University of Alberta

GRID DISCRETIZATION EFFECTS IN THE PRESENCE OF REALISTIC GEOLOGICAL HETEROGENEITIES

By

Hanh Nguyen ©

A thesis submitted to the Faculty of Graduate Studies and Research in partial fulfillment of the requirements for the degree of Master of Science

in

Petroleum Engineering

Department of Civil and Environmental Engineering

Edmonton, Alberta

Spring 2001

National Library of Canada
Acquisitions and Bibliographic Services
395 Wellington Street
Ottawa ON K1A 0N4
Canada

Bibliothèque nationale du Canada
Acquisitions et services bibliographiques
395, rue Wellington
Ottawa ON K1A 0N4
Canada

Your file Votre référence

Our file Notre référence

The author has granted a non-exclusive licence allowing the National Library of Canada to reproduce, loan, distribute or sell copies of this thesis in microform, paper or electronic formats.

L'auteur a accordé une licence non exclusive permettant à la Bibliothèque nationale du Canada de reproduire, prêter, distribuer ou vendre des copies de cette thèse sous la forme de microfiche/film, de reproduction sur papier ou sur format électronique.

The author retains ownership of the copyright in this thesis. Neither the thesis nor substantial extracts from it may be printed or otherwise reproduced without the author's permission.

L'auteur conserve la propriété du droit d'auteur qui protège cette thèse. Ni la thèse ni des extraits substantiels de celle-ci ne doivent être imprimés ou autrement reproduits sans son autorisation.

0-612-60481-0

Canada

University of Alberta

Library Release Form

Name of Author: Hanh Nguyen

Title of Thesis: Grid Discretization Effects in the Presence of Realistic Geological Heterogeneities

Degree: Master of Science

Year this Degree Granted: 2001

Permission is hereby granted to the University of Alberta Library to reproduce single copies of this thesis and to lend or sell such copies for private, scholarly or scientific research purposes only.

The author reserves all other publication and other rights in association with the copyright in the thesis, and except as herein before provided, neither the thesis nor any substantial portion thereof may be printed or otherwise reproduced in any material form whatever without the author's prior written permission.

Hanh

3A 8901-112 Street,
Edmonton, AB, Canada, T6G 2C5

Date: 17 April, 2001

University of Alberta

Faculty of Graduate Studies and Research

The undersigned certify that they have read, and recommend to the Faculty of Graduate Studies and Research for acceptance, a thesis entitled ***GRID DISCRETIZATION EFFECTS IN THE PRESENCE OF REALISTIC GEOLOGICAL HETEROGENEITIES*** submitted by ***Hanh Nguyen*** in partial fulfillment of the requirements for the degree of Master of Science in Petroleum Engineering.

Dr. Clayton Deutsch *(Supervisor)*

Dr. Ramon Bentsen *(Committee Chair and Examiner)*

Dr. Ergun Kuru *(Committee Member)*

Dr. Carl Mendoza *(Committee Member)*

Date: April 12, 2001

ABSTRACT

Grid discretization has an effect on reservoir characterization. This effect on reservoir description is exaggerated in the presence of realistic reservoir heterogeneity. The discretization and scaling effects in geological modeling, in turn, are also reflected in reservoir flow simulation. This study describes procedures to understand and quantitatively assess grid discretization effects. Different scaling techniques are applied and the results are compared. Also described is the uncertainty in reservoir flow modeling for different types of fluids flowing in the reservoir. In this study, different ranking techniques as a fast way to assess the uncertainty in reservoir modeling are also presented.

The results of this study show that the magnitude of the grid discretization effects depends on the porosity-permeability properties, and the nature of fluids flowing in the reservoir. Recovery factors and breakthrough times increase as the number of cells increases. For the homogeneous reservoir case, the recovery factors for the coarsest grid used in this study, were 4-5 % lower compared to the finest grid. The breakthrough times were 23-30 % lower for the coarsest grid compared to the finest grid. For the reservoir with downscaled porosity-permeability, recovery factors were 6-8 % lower and breakthrough times were 25-36 % lower for the coarsest grid than for the finest grid. For the reservoir with upscaled porosity-permeability, based on the mean values of 100 realizations, the recovery factors were 3-7 % lower and the breakthrough times were 5-9 % lower for the coarsest grid than for the finest grid.

Uncertainty in geological modeling contributes more to the total uncertainty than does the grid discretization. Recovery factors and breakthrough times obtained from a flow simulation using a very coarse grid can be used as fair to good ranking parameters to assess the uncertainty in the reservoir flow simulation.

TABLE OF CONTENTS

I.	**Introduction**	**1**
II.	**Background Theory Behind Geostatistical Modeling**	**5**
1.	Basic statistics and geostatistics concepts	5
2.	Commonly used probability distributions	9
	2.1. Normal (Gaussian) distribution	9
	2.2. Lognormal distribution	11
3.	Variogram	12
4.	Kriging	16
5.	Simulation	18
III.	**Geostatistical Modeling Using Wingslib**	**22**
1.	Data analysis	22
2.	Variogram construction and model fitting	23
3.	Gaussian simulation	24
	3.1. Grid 61 x 1 x 50	24
	3.2. Grid 8 x 1 x 6	28
	3.3. Grid 128 x 1 x 96	28
IV.	**Flow Simulation Using Eclipse**	**47**
1.	Setting up the input file	47
2.	Calculating mobility ratios	48
3.	Output variables to be monitored	49
4.	Presentation of results	50
V.	**Flow Simulation of a Homogeneous Reservoir**	**61**
1.	Parameter setup	61
2.	Convergence of flow parameters	62
3.	Comparison between displacement results in heterogeneous and homogeneous reservoirs	65
4.	Computer CPU time for simulation runs	66

VI. Porosity and Permeability Scaling 72
1. Scaling down the data 72
1.1. Problem setting 72
1.2. Interpretation of the results 72
1.3. Convergence properties 73
1.4. CPU time 74
1.5. Some comments 76
2. Scaling up the data 76
2.1. Arithmetic averaging 76
2.2. Harmonic averaging 77
2.3. Geometric averaging 78
2.4. Power averaging 78
2.5. Flow-based averaging 80
3. Comparison of the results obtained during different scaling techniques 80
VII. Running Eclipse for Hundred Realizations 93
1. Looping in Eclipse 93
2. Interpretation of the flow simulation results 94
2.1. Oil rate plots 94
2.2. Water rate plots 95
2.3. Recovery factor plots 96
2.4. Recovery factors measured at 1 PVWI 96
2.5. Breakthrough times measured at WCT = 0.01 98
2.6. Illustration of displacement process 99
VIII. Analysis of Variance 121
1. Theoretical background 121
1.1. One-factor model 121
1.2. Two-factor model 123
2. ANOVA of simulated data 124
2.1. Recovery factors at 1 PVWI 124

2.2. Breakthrough times 126

IX. Ranking for Fast Uncertainty Assessment 131

1. Motivation for ranking 131
2. Ranking with fast flow simulation 132
3. Study of an "ellipse effect" for breakthrough times 133

3.1. Changing of realization positions on BT plots 133

3.2. Visualizing selected porosity and permeability distributions 134

3.3. Ranking of BTs based on Cardwell and Parsons' technique 136

3.4. Ranking based on the numbers of connected cells between two wells 139

3.5. Ranking by the effective permeability obtained from flow-based scaling 140

3.6. Ranking based on flow rate variances 141

X. Conclusions and Future Work 154

Bibliography ***156***

Appendix 1: Parameter file for porosity simulation - 61 x 50 grid 158

Appendix 2: Parameter file for permeability simulation – cokriging option – 61 x 50 grid 159

Appendix 3: Input data file for eclipse – example for grid 61 x 50, M = 0.4 160

Appendix 4: Explanations of parameters used in input file for Eclipse 165

Appendix 5: Tabulated results of flow simulation 170

Appendix 6: Turbo Pascal program to scale down porosity from 8 x 6 grid to 16 x 12 grid 174

Appendix 7: Unix shell script file to automate running eclipse for 100 times 175

Appendix 8: "Oil rates" versus PVWI for 100 realizations 176

Appendix 9: "Water rates" versus PVWI for 100 realizations 181

Appendix 10: Oil recovery factors for 100 realizations 186

Appendix 11: Recovery factors taken at 1 PVWI 189

Appendix 12: Breakthrough times - PVWI taken at ≈ 0.01 water cut 195

Appendix 13: Turbo Pascal program to convert saturation values from Eclipse 201

Appendix 14: Ranking numbers for recovery factors 202

Appendix 15: Ranking numbers for breakthrough times 208

Appendix 16: Crossplot of ranking numbers of recovery factors and breakthrough times for different grids 214

Appendix 17: Turbo Pascal program to calculate k_{min} for 8 x 6 grid 218

Appendix 18: Turbo Pascal program to calculate k_{max} for 8 x 6 grid 220

Appendix 19: Summary of k_{min} and k_{max} calculations based on Cardwell and Parsons' method 222

Appendix 20: Ranking based on the number of connected cells and permeability scaling 228

Appendix 21: Variances of flow rates 234

LIST OF TABLES

Table 3-1:	Nested variogram model for porosity	30
Table 3-2:	Nested variogram model for permeability	30
Table 3-3:	Well data check	31
Table 4-1:	Fractional flow calculations for the three mobility ratio cases	53
Table 4-2:	Viscosity sets for three mobility ratio cases at different reservoir pressures	53
Table 4-3:	Example of calculating the oil and water rate with respect to pore volume	54
Table 5-1:	Different reservoir discretizations for the homogeneous case	67
Table 5-2:	Summary of runs for different discretizations - homogeneous reservoir	68
Table 5-3:	Computer CPU time for flow simulation – homogeneous reservoir	68
Table 6-1:	Different reservoir discretizations for the heterogeneous case	83
Table 6-2:	Summary of runs for different discretizations – down scaling process	83
Table 6-3:	Computer CPU times for flow simulation - down scaling process	84
Table 7-1:	Realization number in order of oil production rates – 16 x 12 grid	102
Table 7-2:	Summary statistics on recovery factors	103
Table 7-3:	Summary statistics on breakthrough times (PVWI at ~ 0.01 WCT)	104
Table 7-4:	Grid 16 x 12 - different PVWI for water saturation display	105
Table 8-1:	Summary of single factor ANOVA for recovery factors	127

Table 8-2:	Summary of two factor ANOVA for recovery factors	127
Table 8-3:	Summary of single factor ANOVA for breakthrough times	128
Table 8-4:	Summary of two factor ANOVA for breakthrough times	128
Table 9-1:	Correlation coefficients of ranking numbers of RF and BT for different grids	143
Table A5-1:	Tabulated results of flow simulation for 61 x 50 grid, M = 0.4	170
Table A11-1:	Recovery factors taken at 1 PVWI for 100 realizations	189
Table A12-1:	Breakthrough times for 100 realizations	195
Table A14-1:	Ranking numbers of different realizations for recovery factors	202
Table A15-1:	Ranking numbers of different realizations for breakthrough times	208
Table A19-1:	Permeability values calculated based on Cardwell and Parsons' method	222
Table A20-1:	Ranking for 8 x 6 and 128 x 96 grids based on the connected cells	228
Table A21-1:	Flow rate variances for 8 x 6 and 128 x 96 grids	234

LIST OF FIGURES

Figure 1-1:	Flow chart of reservoir modeling	4
Figure 3-1:	Well 1 - porosity versus depth	32
Figure 3-2:	Well 2 - porosity versus depth	32
Figure 3-3:	Well 1 - permeability versus depth	32
Figure 3-4:	Well 2 - permeability versus depth	32
Figure 3-5:	Porosity histogram of the original data	33
Figure 3-6:	Permeability histogram of the original data	33
Figure 3-7:	Well 1 - porosity versus permeability	34
Figure 3-8:	Well 2 - porosity versus permeability	34
Figure 3-9:	Crossplot of porosity - permeability for both the wells	34
Figure 3-10:	Porosity variogram and the fitted model	35
Figure 3-11:	Permeability variogram and the fitted model	35
Figure 3-12:	Grid 61 x 50 - Porosity distribution using anisotropy ratio of 100	36
Figure 3-13:	Grid 61 x 50 - Permeability distribution using anisotropy ratio of 100	36
Figure 3-14:	Histogram of simulated porosity using anisotropy ratio of 100	37
Figure 3-15:	Histogram of simulated permeability using anisotropy ratio of 100	37
Figure 3-16:	Variogram of simulated porosity for anisotropy ratio of 100	38
Figure 3-17:	Variogram of simulated permeability for anisotropy ratio of 100	38

Figure 3-18: Porosity distribution for anisotropy ratio of 10 (see color scale of 3-12) 39

Figure 3-19: Permeability distribution for anisotropy ratio of 10 (see color scale of 3-13) 39

Figure 3-20: Histogram of simulated porosity for anisotropy ratio of 10 39

Figure 3-21: Histogram of simulated permeability for anisotropy ratio of 10 40

Figure 3-22: Variogram of simulated porosity for anisotropy ratio of 10 40

Figure 3-23: Variogram of simulated permeability for anisotropy ratio of 10 41

Figure 3-24: Permeability simulated using cokriging with porosity (see color scale of 3-13) 41

Figure 3-25: Simulated porosity versus cokriged permeability 42

Figure 3-26: Grid 8 x 6 – porosity distribution (see color scale of 3-12) 42

Figure 3-27: Grid 8 x 6 – permeability distribution (see color scale of 3-13) 42

Figure 3-28: Grid 8 x 6 – histogram of simulated porosity 43

Figure 3-29: Grid 8 x 6 – histogram of simulated permeability 43

Figure 3-30: Grid 128 x 96 first realization–porosity distribution (see color scale of 3-12) 44

Figure 3-31: Grid 128 x 96 first realization–permeability distribution (color scale of 3-13) 44

Figure 3-32: Grid 128 x 96 – histogram of simulated porosity for 100 realizations 44

Figure 3-33: Grid 128 x 96 – histogram of simulated permeability For 100 realizations 45

Figure 3-34: Grid 128 x 96 – variograms of simulated porosity for 100 realizations 45

Figure 3-35: Grid 128 x 96 – variograms of simulated permeability for 100 realizations 46

Figure 3-36:	Grid 128 x 96 – simulated porosity versus simulated permeability	46
Figure 4-1:	Fractional flow curve and mobility ratio calculation – favorable M	54
Figure 4-2:	Fractional flow curve and mobility ratio calculation – unit M	55
Figure 4-3:	Fractional flow curve and mobility ratio calculation – unfavorable M	55
Figure 4-4:	Oil production rates for different mobility ratios versus PVWI - 61 x 50 grid	56
Figure 4-5:	Water production rates for different mobility ratios – 61 x 50 grid	56
Figure 4-6:	Cumulative oil production for different mobility ratios versus PVWI- 61 x 50 grid	57
Figure 4-7:	Cumulative water production for different mobility ratios - 61 x 50 grid	57
Figure 4-8:	Injector BHP for different mobility ratios - 61 x 50 grid	58
Figure 4-9:	Producer water cut for different mobility ratio - 61 x 50 grid	58
Figure 4-10:	Oil recovery factors for different mobility ratios - 61 x 50 grid	59
Figure 4-11:	"Oil rate" for different mobility ratios - 61 x 50 grid	59
Figure 4-12:	"Water rates" for different mobility ratios - 61 x 50 grid	60
Figure 5-1:	Calculation of geometric average permeability	69
Figure 5-2:	Recovery factors at 1 PVWI for different discretizations and mobility ratios - homogeneous reservoir	69
Figure 5-3:	Breakthrough times taken at ≈ 0.01 water cuts for different discretizations and mobility ratios - homogeneous reservoir	70

Figure 5-4:	Differences in recovery factors at 1 PVWI from finest grid - homogeneous reservoir	70
Figure 5-5:	Differences in breakthrough times from BT of finest grid - homogeneous reservoir	71
Figure 5-6:	Computer CPU times for homogeneous reservoir case	71
Figure 6-1:	"Oil production rate" versus PVWI for 64 x 48 grid - downscaling process	84
Figure 6-2:	"Water production rates" versus PVWI for 64 x 48 grid - downscaling process	85
Figure 6-3:	Recovery factors versus PVWI for 64 x 48 grid – downscaling process	85
Figure 6-4:	Recovery factors at 1 PVWI for different discretizations and mobility ratios - downscaling process	86
Figure 6-5:	Breakthrough times taken at ≈ 0.01 water cuts for different discretizations and mobility ratios - downscaling process	86
Figure 6-6:	Differences in recovery factors at 1 PVWI from the recovery factor of the finest grid - downscaling process	87
Figure 6-7:	Differences in breakthrough times of different grids from the finest grid - downscaling process	87
Figure 6-8:	Computer CPU times - down scaling process	88
Figure 6-9:	8 x 6 grid – effective versus power averaged permeability in x direction	88
Figure 6-10:	8 x 6 grid – effective versus power averaged permeability in z direction	89
Figure 6-11:	64 x 48 grid – effective versus power averaged permeability in x direction	89
Figure 6-12:	64 x 48 grid – effective versus power averaged permeability in z direction	90
Figure 6-13:	8 x 6 grid – "Oil production rates" using permeability averaged by power law and flow-based techniques	90

Figure 6-14:	8 x 6 grid – "water production rates" using permeability averaged by power law and flow-based techniques	91
Figure 6-15:	8 x 6 grid – water cuts using permeability averaged by power law and flow-based techniques	91
Figure 6-16:	8 x 6 grid – recovery factors using permeability averaged by power law and flow-based techniques	92
Figure 7-1:	Histograms of recovery factors at 1 PVWI for all grids and mobility ratios	106
Figure 7-2:	Box plot of recovery factors measured at 1 PVWI for different grids and M	107
Figure 7-3:	Percentage differences in RF means from the RF mean for the 128 x 96 grid	107
Figure 7-4:	Interquartile range of RFs for different grids and mobility ratios	108
Figure 7-5:	RF's standard deviation for different grids and mobility ratios	108
Figure 7-6:	RF's coefficients of variance for different grids and mobility ratios	109
Figure 7-7:	Histograms of BTs measured in PVWI at ≈ 0.01 WCT for all grids	110
Figure 7-8:	Box plot of breakthrough times for different grids and mobility ratios	111
Figure 7-9:	Percentage differences in BT means from the BT mean of the 128 x 96 grid	111
Figure 7-10:	Interquartile range for BTs for different grids and mobility ratios	112
Figure 7-11:	BT's standard deviation for different grids and mobility ratios	112
Figure 7-12:	BT's coefficients of variance for different grids and mobility ratios	113

Figure 7-13: Realization 33, 16 x 12 grid – porosity distribution (see color scale in 3-12) 114

Figure 7-14: Realization 33, 16 x 12 grid – permeability distribution (see color scale on 3-13) 114

Figure 7-15: Realization 36, 16 x 12 grid – porosity distribution (see color scale on 3-12) 114

Figure 7-16: Realization 36, 16 x 12 grid – permeability distribution (see color scale on 3-13) 114

Figure 7-17: Realization 33, water saturation profile at different PVWI, for M = 0.4 115

Figure 7-18: Realization 33, water saturation profile at different PVWI, for M = 1 116

Figure 7-19: Realization 33, water saturation profile at different PVWI, for M = 1.8 117

Figure 7-20: Realization 36, water saturation profile at different PVWI, for M = 0.4 118

Figure 7-21: Realization 36, water saturation profile at different PVWI, for M = 1 119

Figure 7-22: Realization 36, water saturation profile at different PVWI, for M = 1.8 120

Figure 8-1: Single factor ANOVA for recovery factors at 1 PVWI 129

Figure 8-2: Two factor ANOVA for recovery factors at 1 PVWI 129

Figure 8-3: Single factor ANOVA for breakthrough times 130

Figure 8-4: Two factor ANOVA for breakthrough times 130

Figure 9-1: Crossplot of ranking numbers of RFs for different grids, M = 0.4 144

Figure 9-2: Crossplot of ranking numbers of BTs for different grids, M = 0.4 144

Figure 9-3: Correlation coefficients between recovery factors and breakthrough times of 128 x 96 and of coarser grids 145

Figure 9-4: Three groups of realizations on BT plot for 8 x 6 grid 145

Figure 9-5: Crossplots of d values of 8 x 6 grid for different mobility ratios 146

Figure 9-6: Crossplots of d values of different grids, M = 1 147

Figure 9-7: Porosity distributions of 8 x 6 grid (on the left hand side), and 128 x 96 grid (on the right hand side) 148

Figure 9-8: Permeability distributions of 8 x 6 grid (on the left hand side), and 128 x 96 grid (on the right hand side) 149

Figure 9-9: k_{min}/k_{max} ratios for 8 x 6 and 128 x 96 grids 150

Figure 9-10: Relative differences between k_{min} and k_{max} for 8 x 6 and 128 x 96 grids 150

Figure 9-11: Realization ranking by the connectivity between two wells: 600 md threshold 151

Figure 9-12: Realization ranking by the connectivity between two wells: 500 md threshold 151

Figure 9-13: Realization ranking by the connectivity between two wells: 400 md threshold 152

Figure 9-14: Realization ranking by the effective permeability from flow-based scaling 152

Figure 9-15: Flow rate variances of 8 x 6 grid 153

Figure 9-16: Crossplot of flow rate variances of 8 x 6 and 128 x 96 grids, M = 0.4 153

Figure A8-1: 8 x 6 grid – "oil rate" plots for M = 0.4 (a), M = 1 (b), and M = 1.8 (c) 176

Figure A8-2: 16 x 12 grid – "oil rate" plots for M = 0.4 (a), M = 1 (b), and M = 1.8 (c) 177

Figure A8-3: 32 x 24 grid – "oil rate" plots for M = 0.4 (a), M = 1 (b), and M = 1.8 (c) 178

Figure A8-4: 64 x 48 grid – "oil rate" plots for M = 0.4 (a), M = 1 (b), and M = 1.8 (c) 179

Figure A8-5: 128 x 96 grid–"oil rate" plots for M = 0.4 (a), M = 1 (b), and M = 1.8 (c) 180

Figure A9-1: 8 x 6 grid – "water rate" plots for M = 0.4 (a), M = 1 (b), and M = 1.8 (c) 181

Figure A9-2: 16 x 12 grid – "water rate" plots for M = 0.4 (a), M = 1 (b), M = 1.8 (c) 182

Figure A9-3: 32 x 24 grid – "water rate" plots for M = 0.4 (a), M = 1 (b), M = 1.8 (c) 183

Figure A9-4: 64 x 48 grid – "water rate" plots for M = 0.4 (a), M = 1 (b), M = 1.8 (c) 184

Figure A9-5: 128 x 96 grid – "water rate" plots for M = 0.4 (a), M = 1 (b), M = 1.8 (c) 185

Figure A10-1: 8 x 6 grid – recovery factor plots for all three mobility ratios 186

Figure A10-2: 16 x 12 grid – recovery factor plots for all three mobility ratios 186

Figure A10-3: 32 x 24 grid – recovery factor plots for all three mobility ratios 187

Figure A10-4: 64 x 48 grid – recovery factor plots for all three mobility ratios 187

Figure A10-5: 128 x 96 grid – recovery factor plots for all three mobility ratios 188

Figure A16-1: Ranking plots for RFs, M = 1 214

Figure A16-2: Ranking plots for RFs, M = 1.8 215

Figure A16-3: Ranking plots for BTs, M = 1 216

Figure A16-4: Ranking plots for BTs, M = 1.8 217

NOMENCLATURE

ROMAN LETTERS

a	Lower Bound of an Interval
a	Variogram Range
b	Upper Bound of an Interval
BHP	Bottom Hole Pressure
BT(s)	Breakthrough Time(s)
C	Covariance
Cov	Covariance
cdf	Cumulative Distribution Function
CV	Coefficient of Variance
df	Degrees of Freedom
E	Expected Value
f	Probability Density Function
F	Cumulative Distribution Function
F_w	Water Fractional Flow
FOEW	Oil Recovery Efficiency
FRPV	Reservoir Pore Volume
g	Gaussian pdf
g_o	Standard Gaussian pdf
G	Gaussian cdf
G_o	Standard Gaussian cdf
h	Distance
h	Thickness
i	Data Index
IR	Interquartile Range
j	Data Index
k	Data Index

k	Permeability
k_{ro}	Relative Permeability to Oil
k_{rw}	Relative Permeability to Water
m	Mean
M	Median
M	Mobility Ratio
p	Quantile Value
pdf	Probability Density Function
PVWI	Pore Volume Water Injected
q	Quantile
RC	Reservoir Characterization
RD(s)	Relative Difference(s)
RF(s)	Recovery Factors(s)
R(u)	RV with Zero Mean and Kriging Variance
RV(s)	Random Variable(s)
SD	Standard Deviation
SS	Sum of Squares
S_w	Water Saturation
u	Location
Var	Variance
w	Weight of Data
WCT	Water Cut
WOPR	Well Oil Production Rate
WOPT	Well Oil Production Total
WPI	Well Production Index
WVIW	Reservoir Volume Injected Water
WWCT	Well Water Cut
WWPR	Well Water Production Rate
WWPT	Well Water Production Total
x	Data Value

X	Random Variable
y	Data Value
Y	Random Variable
Y^*	Kriging Estimator
z	Data Value
Z	Random Variable
Z^*	Kriging Estimator
z_p	Data Value Corresponding to p-quantile

GREEK LETTERS

α	Logarithmic Mean of Lognormal Distribution
β^2	Logarithmic Variance of Lognormal Distribution
γ	Variogram
λ	Kriging Weight
μ	Grand Mean
μ	Viscosity
μ_o	Oil Viscosity
μ_w	Water Viscosity
ρ	Correlation Coefficient
σ	Standard Deviation
σ^2	Variance
σ^2_{SK}	Simple Kriging Variance

I. INTRODUCTION

In a reservoir study, reservoir characterization and model selection are very important steps. Saleri and Toronyi [1] have pointed out that reservoir characterization (RC) can be described in terms of three independent components: (i) fluid characterization, (ii) rock characterization, and (iii) geological modeling. The purpose of RC is to capture the geologic and petrophysical features which affect reservoir flow mechanisms. Following their ideas, fluid characterization involves analyses of the areal and vertical variations of the fluids present in the reservoir. Rock characterization involves studies of parameters such as residual oil, relative permeability, capillary pressure, and oil and water finger printing. A geological model, according to the authors' assessment, is the most important and the most complex. The geological model must be able to capture features that directly affect flow. According to these authors, RC forms the foundation for the other simulation steps. Hence, any error in RC can be costly in terms of engineering results.

Geostatistics is a very important tool for RC, especially in the construction of the geological model. It enables estimating petrophysical properties in areas where there are no data available. Geostatistics offers a way of describing the spatial continuity that is an essential feature of many natural phenomena, and it provides adaptations of classical regression techniques to take advantage of this continuity [2].

Another important step in reservoir modeling is to choose the fluid flow simulation model that is best suited to the objectives of the simulation. For a specific simulation task, various simulation models can be used. Each simulation model has certain advantages and disadvantages. Time and cost considerations and computer and labor resources must also be taken into account in the final decision. Grid selection is an important component in model selection. The dimensionality of the model and the well spacing of the reservoir define the resolution required. The resolution dictates the number and coarseness of the cells. Computer resources are usually limited. Grid

determination is an iterative process that balances available computing capacities and modeling needs [1].

Reservoir parameters such as vertical and horizontal permeabilities, relative permeability, and porosity depend on model cell dimensions [1]. These properties are often obtained on a different scale; therefore, the scaling of the available data to the model cell dimensions becomes important. The reservoir may be discretized very finely for geostatistical modeling so that petrophysical data as well as different geological trends and features are better represented. Most flow simulators cannot handle such fine grid systems. Thus, upscaling is necessary.

There are different methods for upscaling the data. One problem in the upscaling process is that extreme high and low values may be diluted and lost; therefore, the heterogeneous character of the reservoir may not be fully described and the result may be the introduction of error into the reservoir performance predictions. Choosing the right scaling techniques and parameters can result in a better prediction of reservoir flow behavior.

This study examines how grid sizes and data scaling affect the reservoir description process, and how information on heterogeneity may be lost as a result of an increase in grid size. From this grid sensitivity study, the uncertainty associated with combining effects of geological realizations and grid sizes is assessed quantitatively.

Three major steps were involved in this study: (1) construction of geological models using geostatistical modeling techniques, (2) upscaling of the geostatistical models, and (3) flow simulation runs to see the effects of different geological realizations on the flow performance of the reservoir. A flowchart describing the procedure used is shown in Figure 1-1.

Data used for this study were from the two wells drilled 600 m from each other; they intersect an approximately 100 m thick reservoir. The data were organized in Wingslib format (simplified Geo-EAS format [3; p. 21]). Only the porosity and permeability data were analyzed. The porosity was measured at 0.1 m intervals over the entire reservoir thickness. The permeability was measured irregularly, but tabulated in the same depth interval as the porosity.

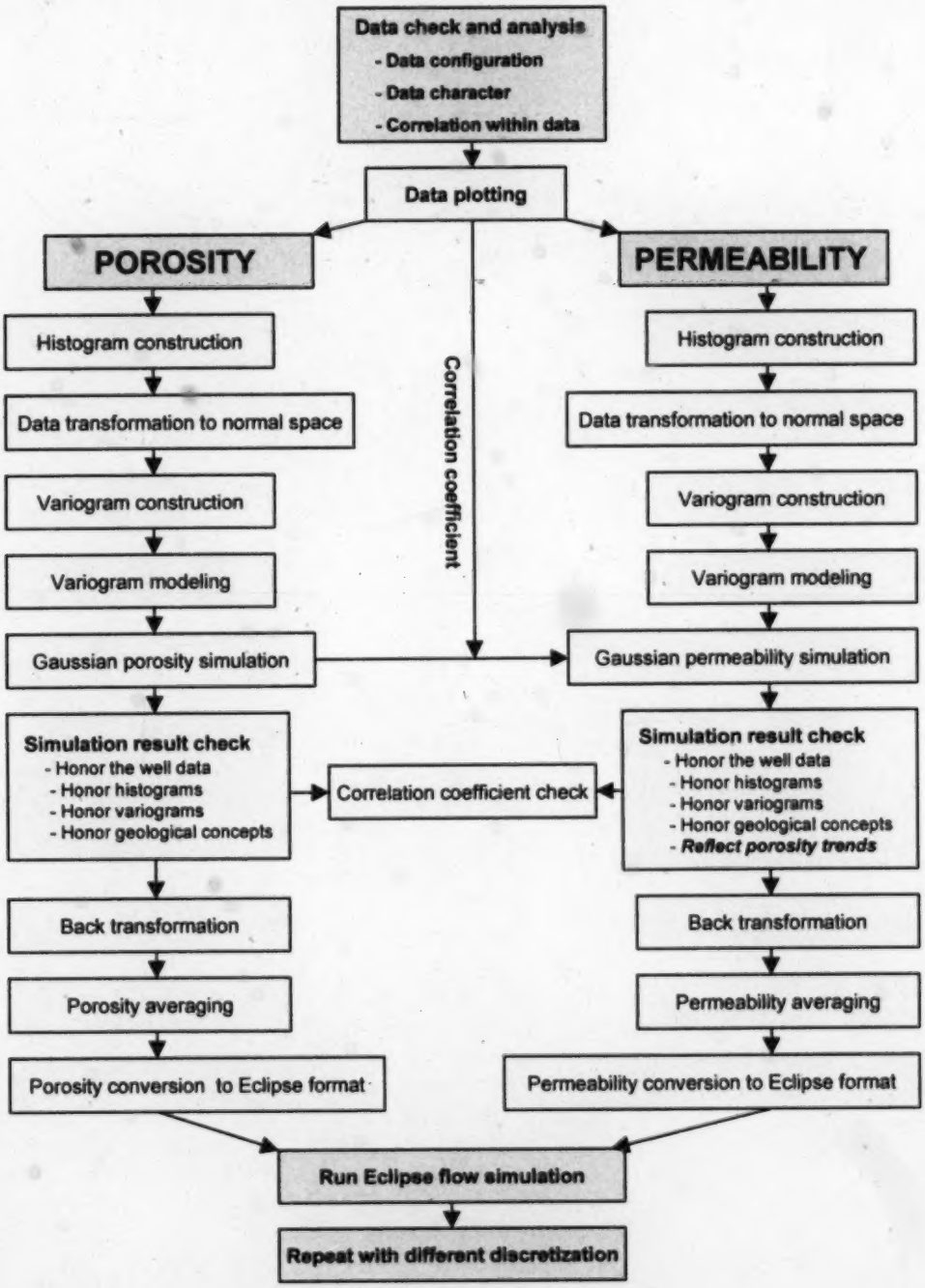

Figure 1-1: Flow chart of reservoir modeling

II. BACKGROUND THEORY BEHIND GEOSTATISTICAL MODELING

1. Basic statistics and geostatistics concepts

Statistics is a mathematical method for collecting, organizing, and interpreting data, as well as drawing conclusions and making reasonable decisions on the basis of such analysis [4]. *Geostatistics* is a branch of applied statistics that emphasizes the geological context of the data, the spatial relationship, and the different volumetric supports and precision between them [4]. Thus, geostatistics considers the spatial structure of the data. Geostatistics offers a collection of deterministic and statistical tools aimed at understanding and modeling spatial variability [3]. One should understand that statistical models are to be used in either the predictive or the stochastic mode until more or better data enables deterministic knowledge of the data. Statistical models should not be used to explain things. That is, statistical correlation does not provide a causal explanation [4].

Predictive statistics enable presenting any unsampled (or unknown) value z in the form of a *random variable* (RV) Z, the probability distribution of which models the uncertainty about z [3]. A RV is a variable that can take a variety of outcome values according to some probability distribution. Variables can be continuous or discrete (categorical). A continuous variable is one that can take on any value between two given values. Porosity and permeability are examples of a continuous variable. Facies or lithology classifications are categorical, because they can have only limited outcomes. An important function that characterizes RVs is the *cumulative distribution function* (cdf). The cdf of a continuous RV Z is defined as:

$$F(z) = \text{Prob}\{Z \leq z\} \in [0,1] \qquad (2\text{-}1)$$

This formula implies that the cdf of the RV Z is the probability of occurrence of all the values of Z that are less than or equal to a threshold value of z. Similarly, the

probability of exceeding any of the threshold values of z can be shown to be:

$$\text{Prob}\{Z \geq z\} = 1 - F(z) \qquad (2\text{-}2)$$

The probability of Z occurring in an interval from a to b (b > a) is the difference in the cdf values evaluated at points b and a:

$$\text{Prob}\{Z \in [a,b]\} = F(b) - F(a) \qquad (2\text{-}3)$$

A *probability density function* (pdf) is the derivative of the cdf; if it is differentiable:

$$f(z) = F'(z) = \lim_{dz \to 0} \frac{F(z+dz) - F(z)}{dz} \qquad \text{if it exists} \qquad (2\text{-}4)$$

Thus, the cdf can be obtained from integration of the pdf:

$$F(z) = \int_{-\infty}^{z} f(z)dz \qquad (2\text{-}5)$$

The *quantile* (q) is another function of RVs. The p-quantile of the distribution $F(z_p)$ is the value z_p for which:

$$F(z_p) = \text{Prob}\{Z \leq z_p\} = p \quad \in [0,1] \qquad (2\text{-}6)$$

Thus, the quantile can be expressed in an inverse form of the cdf: $q(p) = F^{-1}(p)$. The *lower quartile* q(0.25), the *median* (M) q(0.5), and the *upper quartile* values q(0.75) are commonly used. The *interquartile range* (IR) is the difference between the upper and the lower quartiles: IR = q(0.75) – q(0.25).

The next important concept is that of an *expected value*. The expected value is the probability-weighted sum of all the possible occurrences of the RV [5]. The expected value of Z, also called the *mean* of Z, is defined as:

$$E\{Z\} = m = \frac{\sum_{i=1}^{n} w_i z_i}{\sum_{i=1}^{n} w_i} \tag{2-7}$$

where:

E{Z}: expected value of Z

w: weight of the data

n: number of data points

m: mean

Equation (2-7) is used for a discrete case. In a continuous case, the formula can be written as follows:

$$E\{Z\} = m = \int_{-\infty}^{+\infty} z dF(z) = \int_{-\infty}^{+\infty} z f(z) dz \tag{2-8}$$

where f(z) = F'(z) is the probability density function (pdf).

The mean explained above is the moment of order one. The moment of order two is the *variance*. The variance of the RV Z is defined as the expected squared deviation of Z about its mean:

$$Var\{Z\} = \sigma^2 = E\{[Z-m]^2\} = E\{Z^2\} - m^2 \geq 0 \tag{2-9}$$

where:

$\mathrm{Var}\{Z\} = \sigma^2$: variance of RV Z

σ: standard deviation

In discrete form, Equation (2-9) can be written as:

$$Var\{Z\} = \frac{\sum_{i=1}^{n} w_i (z_i - m)^2}{\sum_{i=1}^{n} w_i} \qquad (2\text{-}10)$$

In continuous form, it can be written as:

$$Var\{Z\} = \int_{-\infty}^{+\infty} (z-m)^2 dF(z) = \int_{-\infty}^{+\infty} (z-m)^2 f(z) dz \qquad (2\text{-}11)$$

The variance is a measure of the spread of the data from the mean. The standard deviation (SD), which is the square root of the variance, is also one of the measures of data variability from the mean. The dimensionless *coefficient of variance* (CV) is the ratio of the SD over the mean (SD/m). Other measures of variability include the range which is the difference between the largest and smallest observation, the IR (as defined earlier), and the mean absolute deviation [4].

The statistical definitions described above are applied to univariate distributions. For multivariate, or bivariate distributions in particular, the same idea is applied. Let X and Y be RVs. The cdf of X and Y, $F_{XY}(x,y)$, is defined as:

$$F_{XY}(x,y) = \mathrm{Prob}\{X \le x, \text{and } Y \le y\} \qquad (2\text{-}12)$$

The pdf of a bivariate distribution, f_{XY}, is the derivative of the cdf F_{XY}:

$$f_{XY}(x,y) = \frac{\partial^2 F_{XY}(x,y)}{\partial x \partial y} \tag{2-13}$$

The moment of order two for a bivariate distribution is the *covariance*. The covariance between the two variables is defined as:

$$\begin{aligned} Cov\{X,Y\} &= E\{[X - m_X][Y - m_Y]\} = E\{XY\} - m_X m_Y \\ &= \int_{-\infty}^{+\infty}\int (x - m_X)(y - m_Y) f_{XY}(x,y)dxdy \end{aligned} \tag{2-14}$$

where m_X and m_Y are the means of the RVs X and Y, respectively. The covariance between the same variable is its variance Cov{X,X} = Var{X}; Cov{Y,Y} = Var{Y}

The *correlation coefficient* is a measure of the linear dependence between the two variables.

$$\rho_{XY} = \frac{Cov\{X,Y\}}{\sqrt{Var\{X\}Var\{Y\}}} \in [-1,+1] \tag{2-15}$$

A perfect correlation $|\rho_{XY}| = 1$ implies that X and Y are linearly dependent. Independence between the two variables means the correlation coefficient is zero. However, the reverse statement is not always the case. No correlation does not imply independence between the two variables.

2. Commonly used probability distributions

2.1. Normal (Gaussian) distribution

The Gaussian distribution is fully characterized by its two parameters, the mean m and the variance σ^2. The pdf g(z) of this model can be expressed by the following

equation:

$$g(z) = \frac{1}{\sigma\sqrt{2\pi}} \exp\left[-\frac{1}{2}\left(\frac{z-m}{\sigma}\right)^2\right] \tag{2-16}$$

The standard normal pdf corresponds to a mean of zero and a standard deviation of one. In this case, Equation (2-16) becomes:

$$g_o(z) = \frac{1}{\sqrt{2\pi}} \exp\left[-\frac{z^2}{2}\right] \tag{2-17}$$

The cdf of the Gaussian distribution G(z) has no closed-form analytical expression, but the standard normal cdf $G_o(z)$ is tabulated [5]:

$$G_o(z) = \int_{-\infty}^{z} g_o(z)dz \tag{2-18}$$

$$G(z) = \int g(z)dz = G_o\left(\frac{z-m}{\sigma}\right) \tag{2-19}$$

The Gaussian distribution has characteristic symmetry. It is symmetric about its mean m; therefore, the mean and the median are the same, and g(m+z) = g(m-z).

The Gaussian distribution is related to the central limit theorem, one postulate of which is that the sum of a great number of independent, equally distributed (although not necessarily Gaussian), standardized RVs tends to be normally distributed, that is, if n RV's Zi have the same cdf and zero means, the RV $Y = \sum_{i=1}^{n} Zi$ tends toward a normal cdf, as n increases towards infinity. The most restrictive constraint to the application of the central limit theorem is that all the RV's Zi should be independent

[5]. In laboratory experiments, where the measurement devices are carefully chosen and monitored, it can be expected that the distribution of errors is normal. However, the central limit theorem may not apply in nature.

2.2. Lognormal distribution

The Gaussian distribution is easy to use because of its simplicity, but many experimental distributions tend to be skewed (asymmetric) with a mean different from the median. Moreover, the Gaussian distribution allows negative outcomes, while many earth science variables are non-negative. In order to accommodate these distributions, various transforms of the normal model are defined. One of these transforms is the lognormal distribution.

A positive RV, $Y > 0$ is said to be lognormally distributed if its logarithm $X = \ln(Y)$ is normally distributed.

$$Y > 0 \rightarrow \log N(m, \sigma^2), \text{ if } X = \ln Y \rightarrow N(\alpha, \beta^2) \qquad (2\text{-}20)$$

Lognormal distributions are also characterized by two parameters, a mean and a variance. However, they can be characterized by either the arithmetic parameters (m and σ^2) or the logarithmic parameters (α and β^2). The lognormal cdf is more easily expressed as a function of its logarithmic parameters:

$$F_Y(y) = \text{Prob}\{Y \le y)\} = G_o\left(\frac{\ln y - \alpha}{\beta}\right) \text{ for all } y > 0 \qquad (2\text{-}21)$$

The corresponding pdf is:

$$f_Y(y) = F'_Y(y) = \frac{1}{\beta y} g_o\left(\frac{\ln y - \alpha}{\beta}\right) \qquad (2\text{-}22)$$

The relations between arithmetic parameters and logarithmic parameters are:

$$m = e^{\alpha+\beta^2/2} \qquad \sigma^2 = m^2[e^{\beta^2}-1]$$
$$\alpha = \ln m - \beta^2/2 \qquad \beta^2 = \ln\left(1+\frac{\sigma^2}{m^2}\right) \tag{2-23}$$

The central limit theorem for the lognormal distribution state that the product of a great number of independent, identically distributed RVs tends to be lognormally distributed. Traditionally permeability distributions are assumed to be lognormal. This is more of a convenience than a fact because there is no reason to believe that sources of spatial variability of permeability are all independent, of roughly equal variance, and are multiplicative. There are many other possible models for positively skewed distributions of non-negative variables.

3. Variogram

A variogram, by definition, is a measure of the spatial variability of a variable in an area of interest. Variograms quantify the correlation between any two values of a variable separated by a distance h (usually called the lag distance). Consider two numerical values z(u) and z(u+h) separated by the vector h. The notation u refers to the location coordinates of the vector of a RV Z. The variogram function $2\gamma(h)$ is defined as:

$$2\gamma(h) = E\{[z(u)-z(u+h)]^2\} \tag{2-24}$$

which may be written in the alternate form:

$$2\gamma(h) = \frac{1}{N(h)}\sum_{i=1}^{N}[z(u_i - z(u_i+h)]^2 \tag{2-25}$$

where N(h) is the number of experimental pairs $z(u_i)$ and $z(u_i+h)$ of data separated by the vector h. This is also called the experimental variogram calculation. In the definition of a variogram, the lag distance h is a vector. It can be represented by its modulus and direction. Variograms in a particular direction increase, in general, as the lag distance h increases. This means that the variability between the two data points increases or the correlation between them decreases. This observation is confirmed by common sense; that is, two values in space that are close together tend to be more similar than two that are further apart from each other. Variograms can be calculated in terms of covariances:

$$2\gamma(h) = 2C(0) - 2C(h) \tag{2-26}$$

where:

C(0): covariance at lag distance 0 or a variance of z.

C(h): covariance between z and z(u+h)

A variogram is characterized by eight parameters: three ranges, sill, nugget, and the three rotating angles in a coordinate system. The range is the lag distance at which all successive values are independent of each other. The range can have different values in different directions. The sill is the variogram value corresponding to the range. The sill can be standardized to one. A nugget effect occurs when a variogram has a finite value at lag distance h = 0. Though the intercept at h = 0 should be strictly equal to zero, several factors, such as sampling error and short scale geological variability cause the sample values to be different at a short scale. This causes a discontinuity in the variogram at the origin. The other three parameters are the rotating angles in the different directions from the reference coordinate system. They are azimuth, dip, and plunge corrections. Variograms can be different in different directions. More information about these parameters can be found in Reference [3, p.27].

Variograms carry information about the spatial structure of the data. Thus, variogram interpretation is very useful and it can give additional information about the geological character and trends in the area of interest. A variogram that climbs above the sill may be an indication of a vertical trend. The cyclicity of variograms can often be linked to underlying geological periodicity, but it may be due to limited data. Zonal anisotropy can be inferred from a variogram that is lower than the sill. If that happens in a vertical variogram, one can predict an areal trend. If it is the case for a horizontal variogram, a vertical trend or stratigraphic layering is suspected. Additional relevant information about a study area can help with the interpretation of variograms. Experimental variograms are often noisy because of a lack of data or data accuracy; therefore, experimental points should not be used. Consequently, variogram modeling becomes important and variogram models are used for simulation purposes.

Variogram modeling is important for a number of reasons. First, for mapping, knowledge of variograms for all directions and distances is necessary. The experimental variograms in all distances and directions, in many cases, cannot be constructed because of a lack of data. Secondly, there is a need to incorporate into the analysis other geological knowledge about the area or its analogue. Thirdly, variogram models must be positive definite; therefore, a valid function must be chosen.

There are a number of known legitimate models that are commonly used: nugget, spherical, exponential, and Gaussian. The variogram can be obtained analytically. Any positive linear combination of these models is also positive definite. That makes variogram modeling very flexible. When different variogram models are combined, the resulting model is a nested variogram model. In practice half of the variogram value γ, called the semivariogram, is used more often, and many times it is understood as a variogram.

The *nugget effect* is a variogram value at the origin:

$$\gamma(h) = \begin{cases} 0, \text{if } h = 0 \\ C, \text{otherwise} \end{cases} \tag{2-27}$$

where C is a positive "variance" coefficient; for standardized variograms, C = 1. The *Spherical model* is a commonly encountered variogram shape. The spherical covariance, 1-Sph(h), is the volume of two intersecting spheres. This model is almost linear near the origin:

$$\gamma(h) = CSph\left(\frac{h}{a}\right) = \begin{cases} C\left[1.5\frac{h}{a} - 0.5\left(\frac{h}{a}\right)^3\right] & \text{if } h \le a \\ C & \text{if } h \ge a \end{cases} \tag{2-28}$$

where "a" is the range of the variogram. The *Exponential model* is defined by the following equation:

$$\gamma(h) = CExp\left(\frac{h}{a}\right) = C\left[1 - \exp\left(-\frac{h}{a}\right)\right] \tag{2-29}$$

It is linear near the origin, as is the spherical model, but does not rise as steeply as the latter. Similarly, the formula for the *Gaussian model* is

$$\gamma(h) = C\left[1 - \exp\left(-\frac{h^2}{a^2}\right)\right] \tag{2-30}$$

The Gaussian model is good for continuous variables [4]. In the exponential and Gaussian models, the variogram never reaches the sill. While modeling the variogram, one should try to fit the analytical models as closely as possible to the experimental variogram. Sometimes, it is not an easy task and requires experience and skill. In many cases, when using just one analytical model, it is not possible to fit the experimental variograms. Therefore, a combination of different analytical models,

called nested structures, is required instead. All nested structures act over all the distances and each of them contributes a fraction of the total variance. The variogram models in all three main directions should have the same nugget effect and the same number and types of structures. However each structure can have different range parameters in different directions. The modeling should be conducted in all three main directions simultaneously. More information about variogram construction, interpretation, and modeling can be found in References [2] and [4].

4. Kriging

The basic idea of kriging or linear regression is to estimate an unknown value Z(u) by using a linear combination of n known values Z_α, $\alpha = 1, 2 \ldots n$. These n known values may correspond to the same attribute as Z(u), in which case the process is referred to as "kriging", or to attributes different from Z_o, in which case it is referred to as "cokriging". The estimator that is defined below is a linear estimator:

$$Z^*(u) = \sum_{i=1}^{n} \lambda_i Z(u_i) \qquad (2\text{-}31)$$

where:

$Z^*(u)$: linear estimator at location u

u_i: location of Z

λ_i: weight of $Z(u_i)$

Consider the residual data values $Y(u_i) = Z(u_i) - m(u_i)$, where the mean m(u) could be constant, locally varying, or constant but unknown, and the value $Y^*(u)$ is the estimate $Y^*(u) = \sum \lambda_i Y(u_i)$. The error variance, also called the kriging variance, is defined as:

$$E\{[Y^*(u)-Y(u)]^2\}=\sum_{i=1}^{n}\sum_{i=1}^{n}\lambda_i\lambda_j C(u_i u_j)-2\sum_{i=1}^{n}\lambda_i C(u,u_i)+C(0) \quad (2\text{-}32)$$

where:

$C(u_i,u_j)$: covariance between the data values between locations u_i

$C(u,u_i)$: covariance between the data values at locations u and u_i

C(0): variance

Optimal weights to minimize the error variance are obtained by taking the derivative of the error variance with respect to the weights and setting the derivative equal to zero. Thus, the kriging equation has the following form:

$$\sum_{j=1}^{n}\lambda_j C(u_i,u_j)=C(u,u_i) \quad (2\text{-}33)$$

There are n equations like Equation (2-33). They form a set of n kriging equations, the simple kriging system, with n unknown weights, the solutions of which, if they exist, are the kriging weights. The main controls on the kriging weights are the closeness of the data to the location being estimated (second term on the right hand side in Equation (2-32)), the redundancy between the data (the first term on the right hand side in Equation (2-32)), and the variogram (the last term on the right hand side of Equation (2-32)). Simple kriging (SK) does not constrain the weights; therefore, the kriging weights may have negative values. Ordinary kriging (OK) constrains the sum of weights to be one. There are also many other types of kriging, depending on data character.

Simple kriging has several important properties. Kriging weights give minimum error variance. It takes into account the geometry of the volume estimated, the configuration of the data, the distance between the data locations and the location of the value being estimated, and the structural continuity of the variable being considered. On the other

hand, as Equation (2-33) shows, kriging weights do not depend on the data values. Kriging is locally accurate and smooth, and appropriate to visualizing trends. Kriging is an exact interpolator. It honors data with discontinuity. Despite some very positive properties, kriging also has some limitations.

The most important feature that limits the use of kriging is that the variance of the kriged estimates is too small, and kriged maps look smooth. Using the kriging equation, it can be proved that:

$$Var\{Y^*(u)\} = \sigma^2 - \sigma^2_{SK}(u) \qquad (2\text{-}34)$$

where:

σ^2: complete variance

σ^2_{SK} (u): simple kriging variance (error variance)

The kriging variance has a value of zero at the data locations; thus, there is no smoothing effect. Away from the data locations, the kriging variance is a variance, so the variance of the kriged estimates is zero. A complete smoothing effect takes place in the latter case. Spatial variations of kriging variance depend on the variogram and data spacing. Because of this property, kriging is not used directly for mapping the spatial distribution of an attribute, especially where extreme values are important [4]. Nevertheless, kriging techniques are still an important method for data estimation. It is used for building conditional distributions for stochastic simulation. The smoothing effect can be quantified and corrected by simulation.

5. Simulation

The idea of simulation is to correct the variance and get the right variogram. In kriging, the covariances between data values, and between the data values and predicted values, are correct. Only the covariance between the estimated values

themselves is incorrect. In simulation, it is necessary that the missing kriging variance be added back without changing the covariance reproduction. In order to fulfill that task, a RV with zero mean and a variance equal to the kriging variance is added to the kriged estimator.

$$Y_s = Y^*(u) + R(u) \qquad (2\text{-}35)$$

where:

Ys : simulated value

Y*(u): kriged estimator at location u

R(u): RV with zero mean and kriging variance

Simulated values obtained by adding this RV honor the data and the spatial variability of the data, which is very important for many processes; e.g., extreme values of permeability for flow in a porous medium. Histograms and variograms are also reproduced. It should be noted that, in simulation, there is no best estimator as in kriging. There are different possible models (realizations) that are equiprobable. There is an uncertainty in the simulated values.

Throughout the history of simulation, different simulation techniques and simulation algorithms have been developed and used. Some of them are simpler and therefore are used more often in practice. The others are more complicated to apply and therefore are more of academic interest. Sequential Gaussian Simulation has the simplest theoretical background. Its implementation is not complicated, so it is used and recommended widely.

In Sequential Gaussian Simulation, the following procedure is followed [4]:

- Transform the data to standard normal space (this is the reason why this simulation technique is called Gaussian)

- Establish the grid network and coordinate system
- Input variogram models
- Assign data to the nearest grid node (take the closest data point and assign to the same node)
- Determine a random path through all of the grid nodes

    - ❖ Find nearby data and previously simulated grid nodes (this is why the simulation is called sequential)
    - ❖ Construct the conditional distribution by kriging
    - ❖ Draw a simulated value from the conditional distribution

- Back transform the data
- Check the results to ensure that they

    - ❖ Honor the data
    - ❖ Honor the histograms
    - ❖ Honor the variograms
    - ❖ Honor the geology

- If the results do not honor one or more of these factors, an adjustment is made in the simulation setting.

A flowchart showing the main steps in Gaussian simulation is illustrated in Figure 1-1. The advantage of Gaussian simulation is that the global normal distribution is preserved if Gaussian distributions are always used.

The simplicity in mathematical background of the technique leads to some limitations of the technique. Gaussian distributions maximize entropy; that is, high and low values are disconnected. As a result, the simulation values, sometimes, are not appropriate for permeability. Common features encountered in Gaussian simulation

include maximal spatial disorder beyond the variogram, maximal disconnectedness of extreme values (as mentioned above), maximal connectedness of median values, and symmetric disconnectedness of the extreme low and high values. Another problem associated with Gaussian simulation is ergodic fluctuations. That is, the input statistics, such as variograms and histograms, are not exactly reproduced. The ergodicity assumption, which is necessary for Gaussian and many other simulation techniques, is an assumption about the infinite size of the domain. In many particular simulation assignments, this assumption is not well met.

III. GEOSTATISTICAL MODELING USING WINGSLIB

There are three main steps involved in this part:

- Data analysis: the geological character and important statistical parameters of the data were examined and identified.
- Variogram modeling: construction of variograms of the given data and identifying the analytical models that best fit them.
- Gaussian simulation: use of variogram models to simulate and assign property values to all grid nodes

1. Data analysis

Plots of porosity and permeability versus depth for each of the wells are shown in Figures 3-1 through 3-4. From these plots, it can be seen that the reservoir was heterogeneous with the inclusion of lower porosity and permeability zones. The porosity falls mainly in the range from 0.04 to 0.25. The permeability ranges from 0.1 to 2000 md. These observations were confirmed by the histogram of porosity and permeability (Figures 3-5 and 3-6). The statistics from the histograms show that the porosity has a mean value of 0.17 and a standard deviation of 0.06, while the permeability has a mean of 1176 md and a standard deviation of 1141 md. Despite the fact that the data were scattered, there was a trend of increasing porosity with depth (shows more clearly in well 1). This observation contradicts general observation that porosity decreases with depth. The explanation here is that this trend is probably more related with the way the sediments were deposited. Coarser grains may deposit at the bottom of the reservoir and therefore porosity is higher at deeper level. The permeability, on the other hand, stays more constant at a value of about 1000 md for depths of 50 m and greater. Rough horizontal correlations between the two wells can be inferred, based on sharp peaks in both the porosity and permeability plots.

Crossplots of porosity versus permeability data for both wells have been constructed also (Figures 3-7, 3-8, 3-9). The correlation coefficients between the two parameters were 0.029 for well 1 (quite low), 0.462 (higher) for well 2 and 0.311 for the combined plot. The crossplots were constructed separately for the two wells in order to see the correlation between porosity and permeability in each location. The combined plot was constructed to obtain statistics that will be used in further geostatistical modeling. The general picture was that the permeability increases as the porosity increases.

2. Variogram construction and model fitting

Variograms of porosity and permeability, based on the given data, have been constructed (Figures 3-10 and 3-11) using the variogram calculation program for the irregular spaced data option ("gamv"). The variogram sills were normalized. The data were measured at only two well locations, so only the vertical variograms could be constructed. No horizontal variograms could be presented, because there were only two data points. Also, no declustering operation has been performed, because the data were measured at a regular spacing of 0.1 m down each well. The analytical variogram models were then adjusted to fit the experimental variograms. To construct the 3-D variogram model, the variogram parameters in the horizontal directions (X and Y) have to be assumed. Kupfersberger and Deutsch [6] state that the character of variograms is the same in different directions; that is, only the scales are different. They suggest that the anisotropy ratio should vary from 10 to 100. Different anisotropy ratios in this range were tried for this reservoir. A ratio of 1:100 was finally picked. The reason for making this choice is described later in Section 3.1. The analytical variogram models that best fit the variograms of porosity and permeability, constructed from the original data, are shown in Tables 3-1 and 3-2. These sets of the nested structures are variogram models for porosity and permeability data.

The porosity variogram shows some cyclicity. This may be interpreted as being due to periodic changes in either shale content or sand grain sizes. The permeability variogram also shows some cyclicity, but not so clearly. The porosity and permeability show correlation over a distance of approximately 50 m, at which point they reach the sill. These best fit variogram models for the two parameters will be used in the simulation part.

3. Gaussian simulation

The Sequential Gaussian Simulation program ("sgsim") was used for this particular assignment. The steps illustrated in Figure 1-1 were followed during the sequential Gaussian simulation. In this particular simulation, however, the data were transformed to normal space and back, simultaneously within "sgsim", so that there were no separate steps to transform the data forward and backward.

3.1. Grid 61 x 1 x 50

The first reservoir discretization was a system of 61 x 1 x 50 cells in the x, y and z directions, respectively (3050 cells - 2D problem). The grid size was uniform (10m x 1m x 2m). Note that the wells go through the centers of the first and last cells in the x direction. A reservoir thickness of 100 m was simulated. The coordinates of the reference point (center of the first block in the three directions) were 0 : 0.5 : (-99) m in x, y and z directions, respectively. The option of data transformation was chosen, because the original well data file was used. Two options of kriging were used in the Gaussian simulation: simple kriging and co-located kriging with one secondary variable. In the latter case, the secondary variable used for a permeability simulation was porosity. For the cokriging option, the correlation coefficient of 0.311 was taken from the crossplot of porosity versus permeability, as shown in Figure 3-9. The option of assigning data to the nodes was used; therefore, the data were relocated to the grid nodes, and a spiral search was conducted. The idea of spiral search is to consider

values at grid nodes successively farther away from the point being estimated. More information on spiral search can be found in Reference [3, pp.35,179]. The search angles were set to 0. The search radii in the three directions were taken to be the same as the variogram ranges in the corresponding directions. Only one realization was implemented for all simulations. Details of the parameter file for the Gaussian simulation can be found in Appendix 1 (for porosity) and Appendix 2 (for permeability). Explanation of "sgsim" simulation parameters can be found in Reference [3, pp. 170-175].

The variogram models were kept flexible regarding the ranges in the horizontal directions. Different anisotropy ratios were considered. Variograms based on the simulated data were then constructed (using the program "gam") and compared with the variogram models to see whether they matched each other. Histograms were also constructed and compared with the original data. These criteria helped to determine the quality of the simulation and aided in selection of the appropriate variogram ranges.

First, an anisotropy ratio of 100 was tried and the porosity and permeability were simulated separately. The simulated values seemed to honor the geology, with a layer of high porosity and permeability at the bottom of the reservoir, and with a more heterogeneous layer in the upper part of the reservoir (Figures 3-12 and 3-13). The variograms and histograms of the simulated porosity seemed to honor the input data; that is, there were good histogram and variogram reproduction between the input and the simulated values (Figures 3-14 to 3-17: they matched the statistics and character of the histograms and the character of the variogram curves). On the other hand, the simulated permeability values do not honor the data very well, with a departure of the variogram from the model. The simulated variogram matches reasonably the variogram of the original data. That may mean the variogram model for permeability does not reflect reality.

An anisotropy ratio of 10 was tried also. The resultant plots of simulated data looked more random, with a disconnection of the high and low value zones (Figures 3-18 and 3-19). The variograms of both porosity and permeability reasonably matched the models (Figures 3-22 and 3-23). The statistics and characteristics of the histograms of both the original data and the simulated values were similar (Figures 3-5 and 3-6 compared with Figures 3-20 and 3-21). From the results of the Gaussian simulation, assuming an anisotropy ratio of 10, it can be seen that the connection between porosity and permeability values was not so realistic, from a geological point of view, when compared to the results for a ratio of 100, where layers of low and high values were simulated. The original data were taken from a reservoir formed in a deltaic depositional environment. Lenses of high porosity and permeability sand surrounded by shales are common in such an environment. The simulated data, based on an anisotropy ratio of 100, contain such features, whereas the simulated data, based on an anisotropy ratio of 10, do not. Consequently, even though the variograms and histograms, based on an anisotropy ratio of 10, were closer to those for the original data than were those for an anisotropy ratio of 100, the latter ratio was chosen for further simulation and analysis, because it models better the actual geology. The same ratio of 100 was applied for porosity and for permeability. This iterative and subjective procedure of choosing the anisotropy in horizontal directions was inevitable because there were not enough input data to construct variogram models in horizontal directions.

The permeability was simulated again using the cokriging option, with porosity as a secondary variable. The first reason for using the cokriging option was because there was much more data on porosity than permeability. Secondly, there was a moderate to good correlation between porosity and permeability. Thirdly, the variogram ranges of permeability (spatial correlation between data) were shorter; therefore, using porosity data can help to identify a trend. All other parameters were the same. The permeability distribution is shown in Figure 3-24. If one looks back at the porosity plot, there is a connection between Figure 3-18 (porosity distribution) and Figure 3-24 (permeability

distribution). The permeability was forced to be lower in the upper part of the reservoir, and higher and more connected in the lower part, corresponding to the porosity distribution. The crossplot of simulated porosity and permeability, using the cokriging option, showed a very high contribution in the ranges 0.1 to 0.26 for porosity and 300 - 5000 md for permeability (Figure 3-25). The correlation coefficient was 0.227, which was fairly close to the value of 0.311 from the original data. The discrepancy in some parameters was probably due to the ergodicity assumption, that is, the domain was assumed to be infinite in size. Another factor that may have caused the divergence was the fact that the results of the simulation were not plotted for values in normal Gaussian space. The behavior of the data in normal space is usually better than in real unit space.

It was necessary also to check if the simulation values honored the well data. In order to make the data tracing process easier, coordinates were added to the simulated data set using the "addcoord" program. In theory, the simulator was supposed to assign the data point closest to the block center as the block representative value. In reality, well data at 0.9 m lower than the cell centers were taken. If data were not available at this point, then the closest datum to that point was taken (see Table 3-3). It was not clear if there was some error with the simulation procedure and setup, or with the simulator itself. Nevertheless, considering the fact that the error was minor and the simulation results did honor the well data, the simulated results were accepted for further analysis.

The first 61 x 1 x 50 grid was simulated to establish and check the geostatistical modeling procedure. The two grids, 8 x 1 x 6 and 128 x 1 x 96 were, respectively, the coarsest and finest grids to be examined. The simulated data from the very coarse grid (8 x 6) were used to downscale the reservoir to finer grids, and the data from the very fine grid (128 x 96) were used to upscale porosity and permeability to coarser grids.

3.2. Grid 8 x 1 x 6

The procedure used for the 61 x 50 grid was applied to the 8 x 6 grid. The grid sizes now were 75, 1 and 16.67 m in the x, y, z directions, respectively. The porosity was simulated first using "sgsim". The permeability was simulated using the simulated porosity values and a correlation coefficient of 0.311. The porosity and permeability distributions are shown in Figures 3-26 and 3-27. Histograms of the simulated values were constructed and are shown in Figures 3-28 and 3-29. From these figures, it can be seen that the porosity had an average value of 0.164 (SD 0.048) and the permeability had an average value of 787.16 md (SD 744.14). Both the simulated porosity and permeability had lower averages than the statistics from the original data. This was the case especially for the permeability (in the original data, the porosity has an average value of 0.17 and the permeability an average value of 1176.14 md). The reservoir has a streak of low permeability near the top of the reservoir in the vicinity of well 2. This again can be explained by the use of a finite domain. The number of cells discretized was so few that the original statistics cannot be reproduced. Also, because there were so few points, the variogram reproduction for this grid was so poor that it was not worth presenting it here.

3.3. Grid 128 x 1 x 96

The base model used to upscale to coarser grids utilized a 128 x 1 x 96 grid. The grid sizes were 4.69, 1 and 1.04 m in the x, y, z directions, respectively. The variogram models for porosity and permeability were the same as those mentioned before in Tables 3-1 and 3-2. The number of realizations was 100. Modeling was done simultaneously using the program "sgsim". All other parameters were kept the same. The output for the 100 realizations was unified in two output files, one for porosity and one for permeability. The 2D maps for the first realization of porosity and permeability are shown in Figures 3-30 and 3-31. The porosity and permeability

showed good correlation, that is, high porosity values correspond to high permeability values and low porosity values correspond to low permeability values.

The simulated values were cross-checked by constructing their histograms and variograms for all 100 realizations. The histogram of simulated porosity (Figure 3-32) showed that the porosity has a mean of 0.172 and a SD of 0.054 (the original data had a mean of 0.17 and a SD of 0.6). The simulated permeability values had a mean of 1088.7 md and a SD of 1040.9 (Figure 3-33) (the original permeability data had a mean of 1176.13 md and a SD of 1141.73). It is worth noticing that both the simulated porosity and permeability have zero values. This caused a problem when the data were averaged.

Variograms of porosity and permeability from the 100 realizations were constructed and plotted (Figures 3-34 and 3-35). One hundred variogram output files were created, one after another, for every realization. In the end, 100 variograms of simulated values (of porosity and permeability), the mean of the 100 variograms, and the variogram model, were plotted together. The mean of the 100 variograms and the variogram model for the original data matched reasonably well for both the porosity and the permeability. A better match could not be achieved because of the ergodicity problem.

A crossplot of the simulated porosity and permeability values is shown in Figure 3-36. Only every 200th data point is plotted (because the number of points was too big), so out of 1,228,800 points only 6144 points are present on the plot. The correlation coefficient for this plot is 0.334 (the original data had a correlation coefficient of 0.311).

No	Type	Contributed sill	h_{max} (m)	h_{min} (m)	h_{vert} (m)
	Nugget	0.001			
1	Spherical	0.55	300	300	3
2	Gaussian	0.12	800	800	8
3	Spherical	0.12	2200	2200	22
4	Spherical	0.21	6000	6000	60
		Sum 1			

Table 3-1: Nested variogram model for porosity

No	Type	Contributed sill	h_{max} (m)	h_{min} (m)	h_{vert} (m)
	Nugget	0.001			
1	Spherical	0.56	280	280	2.8
2	Spherical	0.20	940	940	9.4
3	Spherical	0.17	1500	1500	15
4	Spherical	0.07	5400	5400	54
		Sum 1			

Table 3-2: Nested variogram model for permeability

Well 1				
	Porosity		Permeability (md)	
Simulation Depth (m)	Original Depth (m)	Values	Original Depth (m)	Values
1	1.9	0.06		696.1231
3	3.9	0.141		8.108
5	5.9	0.122		0.4152
7	7.9	0.151	7.8	45.328
9	9.9	0.154	9.9	265.172
11	11.9	0.124	11.5	49.969
89	89.9	0.217	89.9	543.816
91	91.9	0.216	91.9	548.421
93	93.9	0.139	93.3	2.087
95	95.9	0.101	95.6	0.134
97	97.9	0.238	97.9	990.034
99	99.9	0.157	99.8	28.165

Well 2			
Simulation Depth (m)	Original Depth (m)	Porosity	Permeability (md)
1	1.9	0.167	274.949
3	3.9	0.214	1151.538
5	5.9	0.197	139.408
7	7.9	0.158	0.05
9	9.9	0.121	0.049
11	11.9	0.172	2280.974
89	89.9	0.236	1513.519
91	91.9	0.196	1000.222
93	93.9	0.25	1666.911
95	95.9	0.243	1550.796
97	97.9	0.25	1563.349
99	99.9	0.211	1159.484

Table 3-3: Well data check

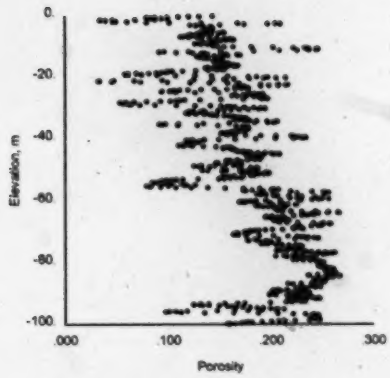

Figure 3-1: Well 1 - porosity versus depth

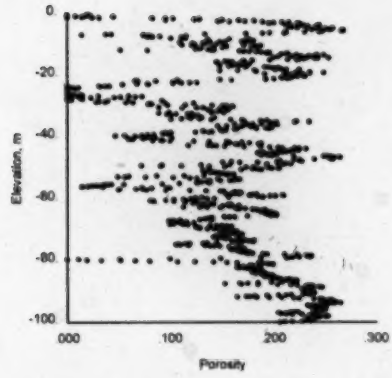

Figure 3-2: Well 2 - porosity versus depth

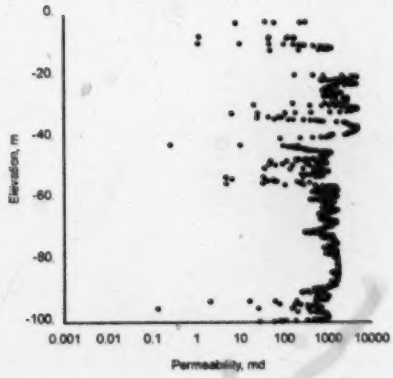

Figure 3-3: Well 1 - permeability versus depth

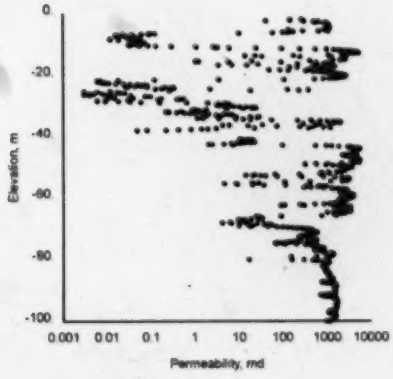

Figure 3-4: Well 2 – permeability versus depth

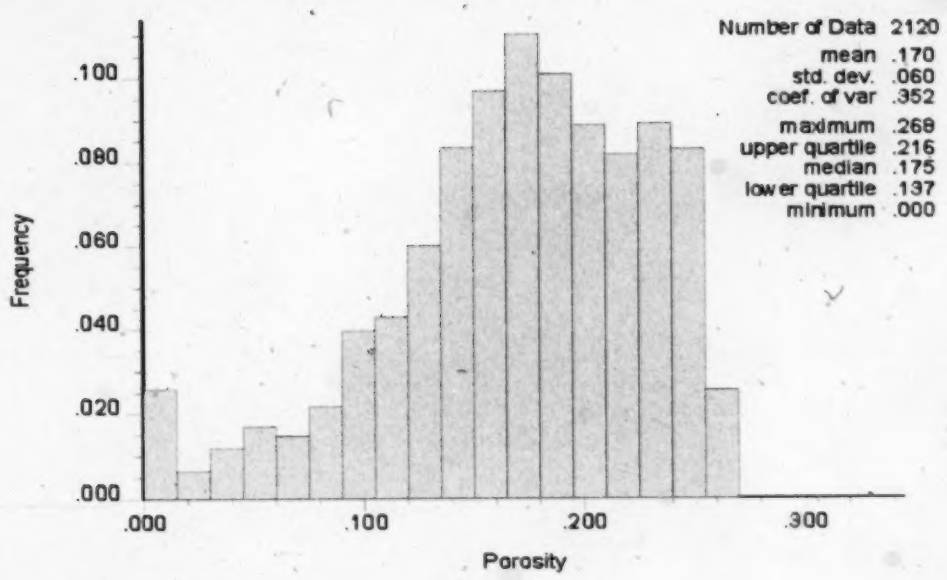

Figure 3-5: Porosity histogram of the original data

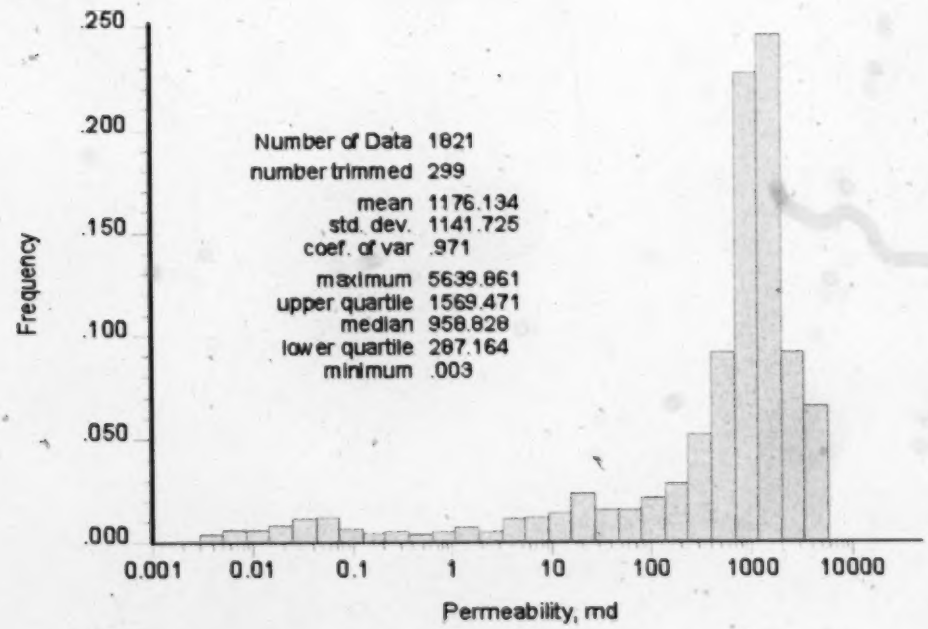

Figure 3-6: Permeability histogram of the original data

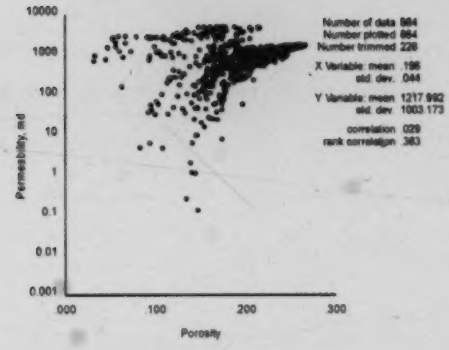

Figure 3-7: Well 1 - porosity versus permeability

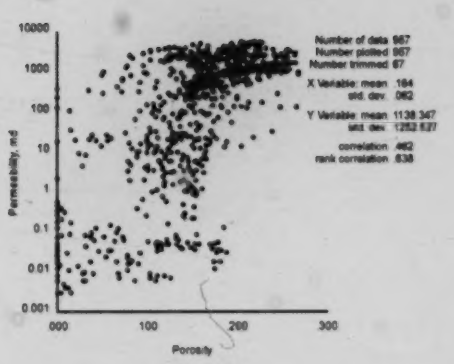

Figure 3-8: Well 2 - porosity versus permeability

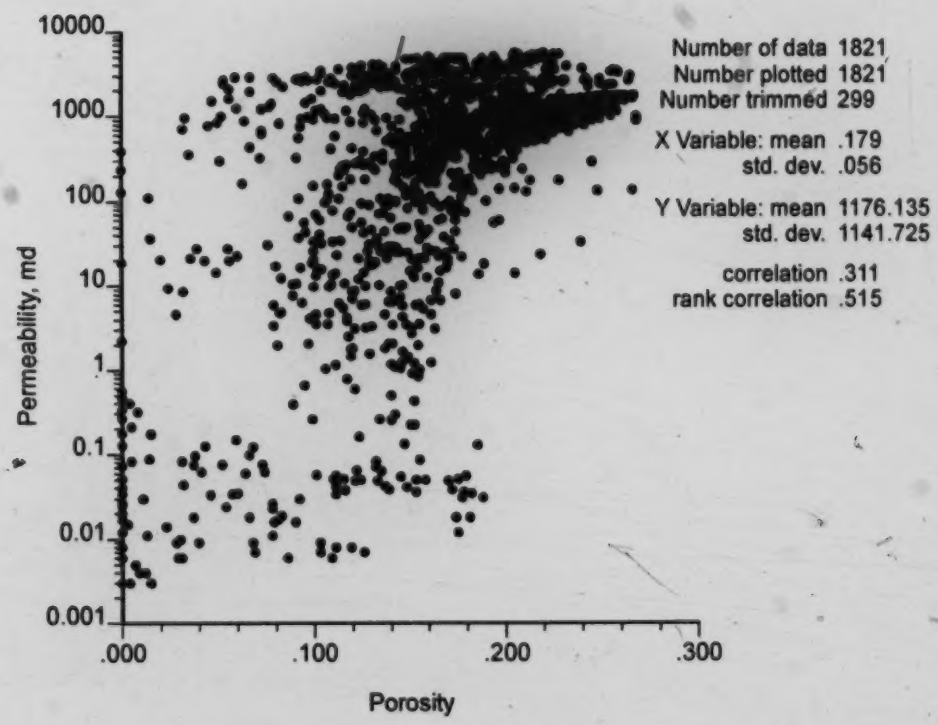

Figure 3-9: Crossplot of porosity - permeability for both the wells

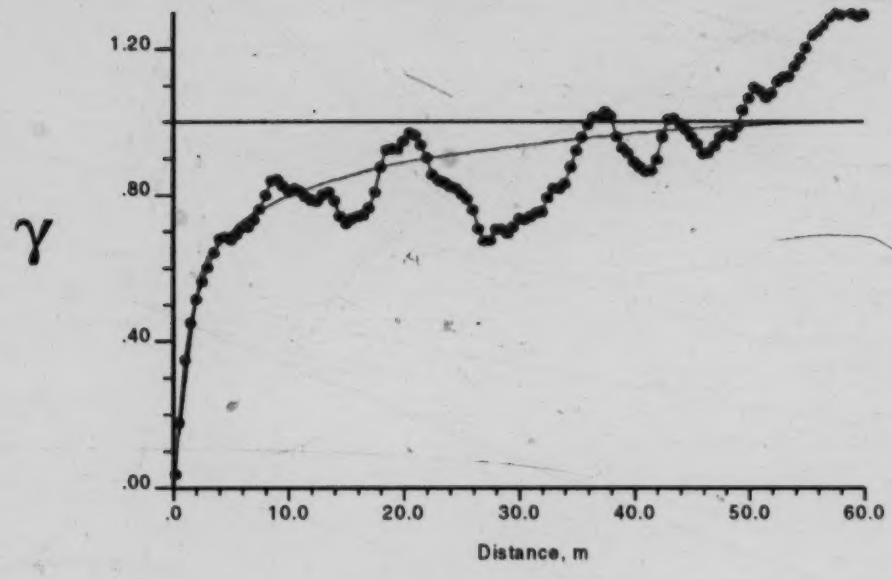

Figure 3-10: Porosity variogram and the fitted model

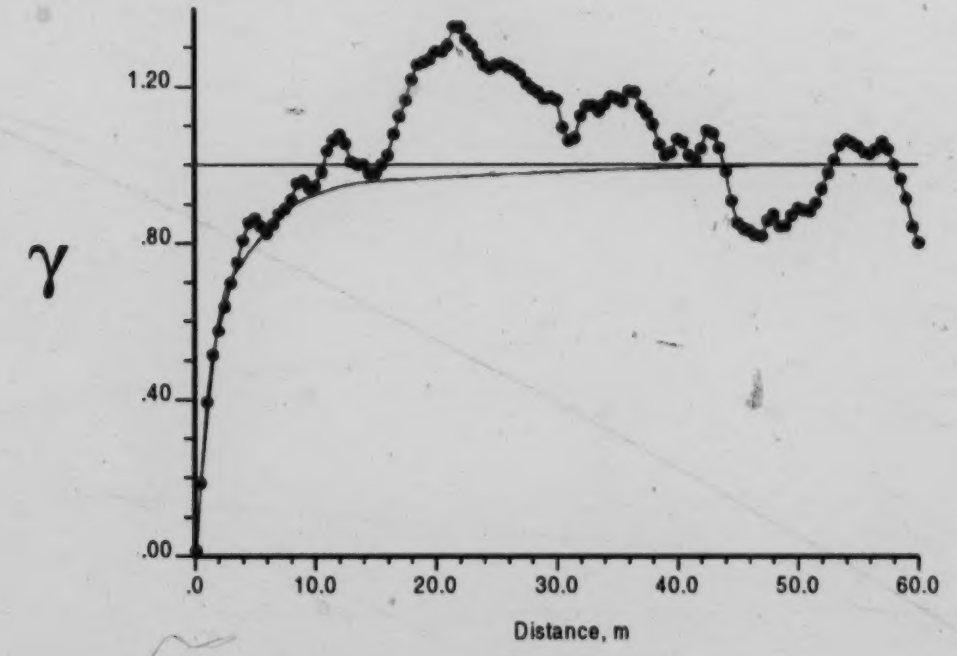

Figure 3-11: Permeability variogram and the fitted model

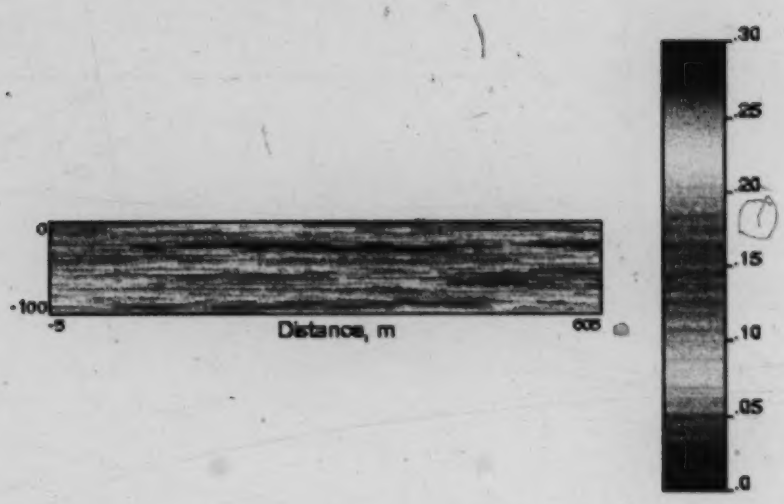

Figure 3-12: Grid 61 x 50 - Porosity distribution using anisotropy ratio of 100

Figure 3-13: Grid 61 x 50 - Permeability distribution using anisotropy ratio of 100

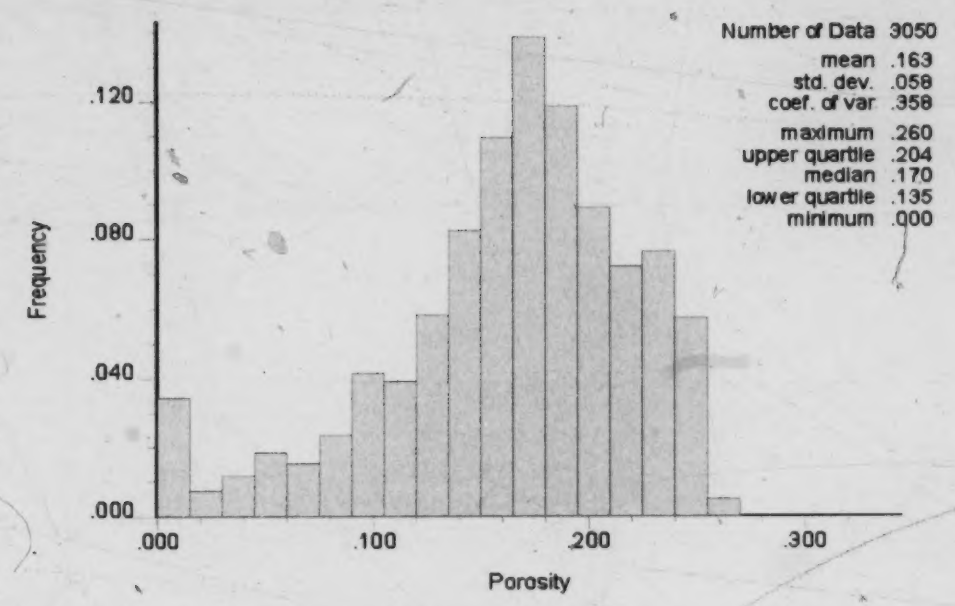

Figure 3-14: Histogram of simulated porosity using anisotropy ratio of 100

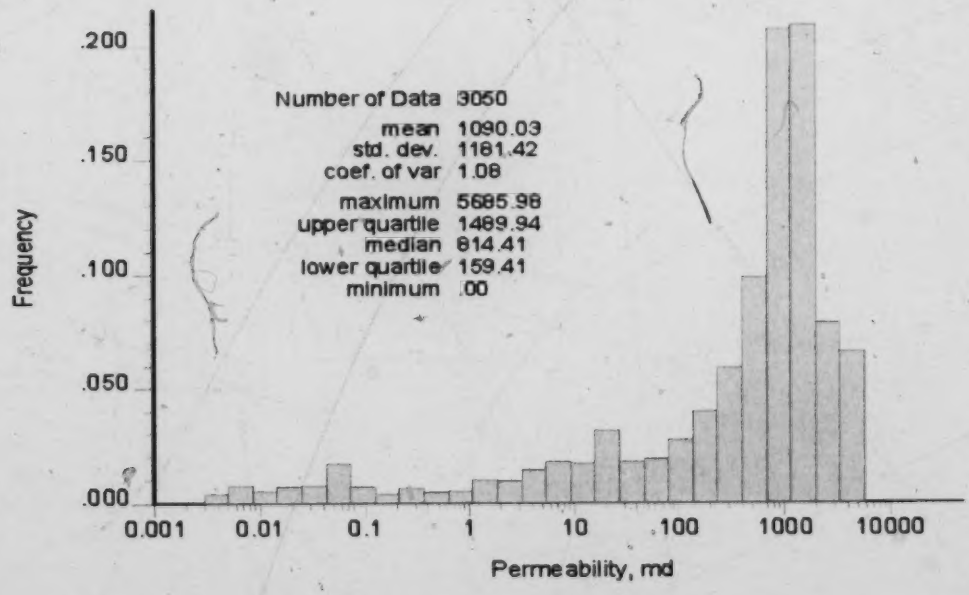

Figure 3-15: Histogram of simulated permeability using anisotropy ratio of 100

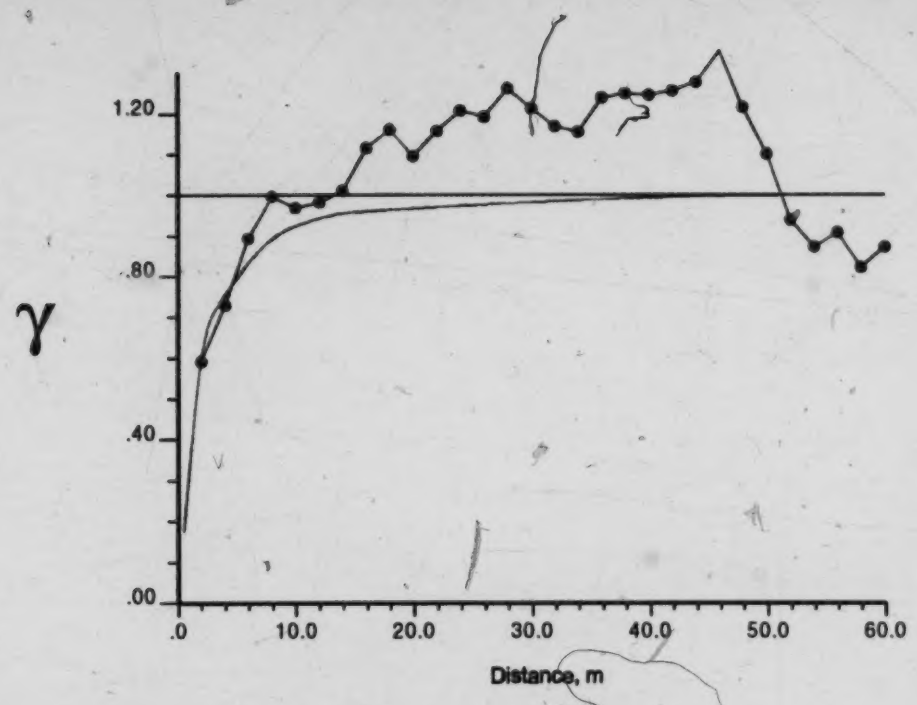

Figure 3-16: Variogram of simulated porosity for anisotropy ratio of 100

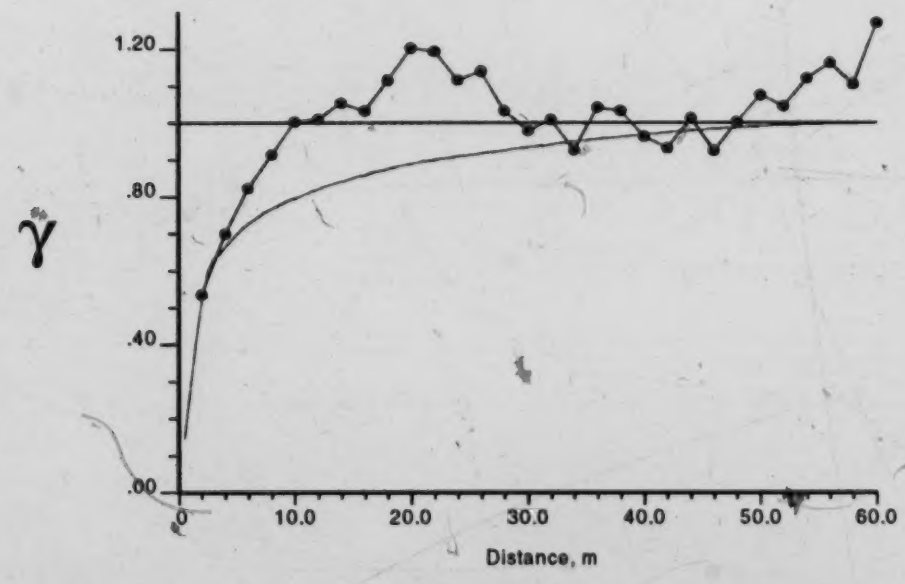

Figure 3-17: Variogram of simulated permeability for anisotropy ratio of 100

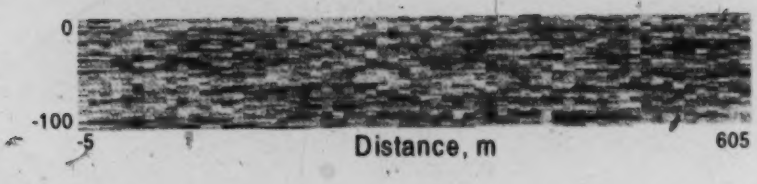

Figure 3-18: Porosity distribution for anisotropy ratio of 10 (see color scale of 3-12)

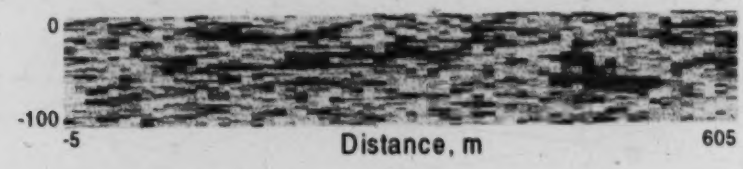

Figure 3-19: Permeability distribution for anisotropy ratio of 10 (see color scale of 3-13)

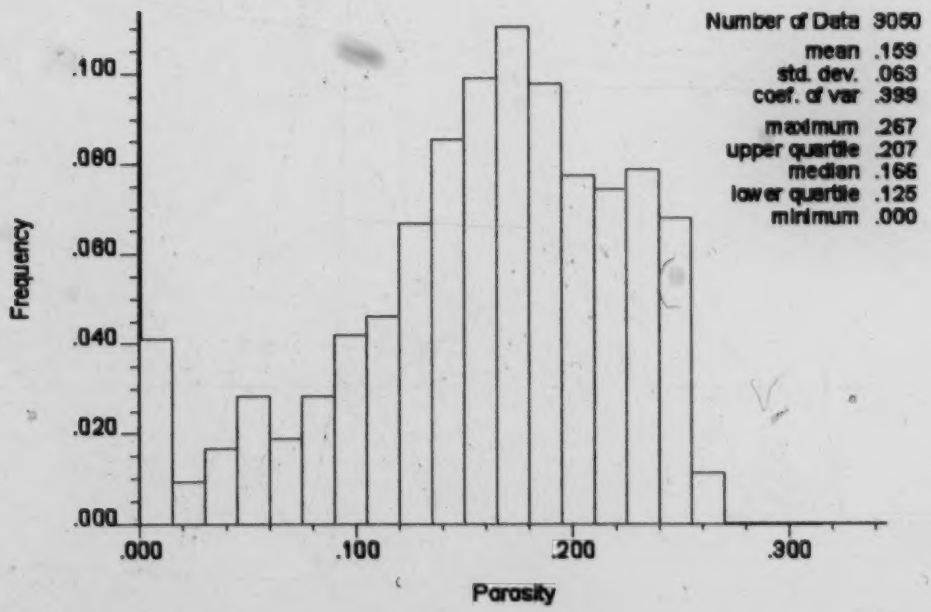

Figure 3-20: Histogram of simulated porosity for anisotropy ratio of 10

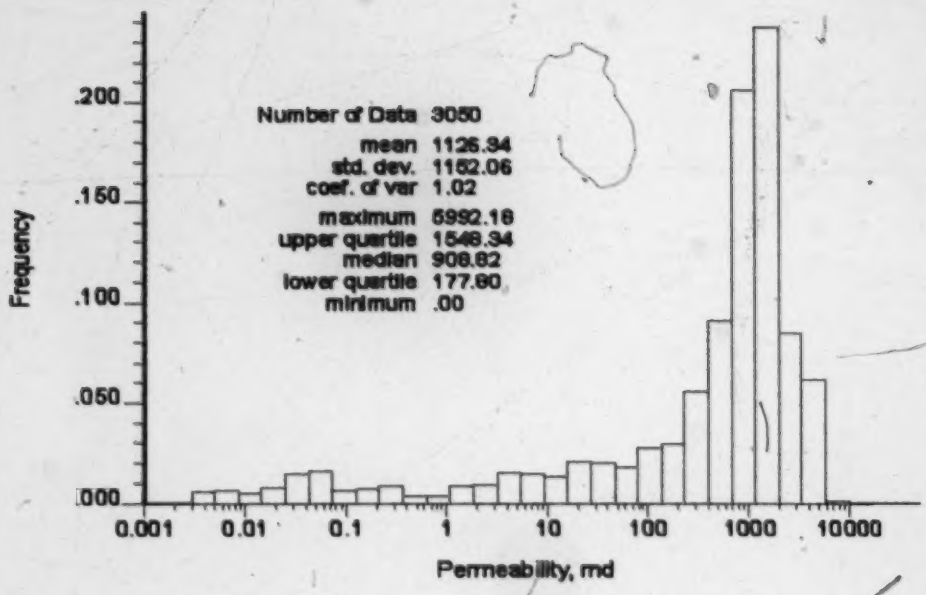

Figure 3-21: Histogram of simulated permeability for anisotropy ratio of 10

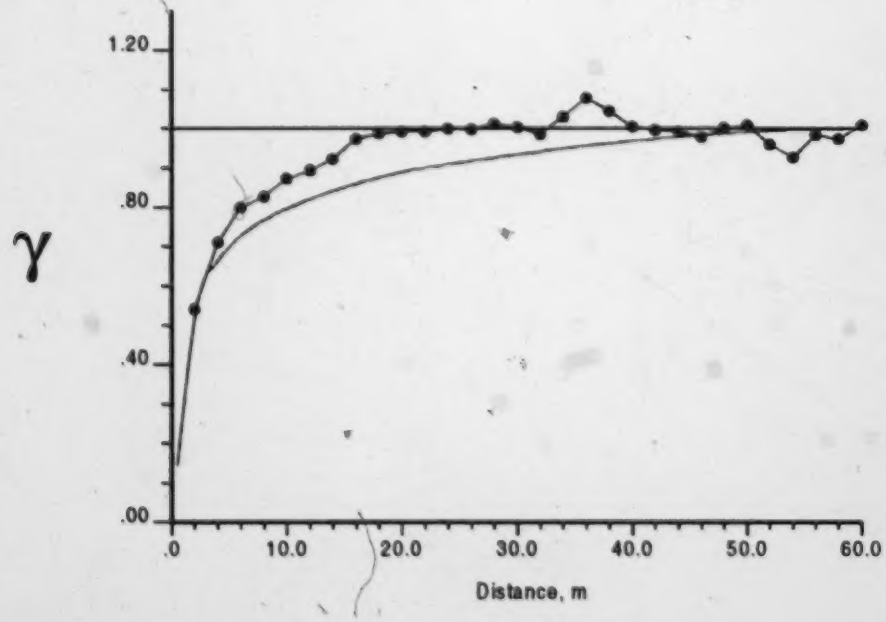

Figure 3-22: Variogram of simulated porosity for anisotropy ratio of 10

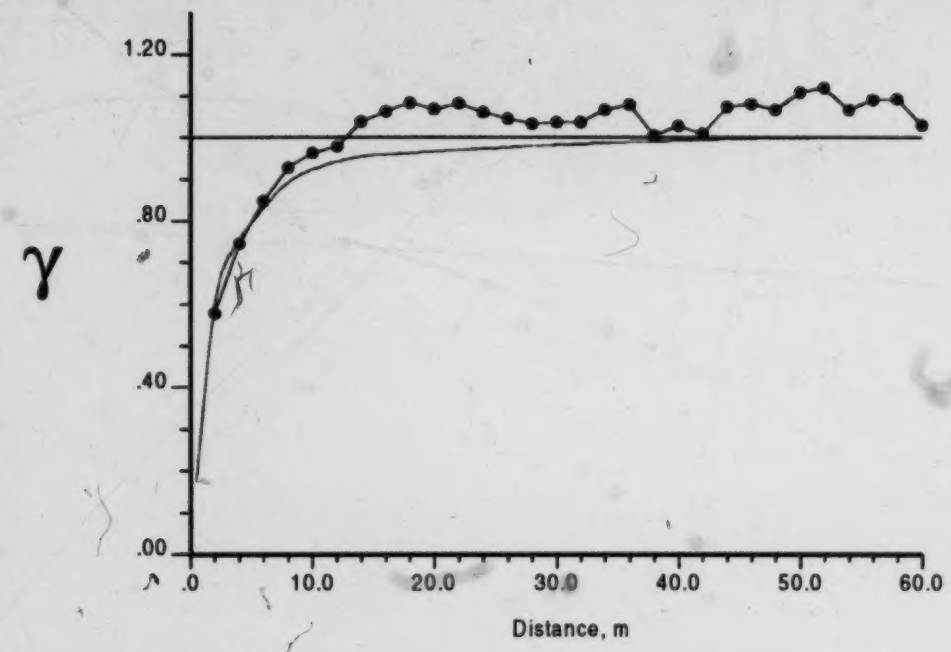

Figure 3-23: Variogram of simulated permeability for anisotropy ratio of 10

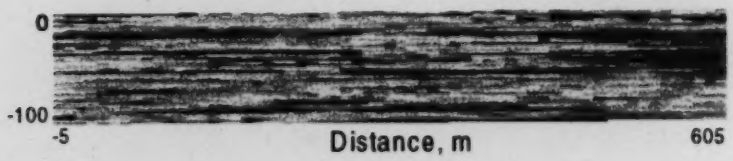

Figure 3-24: Permeability simulated using cokriging with porosity (see color scale of 3-13)

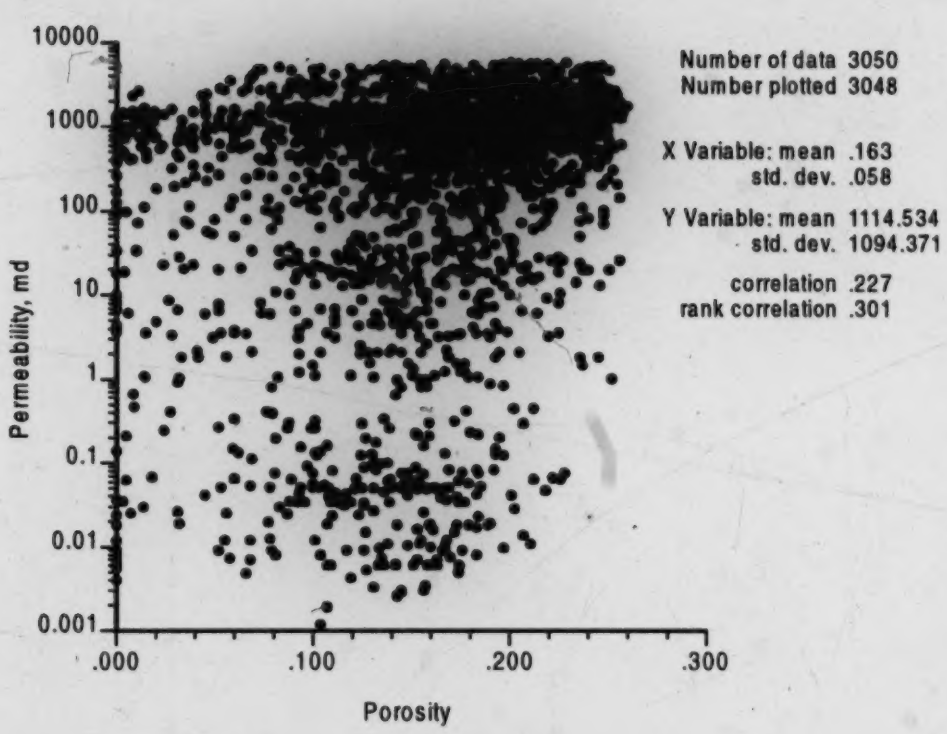

Figure 3-25: Simulated porosity versus cokriged permeability

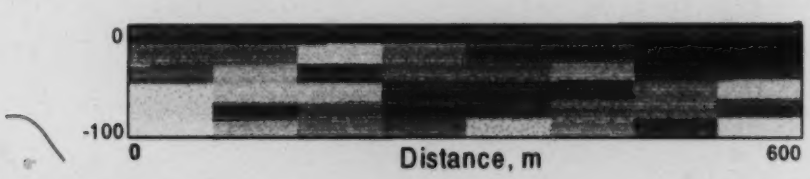

Figure 3-26: Grid 8 x 6 – porosity distribution (see color scale of 3-12)

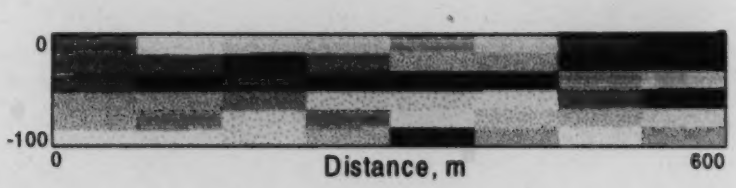

Figure 3-27: Grid 8 x 6 – permeability distribution (see color scale of 3-13)

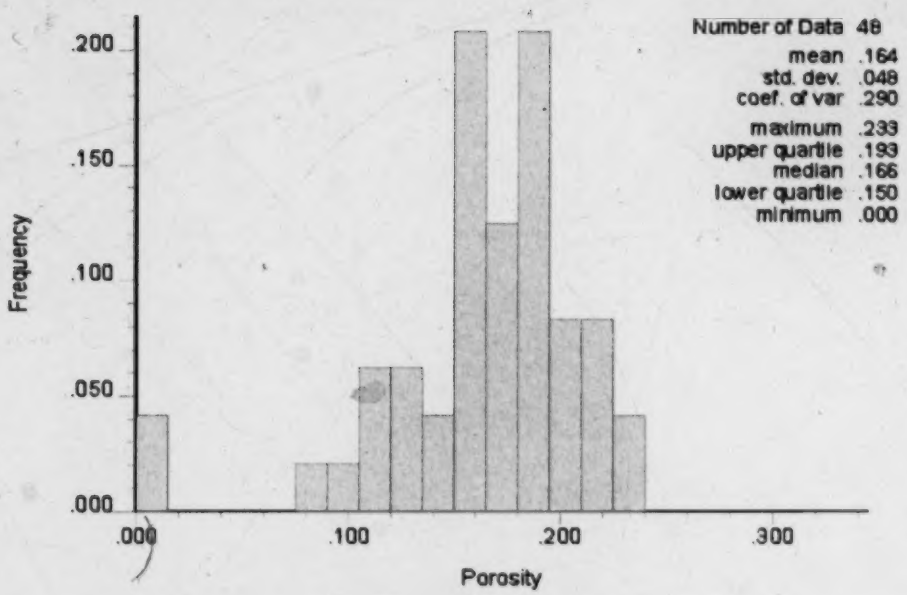

Figure 3-28: Grid 8 x 6 – histogram of simulated porosity

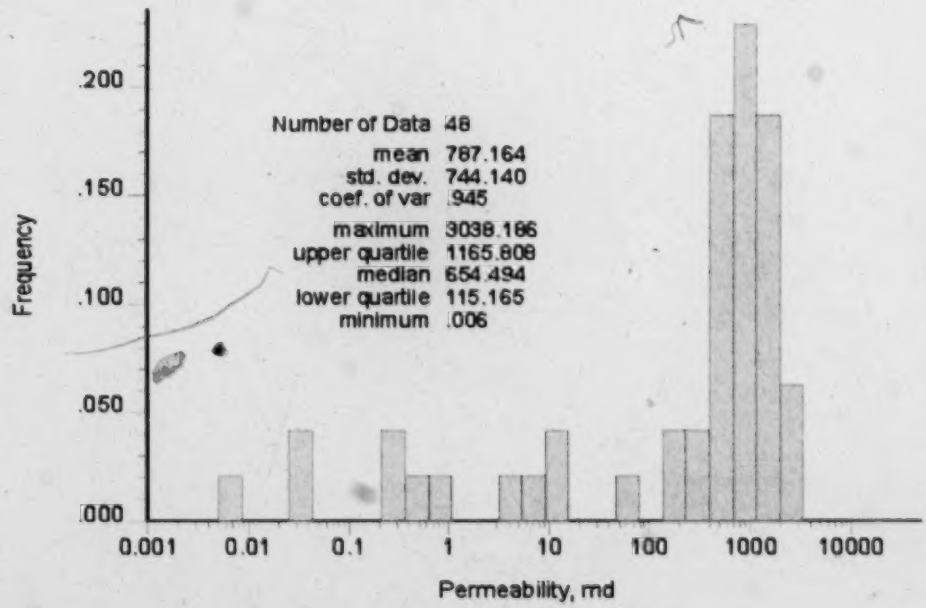

Figure 3-29: Grid 8 x 6 – histogram of simulated permeability

Figure 3-30: Grid 128 x 96 first realization – porosity distribution (see color scale of 3-12)

Figure 3-31: Grid 128 x 96 first realization – permeability distribution (color scale of 3-13)

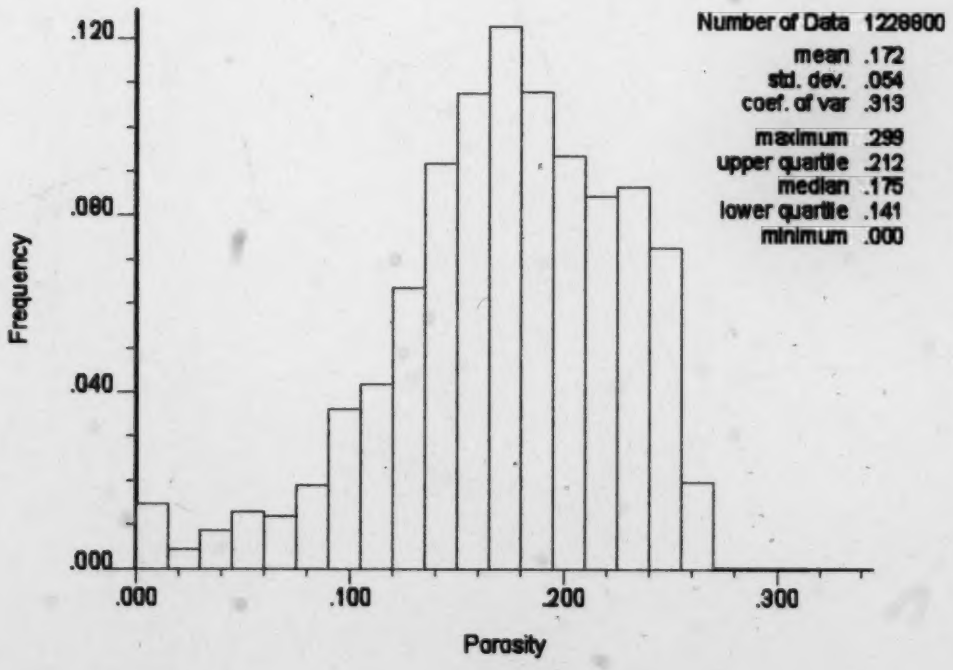

Figure 3-32: Grid 128 x 96 – histogram of simulated porosity for 100 realizations

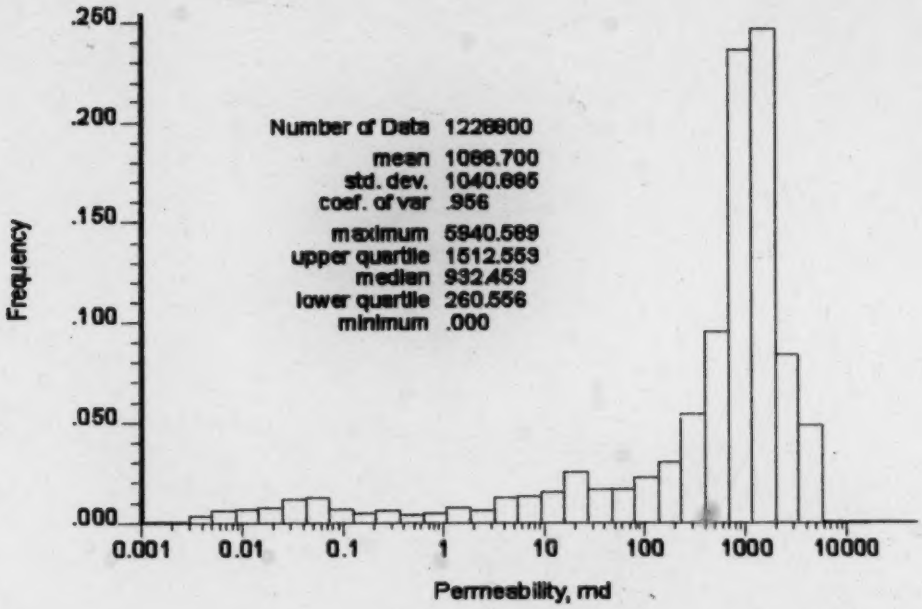

Figure 3-33: Grid 128 x 96 – histogram of simulated permeability for 100 realizations

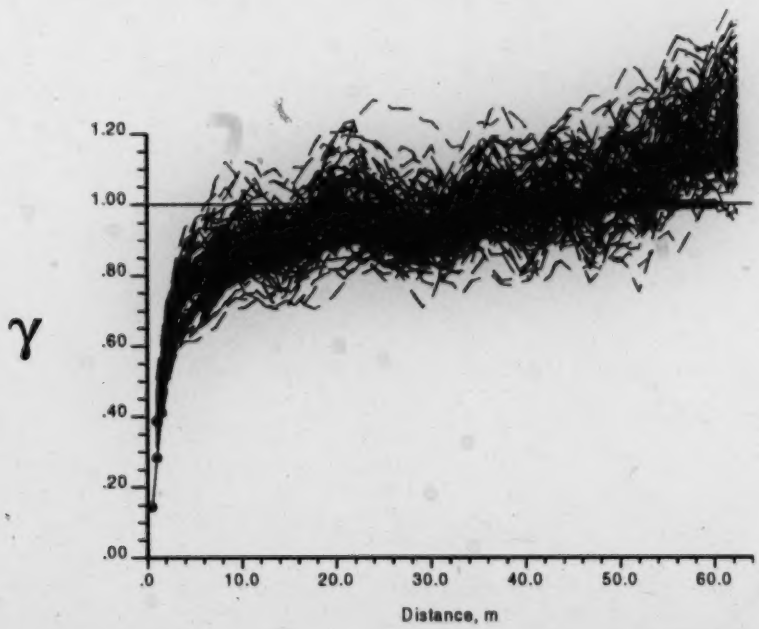

Figure 3-34: Grid 128 x 96 – variograms of simulated porosity for 100 realizations

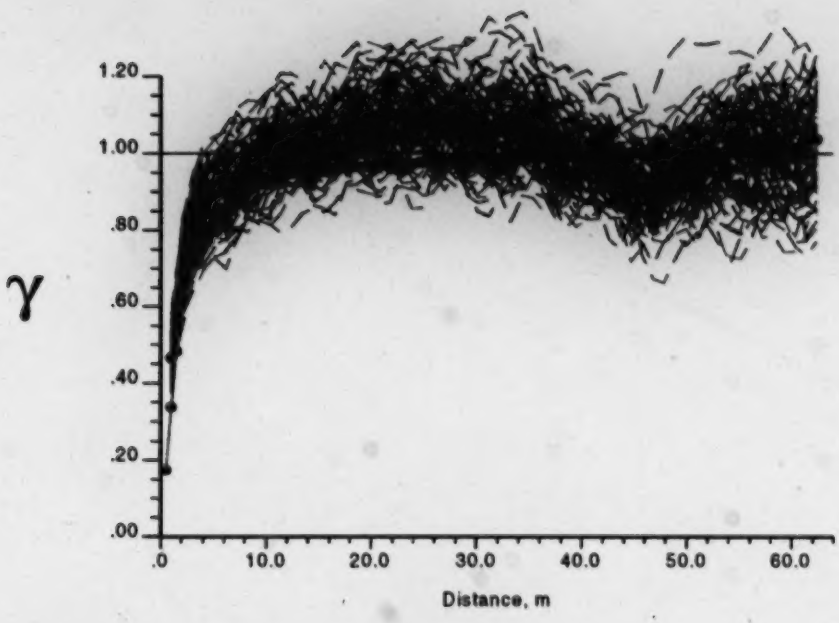

Figure 3-35: Grid 128 x 96 – variograms of simulated permeability for 100 realizations

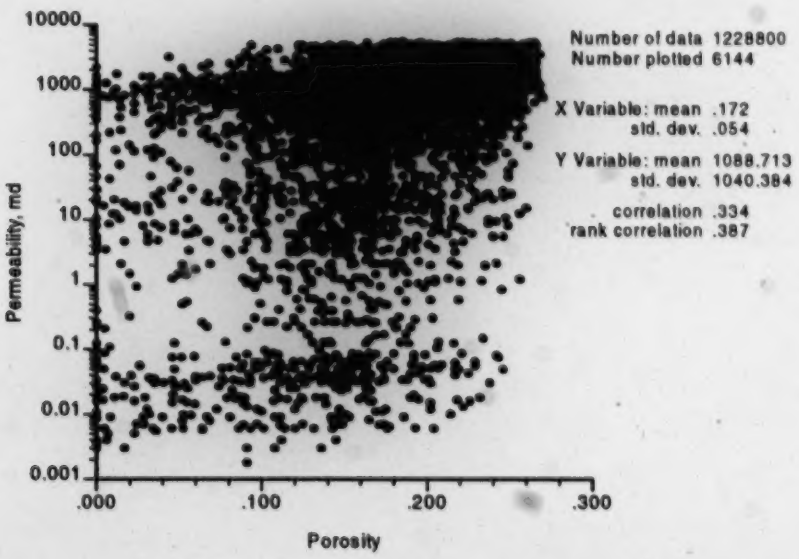

Figure 3-36: Grid 128 x 96 – simulated porosity versus simulated permeability

IV. FLOW SIMULATION USING ECLIPSE

Eclipse is a Schlumberger GeoQuest suite of reservoir flow simulators. Eclipse 100 used in this study is one among this series of flow simulators; it is a fully implicit, three-phase, three-dimensional, general purpose black oil simulator with gas condensate options.

1. Setting up the input file

To test and establish the procedure to run simulations in Eclipse, the results of the geostatistical modeling done for the 61 x 1 x 50 grid system were input into the Eclipse simulator. The cell sizes and reservoir dimensions were kept the same as in the geostatistical modeling.

The simulated values of porosity and permeability for the 3050 cells were converted to Eclipse format, using the program "gsl2ecl", before being input into the flow simulator Eclipse. This was necessary because the format of the output data from Wingslib was different from the format required by Eclipse. The main difference was in the coordinate system. When using Wingslib, the convention was that the z-axis was associated with the positive upward direction, while, when using Eclipse, the convention was that the z-axis was associated with the positive downward direction. In other words, in Wingslib, the z-axis was associated with elevation [3; p. 22], while in Eclipse, the z-axis was associated with depth [7].

Setting up the model and parameters for Eclipse in this case was simple. The system consisted of two wells, one of which (well No.1) was an injection well, and one of which was a production well (well No. 2). The depth to the top of the reservoir was 2000 m. The pressure at this point (reference depth) was 100 bars. A two-phase problem, water and oil, was considered. The initial water saturation was 25 % and the injection rate was 100 m^3/day. The BHP for the injector was kept under 500 bars. The

minimum BHP of the injector was kept above 20 bars. The limiting oil production rate was 1 m^3/d.

2. *Calculating mobility ratios*

In order to see the effects of discretization on the flow of fluids with different properties, three oils with different viscosities were considered for the simulation. Thus, there were displacements with three different mobility ratios: favorable ($M \leq 1$), unity (1) and unfavorable ($M > 1$). For this simulation assignment, the default dead oil viscosity set - viscosity versus pressures - was used (see Appendix 3, parameter PVDO). This was the base set and it was used to calculate the mobility ratios.

The procedure applied to construct the fractional flow curves and calculate the mobility ratios was taken from Craig's waterflooding monograph [8, Appendix E]. Tables 4-1 to 4-2 and Figures 4-1 to 4-3 demonstrate how the mobility ratios were calculated. Fractional flow, F_w, was calculated using the following formula:

$$F_w = \frac{1}{1 + \frac{\mu_w}{k_{rw}} \frac{k_{ro}}{\mu_o}} \qquad (4\text{-}1)$$

where:

μ_o: oil viscosity

μ_w: water viscosity

k_{ro}: relative permeability to oil

k_{rw}: relative permeability to water

The oil viscosity at 100 bars was used to construct the fractional flow curves. The reason for choosing the viscosity to be calculated at 100 bars was because the original reservoir pressure was 100 bars and the average viscosity at different pressures from 1 to 200 bars (0.88 mPas) was close to this number (0.868 mPas) (Table 4-2). The water

viscosity was taken as 0.47 mPas (parameter PVTW). In order to construct the fractional flow curve, the data set of relative permeability to oil and water as a function of water saturation at 100 bars was used (Appendix 3, SWOF parameter).

The mobility ratio was calculated using the formula:

$$M = \frac{\mu_o}{\mu_w} \frac{k_{rw}(S_{wa})}{k_{ro}(S_{wi})} \qquad (4\text{-}2)$$

where S_{wa} is the average water saturation behind the flood front prior to breakthrough. The parameter S_{wa} can be obtained by drawing a tangent from the point S_{wi} to the F_w curve. If the tangent is extended until it intersects the horizontal line corresponding to $F_w = 1$, the water saturation reading was S_{wa} (see Figures 4-1 to 4-3).

Using Equation (4-2), the mobility ratio for the favorable case was calculated to be 0.4. By trial and error, the viscosity values for the unit mobility case were obtained by multiplying the viscosity set in the favorable mobility case by 4. In the unfavorable M case, the viscosity set was multiplied by 20 and M was determined to be1.85.

3. Output variables to be monitored

The monitoring period was 320 days for M = 0.4 and 1, and 400 days for M =1.8. Four-day time steps were used. Thus, the number of time steps was 80 for the previous cases and 100 for the last case. The well performance parameters recorded were: BHP, oil and water production rates (WOPR, WWPR), total oil and water produced (WOPT, WWPT), production index (WPI), oil recovery efficiency (FOEW), water cut (WWCT), reservoir volume injected water (WVIW), and reservoir pore volume (FRPV). One parameter was calculated, the water injected measured in pore volumes (PVWI). This was done outside Eclipse by dividing WVIW by FRPV, because, in Eclipse, there was no such parameter.

The remaining properties of the reservoir rock and fluid can be found in Appendix 3 (for a 61 x 50 grid, M = 0.4). Explanations concerning the proper use of the Eclipse parameters in the input file can be found in Appendix 4. The simulation results were tabulated in Appendix 5 for the favorable mobility ratio case. The results for the other mobility ratios had a similar format; therefore, they were not presented here.

Presentation of results

Figures 4-4 to 4-10 present illustrations of the simulation results for the three mobility ratio sets. On the abscissas of Figures 4-4 to 4-10, PVWI was used instead of time. Dimensionless time (PVWI) was used instead of real time, because it gives more insight into what is happening during the displacement process.

For the M = 0.4 case, the wells were shut in at day 266 (Time Step 69) and the run stopped before the designed time, because the oil production rate fell below the limiting oil rate of 1 sm^3/day. The oil production rate peaked right after the system was opened for flow at around 90 sm^3/d. The oil production rate was kept at this level until approximately 0.3 PVWI (probably breakthrough) when the rate started to decline dramatically and reached its economic limit (Figure 4-4). Also the water production rate increased abruptly at about 0.33 PVWI (Figure 4-5). This observation was supported by the increasing water cut of the producer at this point in time (Figure 4-9). The water cut increased from almost 0 to 0.8 between 0.3 and 0.4 PVWI. At 1 PVWI, approximately 3,500 sm^3 of oil and 6,100 sm^3 of water were produced (Figures 4-6 and 4-7). At this time, the recovery factor was 53 % (Figure 4-10). The BHP of the injector increased gradually to 200 bars at 0.37 PVWI, then slightly decreased to 170 bars at 2 PVWI (Figure 4-8). The BHP of the producer was kept at 20 bars.

The next two runs were completed for mobility ratios of 1 and 1.8, the results of which are shown in Figures 4-4 to 4-10. The oil flow rate dropped earlier ($\approx$ 0.2 and $\approx$ 0.1

PVWI for M = 1 and 1.8, respectively). This means an earlier breakthrough for these systems: 0.24 and 0.12 PVWI, respectively, at WCT ≈ 0.01. The recovery factors were lower at 45 % and 33 % for M = 1 and 1.8, respectively (Figure 4-10). It was observed that the higher the value of M, the lower the oil production and the higher the water production. These were logical results, because in the case of a favorable value of M, the displacement was piston like. When the mobility ratio increases, there will be water channeling as the flow of injected water tries to reach the producer. Thus, the displacement efficiency was worse, and earlier breakthrough was observed. The BHP of the injector for M = 1 reached ≈ 370 bars and decreased to ≈ 200 bars at 2 PVWI (Figure 4-8). For M = 1.8, it was consistently high at 500 bars until 0.75 PVWI, then declined to 400 bars (Figure 4-8). It should be noted that, when the pressure in the reservoir reaches the pressure limit of 500 bars, no water can be injected.

There was one discrepancy when the production and recovery curves for the three mobility ratios were compared. The recovery factor for M =1.8 was almost half that for M = 0.4, but in the oil production plot, the areas under the curves, which should reflect the recovery, do not have such a proportion (only one third). That is, the oil production curves do not reflect true reservoir performance. A review of the possible reasons for this phenomenon revealed that a non-constant water injection rate caused the distortion. The oil production rate was a volume over time (sm^3/day), but this time in days was not used in this case (the dimensionless PVWI was used instead). The oil plots do not reflect the true relationship between the water injected and the oil produced. In order to obtain the proper recovery factor proportion, it is necessary to calculate the oil rate as a volume over dimensionless time (PVWI). That is, the oil production rate should be normalized to PVWI, and has a unit of sm^3/PVWI. The new "oil rate" was defined as follows using the cumulative oil production data, for each simulation time step:

$$\text{"OIL RATE"} = \frac{\Delta \text{ Cumulative Oil Produced}}{\Delta \text{ Pore Volume Water Injected}} \qquad (4\text{-}3)$$

Similarly, the water production curves were corrected using the cumulative water production curve. The new "water rate" was defined as

$$\text{"WATER RATE"} = \frac{\Delta \text{ Cumulative Water Produced}}{\Delta \text{ Pore Volume Water Injected}} \qquad (4\text{-}4)$$

An example of how to calculate the new "oil rate" and "water rate" is illustrated in Table 4-3.

The corrected oil and water production rates are shown in Figures 4-11 and 4-12. Now it can be seen that the areas under the curves on the oil rate plot are the cumulative oil productions. There is an interesting feature on the curve for M = 0.4. It has a peak after the first time step. It is simply an artificial feature that appeared only when the oil rate was recalculated. The original oil production rate had a smooth curve. As was the case for the oil production rate, the areas under the curves on the water production rate plots are the cumulative water production.

S_w	K_{ro}	K_{rw}	F_w for M=0.4	F_w for M=1	F_w for M=1.8
0.25	1	0	0	0	0
0.315	0.8044	0.0026	0.0059	0.8081	0.9960
0.365	0.6301	0.0065	0.0187	0.8415	0.9881
0.415	0.4771	0.0134	0.0493	0.8717	0.9703
0.465	0.3453	0.0244	0.1154	0.8972	0.9349
0.515	0.2348	0.041	0.2438	0.9165	0.8741
0.565	0.1455	0.0651	0.4524	0.9277	0.7911
0.615	0.0775	0.0987	0.7016	0.9292	0.7097
0.665	0.0307	0.1443	0.8967	0.9198	0.6544
0.715	0.0052	0.2045	0.9864	0.8990	0.6272
0.75	0	0.257	1	0.8778	0.6184
1	0	1	1	0.6487	0.5449

Table 4-1: Fractional flow calculations for the three mobility ratio cases

	Favorable	Unit	Unfavorable
P(bars)	Original μ_o (mPas)	Original μ_ox4 (mPas)	Original μ_ox20 (mPas)
1	0.758107	3.032428	60.64856
25	0.772	3.088	61.76
50	0.7952	3.1808	63.616
60	0.8069	3.2276	64.552
70	0.82	3.28	65.6
80	0.8345	3.338	66.76
90	0.8504	3.4016	68.032
100	0.8677	3.4708	69.416
125	0.9171	3.6684	73.368
150	0.9752	3.9008	78.016
175	1.0421	4.1684	83.368
200	1.1177	4.4708	89.416
Average	**0.880**	**3.519**	**70.379**

Table 4-2: Viscosity sets for three mobility ratio cases at different reservoir pressures

Time (days)	PVWI	WOPT (sm^3)	WWP (sm^3)	ΔPVWI	ΔWOP (sm^3)	ΔWWPT (sm^3)	Oil Rate (sm^3/PV)	Water Rate (sm^3/PV)
0	0.0000	0.0	0.000	0.0000	0	0.0000	0.0	0.0000
4	0.0391	346.6	0.051	0.0391	346.6	0.0513	8864.0	1.3125
8	0.0782	701.0	0.104	0.0391	354.3	0.0522	9069.1	1.3361
12	0.1172	1054.4	0.155	0.0390	353.4	0.0518	9053.6	1.3267
16	0.1562	1405.0	0.206	0.0390	350.6	0.0511	8995.0	1.3112

Table 4-3: Example of calculating the oil and water rate with respect to pore volume

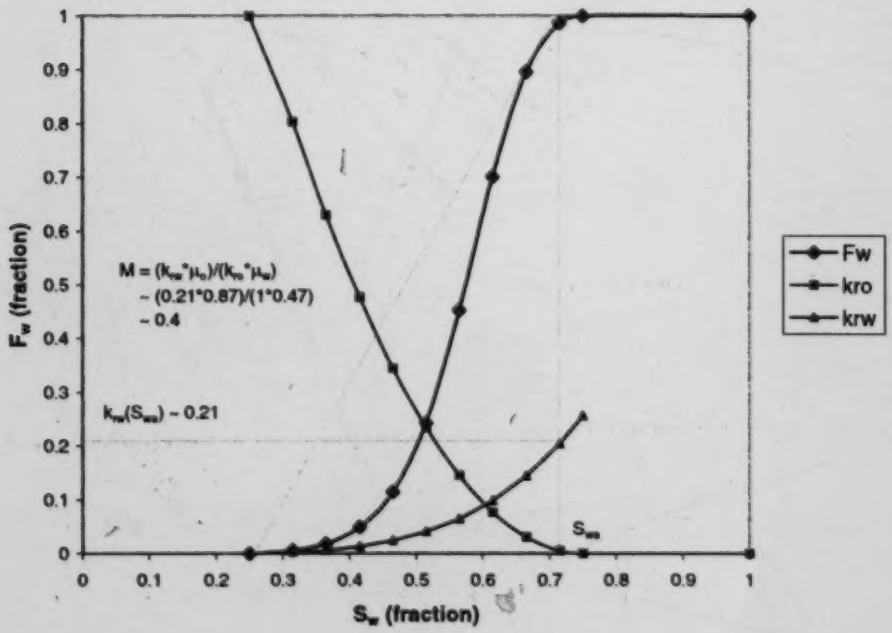

Figure 4-1: Fractional flow curve and mobility ratio calculation – favorable M

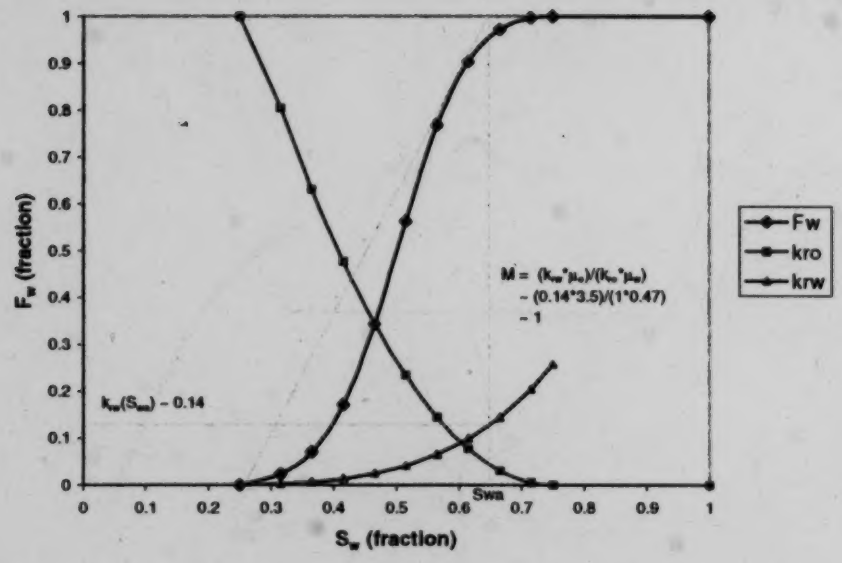

Figure 4-2: Fractional flow curve and mobility ratio calculation – unit M

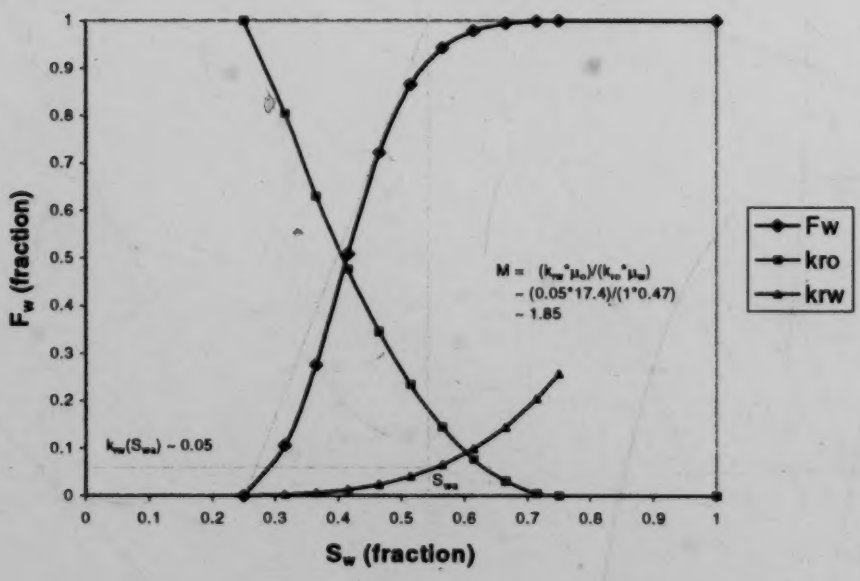

Figure 4-3: Fractional flow curve and mobility ratio calculation – unfavorable M

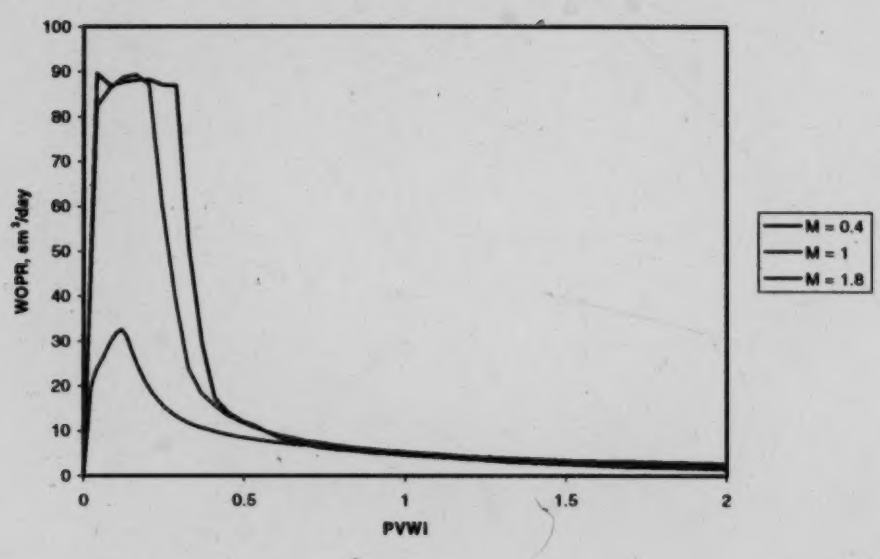

Figure 4-4: Oil production rates for different mobility ratios versus PVWI - 61 x 50 grid

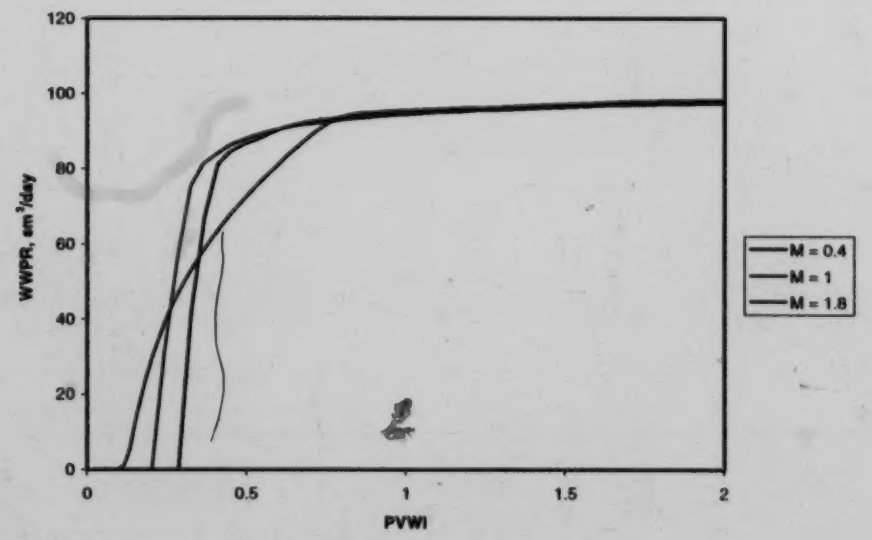

Figure 4-5: Water production rates for different mobility ratios – 61 x 50 grid

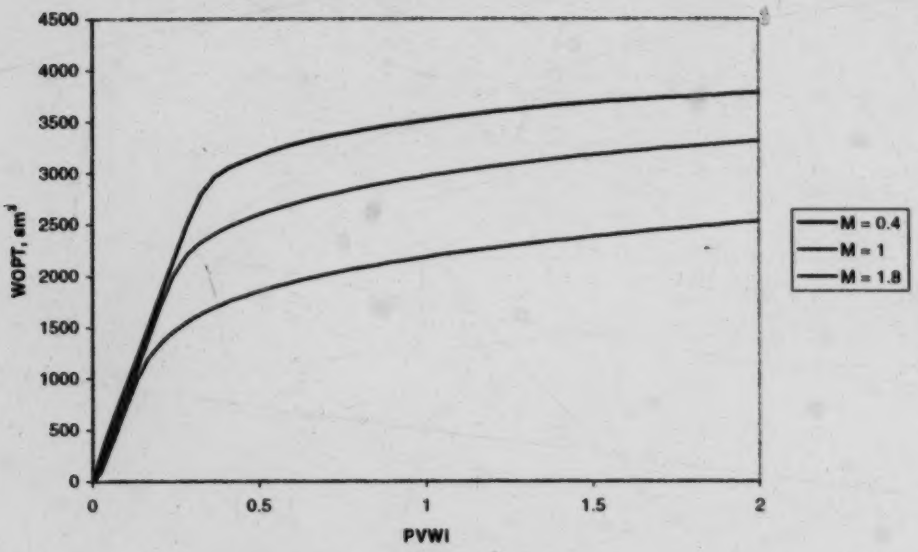

Figure 4-6: Cumulative oil production for different mobility ratios versus PVWI - 61 x 50 grid

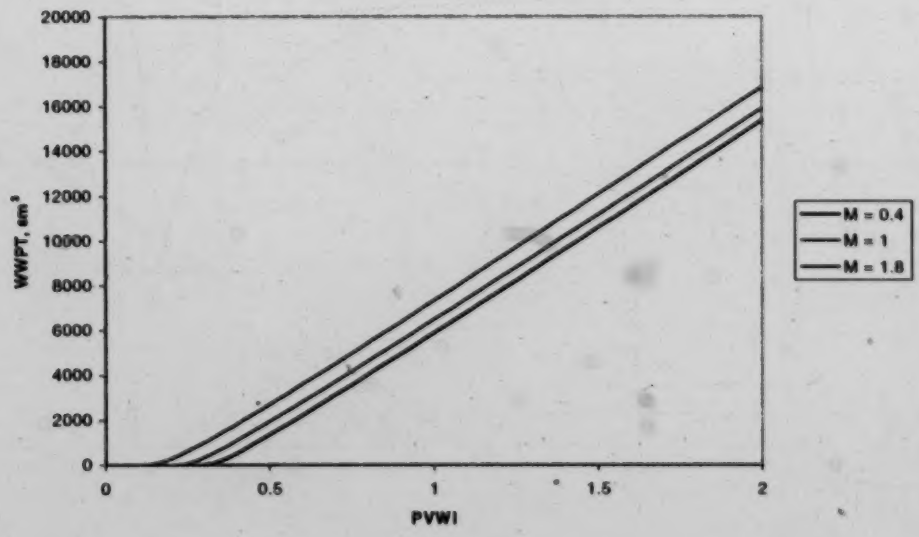

Figure 4-7: Cumulative water production for different mobility ratios - 61 x 50 grid

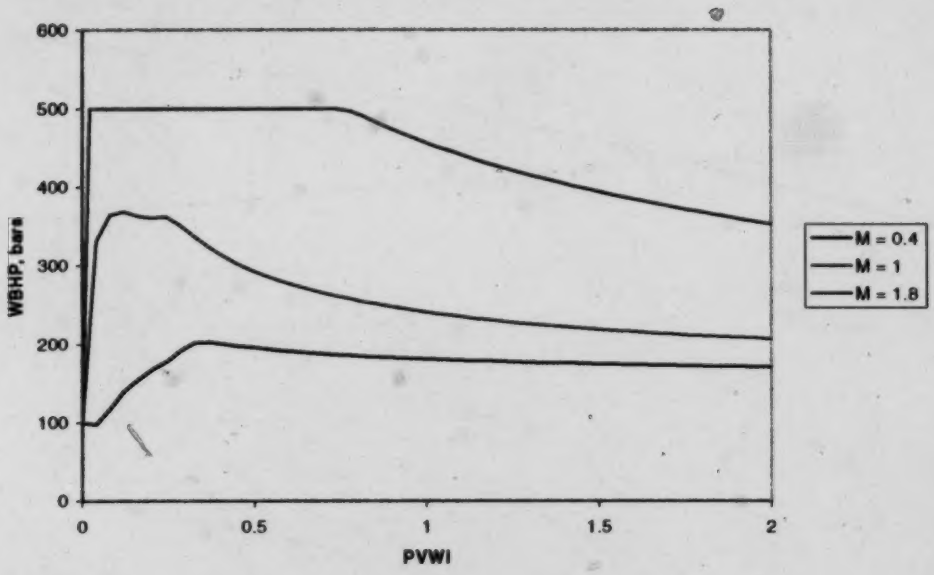

Figure 4-8: Injector BHP for different mobility ratios - 61 x 50 grid

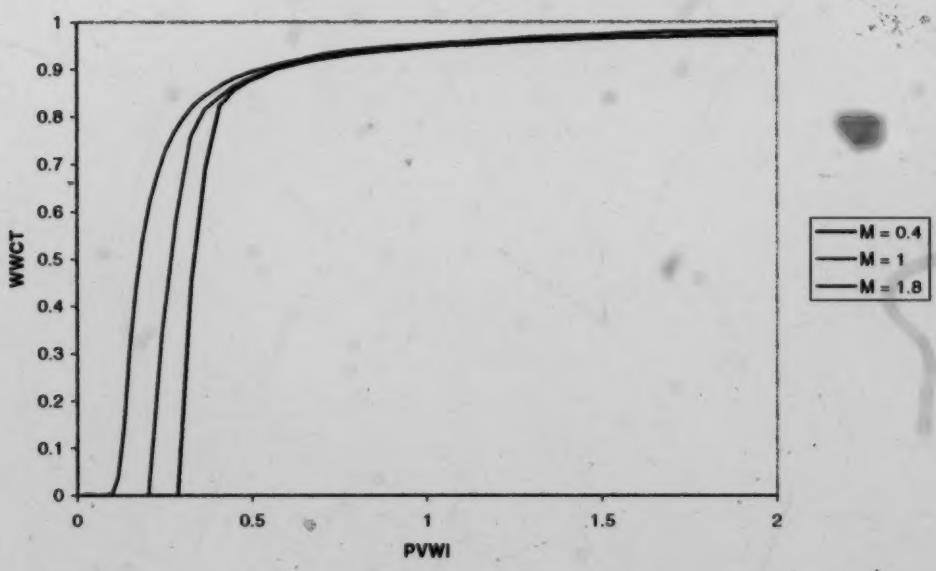

Figure 4-9: Producer water cut for different mobility ratio - 61 x 50 grid

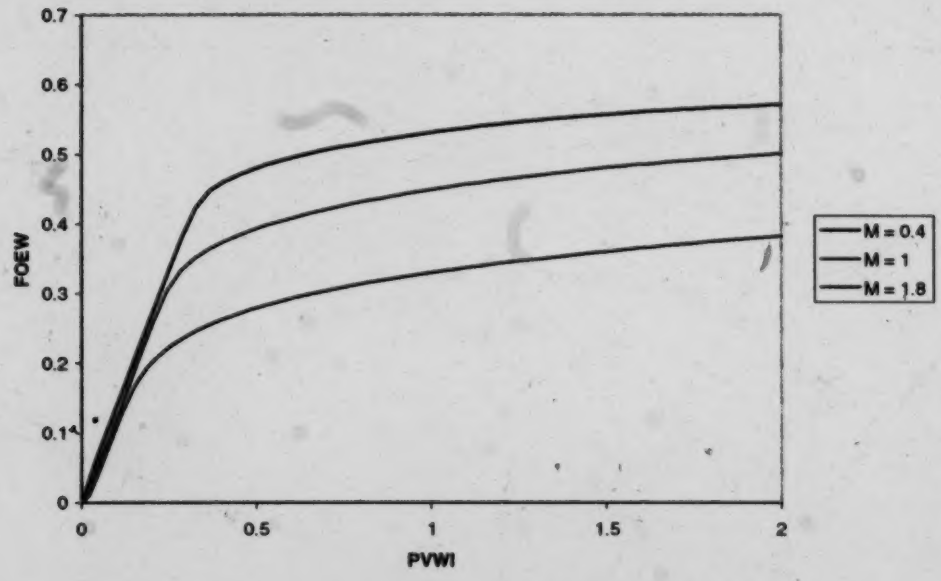

Figure 4-10: Oil recovery factors for different mobility ratios - 61 x 50 grid

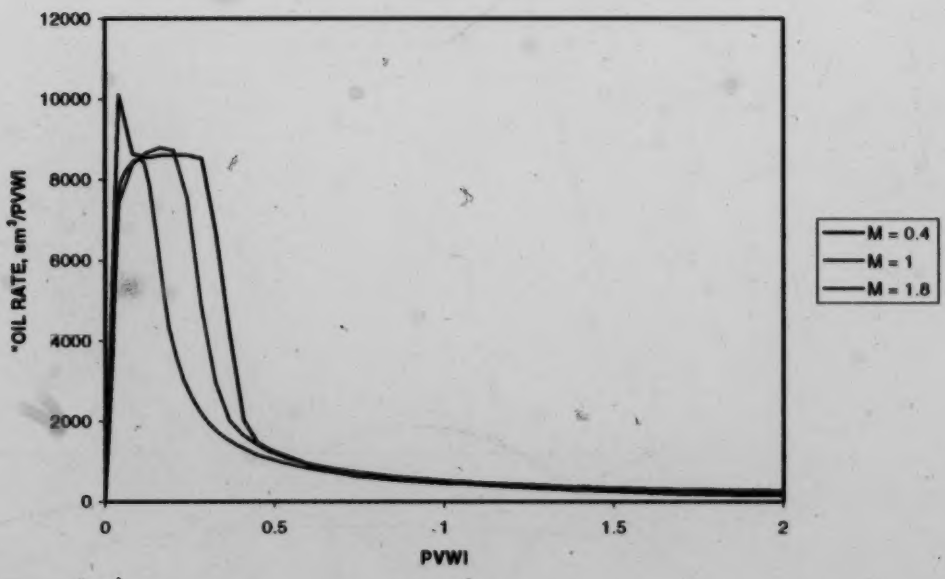

Figure 4-11: "Oil rate" for different mobility ratios - 61 x 50 grid

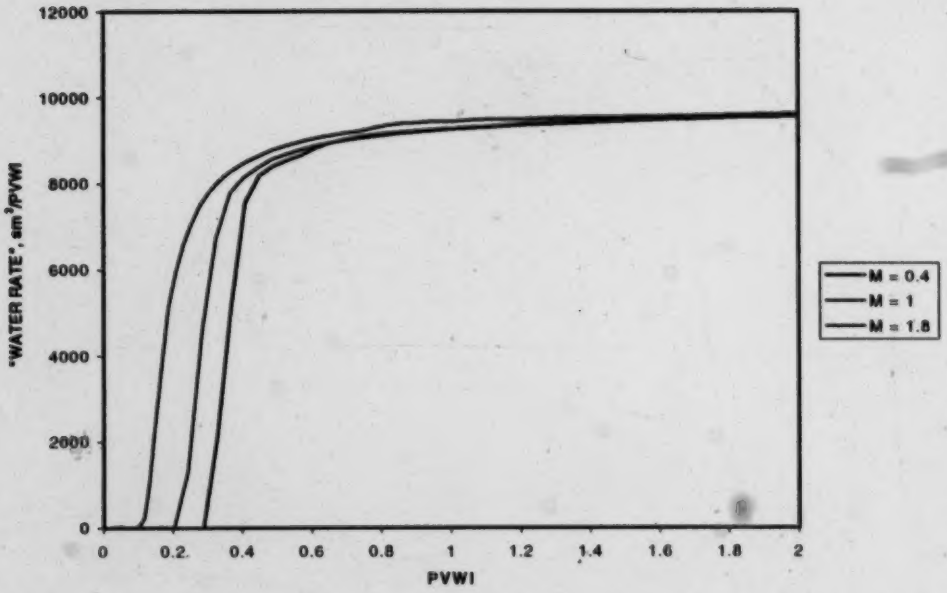

Figure 4-12: "Water rates" for different mobility ratios - 61 x 50 grid

V. FLOW SIMULATION OF A HOMOGENEOUS RESERVOIR

1. Parameter setup

In order to see the effects of discretization alone, the flow performance of a homogeneous reservoir was simulated. The reservoir simulated was assumed to be homogenous and isotropic. This means the porosity was the same everywhere and the permeability was the same in all three directions. In order to keep the properties of the homogenous reservoir close to those of a realistic heterogeneous reservoir, the average porosity and permeability of the reservoir were used. The average reservoir porosity was calculated by arithmetic averaging of the porosity values from the well data. The average porosity was 0.17. Permeability cannot be averaged by taking the arithmetic average. Instead, geometric averaging was used:

$$\bar{k}_{geom} = \exp\left(\sum_{i=1}^{n} \frac{\ln(k_i)}{n}\right) \qquad (5\text{-}1)$$

The arithmetic average of the natural logarithm of permeability ln(k) was found by plotting the histogram of the logarithm of permeability (Figure 5-1). The geometric average permeability was 322.107 md.

Next, several different reservoir discretizations were implemented. The cell sizes used are shown in Table 5-1. After each discretization, the number of cells in each direction nearly doubled. This results in the total number of cells increasing four times. The wells go through the centers of the first and last cells in the x direction. The size of the reservoir was slightly different for each of the different grid systems.

Two parameters were monitored: the recovery factor at one pore volume water injected (1 PVWI) and the time to breakthrough for the different mobility ratios. The input files for Eclipse were the same as those for the heterogeneous case. The only

difference was that the averages of porosity and permeability were used for the models, so there was no need to introduce the geostatistically simulated porosity and permeability into the model. A summary of the runs is shown in Table 5-2. Plots of the results are illustrated in Figures 5-2 and 5-3.

The runs for the last two grid systems were very slow. The Eclipse simulation did not converge. Only one run for the 241 x 200 grid, with a favorable mobility (M = 0.4), finished successfully. The reason why Eclipse did not converge was because, maybe, these grids were so fine, and there were no solutions for flow equations that satisfied Eclipse solution tolerance.

2. *Convergence of flow parameters*

In Figure 5-2, the recovery factors calculated at 1 PVWI are plotted versus the number of cells on a logarithmic scale. For all three mobility ratios, the recovery factors increase as the number of cells increases, in a range from 0.59 to 0.63 for M = 0.4, in a range from 0.52 - 0.54 for M = 1, and in a range from 0.41 - 0.43 for M = 1.8. It was obvious that the higher the mobility ratio, the smaller the amount of oil produced at 1 PVWI. On the other hand, the ranges for different mobility ratios were slightly different, larger for M = 0.4 and smaller for M = 1.8. As a result of this, the slope of the RF curve is larger for the M = 0.4 case than it is for the M = 1.8 case.

For the M = 0.4 case, the curve was relatively flat and its slope decreased as the number of cells increased. This indicates that the system is approaching convergence. Unfortunately, for the other mobility ratios, the final runs could not be completed successfully as it was explained earlier. Consequently, it is difficult to state that the same trend will hold for the other mobility ratios. Nevertheless, it can be inferred from Figure 5-2 that the convergence behavior of the M = 0.4 case can be applied to the other mobility ratios as well. Such convergence is associated only with discretization effects. In order to quantify the difference in the RFs, the RF of the finest grid was

assumed to be the true value and the percentage differences with respect to the other grids were calculated. Figure 5-4 shows the results of this calculation. The percentage differences between the different mobility ratios were very similar, although the absolute values were very different. A maximum difference of around 4-5 % occurs at the coarsest grid. In general, the difference decreases as the grid gets finer. However, there is one exception at the 121 x 100 grid, M = 0.4 case, with the RF for this grid higher than the RF of the finest grid. This creates a negative point in Figure 5-4. This negative point does not create big concern because the magnitude is relatively small. Another observation regarding the Eclipse run for this grid is that there was a convergence warning during the simulation, therefore the accuracy of the simulation results may not meet the standard setup for Eclipse.

Breakthrough is considered to occur when the water cuts reach ≈ 0.01. In some cases, it was difficult to locate the exact breakthrough time, because the water cut increased sharply over one time step. The breakthrough time was measured in PVWI because of the distortion effects related with time. Figure 5-3 shows breakthrough times versus PVWI. The trend was that the higher the mobility ratio, the earlier the breakthrough time. This is an interesting behavior, because this was a homogeneous system. This observation was easier to explain for heterogeneous reservoirs, where the earlier breakthrough for a high mobility ratio displacement can be explained by water channeling. Viscous fingering occurs when the flow is forced to go faster through higher permeable zones and, therefore, the displacement front is not stable. As a result, water will appear faster at the end of the system. It appears that, even for a homogenous reservoir, in the case of an unfavorable displacement, viscous fingering may take place.

This observation can be explained by instability theory which predicts that unfavorable mobility ratio displacements will be unstable, even if the reservoir is homogeneous. Collins [9] derived an equation to show the relationship between the size of a viscous finger and mobility ratio. According to the author, the length of the

perturbation from the plane displacement front grows exponentially with time after inception of the perturbation if $M > 1$, or decays exponentially with time if $M < 1$. For $M = 1$, it does not change with time. In other words, if the mobility ratio is unfavorable, any small perturbation of the front gives rise to irregularities which grow very rapidly; therefore, the displacement is not stable. For a favorable mobility ratio, the front is stable. The critical point is the fact that some type of heterogeneity or perturbation is required to initiate the instability and hence fingering. Because an infinity of random perturbations is present in the most uniform porous medium imaginable, fingering will always occur if $M > 1$, even in a homogeneous reservoir. Gravity and capillarity may act to eliminate fingers as they are formed [9]. On the other hand, heterogeneity enhances the growth of viscous fingering. The conclusion to draw here is that mobility ratio is the most important factor in the development of viscous fingering.

In Figure 5-3, there is an indication of convergence for $M = 0.4$, but it is harder to predict the behavior of the other mobility ratios as the grid system gets finer. As Figure 5-3 shows, for $M = 1$, the breakthrough times (in PVWI) increase significantly for the first three coarse grids, then flatten out for the last two finer grids. For the case of $M = 1.8$, the picture is more complicated. The BT times increase for the first two coarse grids, and then decrease, as the grids get finer. Maybe, for different grids, the water channels differently. Different paths lead to different BT times. Figure 5-5 shows the difference between the BT for the finest grid and for the other grids. The calculation was done in a way that is similar to the way used for the RF. Unlike the RF, there was a very big difference in BT between different grids, up to 30 % in the case of the coarsest grid. The unfavorable mobility ratio case shows unpredictable behavior with three negative points in the curve for $M = 1.8$ in Figure 5-5. The reason for this unpredictable behavior was explained earlier.

3. *Comparison between displacement results in heterogeneous and homogeneous reservoirs*

For the 61 x 50 grid, there are two sets of results: one for the heterogeneous reservoir case and one for the homogeneous case. To see the differences in the flow performance, two key parameters were compared: the recovery factor at 1 PVWI and the breakthrough time. The RFs for the different mobility ratios were higher for the homogeneous case: 0.62, 0.54 and 0.43 as compared to 0.52, 0.45 and 0.33 for the heterogeneous case. The breakthrough times (in PVWI), for the homogeneous reservoir case, were 0.46, 0.34 and 0.18 as compared to 0.33, 0.24 and 0.12 for the heterogeneous case. Obviously, the displacement efficiency in the homogenous reservoir was better than in the heterogeneous reservoir (higher recovery and delayed breakthrough times). This difference in behavior can be explained by the reservoir character. The recovery for the heterogeneous model is poorer because this model permits by-passed oil (that may be recovered later) and channeling through high permeability streaks that causes earlier breakthrough and less recovery. Another question is the way the permeability was averaged (geometric averaging). The geometric average is accurate if the permeability values are random and log-normally distributed. The domain for the averaging process is assumed to be infinite. In addition, the averaging technique is developed for a single phase displacement problem. In the two well data set, the permeability was not perfectly lognormal (Figures 3-6 and 5-1). There is a spatial correlation between the permeability data also. This lack of normality and the correlation between the data may be the reason for the inaccuracy in the estimation of the average permeability. Also, the multiphase nature of the flow in this problem can be a factor. Scaling laws for a single phase flow problem cannot capture the complexity associated with multiphase flow scaling. Therefore, replacing the heterogeneity of the reservoir with single values of permeability and porosity in an attempt to reproduce some flow parameters will still leave other parameters poorly reproduced. Further discussion about averaging techniques will be presented later.

4. Computer CPU time for simulation runs

Another parameter that can be useful is the computer CPU times. A summary of the CPU times used for the runs is shown in Table 5-3. A plot of CPU time (seconds) versus the number of cells is presented in Figure 5-6. The number of time steps required for the 61 x 50 and finer grid systems was, for M = 1.8, 150, while the other grid sizes required 80 time steps (4 days per time step). The time and the number of cells were plotted on a logarithmic scale. As the number of cells in the system increases, the CPU time required increases. The three data sets are very close to each other. This means, for the homogeneous reservoir case, that fluid type does not play an important role in the simulation time. Several curves were drawn in an attempt to fit the data points. The observation was that the relationship between CPU time and the number of cells does not follow any simple power law. It appears that for the 1,000 - 10,000 grid cell range, the simulation time required increases as the square of the number of cells.

Grids	Number of cells	Dx (m)	Dy (m)	Dz (m)
7 x 5	35	100	1	20
16 x 12	192	40	1	8.33
31 x 25	775	20	1	4
61 x 50	3050	10	1	2
121 x 100	12100	5	1	1
241 x 200	48200	2.5	1	0.5
481 x 400	192400	1.25	1	0.25

Table 5-1: Different reservoir discretizations for the homogeneous case

Grids	No of cells	RF	% RF	BT (PV)	% PV
M = 0.4					
7 x 5	35	0.593	4.968	0.344	26.338
16 x 12	192	0.61	2.244	0.418	10.493
31 x 25	775	0.618	0.962	0.447	4.283
61 x 50	3050	0.619	0.801	0.461	1.285
121 x 100	12100	0.626	-0.321	0.467	0.000
241 x 200	48200	0.624	0.000	0.467	0.000
M = 1					
7 x 5	35	0.519	4.596	0.251	29.494
16 x 12	192	0.531	2.390	0.3	15.730
31 x 25	775	0.537	1.287	0.338	5.056
61 x 50	3050	0.542	0.368	0.342	3.933
121 x 100	12100	0.544	0.000	0.356	0.000
241 x 200	48200				
M = 1.8					
7 x 5	35	0.411	4.196	0.129	23.214
16 x 12	192	0.42	2.098	0.178	-5.952
31 x 25	775	0.425	0.932	0.183	-8.929
61 x 50	3050	0.427	0.466	0.18	-7.143
121 x 100	12100	0.429	0.000	0.168	0.000
241 x 200	48200				

Table 5-2: Summary of runs for different discretizations - homogeneous reservoir

Grids	Number of cells	M = 0.4	M = 1	M = 1.8
7 x 5	35	2	2.1	3.6
16 x 12	192	3.2	3.3	5
31 x 25	775	8.2	7.9	10.9
61 x 50	3050	42.8	29.2	40
121 x 100	12100	461.9	336.1	392
241 x 200	48200	2408.9	no convergence	no convergence

Table 5-3: Computer CPU time for flow simulation – homogeneous reservoir

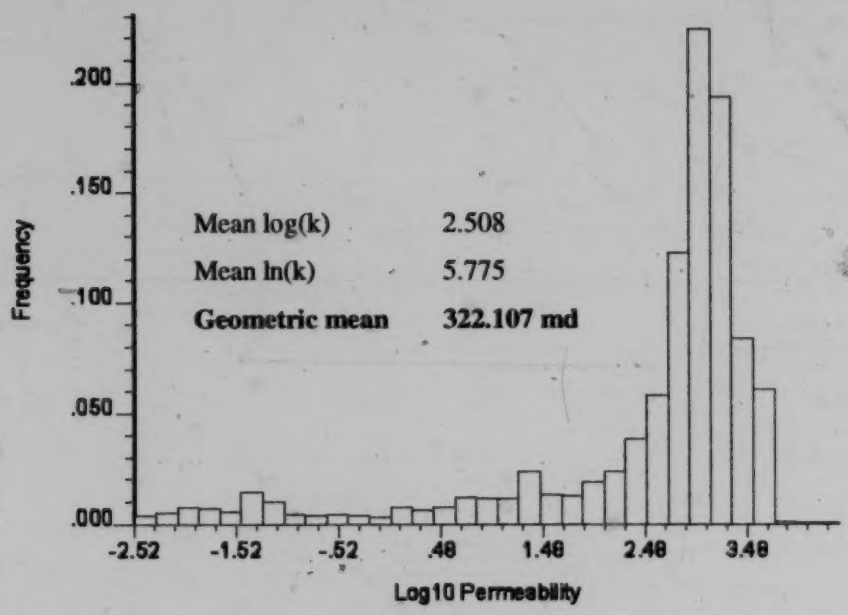

Figure 5-1: Calculation of geometric average permeability

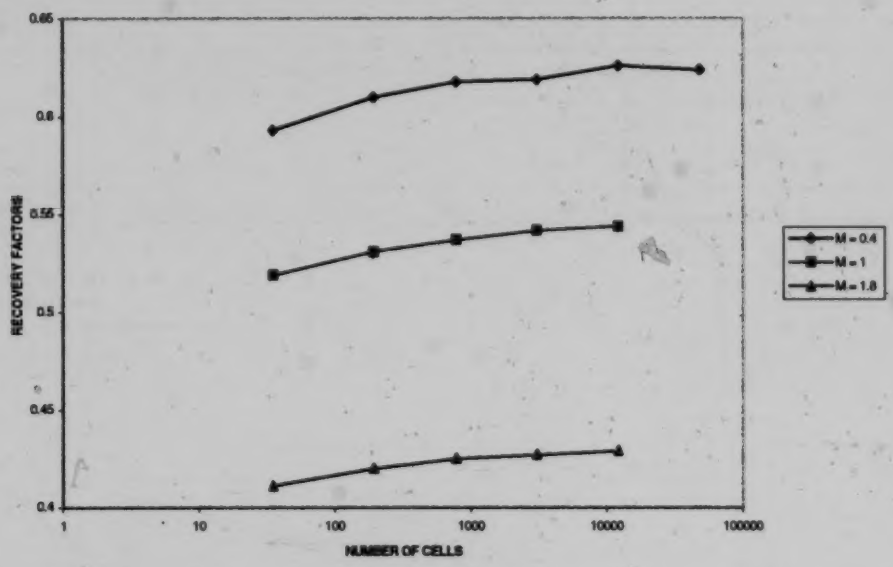

Figure 5-2: Recovery factors at 1 PVWI for different discretizations and mobility ratios - homogeneous reservoir

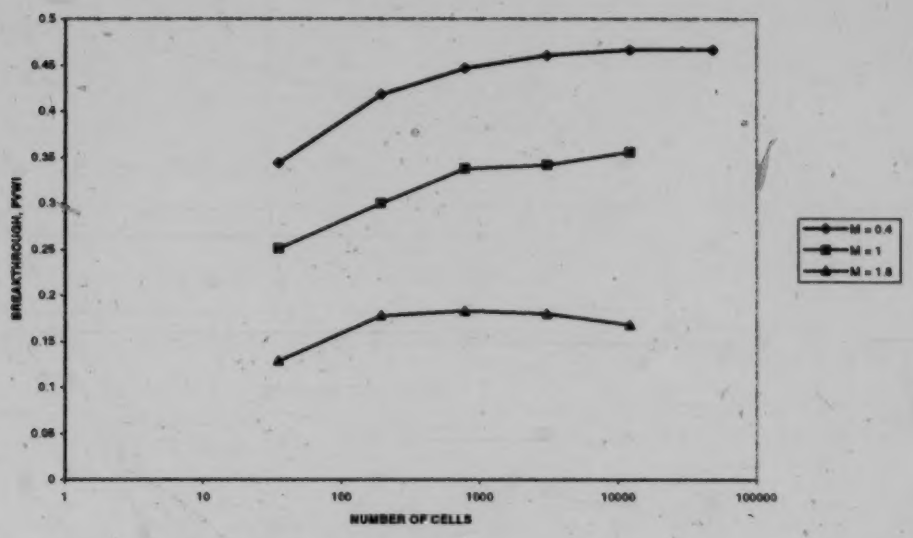

Figure 5-3: Breakthrough times taken at ≈ 0.01 water cuts for different discretizations and mobility ratios - homogeneous reservoir

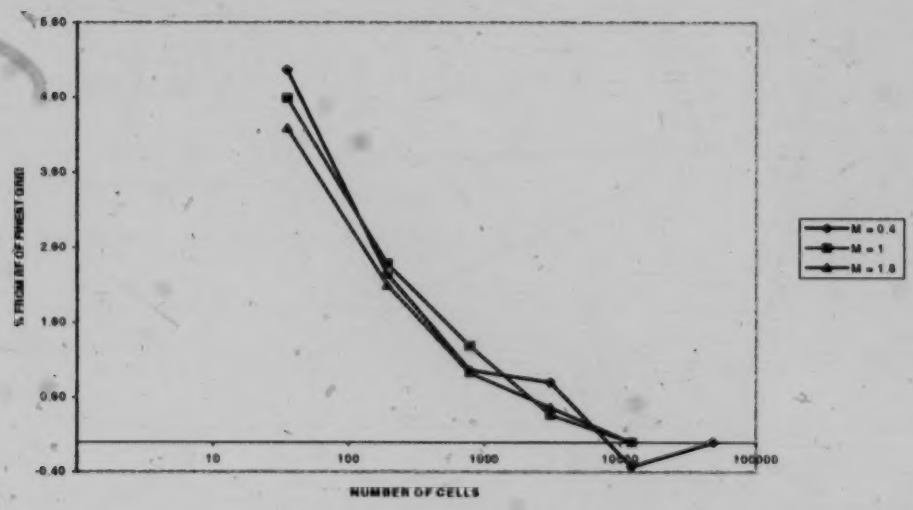

Figure 5-4: Differences in recovery factors at 1 PVWI from finest grid - homogeneous reservoir

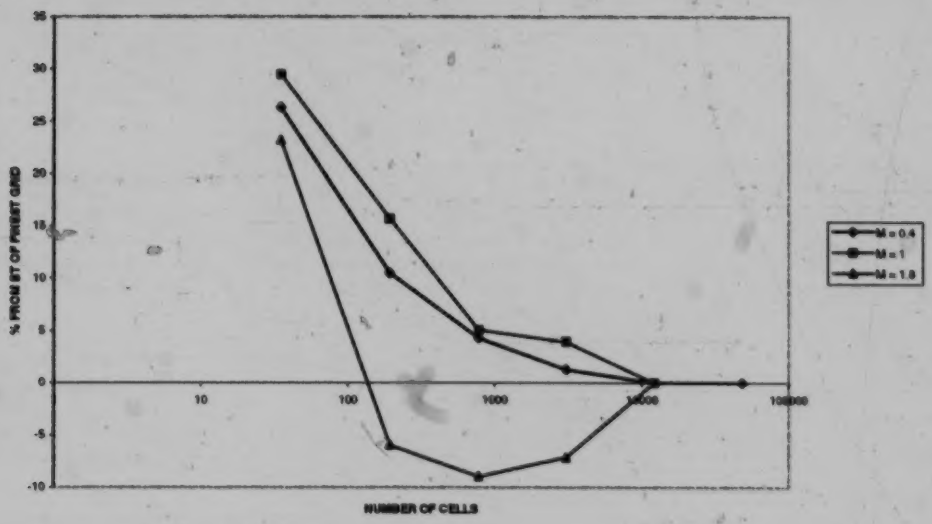

Figure 5-5: Differences in breakthrough times from BT of finest grid - homogeneous reservoir

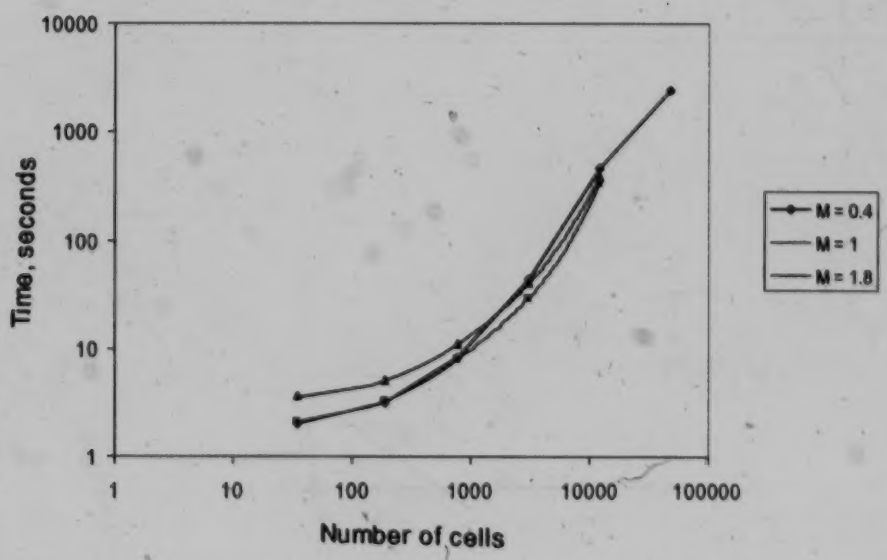

Figure 5-6: Computer CPU times for homogeneous reservoir case

VI. POROSITY AND PERMEABILITY SCALING

There are two types of scaling of data that have different support volumes. The first type is downscaling, where the original data have a larger support volume and data at a finer scale are obtained. The second type is upscaling, where data from small supporting volumes have to be averaged to obtain representative values for a bigger volume. Depending on the nature of the data, one of two approaches can be applied. In this study, two scaling approaches were considered

1. Scaling down the data

1.1. Problem setting

The reservoir was simulated geostatistically at a very coarse scale of 8 x 1 x 6. The procedure and results of the simulated model were explained in Section 3.2 of geostatistical modeling. Five grid systems were simulated from very coarse to very fine, starting with an 8 x 6 grid and finishing with a 128 x 96 grid (2-D problem). The reservoir size was kept the same and the wells were allowed to go to the limit of the reservoir (edges of the first and last cells in the x direction). The cell sizes for these grids can be seen in Table 6-1. In this grid set, the number of cells was close to the number used for the homogeneous case. The number of cells in the x and z directions double exactly each time; therefore, the total number of cells is four times greater as one goes from one grid to the next.

1.2. Interpretation of results

The porosity and permeability for the finer grids were obtained from a scale down of the data for the coarse 8 x 6 grid. The scale down approach was simple. Each data point from the 8 x 6 grid was assigned to four cells of the next finer grid (16 x 12). The data for the next finer grid (32 x 24) was obtained similarly from the 16x12 grid.

In order to assign the data and organize them in a way similar to the Wingslib data output, a program was written in Turbo Pascal. An example of the program to convert the porosity from an 8 x 6 grid to 16 x 12 is illustrated in Appendix 6. Other programs used for this purpose were similar, except that the names of the input and output files were different.

The newly scaled data were introduced into the Eclipse input files so that they could be used for all the grids. The run of the finest 128 x 96 grid, M = 1, did not complete successfully (under the conditions specified in the Eclipse input file, there was no possibility of water being injected into the reservoir). The results are shown in Figures 6-1 to 6-7, where the results for the 64 x 48 grid are used for illustration purposes. The adjusted oil rate plot (Figure 6-1) shows that, in the beginning, the rates were high (≈ 8,500 sm^3/PVWI) and comparable among different mobility ratios. However, the rate for M = 1.8 dropped earlier (≈ 0.11 PVWI), while that for M = 0.4, was maintained constant until later (≈ 0.33 PVWI). The decrease in the rate for M = 1 took place at an intermediate time (≈ 0.23 PVWI). The point at which the rates decrease rapidly corresponds to the breakthrough time in Figure 6-2. The reason why the BT time for M = 1.8 was earlier than the other cases was explained before (water channeling). The recovery factor for this grid (Figure 6-3) was lower than that for the homogenous case (Figure 5-2) or that of the heterogeneous reservoir case (without scaling) (Figure 4-6), when using the same grid. The probable explanation for this behavior is that, in the original simulated data for the 8 x 6 grid, there was a streak of very low porosity and permeability (Figures 3-26 and 3-27). For finer grids, the low values will still be the same and they can block the flow significantly.

1.3. Convergence properties

The RFs and BT times for all of the simulated grids are compared in Table 6-2. In Figure 6-4, the recovery factors calculated at 1 PVWI are plotted versus the number of cells on a logarithmic scale. For the three mobility ratios, the recovery factors

gradually increase as the number of cells increases. The maximum RFs (at convergence) increase from 0.27 to 0.46 as the mobility ratio increases from 0.4 to 1.8. That is, the higher the mobility ratio, the lower the recovery. Recovery values for all of the grids are lower than the corresponding ones for the homogeneous cases. Breakthrough is assumed to occur when the water cut reaches 0.01. With the water cut parameter, the trend is that the higher the mobility ratio, the earlier the breakthrough time. There is an indication of convergence for M = 0.4 as the breakthrough time increases sharply for the small grid system and then flattens out for the larger grid system (Figure 6-5). For M =1, it is hard to say whether convergence occurs, because there is no data point for the largest discretization. For M = 1.8, the breakthrough time increases gradually as the number of cells increases.

The differences, for various grid sizes, in RF and BT, as compared with the results for the finest grid size are shown in Figures 6-6 and 6-7. The general trend is that the coarser grid, the bigger the difference from the reference values. The RF for the M = 0.4 curve shows the greatest difference, reaching 8 % for the 8 x 6 grid (Figure 6-6). For M = 1 and 1.8, the values are close to each other and lower than for the M = 0.4 curve, reaching a 6 % difference from the finest grid for the 8 x 6 grid. The BT times exhibit an even larger difference. The biggest difference was 37 % for M = 1, and the 8 x 6 grid (Figure 6-7). The curve for M = 0.4 shows that it differs less from the reference point than do the other two mobility ratios.

1.4. CPU time

Another important parameter is the computer CPU time, because it is directly related to computing resources. A summary of CPU times used for the runs is presented in Table 6-3. A plot of computer CPU times versus grid number is presented in Figure 6-8, where the time and the cell numbers are plotted on a logarithmic scale. It should be mentioned that the number of time steps for M = 1.8 was usually larger (110 time steps for 16 x 12 to 64 x 48; 150 for 128 x 96) while 80 time steps were sufficient for

the other simulations (4 days per time step). From Figure 6-8, it can be seen that as the number of cells increases, the CPU time increases. For M = 1, and a grid size of 128 x 96, the time was unusually shorter, because the time was cut short due to the fact that no water could be injected into the reservoir. In the cell range of 1,000 – 10,000, it seems the time required for a simulation run increases as the square of the number of cells.

It was also interesting to observe that the times required for the simulation of an unfavorable mobility ratio case were less then those required for the favorable mobility ratio cases. One possible explanation is that for the unfavorable mobility ratio case, the iteration of the flow equations converged faster. Such an explanation is difficult to defend, because common wisdom suggests the opposite; that is, flow simulations for the unfavorable mobility ratios should be more difficult. The reality may be just the opposite; the injected water may find it difficult to force its way through a very viscous oil bank. When the path is established, the system is stable, as injected water will continue to take the same path to the outlet. With a favorable mobility ratio, the injected water has to maintain a smooth flooding front; therefore, it is harder to maintain the system stable mathematically.

The CPU times for this heterogeneous system are presented in Figure 6-8. The required CPU times for heterogeneous systems were higher than those for homogeneous systems (see Figure 5-6), especially for the finer grids and the more favorable mobility ratios (more then six times for a 128 x 96 grid, M = 0.4; 2 times for M = 1.8). These numbers were not for the full heterogeneous reservoir at a fine grid, because of the scaling down effects. The conclusion to be drawn here is that the computer resources should be reviewed carefully to prepare for the simulation of a very fine gridded heterogeneous reservoir, as the CPU time can increase dramatically

1.5. Some comments

Scaling down is not a common practice, because resolution is lost during the scaling down process. The reservoir properties may look unrealistic for the finer grids. More importantly, the simulation results may be biased depending on the original model for the coarser grid.

In practice, very fine geostatistical models can be created. Problems may arise when a flow simulator can handle only a limited number of cells. This depends on computer resources and the objective of the simulation. Therefore, the process of scaling up plays an important role.

2. Scaling up the data

One important consideration in the description of a heterogeneous reservoir is the problem of averaging from one scale to another. Averaging means finding a unique value for the bigger volume that is representative of the set of smaller measurements that can be obtained and processed within it [10]. For different variables, different averaging approaches should be applied. If the variables are additive, such as porosity or saturation, a simple arithmetic averaging can be applied. However, there are other parameters, such as permeability and mobility, that are not additive; therefore, arithmetic averaging cannot be used. Different methods developed by different authors to determine the effective permeability of a block can be found in the literature. Only the basic averaging techniques for permeability are addressed below.

2.1. Arithmetic averaging

If strata can be treated as being parallel, thickness-weighted arithmetic averaging should be used in the calculation of horizontal flow [11]:

$$\bar{k}_{arith} = \frac{\sum_{i=1}^{n} k_i h_i}{\sum_{i=1}^{n} h_i} \qquad (6\text{-}1)$$

where:

k_i – layer permeability

h_i – layer thickness

n – number of layers

If the thickness is the same for every layer, then the arithmetic average becomes:

$$\bar{k}_{arith} = \frac{\sum_{i=1}^{n} k_i}{n} \qquad (6\text{-}2)$$

2.2. Harmonic averaging

Harmonic averaging should be used in calculating permeability for series flow, that is, flow across layers. The harmonic average is:

$$\bar{k}_{harm} = \frac{\sum_{i=1}^{n} h_i}{\sum_{i=1}^{n} h_i / k_i} \qquad (6\text{-}3)$$

With constant thickness, Equation (6-3) becomes:

$$\bar{k}_{harm} = \frac{n}{\sum_{i=1}^{n} 1/k_i} \qquad (6\text{-}4)$$

2.3. Geometric averaging

For randomly distributed permeabilities, the geometric average (or log mean) applies:

$$\bar{k}_{geom} = \sqrt[n]{k_1 k_2 k_3 ... k_n} \qquad (6\text{-}5)$$

Note that Equation (6-5) is equivalent to Equation (5-1), which is written in logarithmic form. If permeabilities are randomly distributed both the horizontal and the vertical permeabilities normally should be obtained by geometric averaging. Warren and Price [12] showed experimentally that the most probable behavior of a heterogeneous system approaches that of a uniform system having a permeability equal to the geometric mean. It can also be shown analytically that the median of a log normal distribution is the geometric mean [4; lecture1].

2.4. Power averaging

Power law averaging has been used extensively in research work on upscaling, in recent years. The formula for power averaging is:

$$\bar{k}_{pow} = \left[\frac{\sum_{i=1}^{n} h_i k_i^w}{\sum_{i=1}^{n} h_i} \right]^{\frac{1}{w}} \qquad (6\text{-}6)$$

where w is the power averaging exponent

Journel et al. [10] stated that, for a rock with a shale content p of less than 0.5, the power average provides a good fit to the curve of effective permeability (k_{eff}) versus p. The effective permeability is calculated for scaled-up blocks using the data from a very fine scale simulation. The average power was determined empirically. In that

study, using a power w of 0.57 and 0.12, a good fit was obtained for the x and z directions, respectively. According to them, the averaging power increases with the correlation range in the direction of flow, with an upper bound of w = 1 corresponding to arithmetic averaging for perfect correlation and laminar flow. The lower limit was –1, which corresponds to the harmonic average used for layers in series. Cardwell and Parsons [13] proved that the effective permeability of a group of heterogeneous blocks lies between the arithmetic and the harmonic averages. A power w range from –1 to 1 is consistent with this conclusion. It can be proved that when the power w approaches zero both from a negative or positive side, the power average approaches the geometric average, and actually reaches the geometric average at the zero limit [14].

Choosing the right exponent for a particular set of data is a crucial step for the power averaging technique. Deutsch [14] proposed a geostatistical approach to estimate the exponent w. He shows that a weighted indicator correlation in the flow direction may be used to predict w. This indicator correlation may be inferred if detailed information, such as appropriate well logs or outcrop data, are available. The indicator correlation may also be inferred from structural hypotheses regarding the shale bodies and corresponding indicator variograms. If this technique is reasonably applied, more accurate estimates than geometric averaging can be expected. Desbarats [15] presented an expression for scaled-up permeability in terms of log-variance and the power averaging exponent. From numerical studies of 3D, isotropic, log normal permeability distributions with small log-variance, he found an empirical power averaging exponent of 1/3 to be appropriate for scale-up. Deutsch suggests an exponent range of 0.5 to 1 in the horizontal x and y directions. For the vertical direction, the range should be from -1 to 0. For the two well data set, a w-value of 0.6 was chosen for the x and y directions and a value of -0.5 for the z direction.

Power law averaging is faster than the pressure solver techniques, which will be defined in Section 2.5, but it is not easy to use in practice because one needs to determine experimentally the power averaging exponent w by means of a fine-grid

simulation. The exponent can vary from one coarse-grid block to another. As a result, the use of a constant exponent for all coarse-grid blocks may result in large error [16]. A comparison between simulations using permeability obtained using power averaging and permeabilities obtained using flow-based techniques is made later.

2.5. Flow-based averaging

An accurate way of calculating the effective permeability of large coarse-grid blocks containing many fine-grid blocks is to solve flow equations with constant pressure and no-flow boundary conditions, or periodic boundary conditions. However, using this approach requires extensive computation. This approach is referred to by many researchers as the pressure solver technique, because the approach solves for the fine-grid pressure distribution first and then calculates the effective permeability using the calculated pressure drops and fluxes and Darcy's equation [16].

3. Comparison of the results obtained using different scaling techniques

Two averaging techniques were applied to the simulated porosity and permeability for the128 x 96 grid (the finest grid): power and flow-based averaging. The various grids used and their sizes are presented in Table 6-1. Two programs were used: "powavg" and "flowsim". Porosity was averaged arithmetically. Because the arithmetic average can be obtained by power averaging with w = 1, "powavg" can be used to get the scaled up porosity. For the x and y directions, a value of w = 0.6 was used, and for the z direction a value of w = –0.5 was used. In the flow averaging method, the idea is to find the effective permeability in different directions by solving Darcy's flow equation. In this method, no flow boundary conditions were set up for directions other than the one of interest. Pressures were kept constant. The program ("flowsim") solves for the effective flow rate (Q_{eff}) and then calculates the effective permeability in this direction using Darcy's law.

Some problems were encountered using the programs for averaging. Sometimes, during the simulation process, there was a warning saying that the system of equations did not converge after 2,500 iterations. Because the tolerance of the program was set at a very small value and this happened only in a few blocks, this was not a large concern from the point of view of accuracy. For power averaging in the z direction, with w = -0.5, a permeability value of zero causes the program to stop because of a division by zero. It is recommended that the input data be checked prior to running the "powavg" program. If the data set contains zero values, these should be changed to some small value (say 0.0001).

To compare the results of the two averaging methods, only the results from the first realization of the geostatistical simulation were used. The crossplots of the results from the two methods in the x and z directions are shown in Figures 6-9 to 6-12. These results are for the 64 x 48 and 8 x 6 grids (the first and last grid for scaling up). The purpose of these figures is to determine the correlation coefficients. A correlation coefficient of 1 corresponds to a perfect linear relationship. If there is a perfect correlation, all the points should fall on the 45° line. All the figures show almost perfect correlation with correlation coefficients ranging from 0.98 to 0.999.

The plots for the 64 x 48 grid show a better correlation with points staying very close to the line. This can be explained by the fact that, for this grid, there were only four data points considered for the up scaling process to obtain the representative permeability value for the coarser block. With the 8 x 6 grid, the number of small blocks was 16. Thus, for the 8 x 6 grid, there were fewer points and the points stay further from the perfect correlation line. In the z direction, there were many points located in the region near zero. This is probably related to the properties of permeability. If there is only one block having a low permeability, the permeability of a bigger block will be low as well. Because scaling up the permeability to the 8 x 6 grid from the 128 x 96 grid takes 16 blocks, there will be a greater chance that one of

the permeability values will be low and, consequently, the permeability of the scaled block will be low as well.

To compare how the averaged permeability derived using different averaging techniques can affect the flow performance of the reservoir, a flow simulation using Eclipse was carried out on an 8 x 6 grid. All three mobility cases were simulated. Oil and water production rates, water cuts and the recovery factors were the parameters monitored. The results for this simulation can be seen graphically in Figures 6-13 through 6-16. The results obtained using the two averaging methods are very similar in character, especially for M = 0.4 and 1.8. The recovery curves are almost identical for these two mobility ratios. For M = 1, the curves are still very close. Based on the results presented above, it can be concluded that the power averaging method, even though more approximate, gives results comparable to those obtained using flow simulation. The power averaging results can be improved by adjusting the exponent w. Thus, permeability averaging can be done quickly and simply by using the power averaging method.

In this study, one hundred (100) realizations obtained using geostatistical modeling were scaled up using the flow-based averaging method. The results of this operation were used for flow simulation of all one hundred realizations.

Grids	Number of cells	Δx (m)	Δy (m)	Δz (m)
8 x 6	48	75	1	16.6667
16 x 12	192	37.5	1	8.3333
32 x 24	768	18.75	1	4.1667
64 x 48	3072	9.375	1	2.0833
128 x 96	12288	4.6875	1	1.0417

Table 6-1: Different reservoir discretizations for the heterogeneous case

Grids	No. cells	RF	% RF	BT (PV)	% PV
M = 0.4					
8 x 6	48	0.423	7.843	0.245	25.305
16 x 12	192	0.441	3.922	0.286	12.805
32 x 24	768	0.449	2.179	0.327	0.305
64 x 48	3072	0.455	0.871	0.327	0.305
128 x 96	12288	0.459	0	0.328	0
M = 1					
8 x 6	48	0.339	6.09418	0.147	35.8079
16 x 12	192	0.352	2.49307	0.183	20.0873
32 x 24	768	0.357	1.10803	0.22	3.93013
64 x 48	3072	0.361	0	0.229	0
128 x 96	12288				
M = 1.8					
8 x 6	48	0.27	5.59441	0.084	32.2581
16 x 12	192	0.279	2.44755	0.102	17.7419
32 x 24	768	0.282	1.3986	0.112	9.67742
64 x 48	3072	0.285	0.34965	0.114	8.06452
128 x 96	12288	0.286	0	0.124	0

Table 6-2: Summary of runs for different discretizations – down scaling process

Grids	Number of cells	M = 0.4 (sec)	M = 1 (sec)	M = 1.8 (sec)
8 x 6	48	2.5	2.4	2.3
16 x 12	192	4	3.5	3.9
32 x 24	768	12.5	9	6.6
64 x 48	3072	219.9	100	42
128 x 96	12288	2878.2	590	805.8

Table 6-3: Computer CPU times for flow simulation - down scaling process

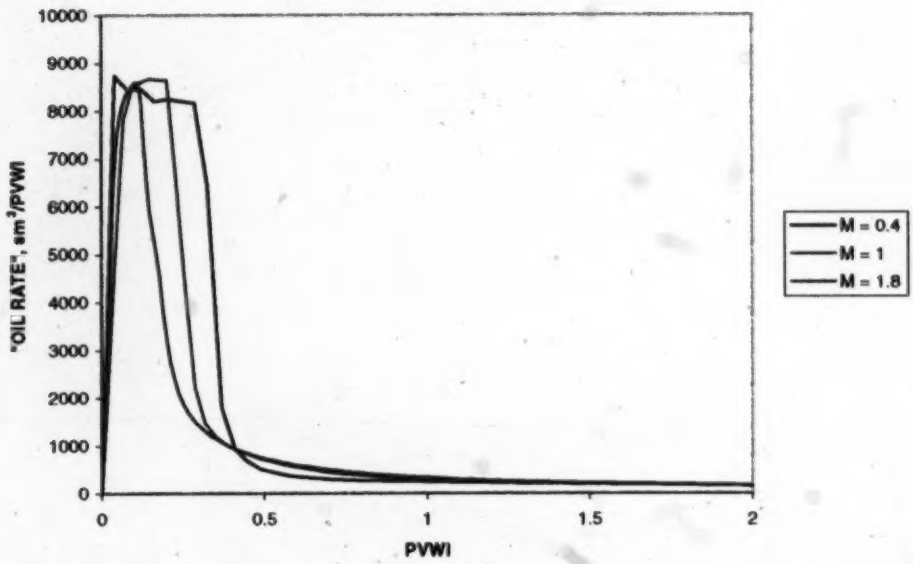

Figure 6-1: "Oil production rate" versus PVWI for 64 x 48 grid - downscaling process

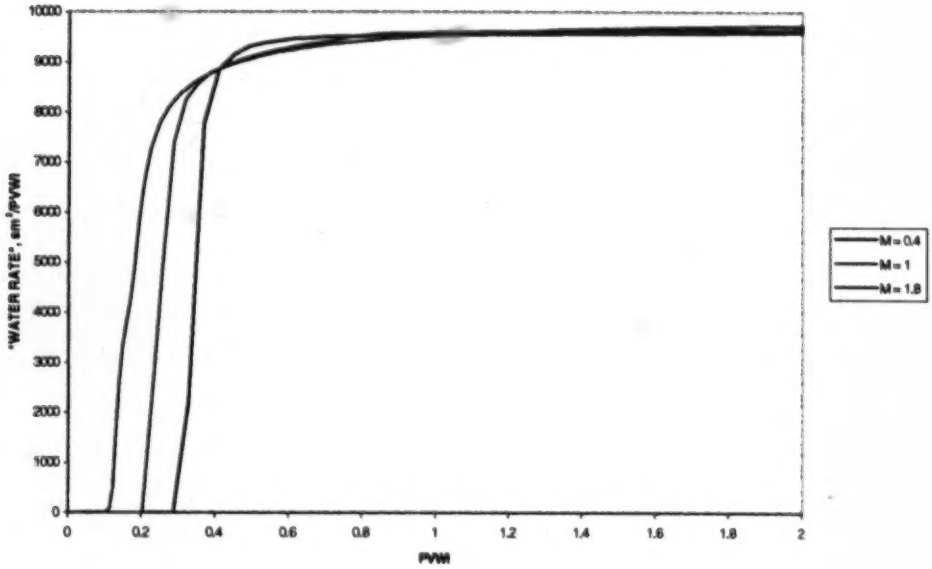

Figure 6-2: "Water production rates" versus PVWI for 64 x 48 grid - downscaling process

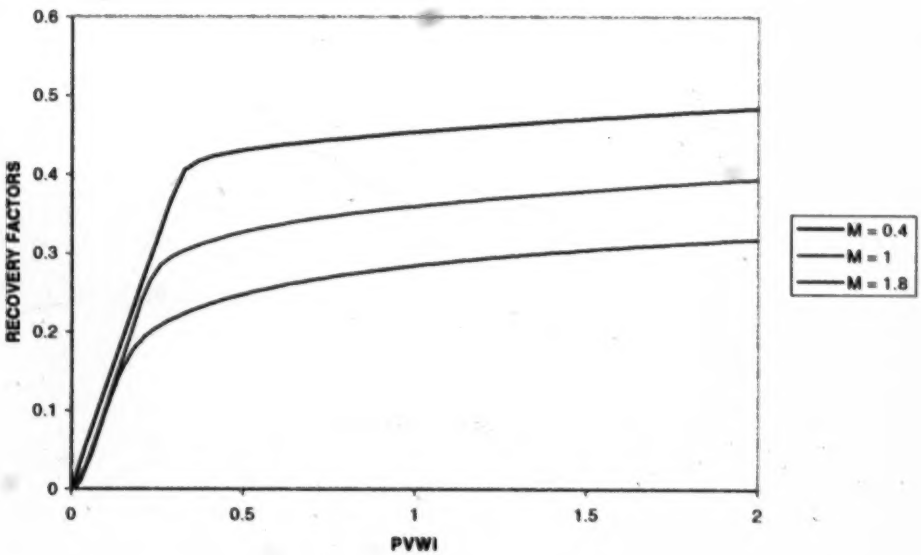

Figure 6-3: Recovery factors versus PVWI for 64 x 48 grid – downscaling process

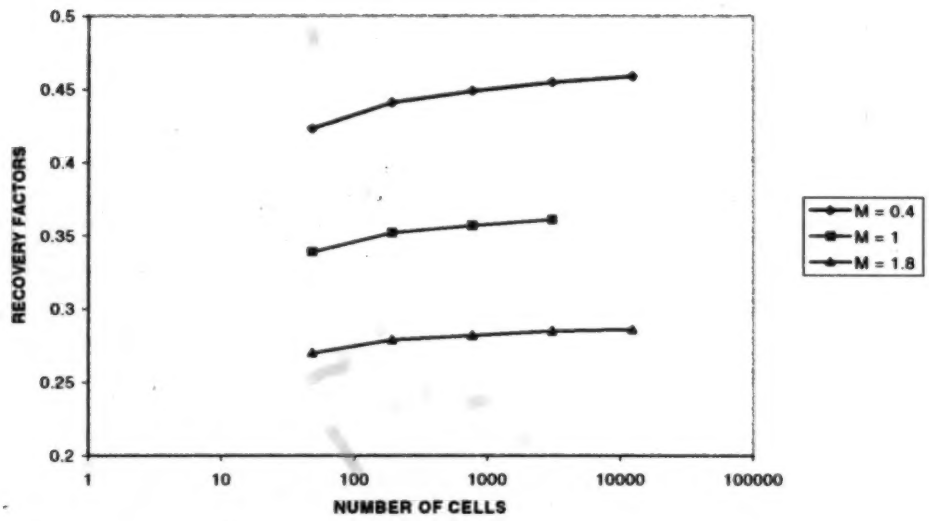

Figure 6-4: Recovery factors at 1 PVWI for different discretizations and mobility ratios - downscaling process

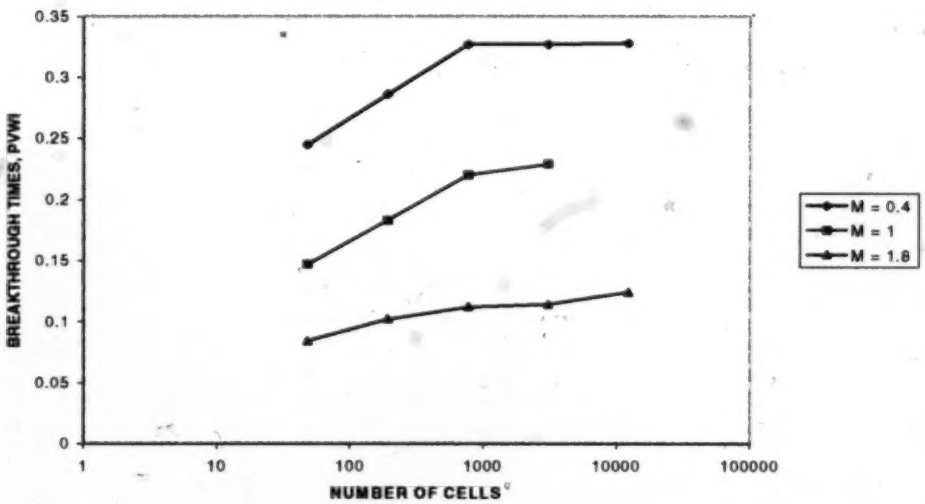

Figure 6-5: Breakthrough times taken at = 0.01 water cuts for different discretizations and mobility ratios - downscaling process

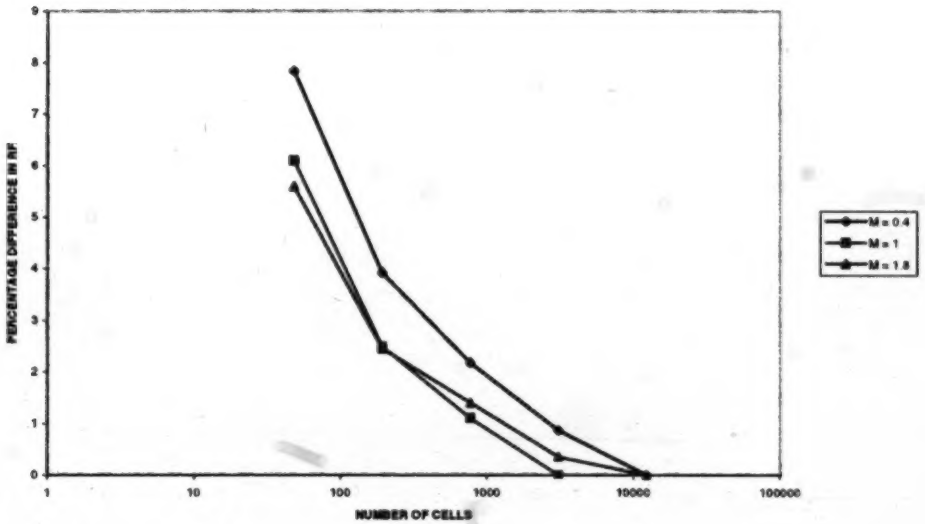

Figure 6-6: Differences in recovery factors at 1 PVWI from the recovery factor of the finest grid - downscaling process

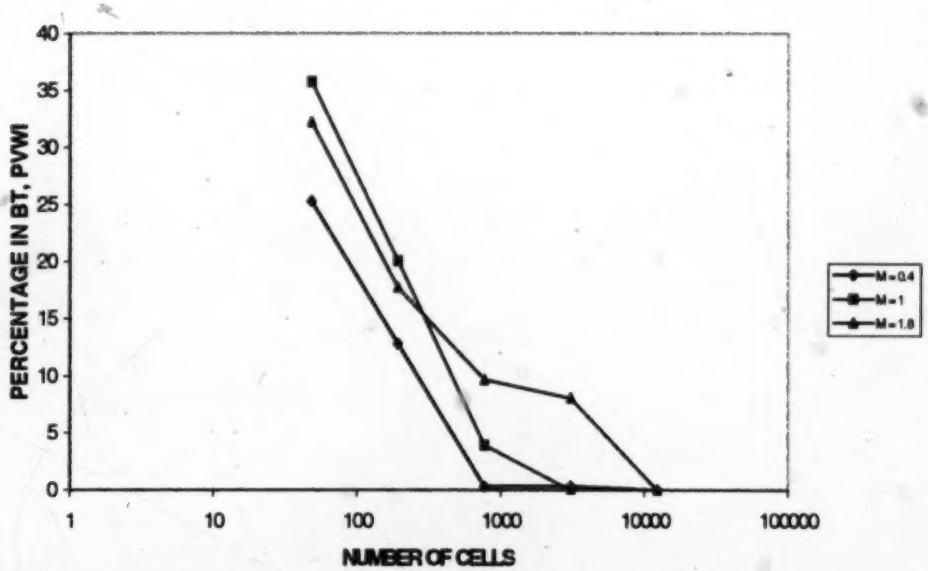

Figure 6-7: Differences in breakthrough times of different grids from the finest grid - downscaling process

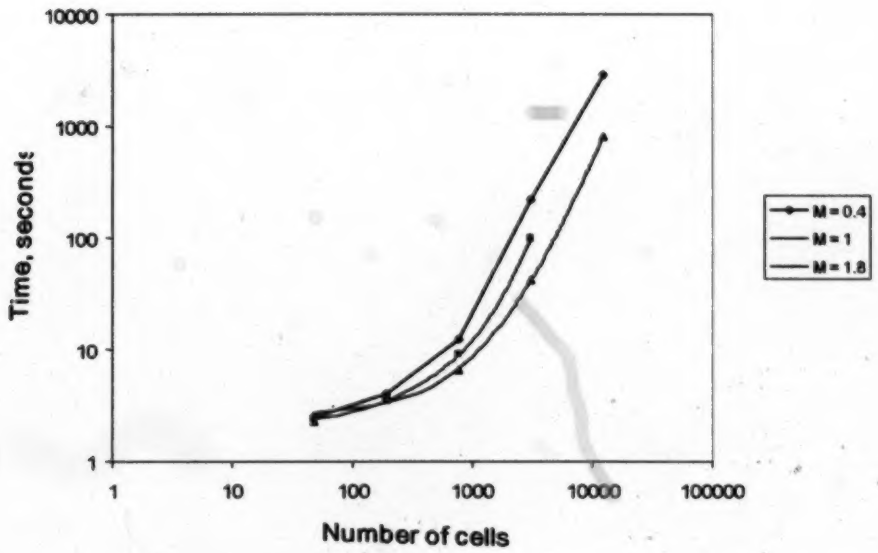

Figure 6-8: Computer CPU times - down scaling process

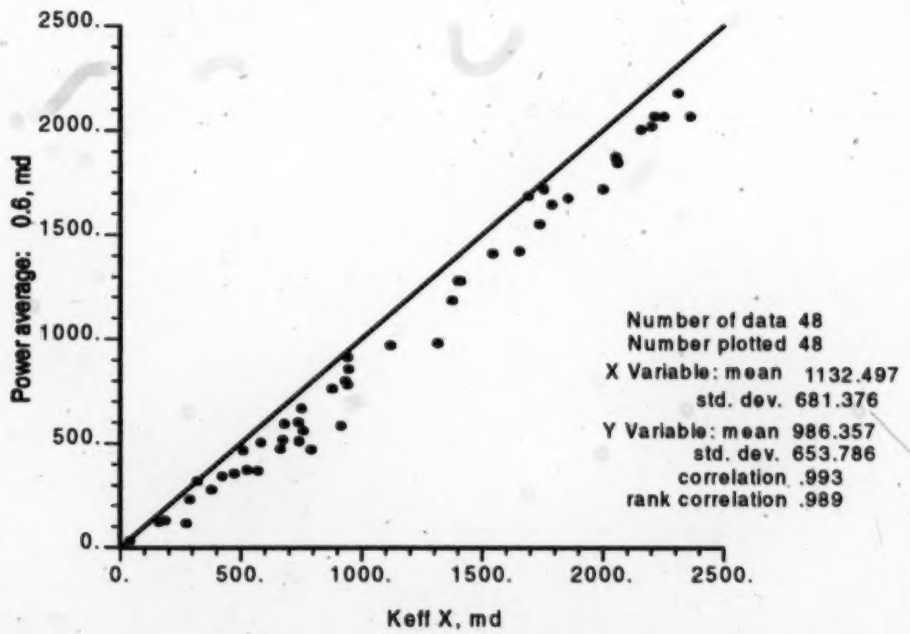

Figure 6-9: 8 x 6 grid – effective versus power averaged permeability in x direction

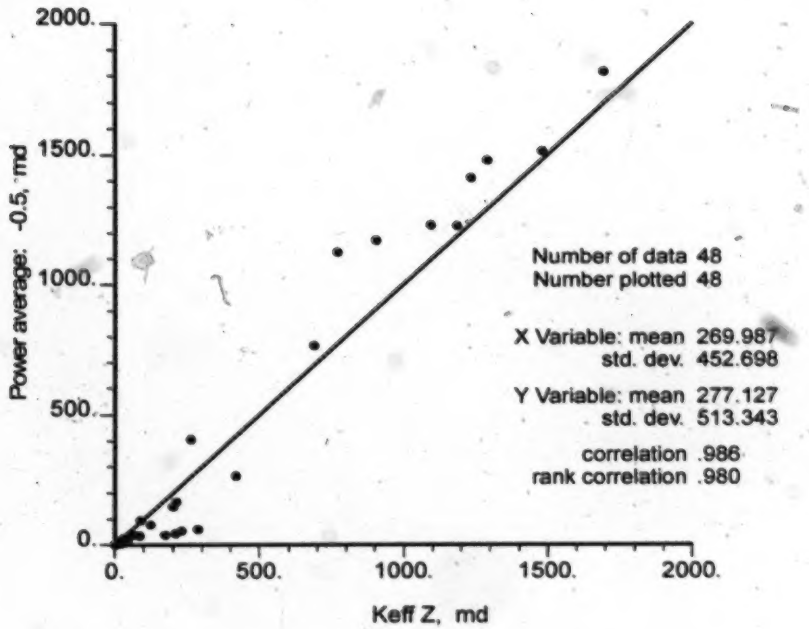

Figure 6-10: 8 x 6 grid – effective versus power averaged permeability in z direction

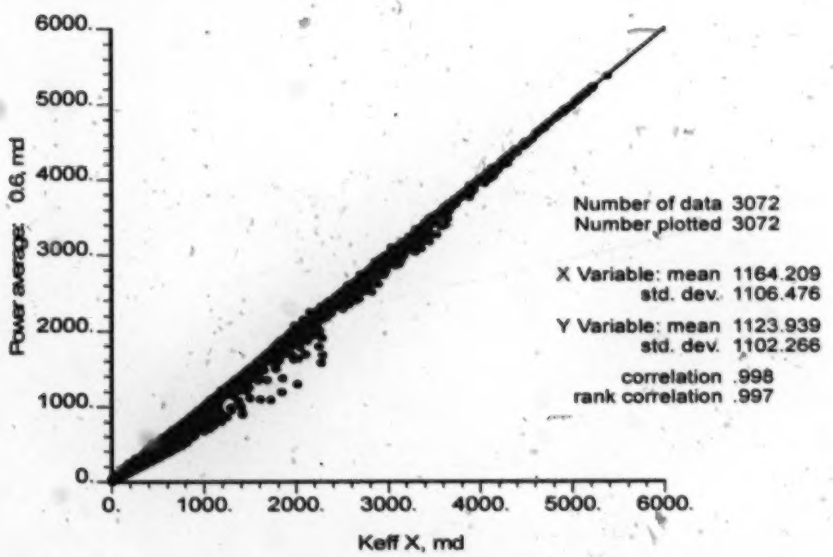

Figure 6-11: 64 x 48 grid – effective versus power averaged permeability in x direction

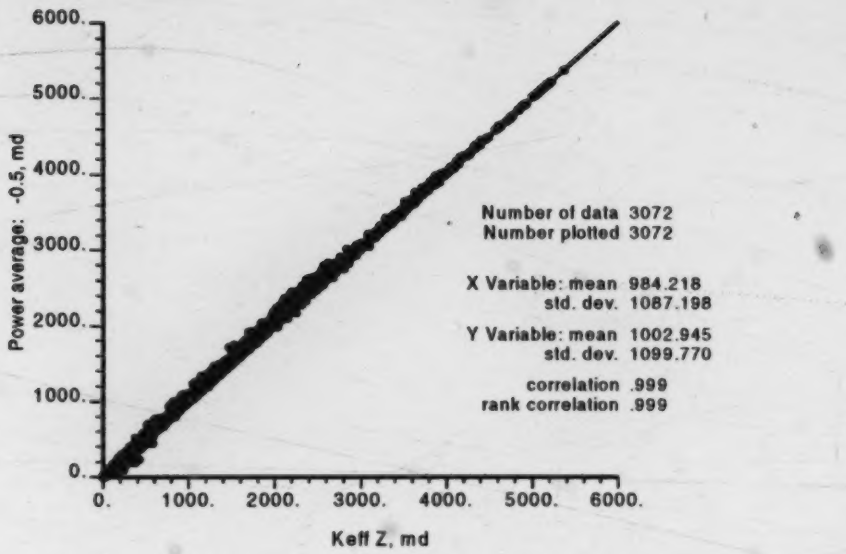

Figure 6-12: 64 x 48 grid – effective versus power averaged permeability in z direction

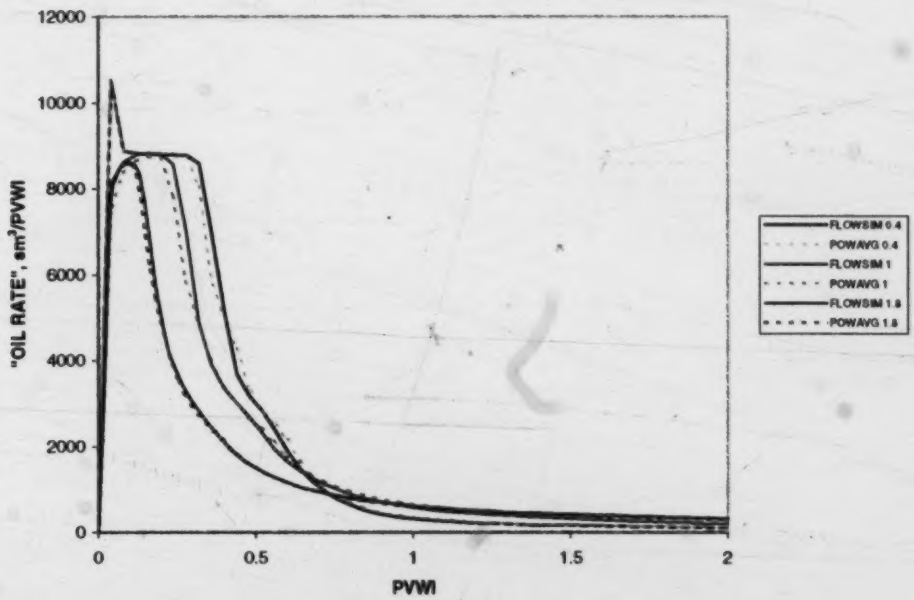

Figure 6-13: 8 x 6 grid – "Oil production rates" using permeability averaged by power law and flow-based techniques

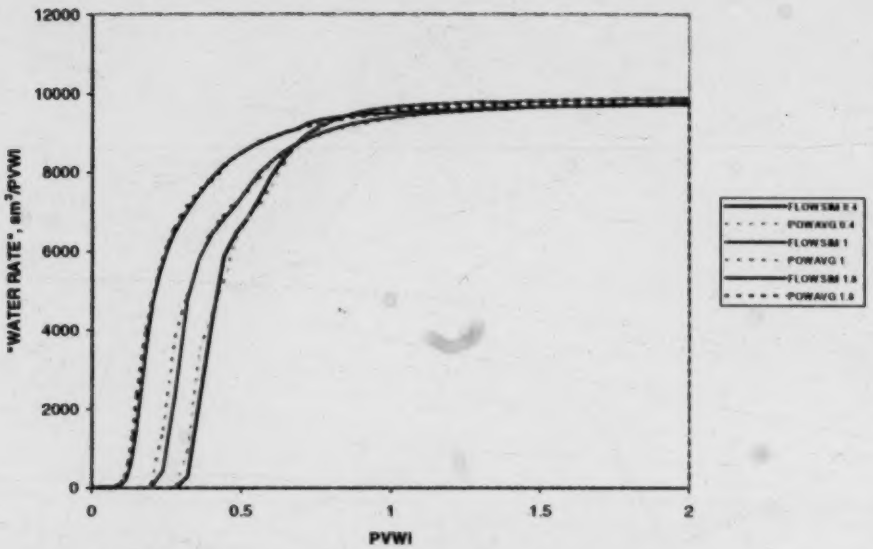

Figure 6-14: 8 x 6 grid – "water production rates" using permeability averaged by power law and flow-based techniques

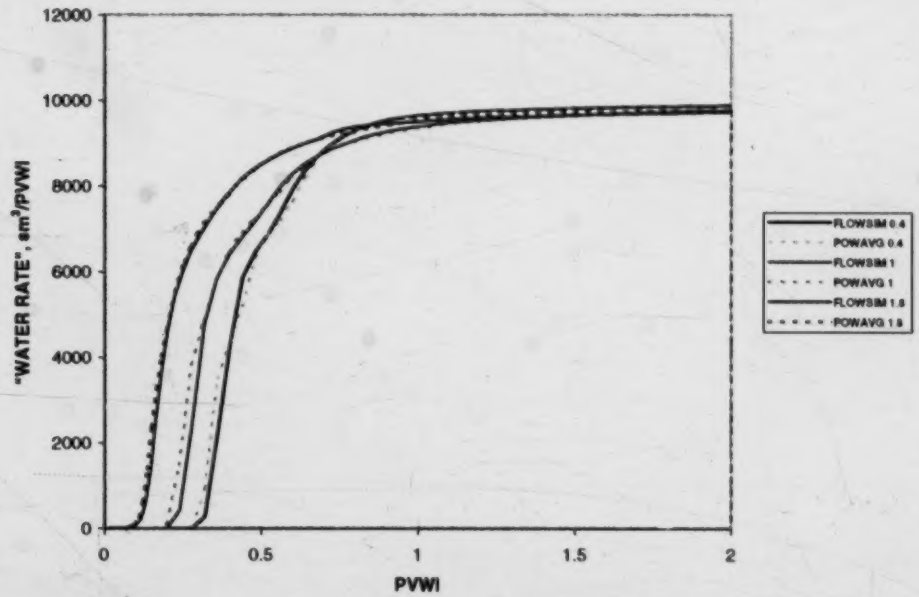

Figure 6-15: 8 x 6 grid – water cuts using permeability averaged by power law and flow-based techniques

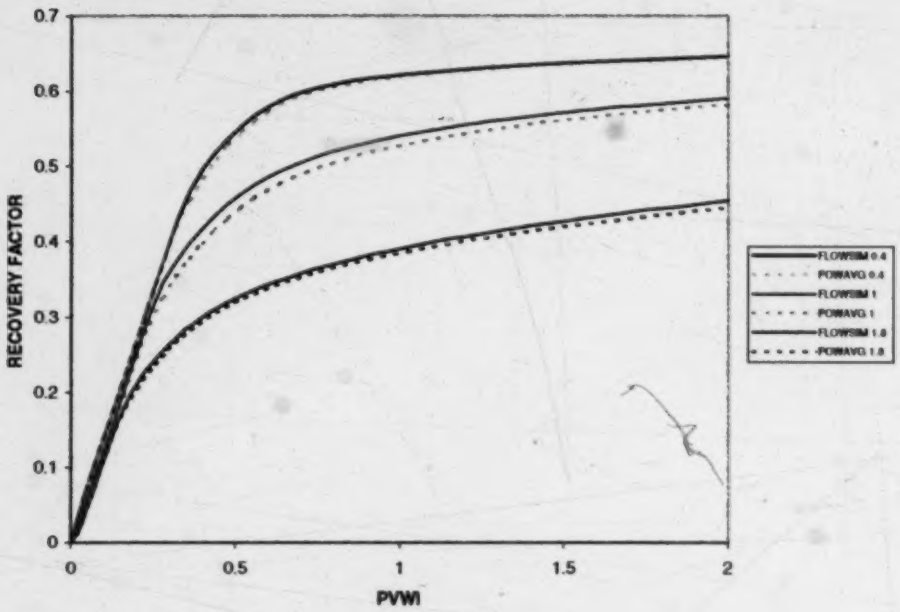

Figure 6-16: 8 x 6 grid – recovery factors using permeability averaged by power law and flow-based techniques

VII. RUNNING ECLIPSE FOR A HUNDRED REALIZATIONS

1. Looping in Eclipse

The results from all hundred Wingslib simulation realizations were used in Eclipse. There were five grids to be simulated (Table 6-1). For every grid, the properties of the three fluids used to create the three mobility ratios were entered into Eclipse separately. The purpose of running so many realizations was to evaluate the uncertainties in flow simulation results associated with gridding, and with the nature of the fluids (viscosity-mobility ratios) in the presence of realistic geological heterogeneities. One hundred realizations were used because, with such a number, reasonably reliable statistics of the flow parameters could be inferred. The decision was based on the central limit theorem which states that the uncertainty in calculated statistics is proportional to the uncertainty in one component divided by the number of components [4]. If the number of components (realizations) is 100, as in this study, the uncertainty in the calculated statistics will be only one one-hundredth of the uncertainty in the results of one realization.

The task of running Eclipse 1,500 times makes manual operation of the simulator unrealistic. A program written in shell script of the Unix system was used to automate the process of running Eclipse for a hundred times. An example of this program for the 8 x 6 grid is available in Appendix 7. Other simulation parameters were kept the same. The permeability now has a different value in each of the three directions, PERMX, PERMY and PERMZ. For the finest grid (128 x 96), there was only one permeability set (because it was the original data for the averaging process). Therefore, the permeability in the three directions was assumed to be the same. This is a reasonable assumption, because the cell sizes were very small. The conversion of the porosity and permeability into Eclipse format, using the program "gsl2ecl", was done simultaneously, in association with running Eclipse.

2. Interpretation of the flow simulation results

Several flow parameters were observed. Among them were the "oil rate", "water rate", recovery factors and water cuts. The oil and water rates were adjusted to overcome the effects of unsteady water injection (due to high reservoir pressure). All parameters were plotted against pore volumes of water injected (PVWI). For all 100 runs of every grid and mobility ratio, the recovery factors at 1 PVWI were extracted. The breakthrough times were taken at a water cut of approximately 0.01 and recorded in PVWI.

2.1. Oil rate plots

Equation (4-3) was used to calculate the "oil production rates". The units of "oil rate" were sm^3/PVWI. The plots of oil rate versus PVWI are shown in Appendix 8. This series of plots was constructed for all of the grids and mobility ratios. The general picture is that for the favorable mobility ratio, M = 0.4, the oil rate at the beginning increases sharply (the highest rates were seen after the first time step at ≈ 12,000 sm^3/PVWI), then drops and flattens out for some time (at rates approximately from 8,000 to 10,000 sm^3/PVWI). At the end, the oil rate gradually decreases. Some realizations can stop earlier, when the oil flow rate fell below the restriction of 1 sm^3/day. During the period of constant flow, the oil rates show the widest range of difference. After the constant rate period, the oil rate drops gradually, because the reservoir was gradually being swept out.

For M = 0.4, a peak at the beginning after the first step was observed for all the realizations. As explained earlier in Part IV (simulation using Eclipse), this peak was not associated with any special event. This was an artificial effect which appeared when the oil production rate was adjusted. The peak is not observed when the normal oil production rates, sm^3/day, are plotted.

For the unit mobility ratio and the unfavorable mobility ratio cases, the oil rate pattern remains the same, except that there were no peaks at the beginning. The oil rates after the first time step were smaller than those of the following time steps. The period of constant rate was also shorter.

In order to see if every realization appears in the same order on the oil rate plots for all the mobility ratios, the oil rates at around 0.1 PVWI were recorded. The point 0.1 was picked because, at that time, the plots show the biggest range in oil rates for all mobility ratios. The 16 x 12 grid was used for this ranking because, from the plots, the oil rates appeared to be more parallel during the period of constant rates. Table 7-1 shows that the order is not quite the same. The highest rate occurs in Realization 33 for all M. The lowest rate occurs in Realization 36 for M = 0.4 and 1 and in Realization 38 for M = 1.8. By taking a closer look at the table, it can be seen that, in many cases, the order is fairly close among the different mobility ratios.

2.2. Water rate plots

In order to adjust for the effects of a non-constant water injection rate, the water production rate was recalculated in a manner similar to that used for the oil production rate (Equation (4-4)).

Appendix 9 shows the "water rates" for 100 realizations for all of the grids and mobility ratios. The water rate plots look very similar for all of the grids. There are, however, differences in the water breakthrough times. The unfavorable value of M has the earliest breakthrough at around 0.1 PVWI, followed by the case of M =1 (at ≈ 0.2 PVWI) and M = 0.4 (at ≈ 0.3 PVWI). The reason for this is that, for the unfavorable mobility ratios, displacement channels or viscous fingers are often observed in the system. These channels reach the producer faster than in the case of a favorable mobility ratio, where a more stable, piston-like displacement is taking place. If one looks back at the oil rate plots, the breakthrough times (in PVWI) coincide with the

end of the period of constant oil production rates. After breakthrough, the rate of water production rises sharply. After approximately 0.8 PVWI, the water production rates remain more or less constant and high at about 8,000 to 10,000 sm^3/PVWI. This is opposite to the time when the oil production rates decline and stay very low. Again, there is a great range in water production profiles for 100 realizations. The uncertainty in the water breakthrough times is discussed in more detail later.

2.3. Recovery factor plots

Plots in Appendix 10 present the recovery factors versus the water injected in pore volume (PVWI) for all of the grids. In these plots, the curves for the three mobility ratios are combined to obtain a comparison among the recoveries obtained under different displacement conditions. As can be seen clearly from these figures, the recovery for M = 0.4 is much higher than that for an unfavorable mobility ratio displacement (M = 1.8). At 2 PVWI, the recovery for M = 0.4 can reach ≈ 0.6 while for M = 1, the RF is around 0.5 and for M = 1.8, it is only ≈ 0.4. During the whole displacement process, the more favorable the mobility ratio, the greater the recovery. The difference range in RF for different realizations depends on the grid size and the mobility ratio. That is, different grid sizes and mobility ratios can give rise to different flow simulation results.

It is worth noticing that, in the beginning, the RF plots were linear. This corresponds to the period before breakthrough, when the oil production rates are more or less constant. The recovery curves then gradually flatten out as the oil production rates drop.

2.4. Recovery factors measured at 1 PVWI

In order to compare quantitatively the flow performances of the different realizations, for every grid size and mobility ratio, the oil recovery factors at ≈ 1 PVWI were

recorded. Appendix 11 shows the RF for all the grids and realizations at ≈ 1 PVWI. Based on this data, histograms of the RF were constructed. Figure 7-1 shows the RF histograms and Table 7-2 shows the summary statistics for the data. It is clear from the histograms that the ranges of the RF for different values of M did not overlap (for M = 0.4, the RF range is 0.57 - 0.63; for M = 1 the range is 0.48 - 0.56; and for M = 1.8, the range is 0.33 - 0.41). Based on these statistics, a box plot of the RF was drawn, where the maximum, mean, minimum, upper and lower quartiles values are shown (Figure 7-2). A line was drawn through all the means. This plot reveals that, for every mobility ratio set of results, the mean decreases as the number of cells increases.

If one takes a 128 x 96 grid (the finest) as the most accurate result, and calculates the difference between the RF mean of the 128 x 96 grid and the mean of the RF of the other grids within each M group (Figure 7-3), it turns out that the 8 x 6 grid is farthest from the reference point (up to 7 %). The M =1.8 series shows the most difference between the grids, followed by M = 0.4 and 1.

The interquartile ranges, IR-difference between the upper and lower quartiles, show that, within every mobility ratio group, the IR increases as the grid becomes finer (Figure 7-4). The graphs of RF's standard deviation (SD) (Figure 7-5) and coefficient of variance (SD/mean) (Figure 7-6) confirm this observation. This suggests that the uncertainty of this parameter increases as the grid system becomes finer. This is understandable because the larger the number of grids, the larger the number of possible combinations of porosity and permeability values. This results in different flow performances between realizations.

The order of the curves on the IR, SD, and the coefficient of variance plots, however, is different. For the IR and SD plots, the order from highest to lowest is M = 1, 1.8 and 0.4, while for the coefficient of variance plot, the order is M = 1.8, 1 and 0.4. In normal situations, where the mean is the same, the dimensionless coefficient of variance is probably the best parameter to describe the uncertainty. In this case, the

mean for M = 1.8 is significantly lower and, therefore, the coefficient of variance was higher. This higher value does not reflect the level of variance in the RFs for this mobility ratio. The standard deviation is possibly the right statistical parameter to describe the variance between different grids and mobility ratios. Following this criterion, the finer grid will have higher uncertainty than the coarser grid. The unit mobility ratio case has the highest variance. Maybe, the situation for M = 1 is a no-win situation where there is no dominant flow of either water or oil. A pictorial illustration presented later confirms this explanation of the flow process.

2.5. Breakthrough times measured at WCT =0.01.

Another important parameter for the displacement is the breakthrough time. Conventionally, the breakthrough time (BT) is assumed to occur when the water cut reaches ≈ 0.01. The PVWI at this time (or the time step that shows a higher water cut, in situations where there is a sharp increase in water cut) was recorded and put in Appendix 12. The data for the histogram modeling of 100 runs were taken from this table. Figure 7-7 shows a plot of all the histograms of BTs. There are distinctive ranges in the histograms for the three mobility ratios. For M = 0.4, the PVWI range is 0.3 - 0.43; for M = 1, the PVWI range is 0.19 - 0.32; and for M = 1.8, the PVWI range is 0.08 - 0.17.

Summary statistics for the BTs are presented in Table 7-3. A box plot of BTs is shown in Figure 7-8. Unlike that for the RFs, the BT box plot shows diversity in character. The mean line increases for the 8 x 6 to 32 x 24 grids, but then stays the same or decreases for the 64 x 48 and 126 x 96 grids. The trend of the mean values of BT among different grids is illustrated more clearly in Figure 7-9. With the BT's mean for the 128 x 96 grid as a reference point, the highest difference in the mean is for the 8 x 6 grid, M = 0.4 (9 %). Except for the favorable M curve, which shows a clear tendency for the mean to increase as the grid gets finer, there is no clear trend for M = 1 or for M = 1.8. Looking back at the box plot, one can see that the decreases in the

mean values are not substantial. It is more like a leveling off of the curve as the grid gets finer.

In the graph of IR versus grid sizes (Figure 7-10), although the trends were not so clear as for the RFs (Figure 7-4), the impression is that, as the grid gets finer, the IR values increase also. This means that the uncertainty is higher for the finer grids. This is confirmed by the graphs of SDs (Figure 7-11) and of the coefficients of variance (Figure 7-12). In Figure 7-12, while the coefficient of variance curves, for M = 1 and M = 1.8, increase slightly as the number of grid blocks increases, the coefficient of variance curve for M = 0.4 remains essentially constant.

The order of the curves is different from graph to graph and from those of corresponding RF plots. The graph of the coefficient of variance is consistent with that for the RFs. It shows a similar trend of increasing for finer grids and higher mobility ratios. The magnitude of the variance, on the other hand, is more similar to the BT curve than to the RF curve, except for M = 0.4. Similar to the RF curve, the breakthrough times for the M = 1.8 series are much earlier than those for the other series, so the coefficient of variance (SD/mean) is higher for higher mobility ratios and cannot be used as a measure of uncertainty. The SD, as well as IR parameters, show that the uncertainty increases as the grid gets finer. Among the three mobility ratios, the M = 1 series shows the highest variance followed by M = 0.4 and 1.8. This order is slightly different from that for the RF curves, which have the order of M = 1, 1.8 and 0.4.

2.6. Illustration of displacement process

To have an idea of how different oils are displaced in the reservoir by injected water, the water saturation of all the cells at different times was recorded and displayed. Realizations 33 and 36 were chosen for illustration purposes. The displacement

process was monitored for the 16 x 12 grid and for all the mobility ratio cases. The reason for choosing these realizations was explained earlier.

To understand what was behind the differences in Realizations 33 and 36, which had the highest and the lowest oil production rates, respectively, plots of porosity and permeability for these realizations were constructed. They are shown in Figures 7-13 to 7-16. From these plots, it can be seen that the porosity and permeability have higher values in the case of Realization 33 than in the case of Realization 36. This suggests that the water should flow more easily through the reservoir defined by Realization 33 than is the case for Realization 36.

In order to compare the displacements, it is desirable to have all the water saturation sets at the same PVWI. Examination of the saturations for all the mobility ratios showed that it was impossible to have the PVWI the same using four-day time steps. Consequently, the simulations for Realizations 33 and 36, and for all the mobility ratio cases, were run again. This enabled choosing the time steps at which the same amount of water was injected. Table 7-4 shows the times in PVWI chosen for the water saturations to be displayed. The range of PVWI was from 0 to ≈ 0.74. This range captured most of the displacement process. After that, the oil and water productions remained stable, so there were less changes of interest to be monitored. Twelve time steps, at which the same amount of water (in PVWI) was injected for both Realizations 33 and 36, as well as for all the mobility ratio cases, were chosen for water saturation profile display. The display is in order of increasing PVWI.

The water saturation values at different time steps were extracted from Eclipse PRT files. In order to plot these data using Wingslib, the data have to be converted into Wingslib format because there is a difference in the data organization, mainly related to the coordinate systems. A program written in the Pascal programming language was used to convert the data. The source codes for this program can be found in Appendix 13.

Figures 7-17 through 7-22 show the water saturation profiles for both realizations and for all three mobility ratio cases. As predicted earlier, the displacement front for the favorable mobility ratio case (Figures 7-17 and 7-20) is more stable than that for the unfavorable mobility ratio case (Figures 7-19 and 7-22). In the cases of M = 1 and M = 1.8, water channeling occurs and, therefore, the water reaches the producer faster. Oil is bypassed in the unit and unfavorable mobility ratio cases. As a result of this, less oil is recovered in these cases.

The water saturation profiles between the two realizations are not so different. In the case of Realization 36, oil seems to be left more in the lower part of the reservoir and the recovery factor is lower than that for Realization 33. The RFs for Realization 33 are 0.625, 0.547, and 0.392 for M = 0.4, 1, and 1.8, respectively; for Realization 36 the RFs are 0.617, 0.519, and 0.4, respectively (Appendix 8). The low permeability zone in the case of Realization 36 (Figure 7-16) blocks the flow more severely as the mobility ratio increases. The BT times for these two realizations are not so different: 0.39, 0.246, and 0.112 PVWI for Realization 33, M = 0.4, 1, and 1.8, respectively; and 0.39, 0.249, and 0.128 PVWI for Realization 36, M = 0.4, 1, and 1.8, respectively (Appendix 12). The RFs and BT times for the realizations 33 and 36 were not the highest and the lowest numbers among all the realizations.

	M = 0.4		M = 1		M = 1.8	
No.	ORATE (sm^3/PVWI)	Realization	ORATE (sm^3/PVWI)	Realization	ORATE (sm^3/PVWI)	Realization
1	10029.2	33	10061.6	33	9796.2	33
2	9896.5	49	9879.9	2	9635.3	49
3	9835.4	2	9812.3	79	9614.8	2
4	9751.6	94	9738.6	62	9577.0	94
5	9731.1	79	9734.3	16	9549.6	43
6	9706.4	16	9729.2	94	9543.5	16
7	9666.1	62	9688.7	49	9511.7	95
8	9641.2	95	9650.5	46	9482.1	79
9	9639.5	43	9638.6	30	9462.4	62
10	9625.5	44	9610.0	95	9453.3	44
45	9045.2	40	9058.6	82	8882.7	39
46	9029.2	77	9054.6	81	8864.8	81
47	9024.9	9	9038.2	27	8853.3	40
48	9022.7	100	9034.6	21	8847.2	21
49	9014.4	81	9007.8	65	8826.9	65
50	9010.6	78	8997.9	55	8807.9	9
51	8995.4	61	8994.6	97	8803.3	4
52	8981.2	65	8988.5	22	8801.6	22
53	8977.7	22	8980.8	9	8783.7	26
54	8965.8	55	8967.1	4	8783.0	55
55	8959.9	39	8932.8	26	8774.6	58
90	8569.1	41	8530.8	14	8331.8	45
91	8528.3	83	8515.9	83	8257.2	74
92	8527.6	38	8511.8	74	8241.4	56
93	8457.6	74	8496.7	93	8224.6	3
94	8390.0	35	8410.3	35	8217.5	35
95	8388.7	51	8390.1	45	8183.3	64
96	8308.2	64	8357.1	64	8141.9	63
97	8303.6	56	8285.7	56	8083.8	41
98	8280.8	45	8188.4	51	8075.2	36
99	8242.2	63	8186.7	63	7502.2	38
100	8126.5	36	8083.3	36		86

Table 7-1: Realization number in order of oil production rates – 16 x 12 grid

Statistics	8 x 6	16 x 12	32 x 24	64 x 48	128 x 96
M = 0.4					
Mean	0.6228	0.6199	0.6149	0.6062	0.6008
SD	0.0044	0.0084	0.0102	0.0115	0.012
Coefficient of variance	0.007	0.0136	0.0166	0.0189	0.02
Max	0.63	0.6334	0.6332	0.6228	0.6243
Upper q	0.6255	0.6256	0.6226	0.6153	0.6102
Median	0.6236	0.6213	0.6155	0.6068	0.6012
Lower q	0.6212	0.6167	0.6081	0.5995	0.5928
Min	0.6002	0.5935	0.5832	0.5791	0.5698
IR	0.0043	0.0089	0.0145	0.0158	0.0174
% from RF 128 x 96	2.51	2.52	2.03	0.84	0
M = 1					
Mean	0.5392	0.5347	0.5307	0.5249	0.5217
SD	0.0111	0.0138	0.0155	0.0162	0.0165
Coefficient of variance	0.0205	0.0259	0.0291	0.0309	0.0317
Max	0.5578	0.5596	0.5624	0.5605	0.5587
Upper q	0.5475	0.5448	0.5427	0.5375	0.5336
Median	0.5415	0.5382	0.5312	0.5248	0.5217
Lower q	0.5348	0.5259	0.5204	0.5143	0.5126
Min	0.5112	0.497	0.4866	0.4775	0.4775
IR	0.0127	0.0189	0.0223	0.0232	0.021
% from RF 128 x 96	2.6	2.1	1.71	0.73	0
M = 1.8					
Mean	0.3952	0.3863	0.3794	0.3718	0.3664
SD	0.0079	0.011	0.0127	0.0131	0.0133
Coefficient of variance	0.0201	0.0285	0.0335	0.0353	0.0362
Max	0.4096	0.406	0.4019	0.3998	0.3959
Upper q	0.4015	0.3941	0.3903	0.3829	0.3763
Median	0.3967	0.3869	0.3794	0.3725	0.3664
Lower q	0.3903	0.3793	0.3702	0.3624	0.356
Min	0.367	0.3486	0.3525	0.3393	0.3329
IR	0.0112	0.0148	0.0201	0.0205	0.0205
% from RF 128 x 96	6.7	4.73	3.72	1.75	0

Table 7-2: Summary statistics on recovery factors

Statistics	8 x 6	16 x 12	32 x 24	64 x 48	128 x 96
M = 0.4					
Mean	0.3496	0.3677	0.3811	0.383	0.3833
SD	0.0214	0.0218	0.0227	0.0228	0.0227
Coefficient of variance	0.0611	0.0593	0.0594	0.0596	0.0592
Max	0.3937	0.4106	0.4327	0.4328	0.4328
Upper q	0.3642	0.3851	0.3991	0.4012	0.4012
Median	0.3513	0.3648	0.3829	0.3842	0.386
Lower q	0.3316	0.3541	0.362	0.3635	0.3643
Min	0.291	0.315	0.3301	0.3302	0.3303
IR	0.0326	0.031	0.0371	0.0377	0.0369
% from BT 128 x 96	8.79	4.07	0.57	0.08	0
M = 1					
Mean	0.246	0.2584	0.2663	0.2606	0.2577
SD	0.0197	0.0229	0.0261	0.0267	0.0268
Coefficient of variance	0.0802	0.0886	0.0978	0.1025	0.104
Max	0.2869	0.3209	0.3216	0.3213	0.3155
Upper q	0.2631	0.2733	0.282	0.2784	0.2763
Median	0.2419	0.2597	0.26676	0.2623	0.2564
Lower q	0.2328	0.2387	0.2447	0.2392	0.2376
Min	0.204	0.2062	0.2056	0.1937	0.1953
IR	0.0303	0.0346	0.0373	0.0392	0.0387
% from BT 128 x 96	4.54	-0.27	-3.34	-1.13	0
M = 1.8					
Mean	0.1108	0.1197	0.1232	0.1221	0.12
SD	0.0078	0.0119	0.0127	0.0153	0.0149
Coefficient of variance	0.0704	0.0991	0.103	0.1251	0.1241
Max	0.129	0.142	0.153	0.1596	0.1637
Upper q	0.1156	0.1282	0.1335	0.1337	0.1297
Median	0.1109	0.1202	0.1252	0.1211	0.1203
Lower q	0.1059	0.1126	0.1128	0.1135	0.1102
Min	0.0864	0.0868	0.0855	0.0873	0.0907
IR	0.0097	0.0156	0.0207	0.0202	0.0195
% from BT 128 x 96	7.67	0.25	-2.67	-1.75	0

Table 7-3: Summary statistics on breakthrough times (PVWI at ~ 0.01 WCT)

No.	Realization 33			Realization 36		
	M = 0.4	M = 1	M = 1.8	M = 0.4	M = 1	M = 1.8
1	0.044	0.044	0.043	0.044	0.043	0.044
2	0.08	0.079	0.077	0.076	0.075	0.077
3	0.107	0.106	0.108	0.109	0.107	0.107
4	0.178	0.176	0.176	0.174	0.18	0.179
5	0.249	0.247	0.248	0.25	0.253	0.251
6	0.32	0.317	0.316	0.315	0.317	0.318
7	0.39	0.387	0.392	0.39	0.393	0.389
8	0.47	0.467	0.47	0.466	0.468	0.467
9	0.532	0.528	0.531	0.531	0.532	0.533
10	0.594	0.599	0.595	0.596	0.597	0.595
11	0.665	0.661	0.663	0.661	0.662	0.661
12	0.736	0.732	0.733	0.736	0.737	0.738

Table 7-4: Grid 16 x 12 - different PVWI for water saturation display

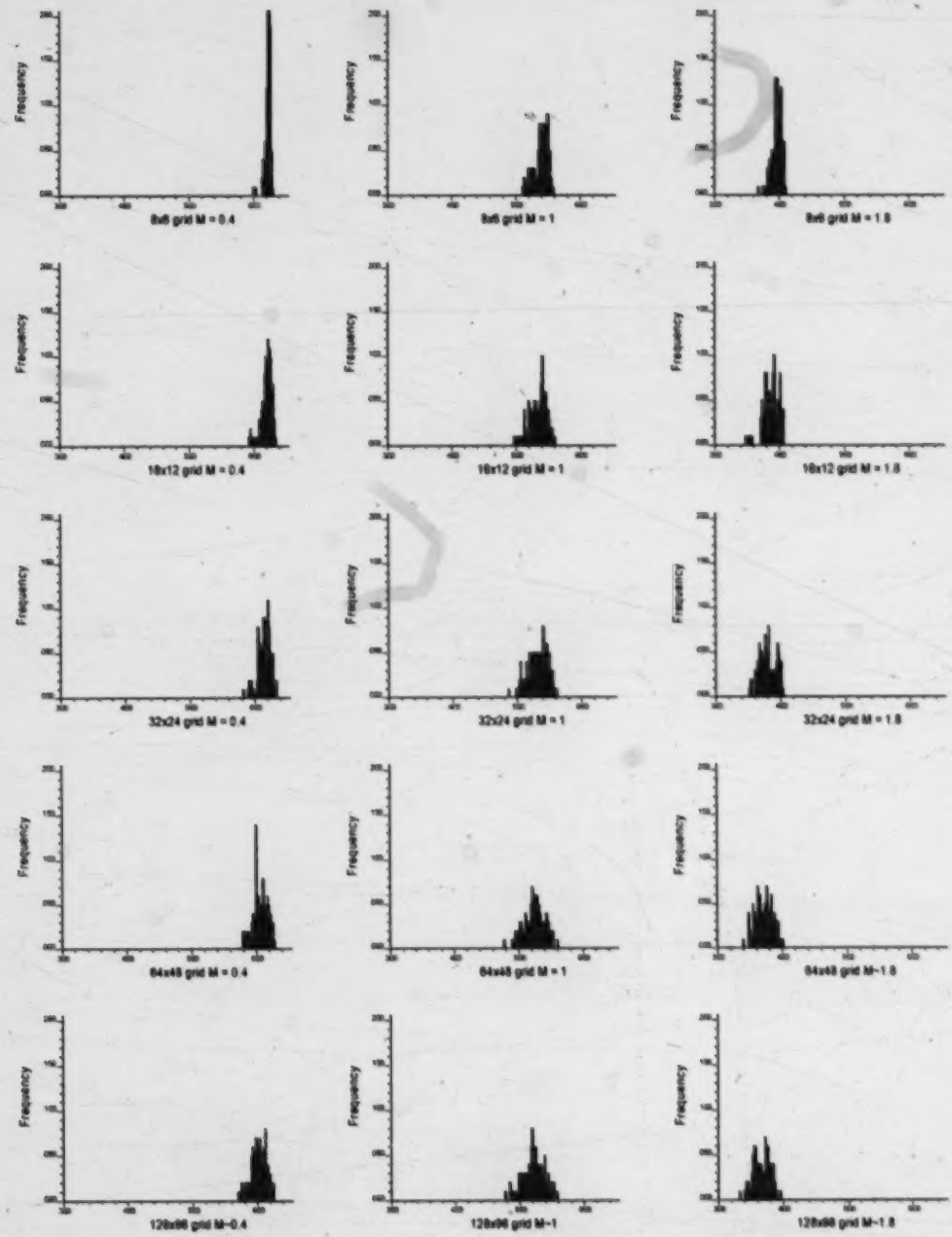
Frequency
8x8 grid M = 0.4
8x8 grid M = 1
8x8 grid M = 1.8
16x12 grid M = 0.4
16x12 grid M = 1
16x12 grid M = 1.8
32x24 grid M = 0.4
32x24 grid M = 1
32x24 grid M = 1.8
64x48 grid M = 0.4
64x48 grid M = 1
64x48 grid M=1.8
128x96 grid M=0.4
128x96 grid M=1
128x96 grid M=1.8

Figure 7-1: Histograms of recovery factors at 1 PVWI for all grids and mobility ratios

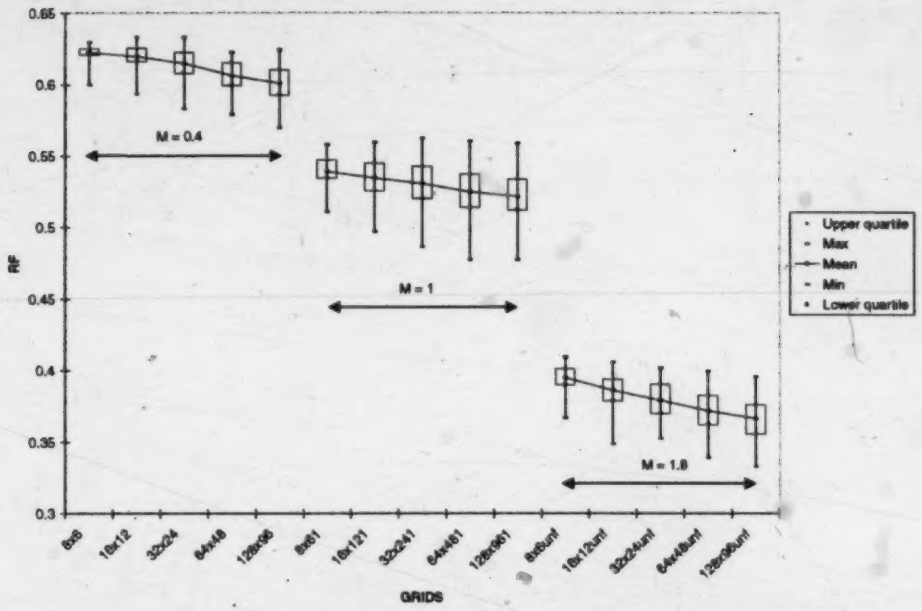

Figure 7-2: Box plot of recovery factors measured at 1 PVWI for different grids and M

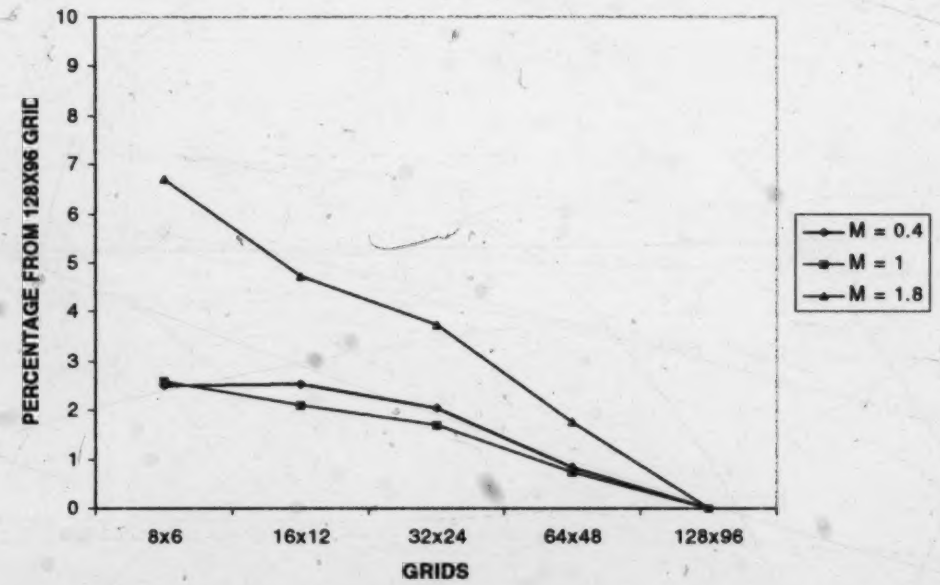

Figure 7-3: Percentage differences in RF means from the RF mean for the 128 x 96 grid

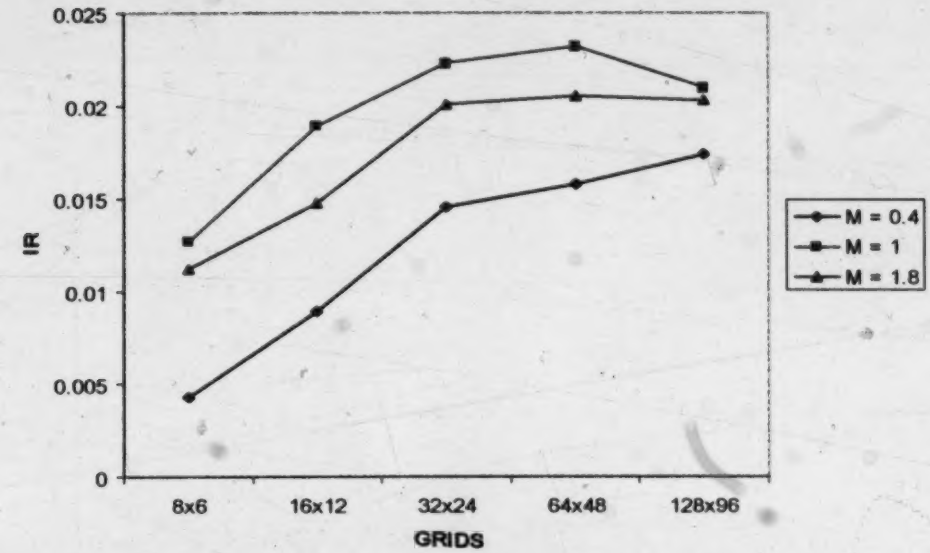

Figure 7-4: Interquartile range of RFs for different grids and mobility ratios

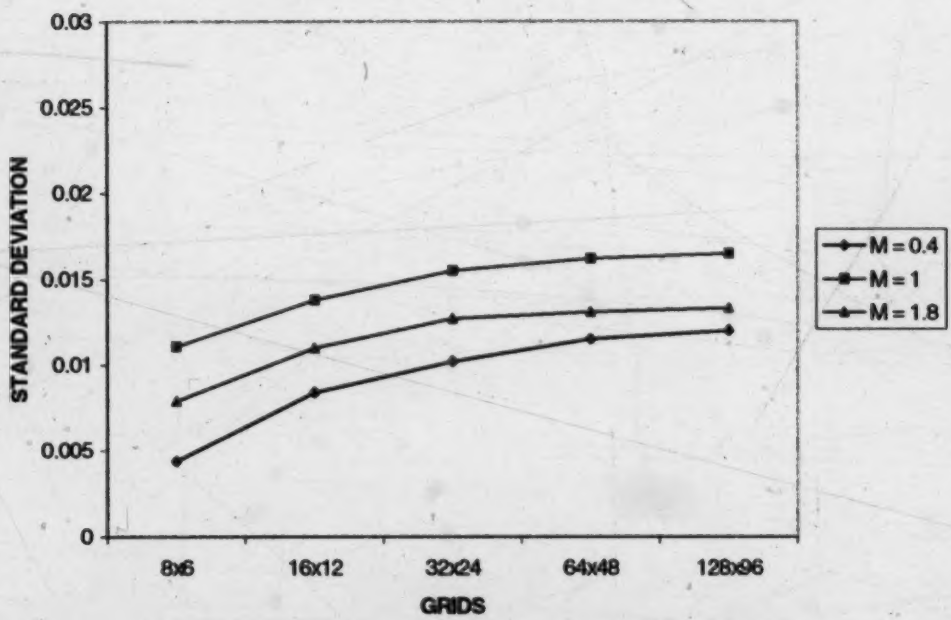

Figure 7-5: RF's standard deviation for different grids and mobility ratios

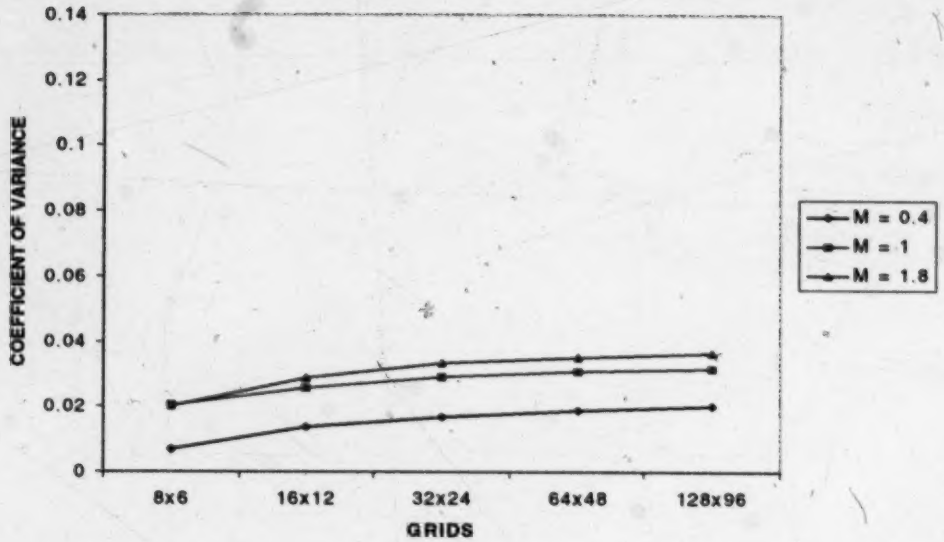

Figure 7-6: RF's coefficients of variance for different grids and mobility ratios

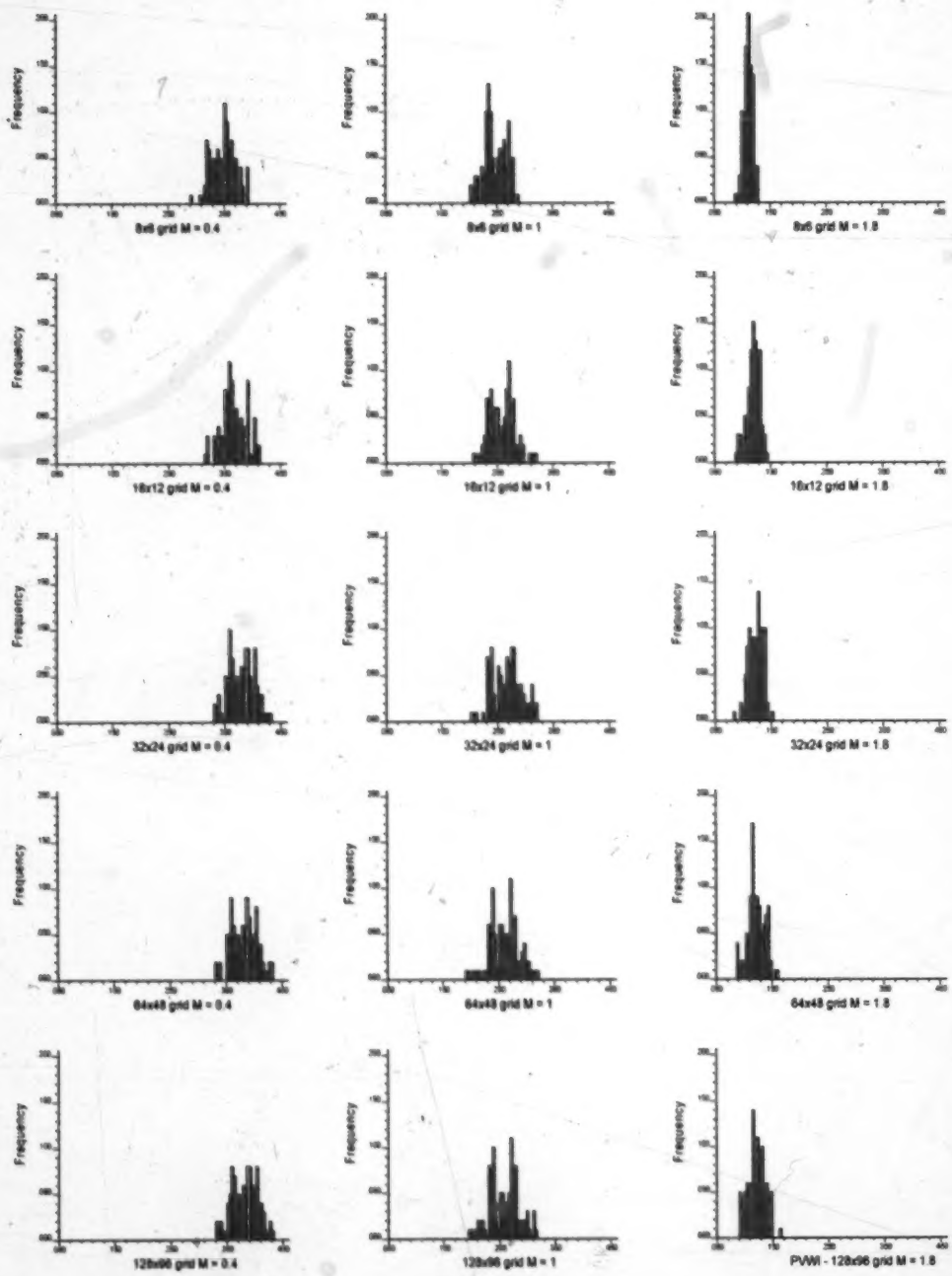
Frequency
8x6 grid M = 0.4
8x6 grid M = 1
8x6 grid M = 1.8
16x12 grid M = 0.4
16x12 grid M = 1
16x12 grid M = 1.8
32x24 grid M = 0.4
32x24 grid M = 1
32x24 grid M = 1.8
64x48 grid M = 0.4
64x48 grid M = 1
64x48 grid M = 1.8
128x96 grid M = 0.4
128x96 grid M = 1
PVWI - 128x96 grid M = 1.8

Figure 7-7: Histograms of BTs measured in PVWI at ≈ 0.01 WCT for all grids

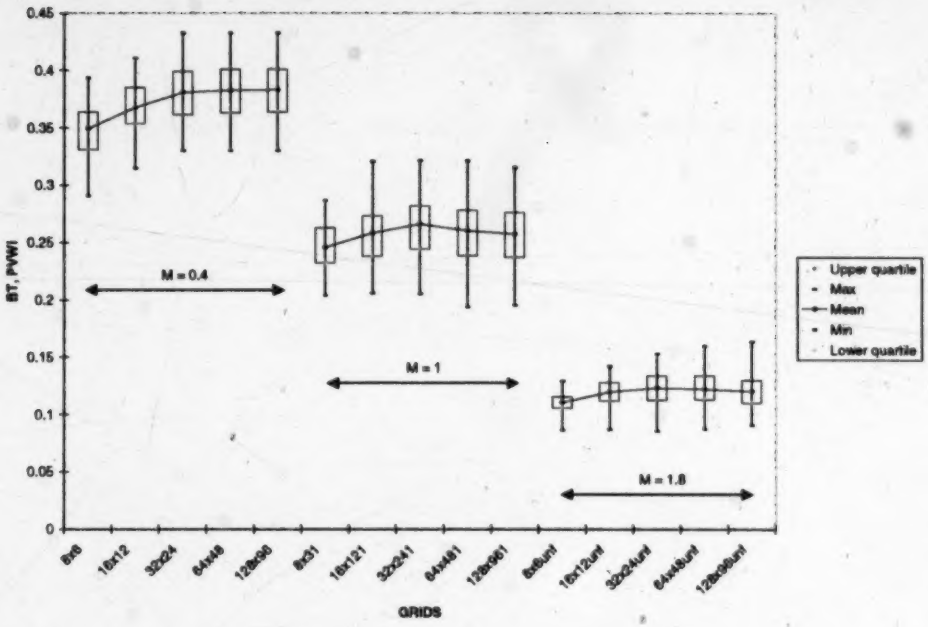

Figure 7-8: Box plot of breakthrough times for different grids and mobility ratios

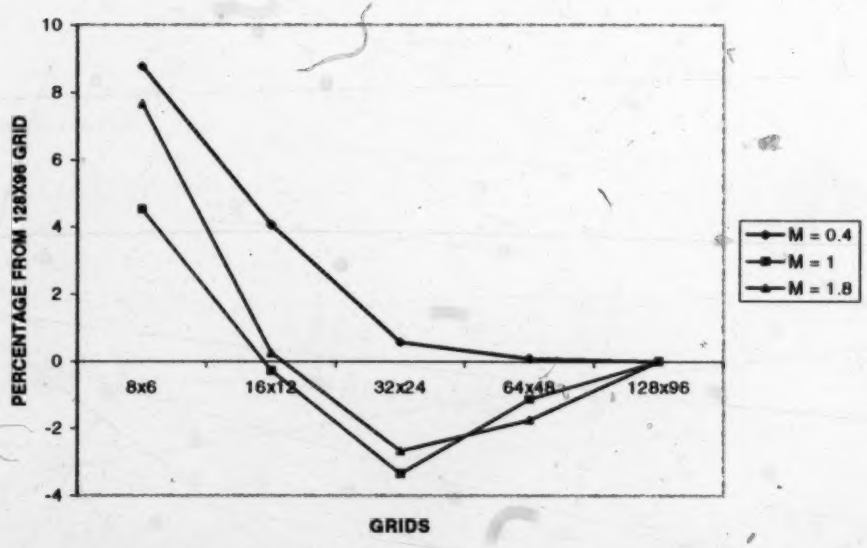

Figure 7-9: Percentage differences in BT means from the BT mean of the 128 x 96 grid

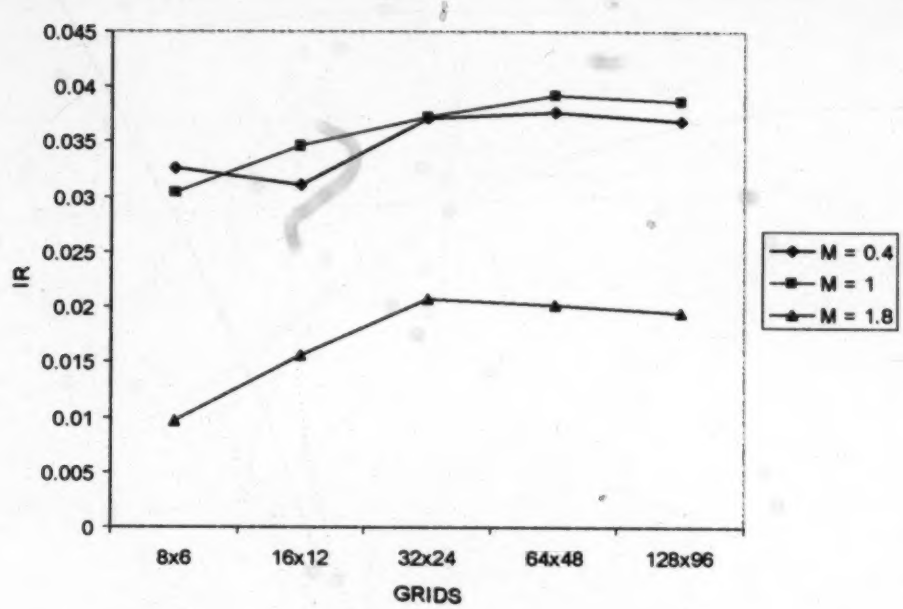

Figure 7-10: Interquartile range for BTs for different grids and mobility ratios

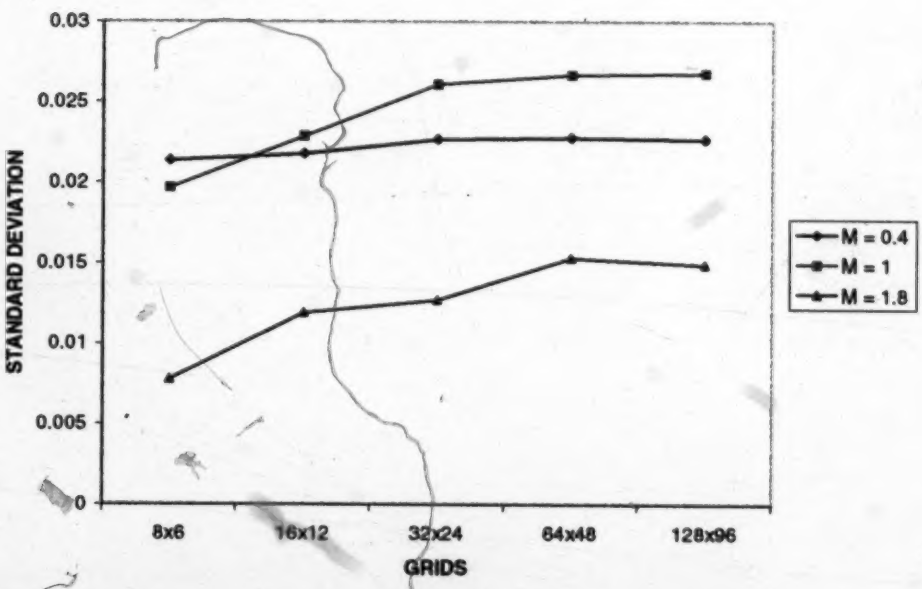

Figure 7-11: BT's standard deviation for different grids and mobility ratios

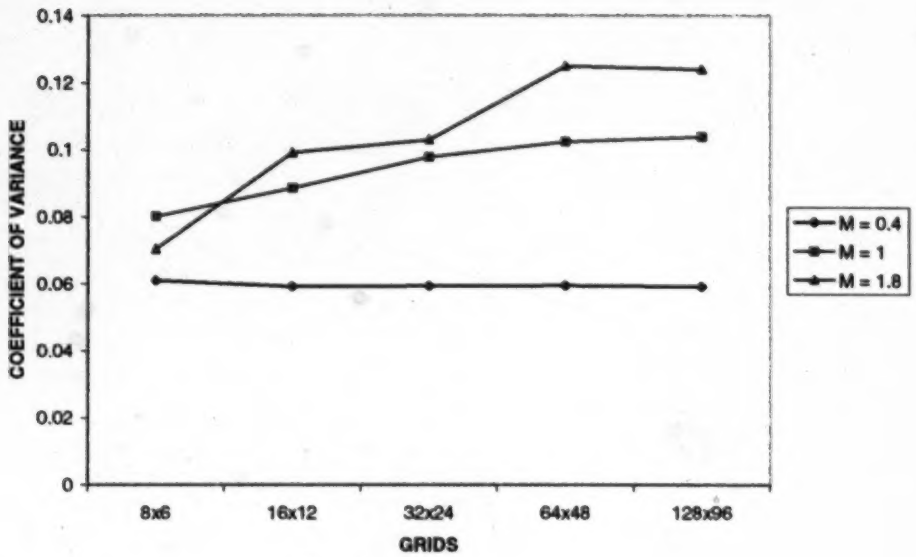

Figure 7-12: BT's coefficients of variance for different grids and mobility ratios

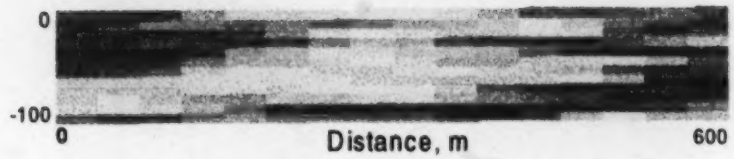

Figure 7-13: Realization 33, 16 x 12 grid – porosity distribution (see color scale in 3-12)

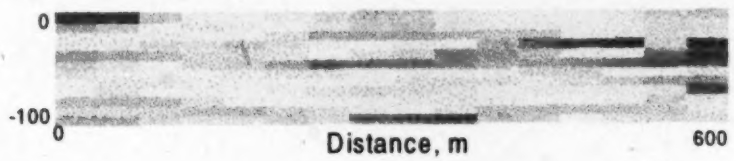

Figure 7-14: Realization 33, 16 x 12 grid – permeability distribution (see color scale on 3-13)

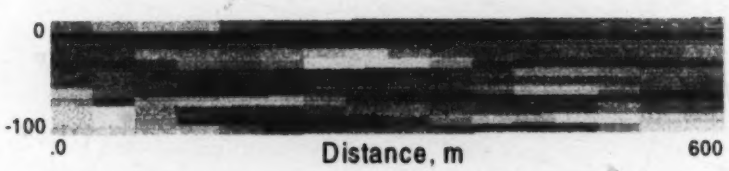

Figure 7-15: Realization 36, 16 x 12 grid – porosity distribution (see color scale on 3-12)

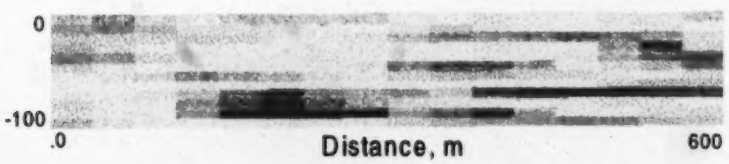

Figure 7-16: Realization 36, 16 x 12 grid – permeability distribution (see color scale on 3-13)

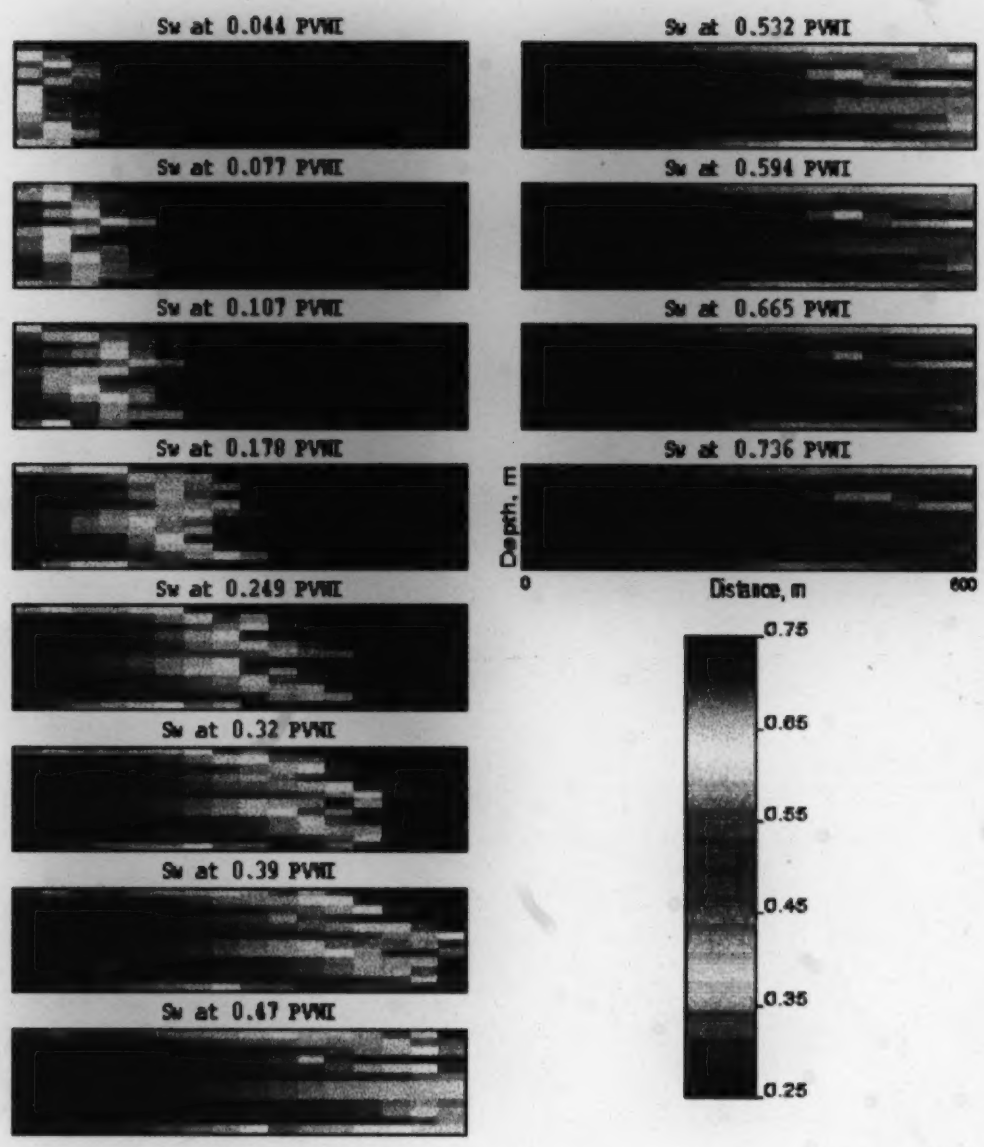

Figure 7-17: Realization 33, water saturation profile at different PVWI, for M = 0.4

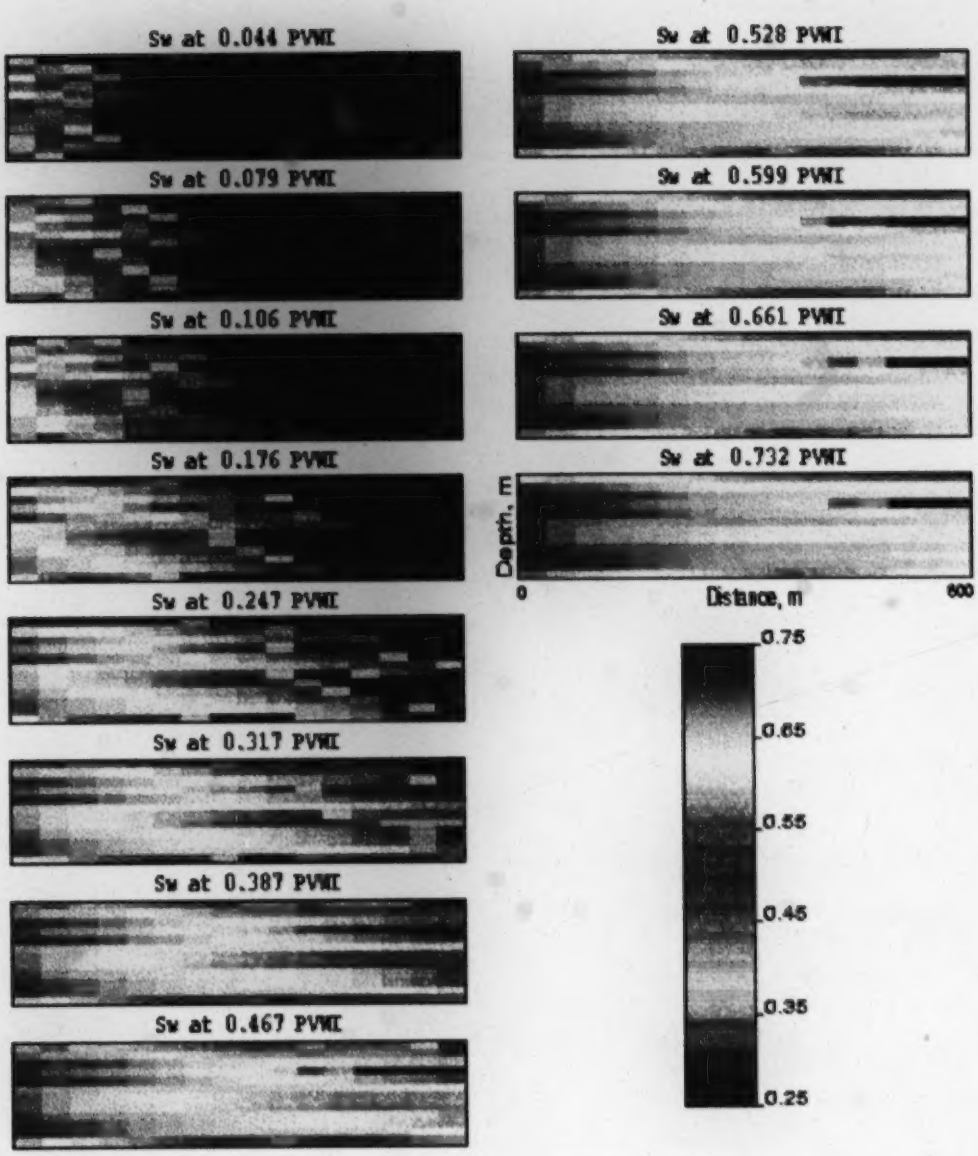

Figure 7-18: Realization 33, water saturation profile at different PVWI, for M = 1

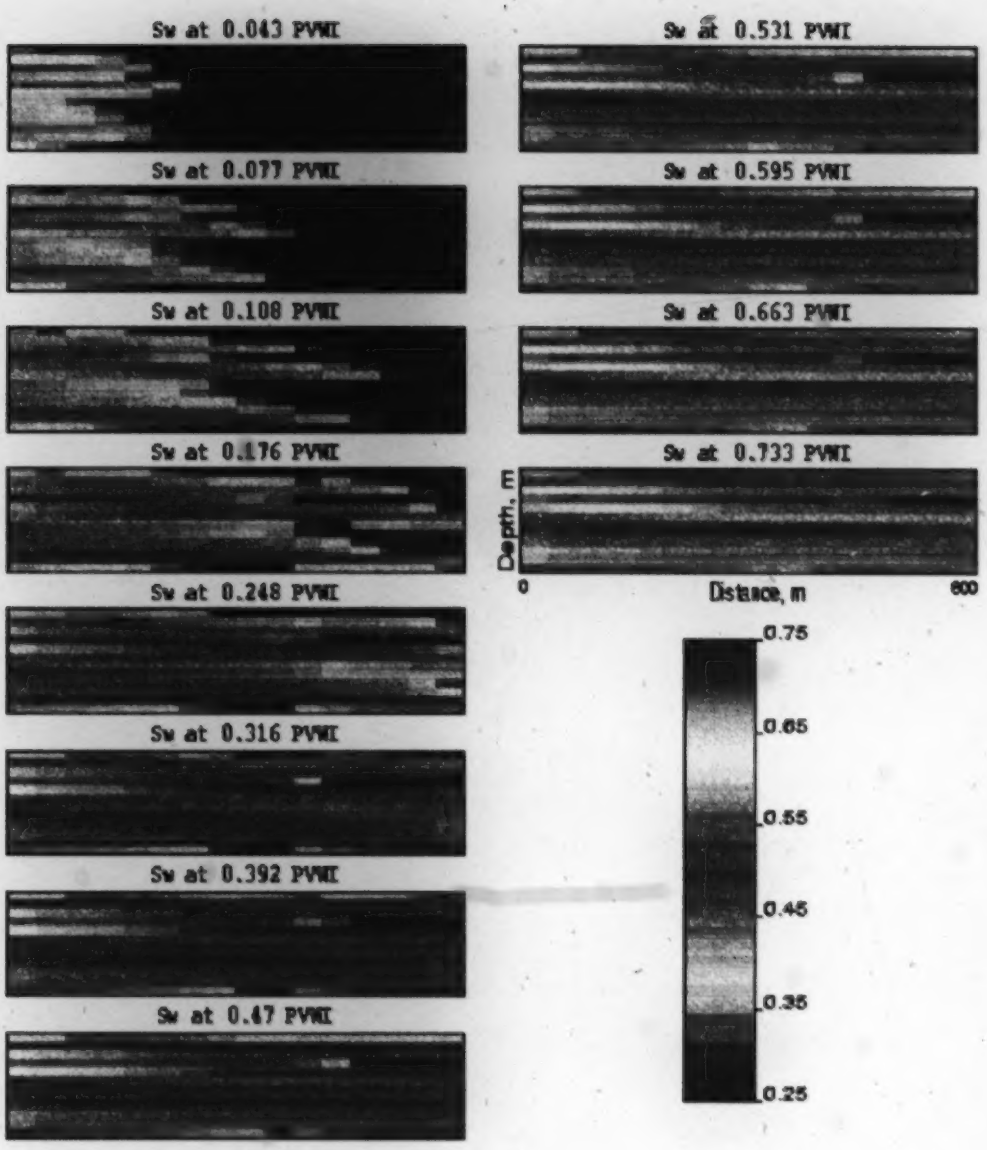

Figure 7-19: Realization 33, water saturation profile at different PVWI, for M = 1.8

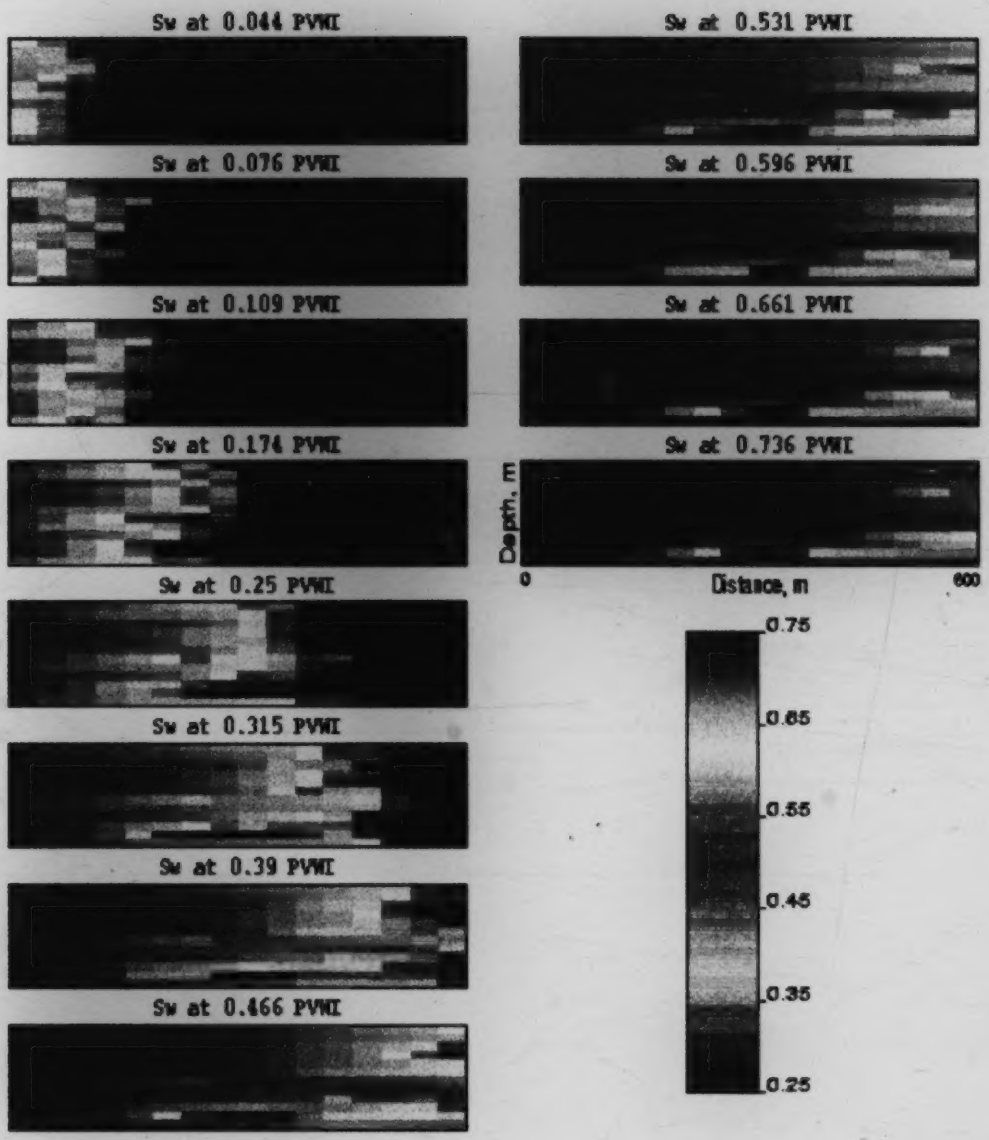

Figure 7-20: Realization 36, water saturation profile at different PVWI, for M = 0.4

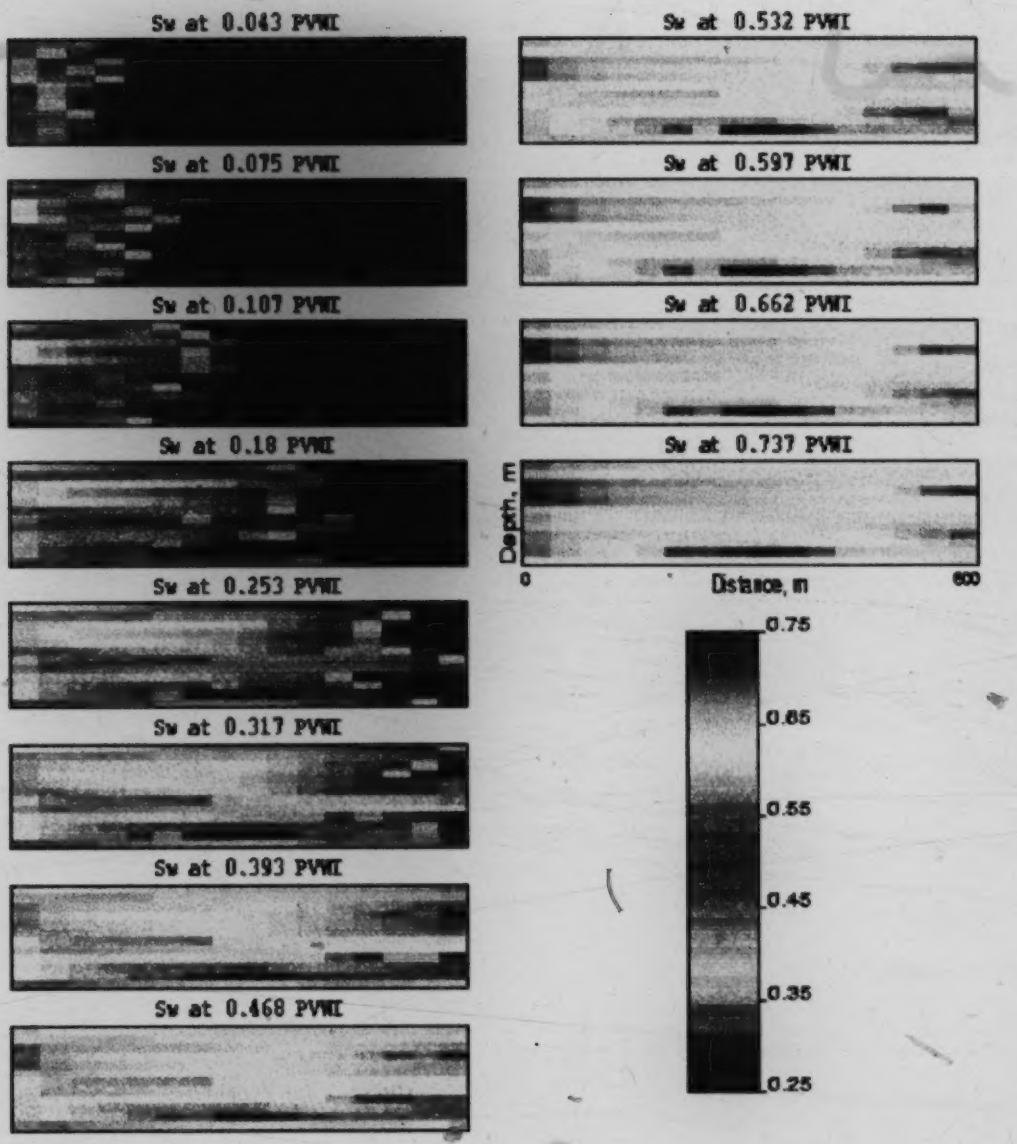

Figure 7-21: Realization 36, water saturation profile at different PVWI, for M = 1

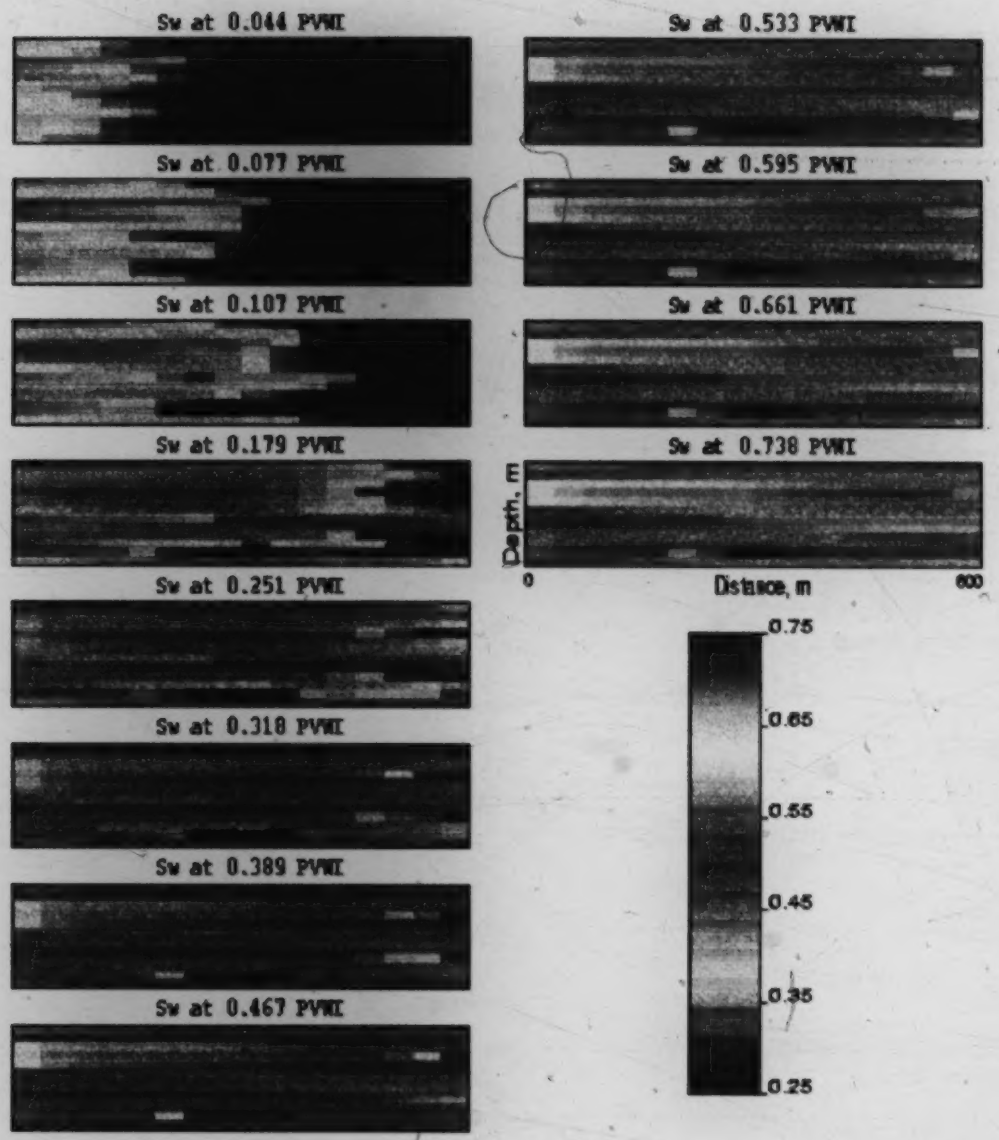

Figure 7-22: Realization 36, water saturation profile at different PVWI, for M = 1.8

VIII. ANALYSIS OF VARIANCE

From the Eclipse simulation results for one hundred realizations and different discretizations, it can be seen that there is uncertainty in the key reservoir performance parameters. This uncertainty is caused by different factors: uncertainty due to the lack of data (different reservoir models from different geostatistical realizations), discretization (related with scaling), and the nature of fluids in the reservoir (different mobility ratios). The question now is how these factors contribute to the overall uncertainty during reservoir simulation. In other words, how quantitatively the overall variability in simulation of reservoir performance parameters is caused by the variability related to these factors. Analysis of variance (ANOVA) is a statistical technique to help to quantify the contribution of different factors to the total variability of the parameters of interest.

The basic problem to which ANOVA is applied is the determination of which part of the variation in the population is due to systematic reasons (called factors) and which part is due to chance [17]. Scheffe [18] defines ANOVA as a statistical technique for analyzing measurements that depend on several kinds of effects operating simultaneously to decide which kinds of effects are important and to estimate the magnitude of these effects. Depending on the number of factors, analysis of variance gives rise to one-way (single factor), two-way (two-factor) or multiple factor models.

1. Theoretical background

1.1. One-factor model

Suppose that we are interested in comparing the means of J different populations, and that we therefore have J samples, one from each population. The sample size of the j^{th} sample is n_j (j = 1, 2,..., J). In this model, the total variation in a set of J samples is divided into two parts: 1) the variation between J samples, and 2) the variation within

the J samples. A model for the composition of any observed value y_{ij}, corresponding to the i^{th} observation in the j^{th} sample, is a linear model [19].

$$y_{ij} = \mu + \tau_j + \varepsilon_{ij} \quad \text{with } j = 1, 2, \ldots, J \quad i = 1, 2, \ldots, n_j \tag{8-1}$$

According to this model, an observation is the sum of three components:

1. The grand mean μ of the "combined" population $\mu = \sum_{j=1}^{J}\sum_{i=1}^{n_j} y_{ij} \Big/ \sum_{j=1}^{J} n_j$
2. A treatment effect τ_j associated with the particular population from which the observation is taken
3. A random-error term ε_{ij}

Equation (8-1) can be written in a form:

$$y_{ij} = \mu_j + \varepsilon_{ij} \tag{8-2}$$

An ANOVA procedure consists of calculating a number of sums of squares (SS). The total sum of squares of the deviation of all measurements with respect to the general mean, called the corrected sums of squares, is given by the following equation:

$$\sum_{j=1}^{J}\sum_{i=1}^{n_j}(y_{ij} - \mu)^2 = \sum_{j=1}^{J}\sum_{i=1}^{n_j}(y_{ij} - \mu_j)^2 + \sum_{j=1}^{J} n_j(\mu_j - \mu)^2$$

$$SS_{TOTAL} = SS_{WITHIN} + SS_{BETWEEN} \tag{8-3}$$

The proof of this equation can be found in [19, p.657]. From Equation (8-3), it can be seen that the total variation has been separated into two sources, between samples and within samples. For each of these sources, a mean square (MS) value can be

determined by taking the ratio of the SS and its degrees of freedom (df). Mean square values are the corresponding variance values.

1.2. Two-factor model

If an investigation of the simultaneous effects of two factors on a variable is necessary, the two-factor model should be used. This model enables examination of the main effects of separate factors as in the one-factor model: the variability that is due to a single variable, and the interaction effect: the variability that is due to the combination of factors [19]. Suppose there are J levels of the first factor and K levels of the second factor, and that there are n observations for each combination of one level from each factor. If y_{ijk} denotes the i^{th} observation in the group with level j on the first factor and level k on the second factor, then the model may be written as follows:

$$y_{ijk} = \mu + \tau_j + \lambda_k + (\tau\lambda)_{jk} + \varepsilon_{ijk} \qquad \begin{matrix} \text{with } i = 1,\ldots,n; \\ j = 1,..,J; \\ k = 1,\ldots,K \end{matrix} \qquad (8\text{-}4)$$

The observation is calculated using five components:

1. A grand mean μ over the entire population
2. A treatment effect τ_j associated with the particular level (j^{th} level) of the first factor
3. A treatment effect λ_k associated with the particular level (k^{th} level) of the second factor
4. An interaction effect $(\tau\lambda)_{jk}$ associated with the particular combination of the j^{th} level of the first factor and the k^{th} level of the second factor
5. A random error-term ε_{ijk}

Suppose that the number of observations in the treatment combination jk is n, the total number of observations for level j is Kn, and the total number of observations for level

k is Jn. The sample mean for the n observations in the treatment jk combination is denoted by $\bar{y}_{jk}$, the sample mean for the Kn observations in factor level j is $\bar{y}_j$, and the sample mean for the Jn observations in factor level k is $\bar{y}_k$. The total sum of squares is calculated from four components [19]:

$$SS_{TOTAL} = \sum_{i}^{n}\sum_{j=1}^{J}\sum_{k=1}^{K}\left(y_{ijk} - \mu\right)^2$$

$$SS_{COLUMN}\,(factor\ \tau) = \sum_{j=1}^{J} Kn(\bar{y}_j - \mu)^2$$

$$SS_{ROW}\,(factor\ \lambda) = \sum_{k=1}^{K} Jn(\bar{y}_k - \mu)^2 \qquad (8\text{-}5)$$

$$SS_{WITHIN}\,(error) = \sum_{i=1}^{n}\sum_{j=1}^{J}\sum_{k=1}^{K}(y_{ijk} - \bar{y}_{jk})^2$$

$$SS_{INTERACTION} = \sum\sum n(\bar{y}_{jk} - \bar{y}_j - \bar{y}_k + \mu)^2$$

2. *ANOVA of simulated data*

In the previous chapter, the recovery factors at 1 PVWI and the breakthrough times were recorded and analyzed. In this part, ANOVA will be applied to these two parameters.

2.1. Recovery factors at 1 PVWI

Single factor model

In this model, the discretization is considered to be a factor. The variability of the RFs between realizations is the variability within a group. Table 8-1 summarizes the ANOVA analysis for the single factor model for three mobility ratio cases. Figure 8-1 illustrates the contribution of the different sources of variation for the different

mobility ratio cases. From Figure 8-1, it can be seen that the total variation is biggest for the mobility ratio case of 1 (0.129) and smallest for the favorable mobility ratio case (0.081). In all three mobility ratio cases, the variation due to discretization is smaller than the variation due to different realizations. If the relative contribution of two sources is compared, it can be seen that the discretization effect contributes less to the total variation in the case of the mobility ratio of 1 (about 16 %) followed by the case of mobility ratio of 0.4 (about 42 %) and M = 1.8 (about 43 %).

The reason why the variability in the RFs is less due to discretization, and more due to the realization, for the unit mobility ratio case is probably, for this mobility ratio, there is a no-win situation where there is no dominant flow of either water or oil. Different realizations with different spatial continuity become more important in determining the flow paths of the fluids in a reservoir. Therefore, the variation due to different realizations contributes more to the total variation in the recovery factors at 1 PVWI.

Two factor model

The two factors to be considered in ANOVA are mobility ratio and discretization. Different realizations are considered replications within a group. For the two factor model, the number of replications within different groups should be the same. The data for Realization 86, M = 1.8, could not be obtained because the run did not complete successfully. Therefore, the values for the RF as well as for the BT for this realization were taken from Realization 87. This assumption was made based on the fact that there were not big differences between the values of RFs and BTs from realization to realization. A summary of the results for the ANOVA analysis for the two factor model is given in Table 8-2. Figure 8-2 illustrates the contribution of the different factors to the total variance of the RFs. From this figure, it is obvious that the dominant source of variation is the mobility ratio ≈ 97.7 %. The part of the variation that is due to different realizations is ≈ 1.6 %. Discretization contributes ≈ 0.7 %, and

the interaction effect between mobility ratio and discretization is very small (≈ 0.03 %).

2.2. Breakthrough times

Single factor model

Similar to the RF case, ANOVA for the BT parameter was implemented. The factor is the discretization. Table 8-3 and Figure 8-3 summarize the results of the ANOVA analysis. A mobility ratio case of 1.8 has the smallest variation of BTs (0.091), followed by M = 1 (0.325) and M = 0.4 (0.333). The proportion of the variation due to discretization is 26, 7 and 11 % for M = 0.4, 1 and 1.8, respectively. Again, the percentage is smallest for the mobility ratio of 1. The reason for this observation can be explained similarly to that for the ANOVA for the RFs.

Two factor model

Table 8-4 and Figure 8-4 summarize the results of the ANOVA analysis for the single factor model for the BT parameter. The two factors are discretization and mobility ratio. Different realizations are considered as replications by chance within each group. Although the exact proportion of the different sums of squares is different, the variation in BT due to mobility ratio is the biggest (95.6 %). Discretization effects contribute less to the total variation than uncertainty in the geological model (resulted in different realizations)(0.5 and 3.7 %, respectively). The variation due to the interaction effect between mobility ratio and discretization is the smallest (0.15 %).

The results of the ANOVA analysis mentioned above were obtained from the 2-D reservoir model. One should be very careful about extending these results to a 3-D reservoir model because the behavior of the fluid flow in 3-D model is more complicated than in a 2-D model.

M = 0.4				
Sources of variation	**Locations**	**SS**	**df**	**MS**
Discretizations	Between Groups	0.034	4	0.00851
Realizations	Within Groups	0.047	495	0.00010
Total		**0.081**	**499**	
M = 1				
Sources of variation	**Locations**	**SS**	**df**	**MS**
Discretizations	Between Groups	0.020	4	0.00505
Realizations	Within Groups	0.109	495	0.00022
Total		**0.129**	**499**	
M = 1.8				
Sources of variation	**Locations**	**SS**	**df**	**MS**
Discretizations	Between Groups	0.052	4	0.01307
Realizations	Within Groups	0.069	494	0.00014
Total		**0.122**	**498**	

Table 8-1: Summary of single factor ANOVA for recovery factors

Sources of variation	**Locations**	**SS**	**df**	**MS**
Mobility ratio	Row	13.966	2	6.9830
Discretization	Column	0.102	4	0.0255
M and discretization	Interaction	0.005	8	0.0006
Realizations	Within	0.225	1485	0.0002
Total		**14.298**	**1499**	

Table 8-2: Summary of two factor ANOVA for recovery factors

M = 0.4				
Sources of variation	**Locations**	**SS**	**df**	**MS**
Discretizations	Between Groups	0.085	4	0.0212
Realizations	Within Groups	0.248	495	0.0005
Total		**0.333**	**499**	
M = 1				
Sources of variation	**Locations**	**SS**	**df**	**MS**
Discretizations	Between Groups	0.022	4	0.0055
Realizations	Within Groups	0.303	495	0.0006
Total		**0.325**	**499**	
M = 1.8				
Sources of variation	**Locations**	**SS**	**df**	**MS**
Discretizations	Between Groups	0.0096	4	0.0024
Realizations	Within Groups	0.0816	494	0.0002
Total		**0.0913**	**498**	

Table 8-3: Summary of single factor ANOVA for breakthrough times

Sources of variation	**Locations**	**SS**	**df**	**MS**
Mobility ratio	Row	16.153	2	8.0766
Discretization	Column	0.091	4	0.0227
M and discretization	Interaction	0.026	8	0.0032
Realizations	Within	0.632	1485	0.0004
Total		**16.902**	**1499**	

Table 8-4: Summary of two factor ANOVA for breakthrough times

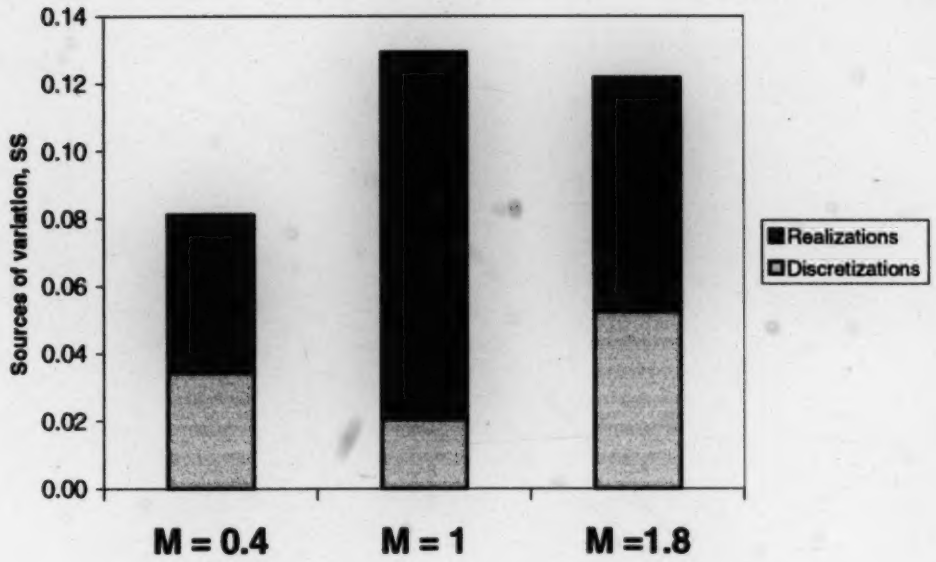

Figure 8-1: Single factor ANOVA for recovery factors at 1 PVWI

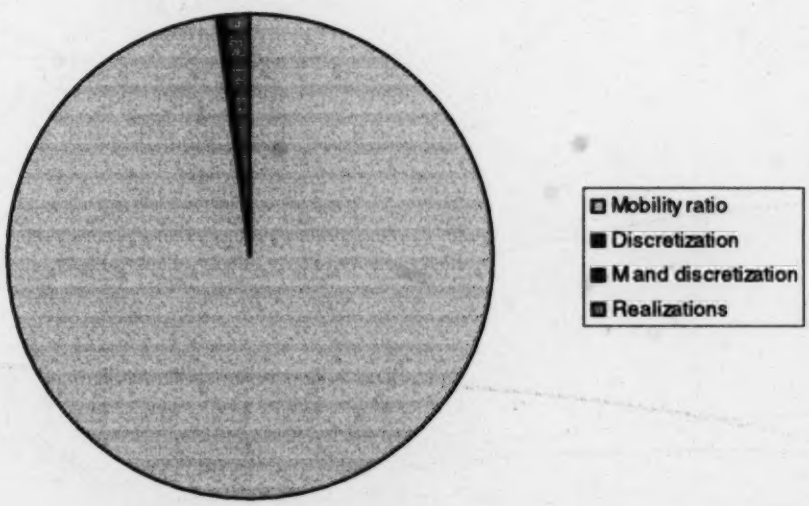

Figure 8-2: Two factor ANOVA for recovery factors at 1 PVWI

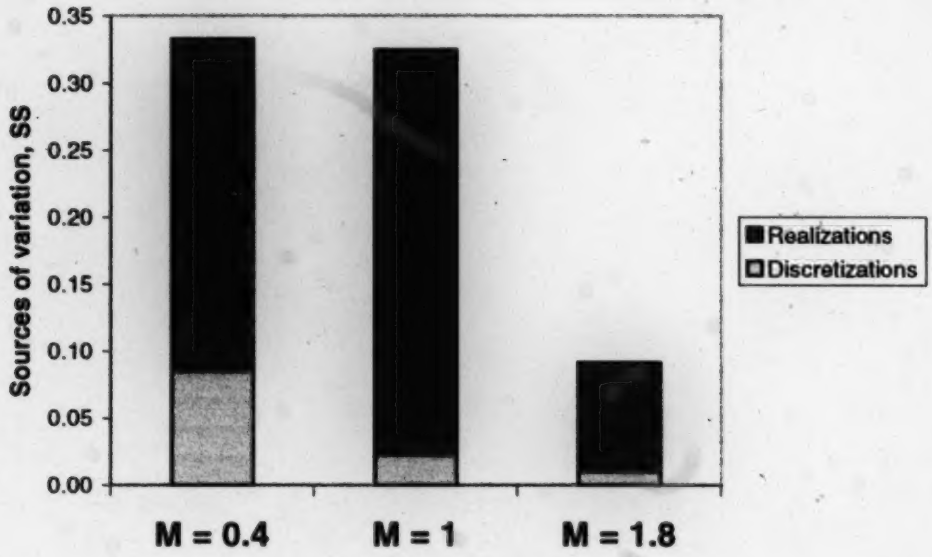

Figure 8-3: Single factor ANOVA for breakthrough times

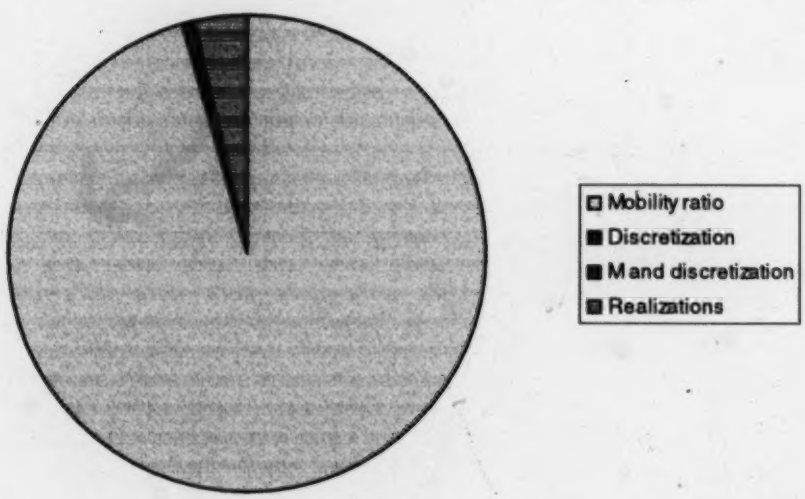

Figure 8-4: Two factor ANOVA for breakthrough times

IX. RANKING FOR FAST UNCERTAINTY ASSESSMENT

1. Motivation for ranking

Uncertainty in any geological model is unavoidable given the scarcity of data available for the modeling of reservoir heterogeneities. Uncertainty involves the risk of making an incorrect decision because the estimates do not agree with reality. Therefore, analysis of the uncertainty associated with a reservoir production forecast is a central concern in the decision making process [20]. In many situations, in order to assess the uncertainty in the geological model, and therefore in the reservoir flow parameters, a large number of geological realizations are constructed. A full flow simulation approach, which involves a simulation for each of the realizations using very fine grids, requires a large amount of CPU time.

An option to reduce the computational effort is to use different ranking techniques. The central idea behind ranking realizations is to use some simple measures to rank the realizations, and then to run the full flow simulation with fewer realizations, say the 5 % - low, 50 % - expected and 95 % - high ones. This allows bounding the uncertainty without performing a large number of fine-scale flow simulations. A simple measure is a good ranking statistic when it correctly identifies low and high realizations [20]. Realization rank is scenario dependent. Ideally, a ranking methodology should lead to the same rank obtained with the flow response of interest [21].

There are several situations where ranking geostatistical realizations is problematic. The first such situation is when each realization leads to nearly the same answer; that is, when the presence of stochastic heterogeneities is more important than the specific differences between the realizations. The second situation is when the aspect of uncertainty being assessed is easy to calculate; for example, the uncertainty in pore volume may be directly assessed by calculating the pore volume of all realizations.

The last situation is when there are so many independent reservoir responses of interest that there is no single ranking index which leads to a unique and reliable ranking [20]. In this study, the problem faced is probably the third situation.

Almost all flow parameters depend on some measure of continuity, connectivity or tortuosity. Ranking tools vary in complexity and require knowledge of the specific problem. More information must be known about the reservoir and production plan to rank realizations based on the more complex ranking measures. In the literature to date, there are two main kinds of ranking techniques: ranking with statistical measures based on simple summary statistics and ranking with a simple fast flow model.

2. Ranking with fast flow simulation

For the fast flow simulation technique, recovery factors and breakthrough times were considered for ranking. For every grid discretization and mobility ratio case, values of these parameters were ranked from the highest (rank number 1) to the lowest (rank number 100). The results of the ranking are presented in Appendix 14 (for the RFs) and Appendix 15 (for the BTs). These ranking numbers were used to find the correlation between different grid sizes.

In the process of plotting the ranked numbers, the flow simulation results for the finest 128 x 96 grid were assumed to be the most accurate (closer to being true). The ranking results of the coarser grids were crossplotted against the ranking of the 128 x 96 grid. Figures 9-1 and 9-2 illustrate crossplots for the RFs and the BTs for the M = 0.4 case. The plots for the other mobility ratios are given in Appendix 16. The straight line represents perfect correlation (correlation coefficient of 1). The general observation is that the finer the grid becomes, the closer the points are to the perfect correlation line. One interesting feature of these plots is that they have an ellipsoid form. This feature is more obvious in the BT plots. The plots are comprised of three main groups of

points: points around, points above, and points below the centerline. Further study to examine the reasons behind this effect is undertaken later.

The correlation coefficients from plots of the ranking numbers were recorded and they are shown in Table 9-1. The data were then plotted in Figure 9-3. From this figure, it can be seen that as a grid gets finer, the correlation coefficients increase and become closer to 1. The range of correlation coefficients for the RFs is from 0.59 to 0.99 and that for the BTs is from 0.38 to 0.85. The correlation coefficients for the RFs are bigger than those for the corresponding values for the BTs. The correlation coefficient curves for the different mobility ratio cases are very close together except for the one for the RFs of M = 1. The coefficient for the latter case goes from a relatively low value of 0.59 for the 8 x 6 grid to a value of 0.89 for the next finer (16 x 12) grid, and departs from the other two curves for the RFs.

The conclusion to be drawn, based on the correlation coefficients between the coarser grids and a very fine grid, is that the RFs and BTs of the reservoir can be fairly well to well predicted, based on the simulation results of the very coarse grids. This conclusion is based on the assumption that the response for a very fine grid (128 x 96) is close to the true reservoir response.

3. Study of the "ellipse effect" for breakthrough times

3.1. Changing of realization positions on BT plots

As mentioned earlier, there is a characteristic grouping of realizations on the BT plots. A classification of these realizations into three different groups is possible: earlier, close-to-true and later BTs. Figure 9-4 illustrates this classification for the 8 x 6 grid, M = 0.4 case. The BT plots for the different grids and mobility ratios appear to be different. One question that arises is whether the points representing realizations are in the same groups on the BT plots, or is there a shift in the positions of each

realization for the different grids and mobility ratios. In order to answer this question, a parameter d is introduced. This is the difference in ranking numbers for each realization between the coarser grids and the finest 128 x 96 grid, within the same mobility case.

Changing between different mobility ratios

The difference between ranking numbers was calculated for the 8 x 6 and 128 x 96 grids for all realizations and for all three mobility ratios. Different combinations of the mobility ratios were plotted. Figure 9-5 illustrates the crossplots of the d values. If the d values for a realization for two mobility ratios cases are positive or negative (quadrants I and III), then there is no shift of a group on the BT plots of these mobility cases; that is, the points stay in either earlier or later BT groups, respectively. If the d values change from positive to negative or vice versa (quadrants II and IV), then there is a change in the groups for this mobility pair. From Figure 9-5, it can be seen that a majority of the d values do not change sign. This means that the majority of realizations stays within the same group in the BT plots for different mobility ratios.

Changing between different grids

The d values were calculated for different grids for a mobility ratio of 1. Figure 9-6 illustrates crossplots of the d values for four grid sizes. Again, the tendency is that the d values do not change sign; that is, many realizations stay in the same BT group for different grids.

3.2. Visualizing selected porosity and permeability distributions

The hypothesis that explains why the BT is significantly earlier or later than the true value is that this effect is related to the connectivity of the porosity and permeability models. There may be a loss in reservoir connectivity as one goes from the finest grid

(original geostatistical model) to the coarser models of scaled up porosity and permeability. In the case of earlier BTs for the coarser grids, the fine grid models may consist of not well connected high porosity and/or high permeability streaks, but the averaged porosity and permeability models may round up the values and give a model better connectivity. The flow of oil in the coarser grids will be easier and faster and this leads to earlier BTs. In an opposite scenario, where the BTs are predicted to be later for the coarser grids than for the finest grid, the connectivity for the finest grid is greater than that for the coarser grids. The original continuous and highly permeable zone may be separated into a few disconnected, but still highly permeable zones, in the coarser models. The displacement would go slower through the disconnected zones; therefore, the BTs would be later than the true BTs. These scenarios may happen even though the overall statistics of the original data still can be reproduced. The only difference in the original models and the models from the averaged values is the spatial continuity of the data which may not be reproduced during the averaging process.

In order to prove the hypothesis, a plot of the BT ranking for the 8 x 6 grid, favorable mobility ratio M = 0.4 case was chosen. Several realizations were chosen, and then porosity and permeability distributions were plotted. The data points corresponding to the realization numbers are identified in Figure 9-4. Realizations 68, 44, and 57 were chosen for the earlier than true BT case (lower part of the plot from the centerline), and Realizations 27, 60, and 56 were chosen to illustrate the later than true BT case (upper part of the plot from the centerline) (see Figure 9-4). These realizations have different positions within the "ellipse" of the 8 x 6 grid. Figures 9-7 and 9-8 illustrate the porosity and permeability distributions in the x direction for the 8 x 6 and 128 x 96 grids. From Figure 9-7, it can be seen that it is hard to draw any conclusions about the connectivity of the different realizations. The permeability distributions (Figure 9-8) give more information about the connectivity for the very fine and very coarse grids. Realization 44 shows less connectivity in the finer grid than in the coarser grid. Realizations 60 and 56 show better connectivity in the lower part of the reservoir in

the finer grid than in the coarser grid. The hypothesis appears to be true, but more confirmative evidence is needed before definitive conclusions can be drawn about the "ellipse effect".

3.3. Ranking of BTs based on Cardwell and Parsons' technique

As noted earlier, visually, there is a characteristic difference in the connectivity of reservoir models for earlier and later BTs. In order to investigate the reasons behind the division of the BTs into three groups, earlier, true and later BTs than the true values, and quantify the difference between these different groups, the permeability distributions for the 8 x 6 and 128 x 96 grids were examined. The purpose of the study is to attempt to visualize the difference in the directional permeabilities. This attempt is based on the Cardwell-Parsons method [13] of calculating the effective permeabilities of a group of heterogeneous blocks. As mentioned in the scaling section, these authors concluded that the effective permeability of a group of heterogeneous blocks lies between the arithmetic and harmonic averages. The following procedure was used to calculate the scaled up permeability [22]:

1. The fine-scale blocks in each row are treated as layers in series and an effective permeability is calculated as a harmonic average. The rows are now treated as layers in parallel to calculate effective permeability as an arithmetic average of harmonic averages. The result of this operation gives a lower bound on the possible effective permeability range (it will be called k_{min}).

2. The fine-scale blocks in a column are treated as layers in parallel and the effective permeability is calculated as an arithmetic average of each column. The columns are then treated as layers in series and the effective permeability is calculated as a harmonic average of the arithmetic averages. It is considered to be the upper bound on the possible effective permeability range (it will be called k_{max}).

The next step is to study the relationship between k_{min} and k_{max}.

Permeability values of one hundred realizations for the 8 x 6 and 128 x 96 grids were used to calculate k_{min} and k_{max}. A series of programs written in Turbo Pascal was used to calculate the effective permeabilities. Appendices 17 and 18 show the Turbo Pascal programs used to calculate k_{min} and k_{max} for the 8 x 6 grid. The programs used for the 128 x 96 grids are similar, and the only difference is the grid size. The ratios k_{min}/k_{max} for each grid were calculated. The relative differences (RD) between k_{min} and k_{max} for each grid size were also calculated using the following equation:

$$RD = \frac{k_{max} - k_{min}}{\frac{k_{max} + k_{min}}{2}} \qquad (9\text{-}1)$$

The ratios between the values of k_{min}/k_{max} and the RDs of the two grids were also calculated. These ratios were then used for ranking different realizations. The realization numbers, and whether they belonged to different groups on the BT graph, were tracked. A summary of the calculations regarding the k_{min}, k_{max} values is given in Appendix 19.

Ranking by k_{min}/k_{max} ratios

For the 8 x 6 grid, the permeability values k_{min} and k_{max} were close to each other, so that the ratio k_{min}/k_{max} was closer to one (from 0.8 to 0.95). The difference between k_{min} and k_{max} for the 128 x 96 grid was much bigger, so that the ratio k_{min}/k_{max} was very low (from 0.19 to 0.5). Note that all the permeability values k_{min} for the same realization were bigger for the 8 x 6 grid than for the 128 x 96 grid. On the other hand, all the permeability values k_{max} for the same realization are smaller for the 8 x 6 grid than for the 128 x 96 grid. Ranking different realizations based on k_{min}/k_{max} values (from the smallest to the biggest) showed that it is not a parameter which can be used

to identify the different groups. Figure 9-9 illustrates the relationship between the k_{min}/k_{max} ratios for the 8 x 6 and 128 x 96 grids. From this figure, one cannot identify different BT groups. The ratio for the 128 x 96 grid is a better indicator. Nine points out of 10 of the earlier BT group fall into the second half of the ranking list, while 17 points out of 23 points of the later BT group fall into the first half of the ranking list.

Ranking by RDs

The RDs for the 8 x 6 grid fall in a range from 0.05 to 0.23. For the 128 x 96 grid, the range is from 0.74 to 1.37. If the ranking is based on the RDs of the 8 x 6 grid, 9 points out of 10 from the earlier BT group fall into the second half of the range, while the later BT group scatter through the entire range. The ranking based on the RDs of the 128 x 96 grid shows an opposite picture from the ranking based on the ratio k_{min}/k_{max} for this grid with 9 points out of 10 of the earlier BT group falling into the first half of the range, and 17 points out of 23 points from the later BT group falling into the second half of the range. The realization numbers were compared and it was noticed that the same realizations appeared in each subgroup in both the ranking by the k_{min}/k_{max} ratios and the RDs. Figure 9-10 illustrates the relationship between the RD values of both 8 x 6 and 128 x 96 grids. From this figure, one cannot identify different BT groups either.

Ranking by the ratios of the k_{min}/k_{max} values of both the 8 x 6 and 128 x 96 grids

The range of this parameter is from 2 to 2.5. It is not clear if there is any trend related to the appearance of any of the BT groups.

Ranking by the ratios of RDs of the two 8 x 6 and 128 x 96 grids

The range of this ratio is from 0.06 to 0.27. Nine points of the earlier BT group fall into the second half of the range. The remaining points are scattered throughout the

whole range and no group identification is possible.

In summary, using the directional effective permeability obtained by Cardwell and Parsons' method is not a good ranking measure to identify points in different BT groups.

3.4. Ranking based on the number of connected cells between two wells

In an attempt to understand and quantify the difference between realizations that leads to the identification of different groups in the BT chart, another ranking technique based on the number of connected cells between the injector and producer was introduced. Two programs were used: "geo_obj" and "rank2loc". The purpose of using these programs is to calculate the number of connected cells, and therefore the reservoir volume, under a chosen threshold permeability value, and to rank different realizations based on these numbers. Cells that have permeability values above a threshold value were assumed to have fluid flowing through them. If the permeability values fell below the threshold value, there was no flow through these cells. The program "geo_obj" identifies and counts all the geo-bodies that have two or more cells that have permeability values above the threshold value and are connected together. The program "rank2loc" counts and ranks all geo-bodies that have cells connecting the injector and the producer. The ranking is based on the number of connected cells between the two wells from the highest cell number (ranked number 1) to the lowest cell number (ranked number 100).

An important parameter for running the ranking program is the threshold permeability value, which defines the permeability limit. If the threshold permeability value is too high, there will be few blocks that are connected between the injector and the producer. This scenario does not represent the true picture where the flow occurs in more blocks of the reservoir. If the permeability threshold value is too low, almost every cell will be connected under the threshold assumption and it will be difficult to

rank different realizations based on the number of connected cells. A trial-and-error approach was used to determine the threshold permeability value that is acceptable for the realization ranking.

At first the permeability threshold was chosen based on the statistics of the permeability for 100 realizations. The upper quartile value of 1512.6 md was chosen to be the threshold value (Figure 3-33). This value turned out to be too high because, for many realizations, especially for the 128 x 96 grid, there were no connected cells between the two wells. Next, the median value of 932.5 md was chosen as the threshold value and it turned out to be too high also. Then the lower quartile permeability value of 260.56 md was tried, and it turned out that this value was too low because many realizations, especially for the 8 x 6 grid, had a very high number of connected cells approaching all 48 cells. The conclusion after this trial-and-error procedure was that the threshold permeability value should be chosen between the lower quartile and the median value of the simulated permeability. Three permeability values were picked as the threshold: 600, 500, and 400 md. Appendix 20 summarizes the results of the rankings for the 8 x 6 and 128 x 96 grids. Figures 9-11, 9-12, and 9-13 show the graphic illustrations of the ranking relationship between the 8 x 6 and 128 x 96 grids for the three permeability thresholds. From these figures, it can be seen that there is no indication that the different groups on the BT plot can be separated. There are differences in the ranking of each realization based on different threshold permeabilities, but with all the thresholds the ranking cannot help to identify different groups of realizations.

3.5. Ranking by the effective permeability obtained from flow-based scaling

The original permeability values (128 x 96 grid) and the scaled permeability values for the 8 x 6 grid were scaled up to one representative effective permeability value using the flow-based scaling technique (program "flowsim"). The result of this ranking is shown in Appendix 20. Figure 9-14 shows the results graphically. It should be noted

that there were many warnings about the non-convergence of the effective permeability during the scaling process for the 128 x 96 grid. This means it was difficult to obtain one representative permeability value for a very finely discretized and highly heterogeneous reservoir. The tolerance for convergence in the "flowsim" program is small, so these messages were ignored. The permeability values scaled from the 128 x 96 and 8 x 6 grids follow the unit line, but again points are not separated as desired into different groups as determined from the BT plot.

3.6. Ranking based on flow rate variances

The idea behind ranking by flow rate variances is that these variances depend on reservoir heterogeneity. The more heterogeneous a reservoir, the greater the variance in the flow rates. If a reservoir is heterogeneous, there will be more chance that viscous channeling occurs. Consequently, the flow in the reservoir is faster through the channels and this leads to an early BT. If one goes back to the hypothesis about reservoir connectivity in different realizations, for the later BT group, there are probably more homogeneous reservoir models for the coarser grids than for the true finest grid. This means there will be less variability in the flow rates for the coarser grids. Similarly, for the earlier BT group, there are probably more heterogeneous reservoir models for the coarser grids than for the finest grid. More channeling occurs in the coarser grids than in the finest grid and the flow rates for the coarse grids will have a larger variance than for the finest grid.

A modified "flowsim" program was used to calculate the flow rates of each realization for the 8 x 6 and 128 x 96 grids, M = 0.4 case. The variance of the flow rates was also calculated and standardized. Appendix 21 summarizes the results of the flow rate calculations. A plot of the flow rate variances of the 8 x 6 grid versus the d value for the 8 x 6 grid (M = 0.4) for 100 realizations is shown in Figure 9-15. Three groups were identified on the plot. From this figure, it can be seen that the hypothesis suggested above regarding the flow rate variances is true. The earlier BT group has a

bigger variance than that for the later BT group. However, it is impossible to identify the three different groups because there is an overlap in the variance ranges for the three groups.

Figures 9-16 shows a crossplot of the standardized flow rate variances between the 8 x 6 and 128 x 96 grids. Standardization was performed in order to obtain the same magnitude of variances for the different grids. Unfortunately, the variances do not fall into three distinct groups as expected. Therefore, no group identification is possible.

The conclusion to be drawn after an attempt to identify different groups on the BT plots is that it is difficult to differentiate realizations using any quantitative measure. This is because the BT is a parameter that is very sensitive to the connectivity character of a reservoir. The results presented above show that directional permeability or even flow rates cannot characterize quantitatively the reservoir connectivity. In other words, the BT is the result of a more complex interaction between the porosity-permeability and flow properties of a reservoir. A simple measure based on effective permeability, flow rates or the number of connected cells cannot capture and predict effectively BTs.

	M = 0.4		M = 1		M = 1.8	
Grids	**RF**	**BT**	**RF**	**BT**	**RF**	**BT**
8 x 6	0.635	0.456	0.593	0.425	0.746	0.382
16 x 12	0.731	0.585	0.889	0.589	0.796	0.604
32 x 24	0.897	0.726	0.954	0.699	0.943	0.769
64 x 48	0.978	0.802	0.987	0.848	0.983	0.823

Table 9-1: Correlation coefficients of ranking numbers of RF and BT for different grids

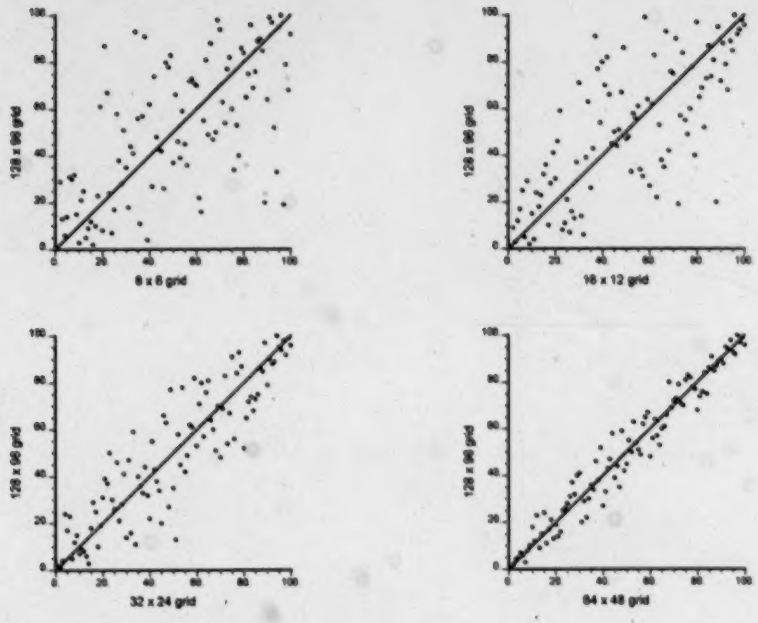

Figure 9-1: Crossplot of ranking numbers of RFs for different grids, M = 0.4

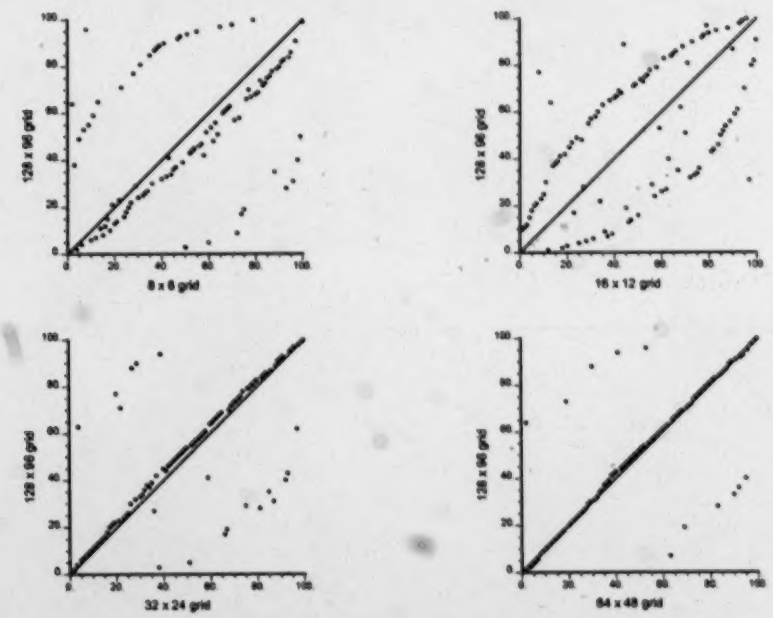

Figure 9-2: Crossplot of ranking numbers of BTs for different grids, M = 0.4

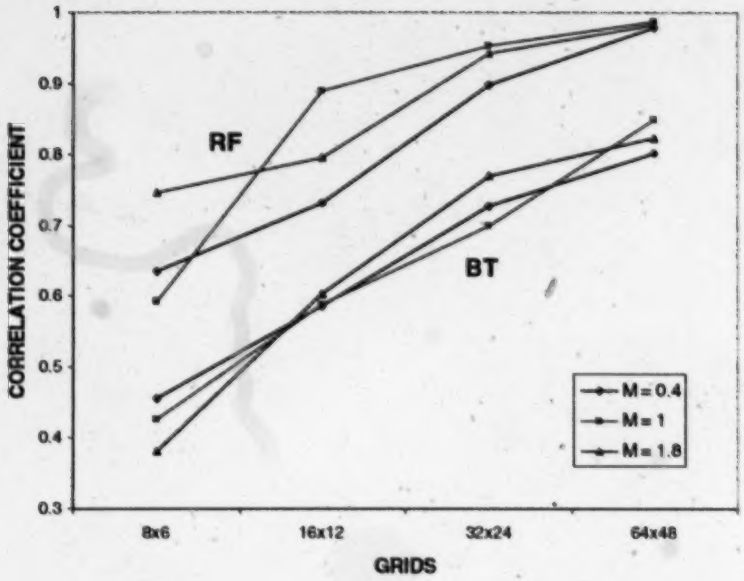

Figure 9-3: Correlation coefficients between recovery factors and breakthrough times of 128 x 96 and of coarser grids

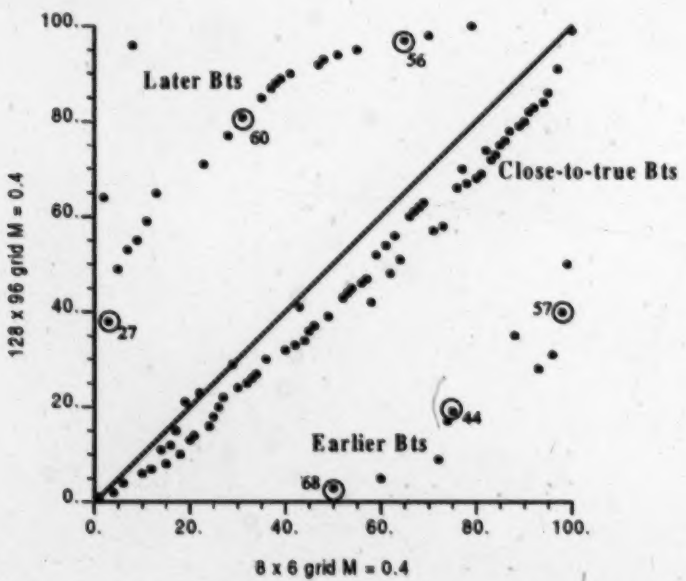

Figure 9-4: Three groups of realizations on BT plot for 8 x 6 grid

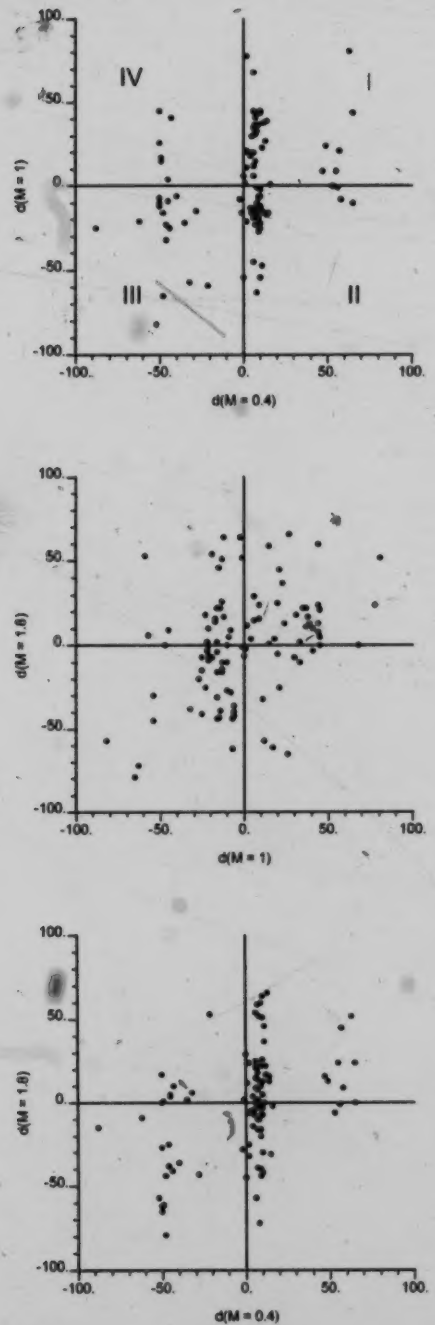

Figure 9-5: Crossplots of d values of 8 x 6 grid for different mobility ratios

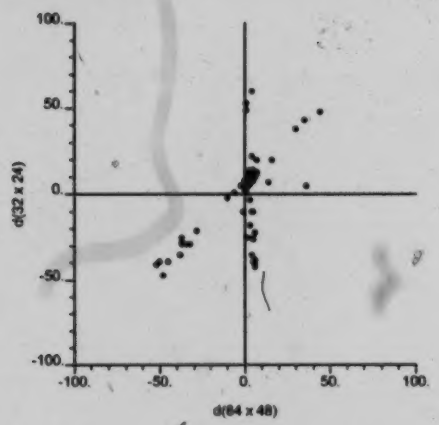

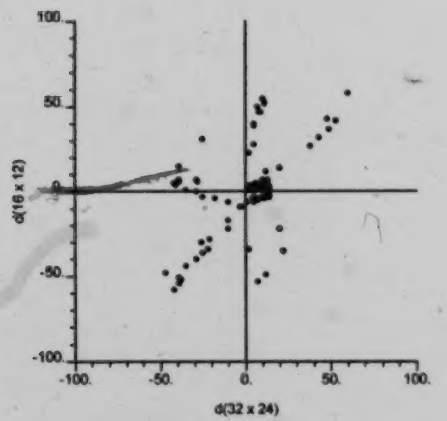

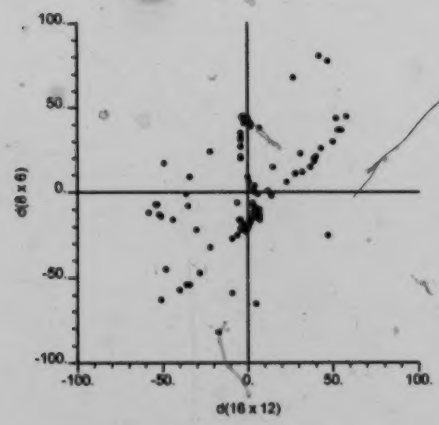

Figure 9-6: Crossplots of d values of different grids, M = 1

Earlier breakthrough times

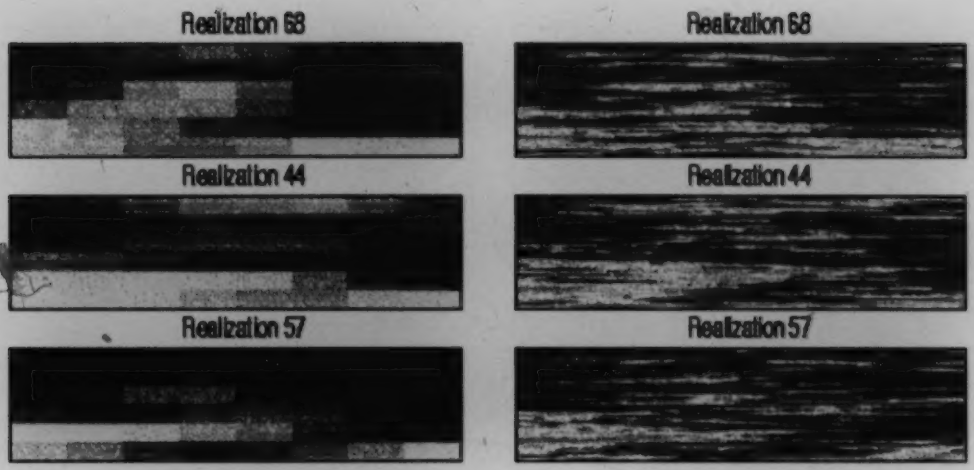

Later breakthrough time

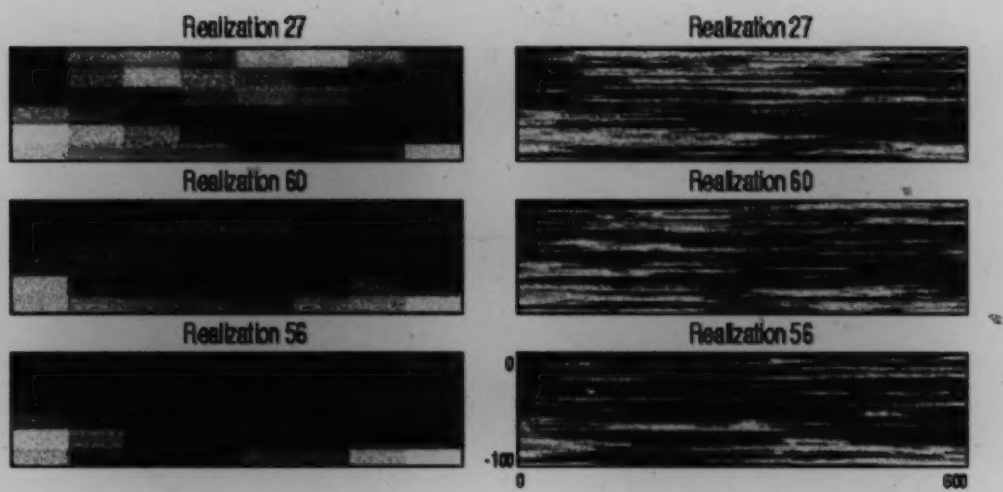

Figure 9-7: Porosity distributions of 8 x 6 grid (on the left hand side), and 128 x 96 grid (on the right hand side)

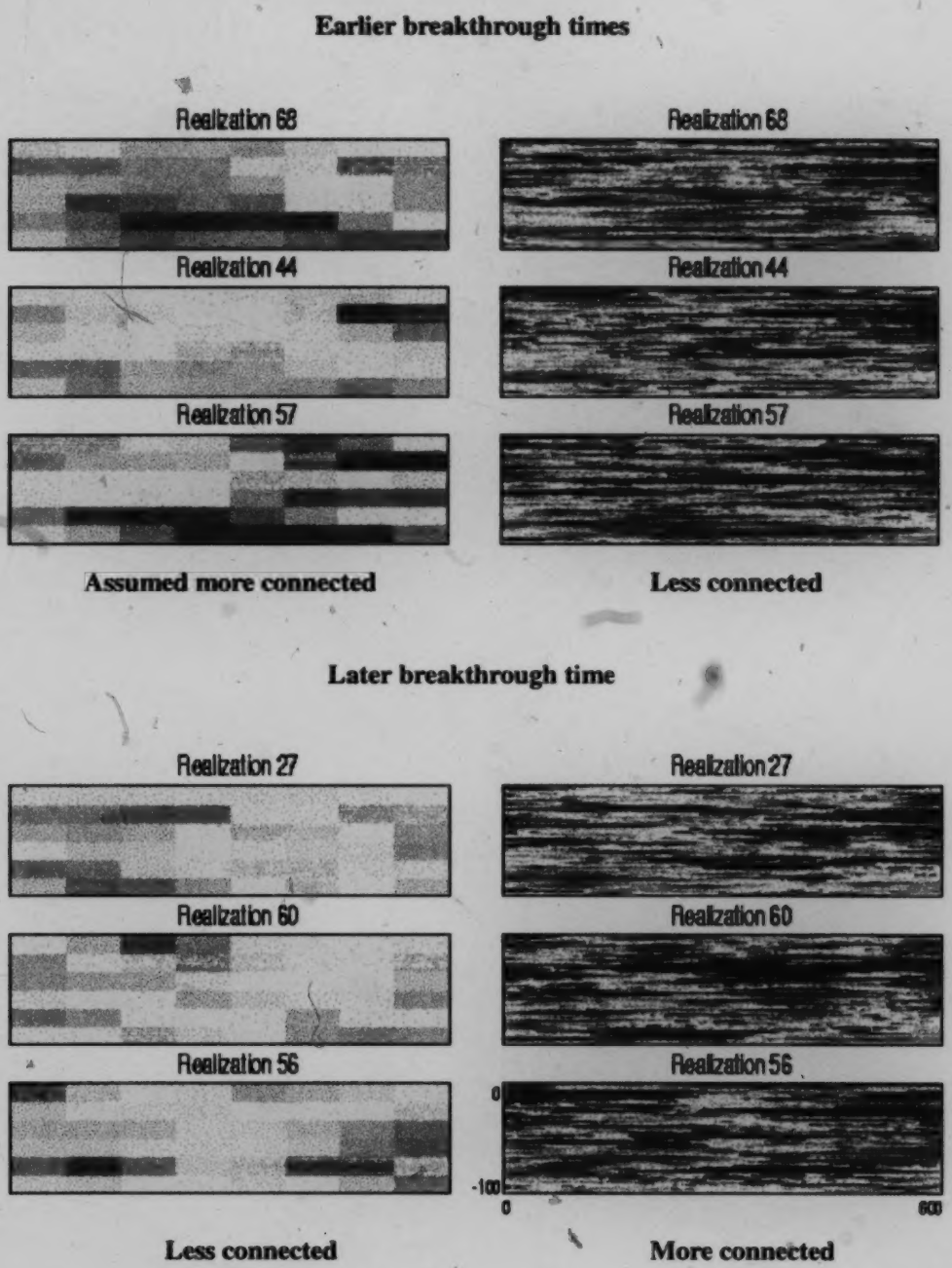

Figure 9-8: Permeability distributions of 8 x 6 grid (on the left hand side), and 128 x 96 grid (on the right hand side)

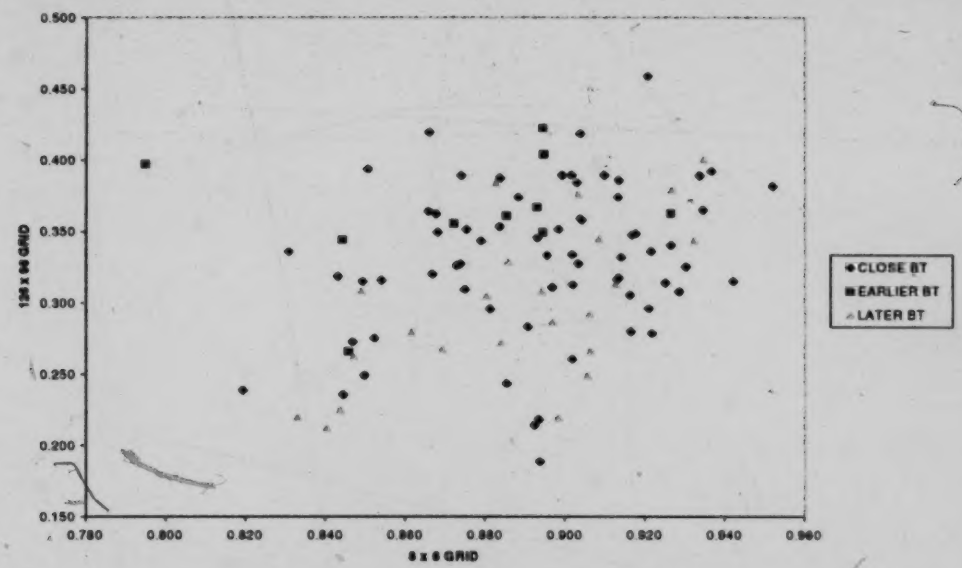

Figure 9-9: k_{min}/k_{max} ratios for 8 x 6 and 128 x 96 grids

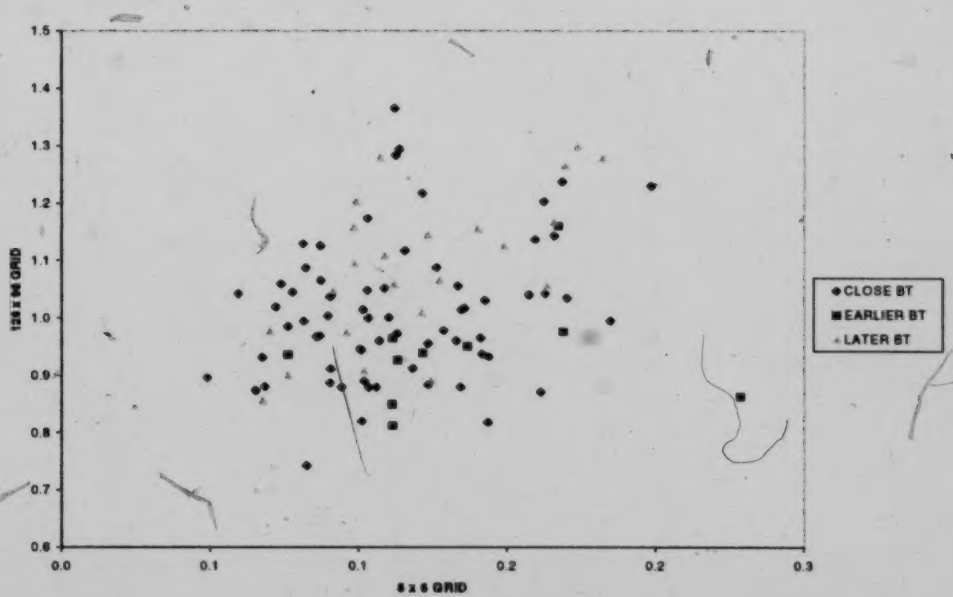

Figure 9-10: Relative differences between k_{min} and k_{max} for 8 x 6 and 128 x 96 grids

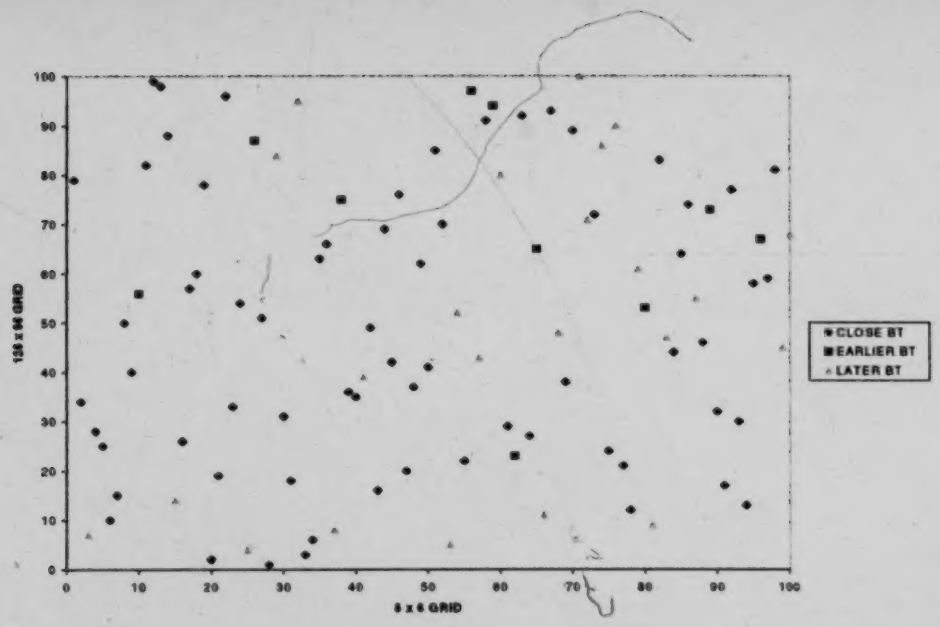

Figure 9-11: Realization ranking by the connectivity between two wells: 600 md threshold

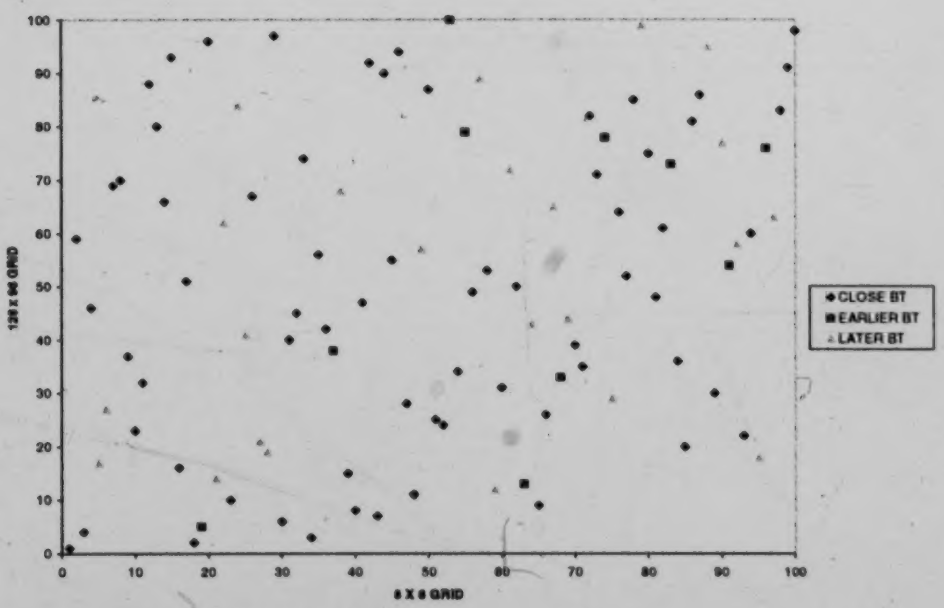

Figure 9-12: Realization ranking by the connectivity between two wells: 500 md threshold

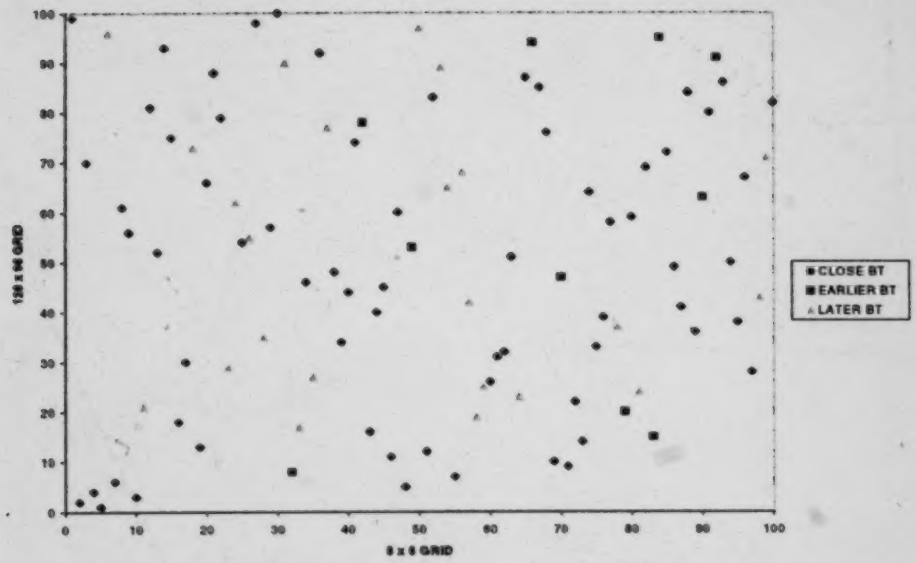

Figure 9-13: Realization ranking by the connectivity between two wells: 400 md threshold

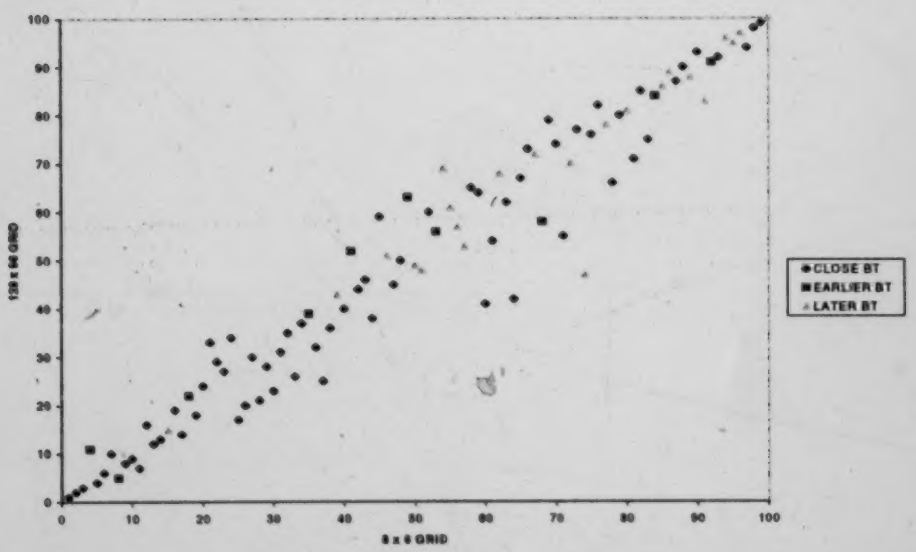

Figure 9-14: Realization ranking by the effective permeability from flow-based scaling

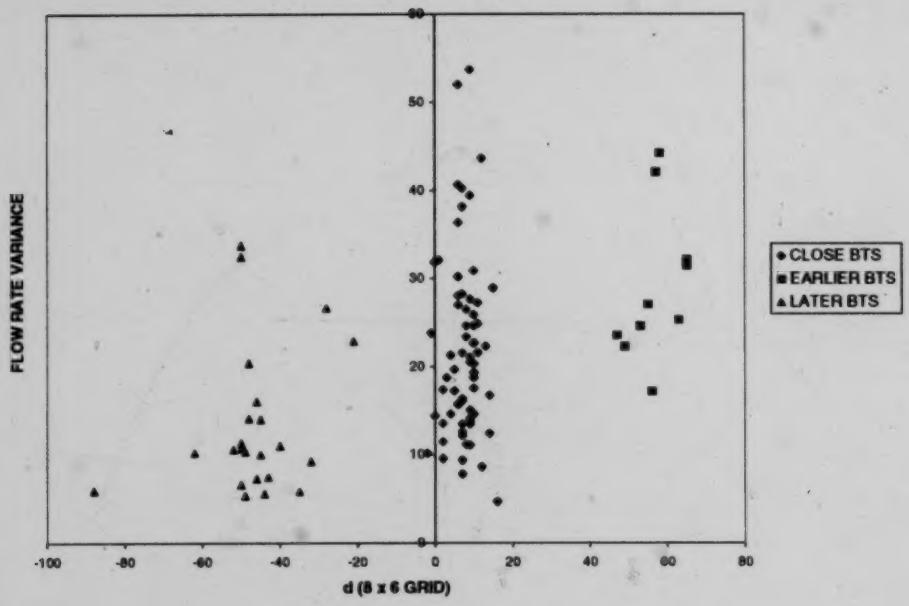

Figure 9-15: Flow rate variances of 8 x 6 grid

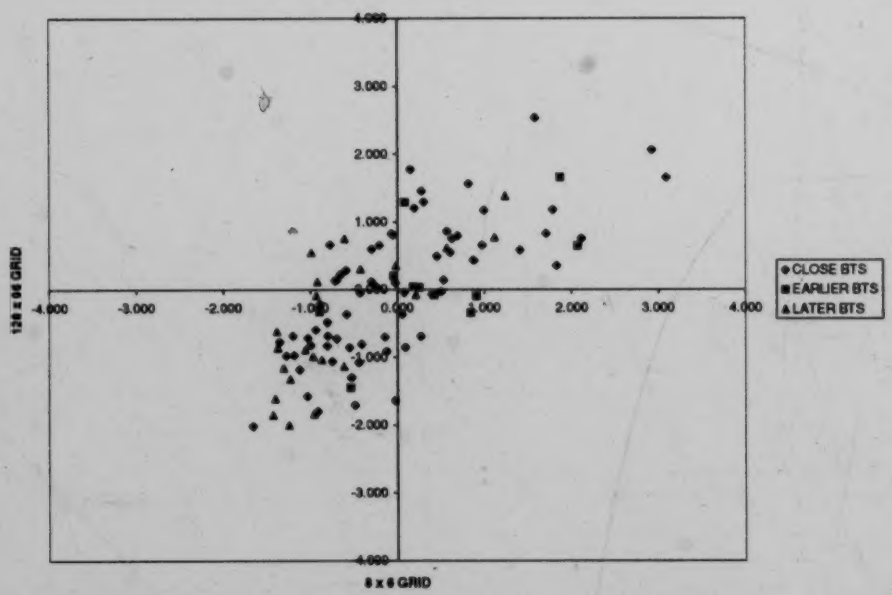

Figure 9-16: Crossplot of flow rate variances of 8 x 6 and 128 x 96 grids, M = 0.4

X. CONCLUSIONS AND FUTURE WORK

Grid discretization effects must always be considered in reservoir simulation. The magnitude of the discretization effect is different depending on the porosity-permeability properties of the reservoir: homogenous or heterogeneous, or obtained from downscaling or upscaling. Grid discretization effects also depend on the nature of the fluid in the reservoir. For the reservoir in this study, in general, RFs and BTs increase as the number of cells increases. For the homogeneous reservoir case, the RFs for the coarsest grid were 4-5 % lower compared to the finest grid, while the BTs were 23-30 % lower for the coarsest grid compared to the finest grid. For the reservoir with downscaled porosity-permeability, RFs were 6-8 % and BTs were 25-36 % lower for the coarsest grid than for the finest grid. For the reservoir with upscaled porosity-permeability, based on the mean values of 100 realizations, the RFs were 3-7 % and the BTs were 5-9 % lower for the coarsest grid than for the finest grid. Recovery factors had more predictable behavior than breakthrough times for different fluid types. This study shows that upscaled permeability values of the reservoir using power and flow-based techniques give very similar reservoir flow responses.

Another conclusion from this study is that it is important to recognize and assess quantitatively sources of uncertainty in reservoir modeling. In this study, three sources of uncertainty in reservoir flow modeling were recognized: differences in fluid types, discretization and scaling, and the uncertainty in the geological model. Differences in fluid types were the biggest source of uncertainty. In the event that the fluid types in the reservoir are known, the uncertainty in geological modeling contributes more to the total uncertainty than the grid discretization; therefore, as many geological realizations as possible should be used in flow simulation during a reservoir study.

Ranking the different geological realizations before running a flow simulation on a fine scale can be used as a tool to enable the use of fewer computing resources in the

task of uncertainty assessment. The RFs and the BTs from the flow simulation of a very coarse grid can be used as fair to good ranking parameters to assess the uncertainty in the reservoir flow simulation. From the in-depth ranking study for the BTs, it was observed that it was difficult to find a simple measure that can quantify reservoir connectivity, which the BTs were very sensitive to. This is an unsolved problem from this study and it should be addressed in a future study. If an effective measure to quantify the connectivity in geological models can be found, better ranking techniques for reservoir flow parameters that are related to connectivity, such as BTs, can be utilized.

The procedure used in this study to assess uncertainty is not restricted to academic studies; it can be applied also to any practical reservoir study. The results of quantitative uncertainty assessment are important in reservoir management and decision making.

BIBLIOGRAPHY

1. N.G. Saleri and R.M. Toronyi: Engineering control in reservoir simulation, SPE paper 18305, 1988.
2. E.H. Isaaks and R.M. Srivastava: An introduction to applied geostatistics, Oxford University Press, 1989, p. 3.
3. C. Deutsch and A. Journel: Geostatistical software library and user's guide, Oxford University Press, 1998.
4. C. Deutsch: Geostatistical methods for modeling earth science data, lecture notes, 1999.
5. A. Journel: Fundamentals of geostatistics in five lessons, short course notes, American geophysical union, 1989.
6. H. Kupfersberger and C. Deutsch: Methodology for integrating analogue geologic data in 3-D variogram modeling, AAPG Bulletin, Vol. 83, No. 8, August 1999, pp. 1262-1278.
7. Eclipse 100 97A, Reference manual, Schlumberger technology corporation, 1997.
8. F. Craig Jr.: The reservoir engineering aspects of waterflooding, SPE monograph, 1993.
9. R. E. Collins: Flow of fluids through porous materials, Research and engineering consultants, Inc., 1990, pp. 196-200.
10. A.G. Journel, C. Deutsch, and A.J. Desbarats: Power averaging for block effective permeability, SPE paper 15128, 1986.
11. C.C. Mattax and R. L. Dalton: Reservoir simulation, SPE monograph, 1990, p. 33.
12. J.E. Warren and H.S. Price: Flow in heterogeneous porous media, SPEJ, Sept. 1961, pp.153-169.
13. W.T. Cardwell and R.L. Parsons: Average permeabilities of heterogeneous oil sands, Trans. AIME, 160 (34), 1945.
14. C. Deutsch: Estimating block effective permeability with geostatistics and power averaging, SPE paper 15991, 1986.

15. A.J. Desbarats: Spatial averaging of hydraulic conductivity in three-dimensional heterogeneous porous media, Mathematical geology, 24 (3), 1992, pp. 249-267.
16. D. Li and B. Beckner: A new efficient averaging technique for scaleup of multimillion-cell geologic models, SPE paper 56554, 1999.
17. D.L. Massart, B.G.M. Vandeginste, S. N. Deming, Y. Michotte and L. Kaufman: Chemometrics: a textbook, Elsevier, 1988.
18. H. Scheffe: The analysis of variance, New York, 1959.
19. D. L. Harnett: Statistical methods, Addison-Wesley publishing company, Inc., 1982.
20. P.R. Ballin, K. Aziz, and A. G. Journel: Quantifying the impact of geological uncertainty on reservoir performing forecast, SPE paper 25238, 1993.
21. C. Deutsch, S. Srinivasan: Improved reservoir management through ranking stochastic reservoir models, SPE paper 35411, 1996.
22. M.A. Malik and L.W. Lake: A practical approach to scaling-up permeability and relative permeabilities in heterogeneous permeable media, SPE paper 38310, 1997.

APPENDIX 1: PARAMETER FILE FOR POROSITY SIMULATION – 61 x 50 GRID

```
************************************************************
* File generated by WinGslib - modify at your own risk
* Version:        1.2.2
* Build code:     245c173/1/2_4_1381
* Date:           Wednesday, August 16, 2000
* Time:           5:14:51 PM
* Author:         Administrator
* Computer name: AMBA2 (129.128.32.52)
* Comment:
************************************************************

                  Parameters for SGSIM
                  ********************

START OF PARAMETERS:
D:\hanh\start\input\data.txt
2 0 4 7 0 0                          -  columns for X,Y,Z,vr,wt,sec.var.
-100 1E+21                           -trimming limits
1                                    -transform the data (0=no, 1=yes)
d:\hanh\start\output\simpor.trn
0                                    -  consider ref. dist (0=no, 1=yes)
d:\hanh\start\input\histsmth.out
1 2                                  -  columns for vr and wt
0 0.3                                -  zmin,zmax (tail extrapolation)
1 0                                  -lower tail option
1 0.3                                -upper tail option
1                                    -debug level (0-3)
d:\hanh\start\output\simpor.dbg
d:\hanh\start\output\simpor.out
1                                    -number of realizations to generate
61 0 10                              -nx, xmin, xsize
1 0.5 1                              -ny, ymin, ysize
50 -99 2                             -nz, zmin, zsize
69075                                -random number seed
0 8                                  -Min and max original data for sim
12                                   -number of simulated nodes to use
1                                    -assign data to nodes (0=no, 1=yes)
1 3                                  -multiple grid search (0=no, 1=yes), num
0                                    -maximum data per octant (0=not used)
6000 6000 60                         -maximum search radii (hmax, hmin, vert)
0 0 0                                -angles for search ellipsoid
51 51 11                             -size of covariance lookup table
0 0 1                                -kType: 0=SK,1=OK,2=LVM,3=EXDR,4=COLC
d:\hanh\start\input\ydata.dat
4                                    -  column
4 0                                  -nst, nugget
1 0.55 0 0 0                         -it, cc, ang1, ang2, ang3
300 300 3                            -a_hmax, a_hmin, a_vert
3 0.12 0 0 0                         -it, cc, ang1, ang2, ang3
800 800 8                            -a_hmax, a_hmin, a_vert
1 0.12 0 0 0                         -it, cc, ang1, ang2, ang3
2200 2200 22                         -a_hmax, a_hmin, a_vert
1 0.21 0 0 0                         -it, cc, ang1, ang2, ang3
6000 6000 60                         -a_hmax, a_hmin, a_vert
```

APPENDIX 2: PARAMETER FILE FOR PERMEABILITY SIMULATION – COKRIGING OPTION – 61 x 50 GRID

```
************************************************************
* File generated by WinGslib - modify at your own risk
* Version:        1.2.2
* Build code:     245c173/1/2_4_1381
* Date:           Wednesday, August 16, 2000
* Time:           6:52:17 PM
* Author:         Administrator
* Computer name: AMBA2 (129.128.32.52)
* Comment:
************************************************************

                  Parameters for SGSIM
                  ********************

START OF PARAMETERS:
D:\hanh\start\input\data.txt
2 0 4 8 0 0                          -  columns for X,Y,Z,vr,wt,sec.var.
-1 1E+21                             -trimming limits
1                                    -transform the data (0=no, 1=yes)
d:\hanh\start\output\simperm-por.trn
0                                    -  consider ref. dist (0=no, 1=yes)
d:\hanh\start\input\histsmth.out
1 2                                  -  columns for vr and wt
0 6000                               -  zmin,zmax (tail extrapolation)
1 1                                  -lower tail option
1 1                                  -upper tail option
1                                    -debug level (0-3)
d:\hanh\start\output\simperm-por.dbg
d:\hanh\start\output\simperm-por.out
1                                    -number of realizations to generate
61 0 10                              -nx, xmin, xsize
1 0.5 1                              -ny, ymin, ysize
50 -99 2                             -nz, zmin, zsize
69069                                -random number seed
0 8                                  -Min and max original data for sim
12                                   -number of simulated nodes to use
1                                    -assign data to nodes (0=no, 1=yes)
1 3                                   -multiple grid search (0=no, 1=yes),
num
0                                    -maximum data per octant (0=not used)
5400 5400 54                           -maximum search radii (hmax, hmin,
vert)
0 0 0                                -angles for search ellipsoid
51 51 11                             -size of covariance lookup table
4 0.311 1                            -kType: 0=SK,1=OK,2=LVM,3=EXDR,4=COLC
D:\hanh\start\output\simpor.out
1                                    -  column
4 0                                  -nst, nugget
1 0.56 0 0 0                         -it, cc, ang1, ang2, ang3
280 280 2.8                          -a_hmax, a_hmin, a_vert
1 0.2 0 0 0                          -it, cc, ang1, ang2, ang3
940 940 9.4                          -a_hmax, a_hmin, a_vert
1 0.17 0 0 0                         -it, cc, ang1, ang2, ang3
1500 1500 15                         -a_hmax, a_hmin, a_vert
1 0.07 0 0 0                         -it, cc, ang1, ang2, ang3
5400 5400 54                         -a_hmax, a_hmin, a_vert
```

APPENDIX 3: INPUT DATA FILE FOR ECLIPSE – EXAMPLE FOR GRID 61 x 50, M = 0.4

```
RUNSPEC=============================================================

TITLE
TWO WELL SIMULATION TEST
DIMENS
     61  1   50 / Number of blocks in x, y, z directions
--Two phase problem oil and water
OIL

WATER
--metric unit
METRIC

--Start of simulation date
START
    16    'MAY'  2000 /

WELLDIMS
--Max #wells   Max#cell/well  Max#group  Maxwell/group
  5            60             3          2  /

FMTOUT

UNIFOUT

SAVE
 /
--
=====================================================================

GRID
--Output  INIT  file-summary  of  data  entered  in  GRID,  PROPS,  REGION
sections
INIT

DX

3050*10 /

DY
3050*1 /

DZ
3050*2  /
--Cell size in x direction 10 m, y-1m, z-2m
TOPS
--Depth of the formation top
61*2000 /

BOX
```

```
1 61 1 1 1 50 / cell from 1 to n in x, y, z directions

INCLUDE
'TWPOR.ECL'
/ file for porosity values converted from geostatistical modeling

BOX
1 61 1 1 1 50 /

INCLUDE
'TWPERM.ECL'
/ file for permeability values converted from geostatistical modeling

BOX
1 61 1 1 1 50 /

COPY
'PERMX'  'PERMY' /
'PERMX'  'PERMZ' /
/ Assume perms in x, y dir are the same as block perms

ENDBOX

BOX
1 61 1 1 1 50 /

MULTIPLY
'PERMZ' 0.1 /
/ perm in z dir is only 0.1 of x,y dir

ENDBOX

--------------------------------------------------------------------

PROPS
SWOF
--Sw  Krw   Kro   Pcow
0.250 0.0000      1.0000  0
0.315 0.0026      0.8044  0
0.365 0.0065      0.6301  0
0.4150      0.0134  0.4771  0
0.465 0.0244      0.3453  0
0.5150      0.0410      0.2348  0
0.565 0.0651      0.1455  0
0.6150      0.0987      0.0775  0
0.665 0.1443      0.0307  0
0.715   0.2045  0.0052  0
0.750   0.2570  0.0000  0
1.00  1.0000      0.0000  0
/
PVTW
--Pref      Bw    Cw    mw
100.0       1.015       4.57E-5 0.47 0.00E00 /

ROCK
```

```
--Pref      Ct
100.0       5.51E-5 /

DENSITY
--Oil Water Gas  @Surface conditions
825.0       1090        0.750 /
--PVT properties of dead oil
PVDO
--p   Bo    mo
1.0    1.1360   0.758107
25.0   1.1336   0.772075
50.0   1.1311   0.7952
60.0   1.1301   0.8069
70.0   1.1291   0.82
80.0   1.1281   0.8345
90.0   1.1271   0.8504
100.0  1.1261   0.8677
125.0  1.1236   0.917075
150.0  1.1211   0.9752
175.0  1.1186   1.042075
200.0  1.1161   1.1179 /

SOLUTION
EQUIL
--Datum depth     p@d.d.      WOC depth
 2000             100.0       3000.0  /

RPTSOL
-- 1 2 3 4 5 6 7 8 9 10 11 12 13 14 15 16 17 18 19 20
   1 0 1 0 0 0 0 2 1  0  0  1  0  0  0  0  0  0  0  0
-- 21 22 23 24 25 26 27 28 29 30 31 32 33 34 35 36 37 38 39 40
   0  0  0  0  0  0  0  0  0  0  0  0  0  0  0  0  0  0  0  0 /
   1
-----------------------------------------------------------------

SUMMARY

RPTONLY
--MONITOR
DATE

WOPR
'P'/ Well oil production rate
WOPT
'P'/ Total oil production
WPI
'P'/ Productivity index
WWPR
'P'/ Water production rate
WWPT
'P'/ Total water production
WWCT
'P'/ Water cut
WBHP
/ Bottom hole pressure
```

```
WWIR
'I'/ Water injection rate
WWIT
'I'/Water injection total
WVIT
'I'/Reservoir volume injection total
FOEW
/ Recovery efficiency: oil produced over IOIP
FRPV
/Pore volume at reservoir conditions

SEPARATE
--Request a neat tabulated output of the summary file data
RUNSUM
RPTSMRY
  1 / Request printed output of keywords in the SUMMARY section

--=================================================================

SCHEDULE
-- Control output from SCHEDULE section
RPTSCHED
-- 1 2 3 4 5 6 7 8 9
   1 0 1 0 0 0 0 2 1
/

TUNING
/
/
12 3 200 1* 45 /

MESSAGES
5000 5000 5000 2000 2000 2000 10000 10000  10000 1000 1000 1000 /

WELSPECS
--Wname     i    j   DDepth BHP
'I'    'INJ'    1    1     2000.0   'LIQ'  2*   'SHUT'/
'P'    'PROD'  61   1     2000.0   'LIQ'  2*   'SHUT'/
/
--Well completion specification data
COMPDAT
--Wname i,j k        kr      W diameter
'I'    2*   1   50 'OPEN'  1* 0.000000 0.12  /
'P'    2*   1   50 'OPEN'  1* 0.000000 0.12  /
/
--Control data for injection well
WCONINJE
--                 inj rate     BHP upper limit
'I' 'WAT' 'SHUT' 'RATE'  100.0   1*  500.0  /
/
--Control data for production well
WCONPROD
'P' 'SHUT' 6* 20/
/
WELOPEN
```

```
'P', 'OPEN'      /
'I', 'OPEN'      /
/
--Economic limit data for production well
WECON
--  min orate      max wcut    workover
'P' 1     1*     0.9    2*  'NONE ' 'NO'    1*  'RATE' /
/
--Time steps 1 day
TSTEP
30*4
/
TSTEP
30*4
/
TSTEP
20*4
/
END
```

APPENDIX 4: EXPLANATIONS OF PARAMETERS USED IN INPUT FILE FOR ECLIPSE

There are six main sections in the input file:

1. RUNSPECT
2. GRID
3. PROPS
4. SOLUTION
5. SUMMARY
6. SCHEDULE

1. RUNSPECT

TITLE: Title of the simulation job
DIMENS: Number of blocks in X, Y and Z directions
OIL:
WATER: Two phase flow problem: oil and water
METRIC: The unit of all parameters is in metric unit system
START: Date the simulation starts
WELLDIMS: 4 parameters in order:
- Maximum number of wells in the reservoir
- Maximum number of cells intersected by wells
- Maximum number of well groups
- Maximum number of wells in one group

SAVE: Create a SAVE file for fast restart

2. GRID

This section specifies the grid system for the run, cell sizes as well as the porosity and permeability values of each cell.

INIT: Output INIT file-summary of data entered in GRID, PROPS, and REGION sections
DX:
DY
DZ: cell sizes in x, y, z directions. The number before the cell sizes is the number of cells that have these sizes
TOP: Depth of the formation top
BOX: create a 3-D array numbering in x, y, z directions.
INCLUDE: read the data from other files specified after the keyword

3. PROPS

Specifies properties of reservoir fluids and rock

SWOF: saturation function if oil and water presented. 4 parameters in order
- Water saturation (Sw)
- Relative permeability to water (krw)
- Relative permeability to oil (kro)
- Capillary pressure (Pcow)

PVTW: PVT properties of water-4 parameters
- Pressure at reference depth
- Water FVF (Bw)
- Water compressibility (c_w)
- Water viscosity (μ_w)

ROCK: rock properties-2 parameters
- Pressure at reference depth
- Rock compressibility (c_r)

DENSITY: density of oil, water and gas at surface conditions
PVDO: PVT properties of dead oil
- Pressures
- Oil FVF (Bo)
- Oil viscosity (μ_o)

4. SOLUTION

Input data to define the initial state (pressure, saturations, Rs, Rv) of every grid block in the reservoir.

EQUIL: Equilibration data specification

- Datum depth (taken at the reservoir top)
- Pressure at datum depth
- Depth of the oil-water contact

RPTSOL: Controls on output from SOLUTION section. The keyword should be followed up to 76 integers, each of which controls a particular form of output. The value of zero or less switches the output off. Optionally, the keyword can be followed by a string of mnemonics to request output to print file

1- Output of initial grid block pressures
2- Output of initial grid block oil saturations
3- Output of initial grid block water saturations
4- Output of initial grid block gas saturations
5- Output of initial grid block solution gas-oil ratios
6- Output of initial grid block vapor oil-gas ratios
7- Output of restart file
8- Output of fluid in place report
    1-Initial fluid in place reported for the whole field
    2-In addition, initial fluids in place are reported for each fluid in place region defined with the FIPNUM keyword
    3-In addition, initial fluids in place are reported for all sets of fluid in place regions defined with the FIP keyword
9- Output of equilibration data
12- Output of analytic (Fetkovich or Carter-Tracy) aquifer

5. SUMMARY

Specifies a number of variables which are to be written to summary files after each time step of the simulation. The graphic post processor may be used to display the variation of variables in the summary files with time and with each other.

RPTONLY: Request that the summary data is only produced at report steps instead of every time step.
DATE: Output the date as three summary quantities DAY, MONTH, YEAR. In addition, the date will be printed in place of the time in the RUNSUM output

All the keywords beginning with W mean parameters of wells

WOPR: Well oil production rate
WOPT: Total oil production
WPI: Productivity index
WWPR: Water production rate
WWPT: Total water production
WWCT: Water cut
WBHP: Bottom hole pressure
WWIR: Water injection rate
FOEW: Recovery efficiency, oil produced over IOIP
WVIW: Volume reservoir water injected
FRPV: Reservoir pore volume

RUNSUM: Request a neat tabulated output of the summary file data
RPTSMRY:
1-Request printed output of keywords in the SUMMARY section
0-Switches it off

6. SCHEDULE:

Controls output from SCHEDULE section

RPTSCHED: The keyword should be followed up to 76 integers, each of which controls a particular form of output. The value of zero or less switches the output off. Optionally, the keyword can be followed by a string of mnemonics to request output to print file.

1- Output of initial grid block pressures
2- Output of initial grid block oil saturations
3- Output of initial grid block water saturations
4- Output of initial grid block gas saturations
5- Output of initial grid block solution gas-oil ratios
6- Output of initial grid block vapor oil-gas ratios
7- Output of restart file
8- Output of fluid in place report
    1- Initial fluid in place reported for the whole field
    2- In addition, initial fluids in place are reported for each fluid in place region defined with the FIPNUM keyword
    3- In addition, initial fluids in place are reported for all sets of fluid in place regions defined with the FIP keyword
9- Output of equilibration data

WELSPECS: General specification data for wells

1- Well name
2- Name of group to which the well belongs
3- I-location of wellhead or heel
4- J- location of well head or heel
5- Datum depth for BHP
6- Preferred phase for the well
7- Drainage radius for productivity/infectivity index calculation (default: 0)
8- Flag for use of a special inflow equation to model the flow of free gas between the completed grid blocks and the well completions (default-STD-standard)
9- Instruction for automatic shut-in
STOP: Stop well above formation (allowing crossflow)
SHUT: Isolate well from the formation

COMDAT: Well completion specification data

1- Well name
2- I location
3- J location
4- first K
5- last K
6- Open/shut flag of connection
7- Saturation table number for connection relative permeabilities (default: the relative permeabilities will be calculated using the same saturation table as the grid block containing the connection.
8- Transmissibility factor for the connection: if enter default, 0 or negative, it will be calculated using the remaining items of data in this record.
9- Wellbore internal diameter at the connection

WCONINJ: Control data for injection well

1- Well name or well name root
2- Injector type
3- Open/shut flag for the well
4- Control mode:
RATE: controlled by surface flow rate
RESV: controlled by reservoir fluid volume rate
BHP: controlled by BHP
BHT: controlled by BHT
GRUP: group control
5- Surface flow rate target or upper limit
6- Reservoir fluid volume rate target or upper limit (default: infinity)
7- BHP target or upper limit

WCONPROD: Control data for production well

1- Well name
2- Open/shut flag for the well

9- BHP target or lower limit

WELOPEN: Shut or re-opens wells or well connection

1- Well name or well name root
2- Open/shut flag for the well or connection

WECON: Economic limit data for production well

1- Production well name
2- Minimum oil flow rate
3- Minimum gas production rate (default: 0)
4- Maximum water cut
5- Maximum gas-oil ratio (default: infinity)
6- Maximum water-gas ratio (default: infinity)
7- Workover procedure on exceeding water cut, GOR, WGR or GLR
NONE: Do nothing
8- End run flag
YES: The run will stop at the next report time if the well is shut or stopped for any reason after being opened
NO: The run will continue regardless
9- Name of the well to be opened when this well is shut (default: no well)
10- Quantity to which the minimum economic limits in items 2, 3, 14 will be applied
RATE: The limit will be applied to the well actual flow rate

TSTEP: Time step

APPENDIX 5: TABULATED RESULTS OF FLOW SIMULATION

Table A5-1: Tabulated results of flow simulation for 61 x 50 grid, M = 0.4

SUMMARY OF RUN INPUT

DAYS	YEARS	WOPR	WOPT	WPI	WWPR	WWPT	WWCT
	years	sm^3/day, P	sm^3, P	P	sm^3/day, P	sm^3, P	P
0	0	0	0	0	0	0	0
4	0.011	89.650	414.85	2286.11	0.013	0.06	0.000
8	0.022	86.991	769.74	2286.20	0.013	0.11	0.000
12	0.033	87.822	1119.97	2286.28	0.013	0.16	0.000
16	0.044	88.187	1472.51	2286.37	0.013	0.22	0.000
20	0.055	88.257	1824.76	2286.45	0.013	0.27	0.000
24	0.066	87.129	2176.63	2286.52	0.013	0.32	0.000
28	0.077	86.934	2524.11	2286.28	0.013	0.37	0.000
32	0.088	51.106	2797.83	1361.03	41.928	86.22	0.451
36	0.099	29.563	2968.37	1004.10	67.088	294.33	0.694
40	0.110	17.330	3051.48	962.91	81.160	603.18	0.824
44	0.120	14.056	3111.44	964.71	84.738	938.09	0.858
48	0.131	12.308	3163.45	982.82	86.638	1281.61	0.876
52	0.142	11.152	3210.11	992.80	87.884	1630.94	0.887
56	0.153	9.712	3252.16	934.90	89.451	1985.25	0.902
60	0.164	8.434	3288.18	919.86	90.846	2346.14	0.915
64	0.175	7.547	3319.84	910.52	91.805	2711.78	0.924
68	0.186	6.892	3348.55	911.56	92.513	3080.59	0.931
72	0.197	6.420	3375.03	918.20	93.023	3451.82	0.935
76	0.208	6.040	3399.84	924.76	93.434	3824.85	0.939
80	0.219	5.718	3423.27	930.22	93.780	4199.38	0.943
84	0.230	5.440	3445.50	934.95	94.069	4575.17	0.945
88	0.241	5.185	3466.69	938.67	94.301	4951.97	0.948
92	0.252	4.964	3486.94	941.40	94.527	5329.66	0.950
96	0.263	4.775	3506.38	942.81	94.748	5708.26	0.952
100	0.274	4.593	3525.08	940.58	94.956	6087.69	0.954
104	0.285	4.404	3543.05	931.70	95.161	6467.96	0.956
108	0.296	4.199	3560.22	922.38	95.392	6849.10	0.958
112	0.307	3.991	3576.54	919.88	95.625	7231.20	0.960
116	0.318	[illegible]	3592.06	921.14	95.842	7614.19	0.962
120	0.32[illegible]	[illegible]0	3606.79	923.93	96.055	7998.03	0.964
124	0.339	[illegible]0	3620.79	926.97	96.260	8382.71	0.966
128	0.350	3.24[illegible]	3634.06	929.88	96.457	8768.21	0.967
132	0.361	3.087	3646.69	932.05	96.637	9154.45	0.969
136	0.372	2.941	3658.69	933.56	96.799	9541.39	0.971

140	0.383	2.806	3670.13	935.73	96.947	9928.94	0.972
144	0.394	2.682	3681.06	938.22	97.080	10317.04	0.973
148	0.405	2.555	3691.49	940.79	97.216	10705.68	0.974
152	0.416	2.425	3701.41	943.28	97.358	11094.87	0.976
156	0.427	2.293	3710.80	945.00	97.504	11484.65	0.977
160	0.438	2.163	3719.66	947.02	97.650	11875.01	0.978
164	0.449	2.045	3728.03	949.09	97.781	12265.93	0.980
168	0.460	1.951	3735.98	951.27	97.886	12657.31	0.980
172	0.471	1.878	3743.56	953.69	97.966	13049.10	0.981
176	0.482	1.816	3750.92	956.42	98.033	13441.13	0.982
180	0.493	1.763	3758.02	959.06	98.091	13833.44	0.982
184	0.504	1.715	3764.88	961.66	98.143	14226.01	0.983
188	0.515	1.669	3771.56	964.35	98.192	14618.78	0.983
192	0.526	1.626	3778.06	967.03	98.238	15011.73	0.984
196	0.537	1.585	3784.40	969.68	98.282	15404.86	0.984
200	0.548	1.545	3790.58	972.29	98.325	15798.16	0.985
204	0.559	1.507	3796.61	974.85	98.366	16191.63	0.985
208	0.569	1.470	3802.49	977.35	98.405	16585.25	0.985
212	0.580	1.434	3808.23	979.78	98.443	16979.02	0.986
216	0.591	1.401	3813.83	982.15	98.479	17372.94	0.986
220	0.602	1.368	3819.30	984.43	98.514	17766.99	0.986
224	0.613	1.336	3824.65	986.63	98.548	18161.18	0.987
228	0.624	1.305	3829.87	988.75	98.581	18555.51	0.987
232	0.635	1.275	3834.97	990.79	98.613	18949.96	0.987
236	0.646	1.245	3839.95	992.74	98.645	19344.54	0.988
240	0.657	1.216	3844.82	994.54	98.676	19739.25	0.988
244	0.668	1.188	3849.57	996.15	98.707	20134.08	0.988
248	0.679	1.162	3854.21	997.29	98.735	20529.02	0.988
252	0.690	1.137	3858.76	997.91	98.762	20924.07	0.989
256	0.701	1.112	3863.21	997.41	98.788	21319.22	0.989
260	0.712	1.089	3867.56	995.56	98.814	21714.47	0.989
264	0.723	1.066	3871.83	992.05	98.839	22109.83	0.989
268	0.734	1.043	3876.00	987.98	98.863	22505.28	0.990
272	0.745	1.019	3880.08	984.44	98.889	22900.84	0.990
276	0.756	0.994	3884.05	981.99	98.917	23296.51	0.990
280	0.767	0	3884.05	0	0	23296.51	0
284	0.778	0	3884.05	0	0	23296.51	0
288	0.789	0	3884.05	0	0	23296.51	0
292	0.799	0	3884.05	0	0	23296.51	0
296	0.810	0	3884.05	0	0	23296.51	0
300	0.821	0	3884.05	0	0	23296.51	0
304	0.832	0	3884.05	0	0	23296.51	0
308	0.843	0	3884.05	0	0	23296.51	0
312	0.854	0	3884.05	0	0	23296.51	0
316	0.865	0	3884.05	0	0	23296.51	0
320	0.876	0	3884.05	0	0	23296.51	0

DAYS	WBHP barsa, I	WBHP barsa, P	WWIR sm^3/day, I	WWIT sm^3, I	WVIT rm^3, I	FOEW	FRPV rm^3
0	100.1	100.1	0	0	0	0	9934.94
4	98.0	20	100	400	406.7	0.0627	9909.47
8	117.4	20	100	800	813.6	0.1163	9912.19
12	141.0	20	100	1200	1220.3	0.1692	9917.25
16	155.6	20	100	1600	1627.0	0.2225	9921.15
20	167.9	20	100	2000	2033.5	0.2757	9925.17
24	178.1	20	100	2400	2440.0	0.3288	9929.36
28	192.3	20	100	2800	2846.2	0.3813	9935.84
32	201.6	20	100	3200	3252.2	0.4227	9940.52
36	202.7	20	100	3600	3658.1	0.4485	9941.64
40	200.5	20	100	4000	4064.0	0.4610	9941.09
44	198.1	20	100	4400	4469.9	0.4701	9940.39
48	195.9	20	100	4800	4875.8	0.4779	9939.79
52	194.0	20	100	5200	5281.7	0.4850	9939.25
56	192.2	20	100	5600	5687.6	0.4913	9938.78
60	190.7	20	100	6000	6093.5	0.4968	9938.36
64	189.3	20	100	6400	6499.4	0.5016	9937.99
68	188.0	20	100	6800	6905.4	0.5059	9937.66
72	186.8	20	100	7200	7311.3	0.5099	9937.37
76	185.7	20	100	7600	7717.3	0.5136	9937.09
80	184.6	20	100	8000	8123.2	0.5172	9936.84
84	183.7	20	100	8400	8529.2	0.5205	9936.62
88	182.9	20	100	8800	8935.2	0.5237	9936.46
92	182.2	20	100	9200	9341.2	0.5268	9936.38
96	181.5	20	100	9600	9747.1	0.5297	9936.29
100	180.8	20	100	10000	10153.1	0.5326	9936.19
104	180.2	20	100	10400	10559.1	0.5353	9936.08
108	179.6	20	100	10800	10965.1	0.5379	9935.98
112	179.0	20	100	11200	11371.0	0.5403	9935.87
116	178.5	20	100	11600	11777.0	0.5427	9935.76
120	177.9	20	100	12000	12183.0	0.5449	9935.66
124	177.4	20	100	12400	12589.0	0.5470	9935.55
128	176.9	20	100	12800	12995.0	0.5490	9935.43
132	176.4	20	100	13200	13401.0	0.5509	9935.30
136	175.9	20	100	13600	13806.9	0.5528	9935.17
140	175.5	20	100	14000	14212.9	0.5545	9935.05
144	175.1	20	100	14400	14618.9	0.5561	9934.93
148	174.7	20	100	14800	15024.9	0.5577	9934.83
152	174.3	20	100	15200	15430.9	0.5592	9934.73
156	173.9	20	100	15600	15836.9	0.5606	9934.63
160	173.6	20	100	16000	16242.9	0.5620	9934.53
164	173.2	20	100	16400	16648.9	0.5632	9934.42
168	172.9	20	100	16800	17054.9	0.5644	9934.32
172	172.6	20	100	17200	17460.9	0.5656	9934.22

176	172.3	20	100	17600	17866.9	0.5667	9934.13
180	172.0	20	100	18000	18272.9	0.5678	9934.03
184	171.7	20	100	18400	18679.0	0.5688	9933.94
188	171.5	20	100	18800	19085.0	0.5698	9933.85
192	171.2	20	100	19200	19491.0	0.5708	9933.77
196	171.0	20	100	19600	19897.0	0.5717	9933.69
200	170.8	20	100	20000	20303.0	0.5727	9933.61
204	170.5	20	100	20400	20709.1	0.5736	9933.53
208	170.3	20	100	20800	21115.1	0.5745	9933.46
212	170.1	20	100	21200	21521.1	0.5753	9933.39
216	169.9	20	100	21600	21927.1	0.5762	9933.33
220	169.8	20	100	22000	22333.2	0.5770	9933.26
224	169.6	20	100	22400	22739.2	0.5778	9933.20
228	169.4	20	100	22800	23145.3	0.5786	9933.14
232	169.3	20	100	23200	23551.3	0.5794	9933.09
236	169.1	20	100	23600	23957.3	0.5801	9933.03
240	169.0	20	100	24000	24363.4	0.5809	9932.98
244	168.8	20	100	24400	24769.4	0.5816	9932.93
248	168.7	20	100	24800	25175.5	0.5823	9932.88
252	168.5	20	100	25200	25581.5	0.5830	9932.84
256	168.4	20	100	25600	25987.5	0.5837	9932.79
260	168.3	20	100	26000	26393.6	0.5843	9932.75
264	168.2	20	100	26400	26799.6	0.5850	9932.70
268	168.1	20	100	26800	27205.7	0.5856	9932.66
272	167.9	20	100	27200	27611.7	0.5862	9932.62
276	167.8	20	100	27600	28017.8	0.5868	9932.58
280	500	0	85.02	27988.2	28409.4	0.5868	10123.21
284	500	0	6.71	28041.2	28462.4	0.5868	10148.50
288	500	0	1.45	28049.8	28470.9	0.5868	10152.43
292	500	0	0.67	28052.5	28473.6	0.5868	10153.62
296	500	0	0.39	28054.0	28475.2	0.5868	10154.29
300	500	0	0.26	28055.1	28476.2	0.5868	10154.74
304	500	0	0.19	28055.8	28477.0	0.5868	10155.05
308	500	0	0.14	28056.4	28477.5	0.5868	10155.29
312	500	0	0.11	28056.8	28477.9	0.5868	10155.48
316	500	0	0.09	28057.2	28478.3	0.5868	10155.63
320	500	0	0.07	28057.4	28478.6	0.5868	10155.75

APPENDIX 6: TURBO PASCAL PROGRAM TO SCALE DOWN POROSITY FROM 8 x 6 GRID TO 16 x 12 GRID

```
Program devide(porfile,fout);
uses wincrt  ;
type
    row = 1..50;
    column =1..70;
    Porarray = Array [row, column] of real;

Var

   i, j, k, l, count: integer;
   Por, por2 : porarray ;
   Porfile,fout: text;

Begin
     assign(fout,'16x12por.out');
     rewrite(fout);
     Assign (porfile, '8x6por.out');
     Reset (porfile);
For i:=1 to 6 do
For j:=1 to 8 do

    Readln (porfile, por [i,j]);
    Close (porfile);

for i:=1 to 6 do
for j:=1 to 8 do
for k:=2*i-1 to 2*i do
for l:=2*j-1 to 2*j do

    por2[k,l]:=por[i,j];

for k:=1 to 12 do
for l:=1 to 16 do

    writeln(fout,por2[k,l]:2:4);
close(fout);
end.
```

APPENDIX 7: UNIX SHELL SCRIPT FILE TO AUTOMATE RUNNING ECLIPSE FOR 100 TIMES

```
set start = 1
set finish = 100
@ sim = $start
while ($sim <= $finish)
sed -e "s/NUM/$sim/g" 8x6perm.par > temp.par
gsl2eclm<<END
temp.par
END
cat 8X6FPP.ECL > middle
cat top middle bottom > 8X6.DATA
@eclipse<<END
99a
8X6
END
cat 8X6.RSM >> 8X6
@ sim = $sim + 1
rm temp.par
rm *.ECL
rm *.FGRID
rm *.DBG
rm *.PRT
rm middle
rm *DATA
rm *RSM
end
```

APPENDIX 8: "OIL RATES" VERSUS PVWI FOR 100 REALIZATIONS

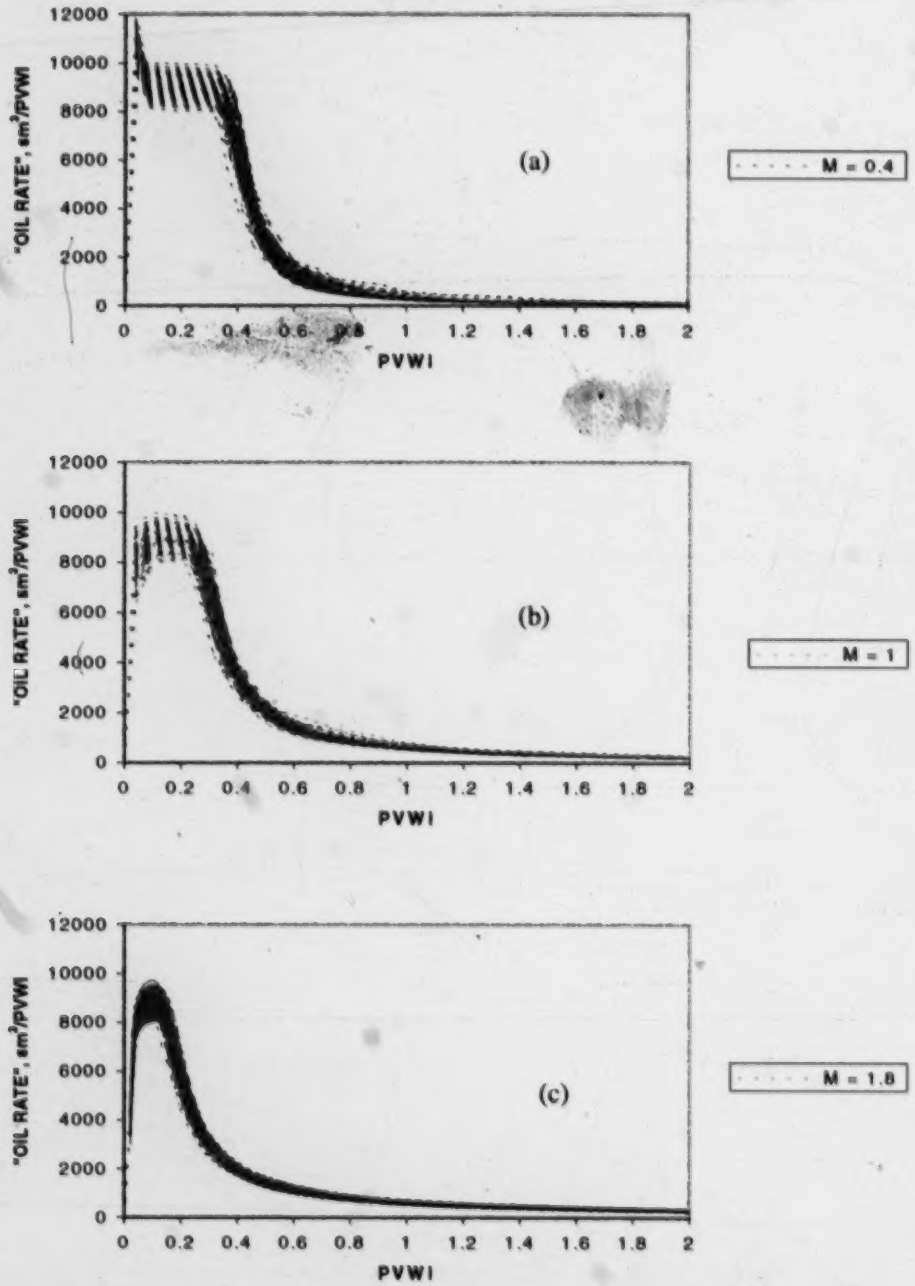

Figure A8-1: 8 x 6 grid – "oil rate" plots for M = 0.4 (a), M = 1 (b), and M = 1.8 (c)

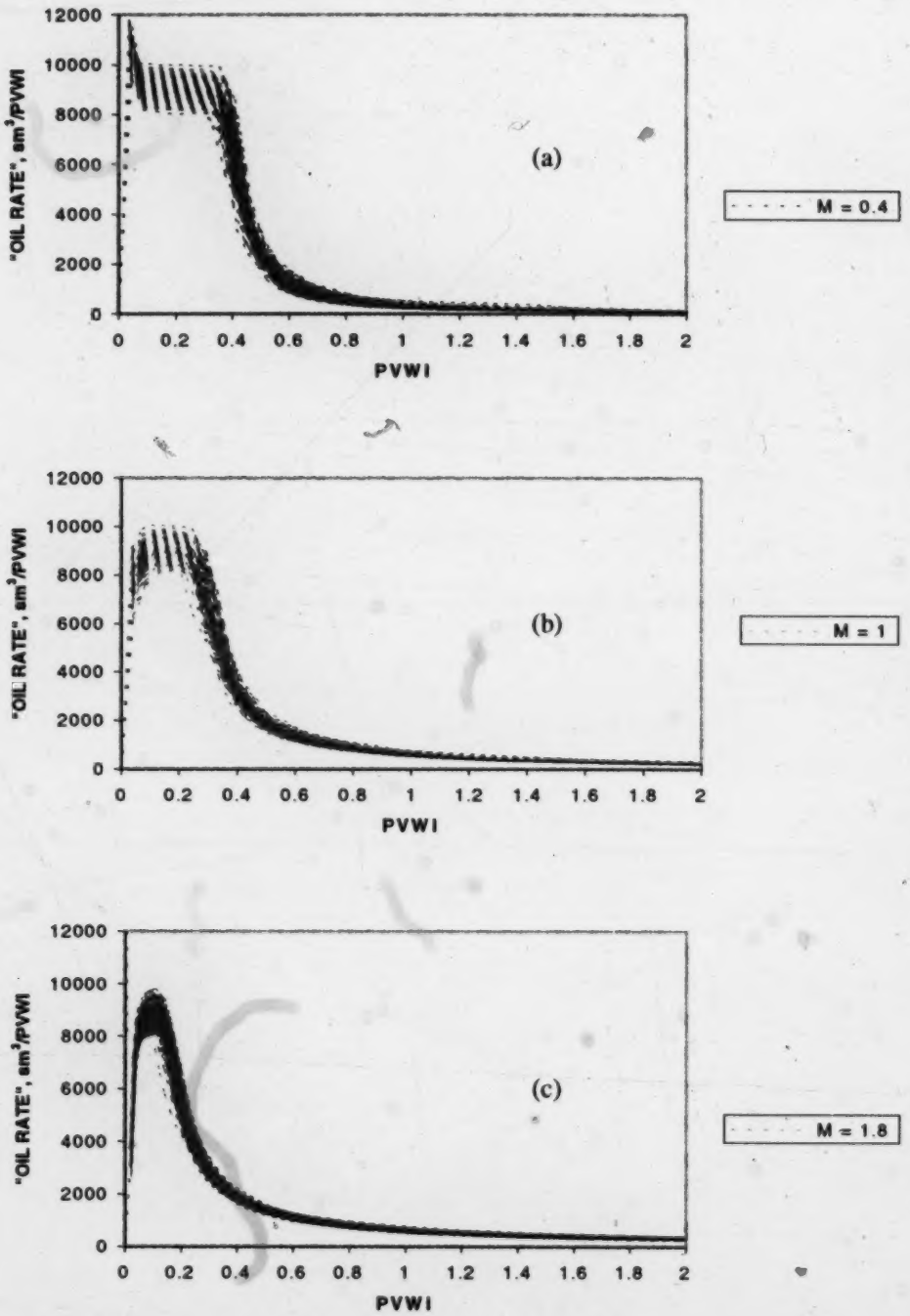

Figure A8-2: 16 x 12 grid – "oil rate" plots for M = 0.4 (a), M = 1 (b), and M = 1.8 (c)

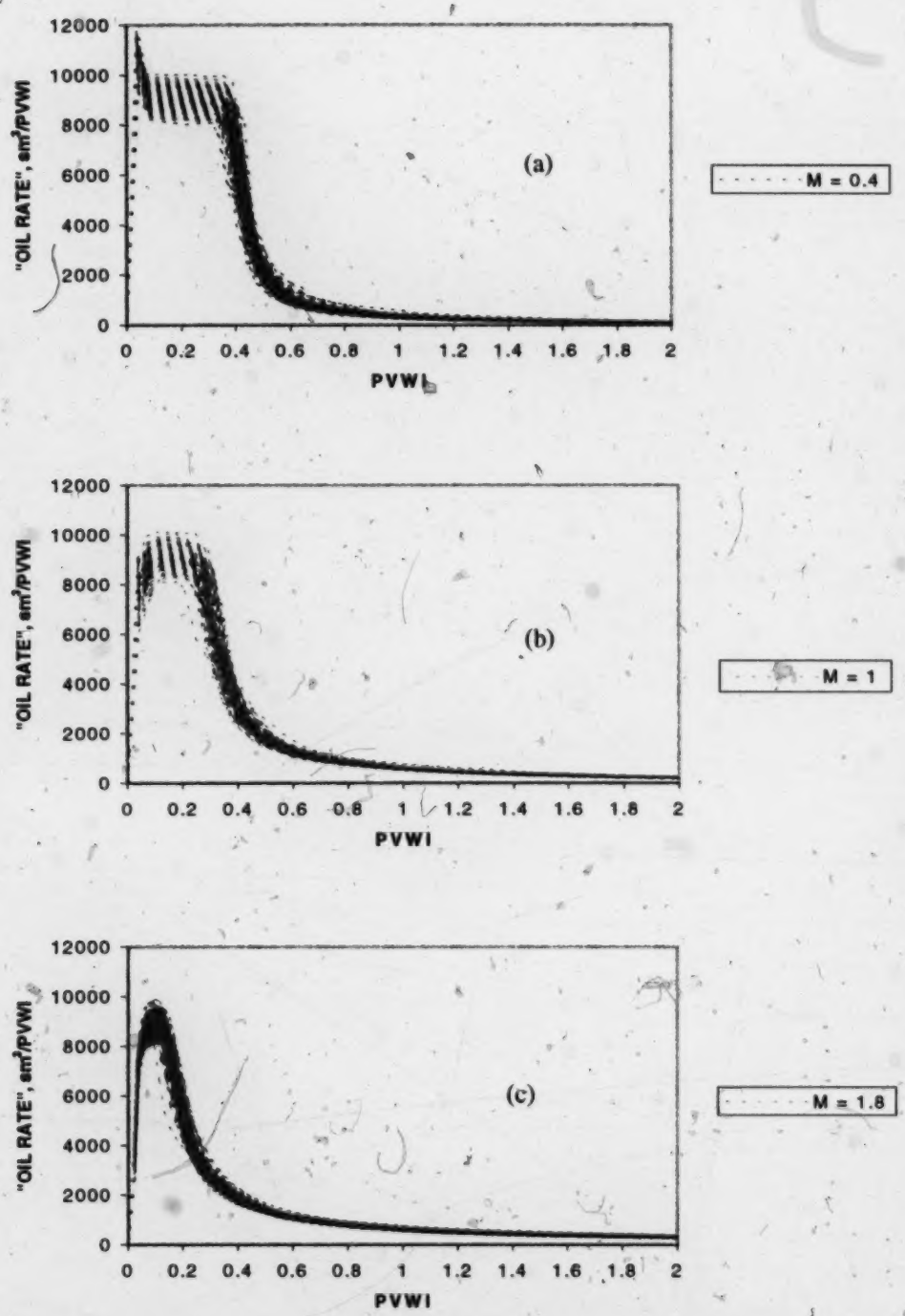

Figure A8-3: 32 x 24 grid – "oil rate" plots for M = 0.4 (a), M = 1 (b), and M = 1.8 (c)

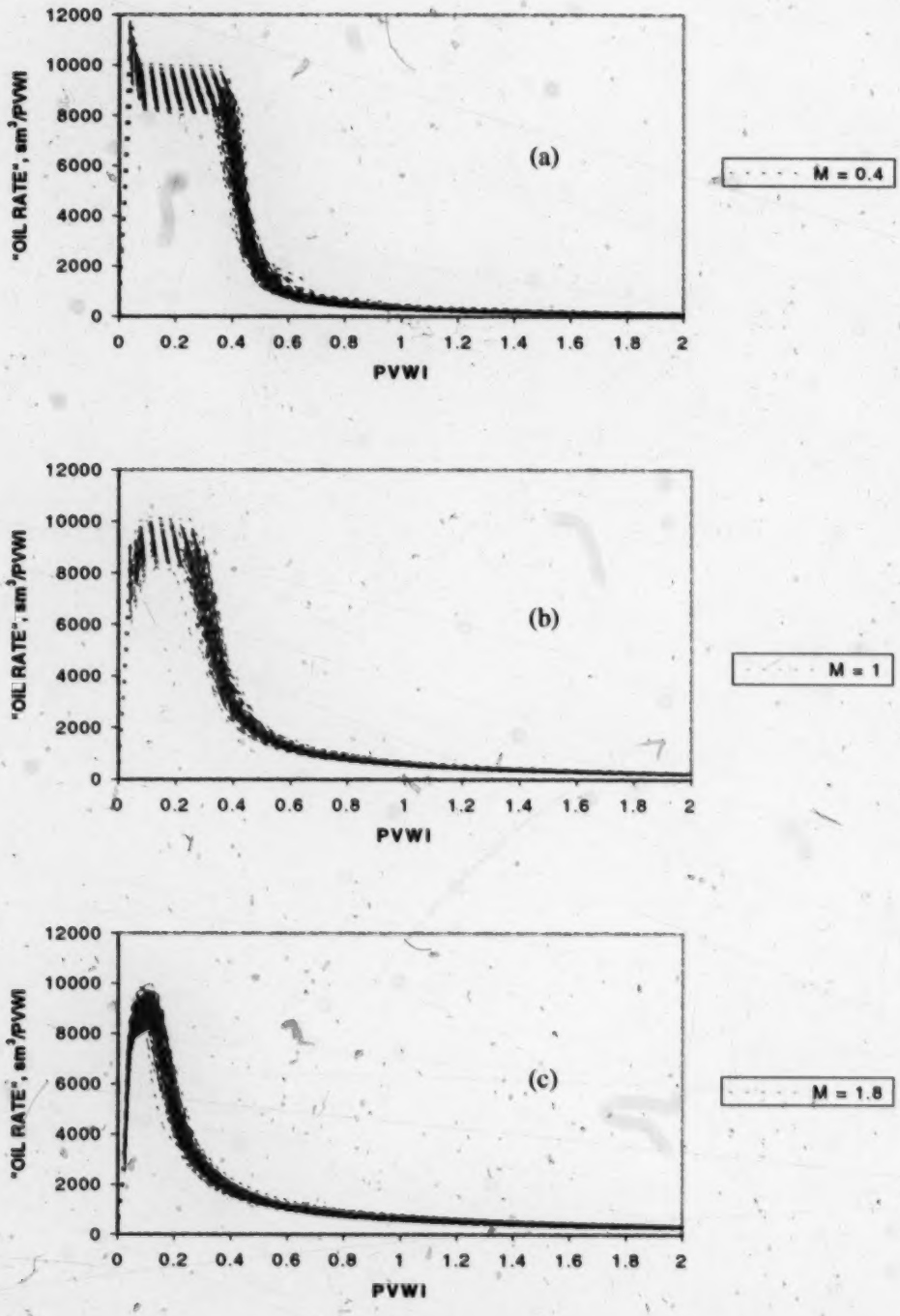

Figure A8-4: 64 x 48 grid – "oil rate" plots for M = 0.4 (a), M = 1 (b), and M = 1.8 (c)

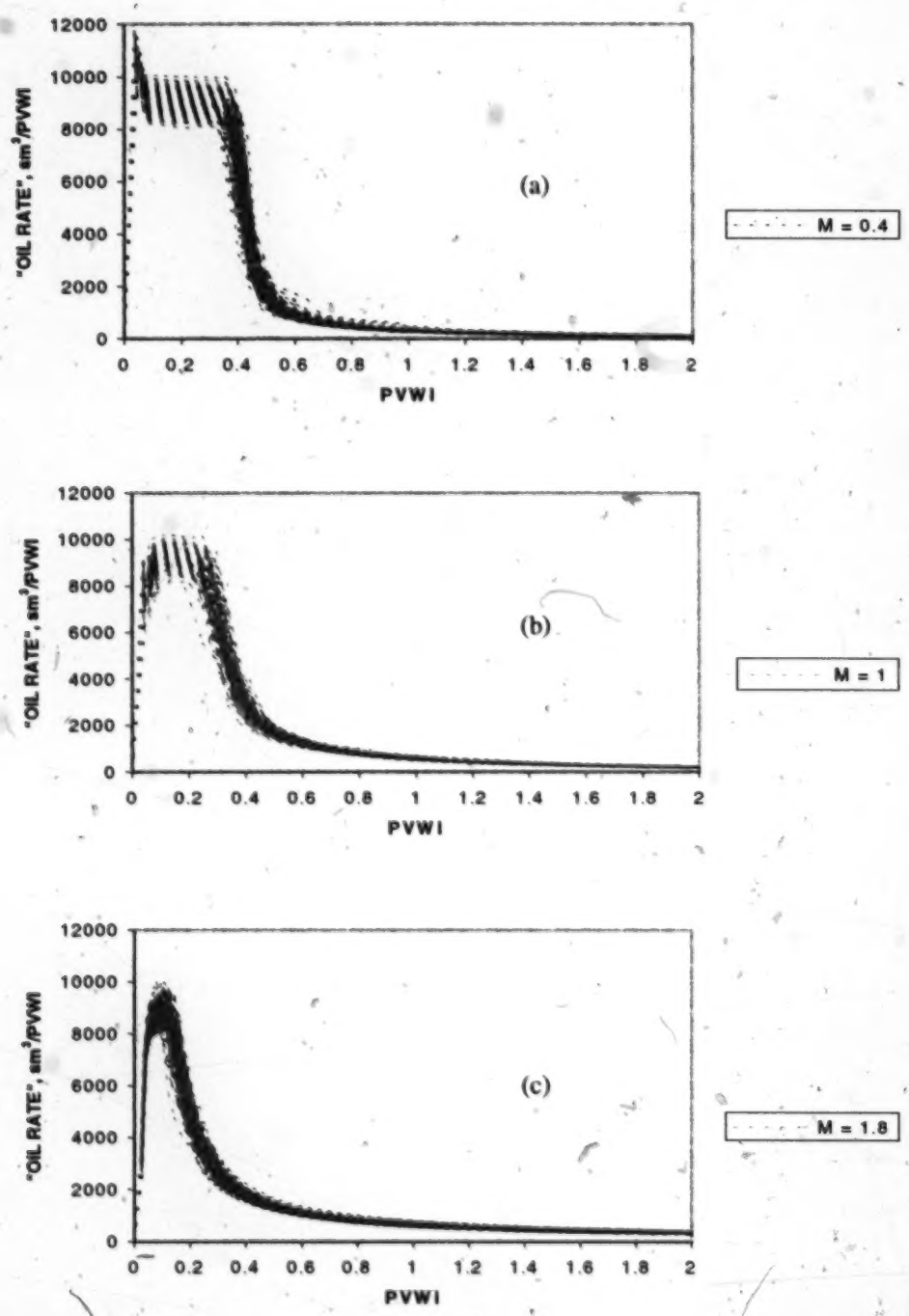

Figure A8-5: 128 x 96 grid–"oil rate" plots for M = 0.4 (a), M = 1 (b), and M = 1.8 (c)

APPENDIX 9: "WATER RATES" VERSUS PVWI FOR 100 REALIZATIONS

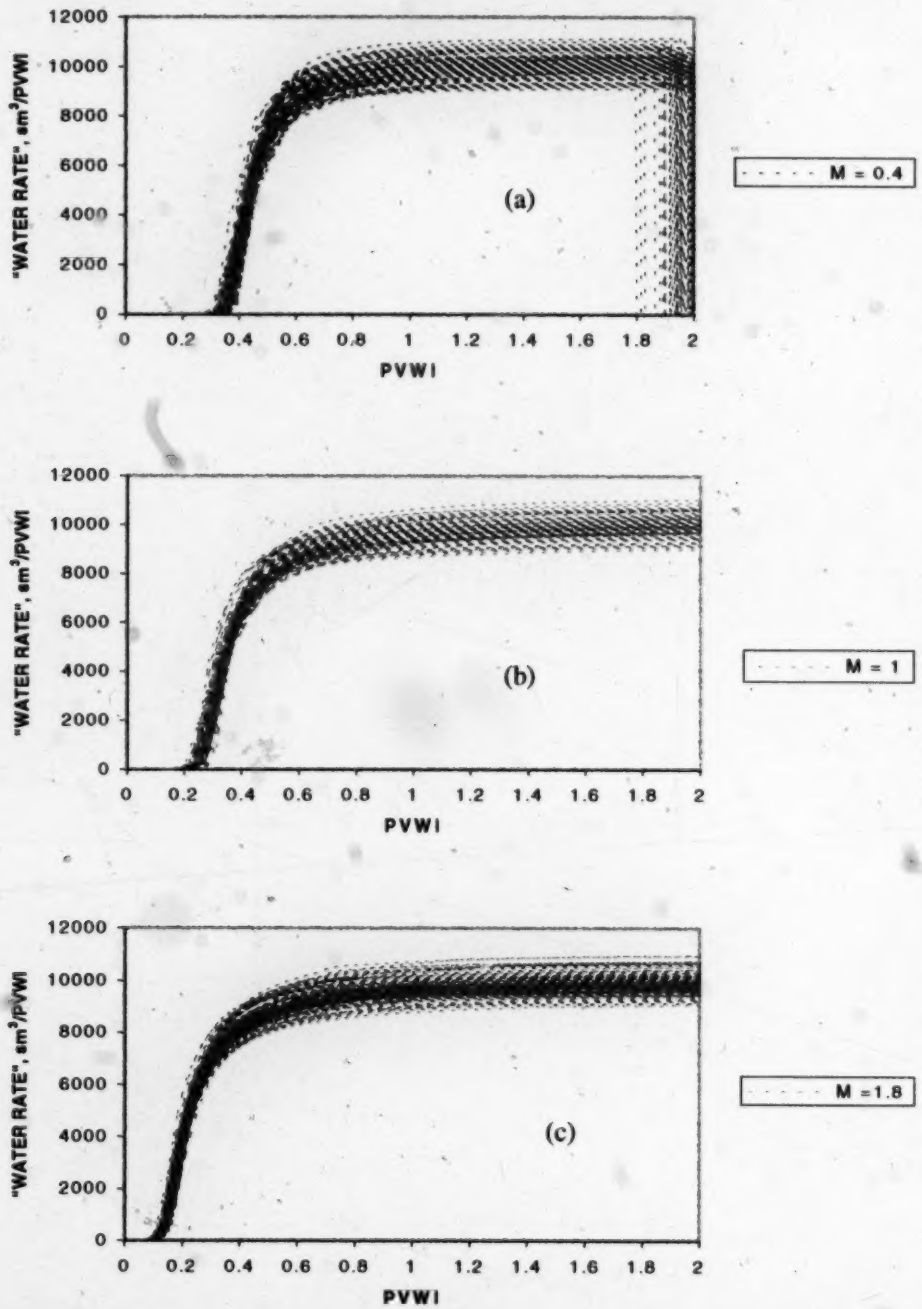

Figure A9-1: 8 x 6 grid – "water rate" plots for M = 0.4 (a), M = 1 (b), and M = 1.8 (c)

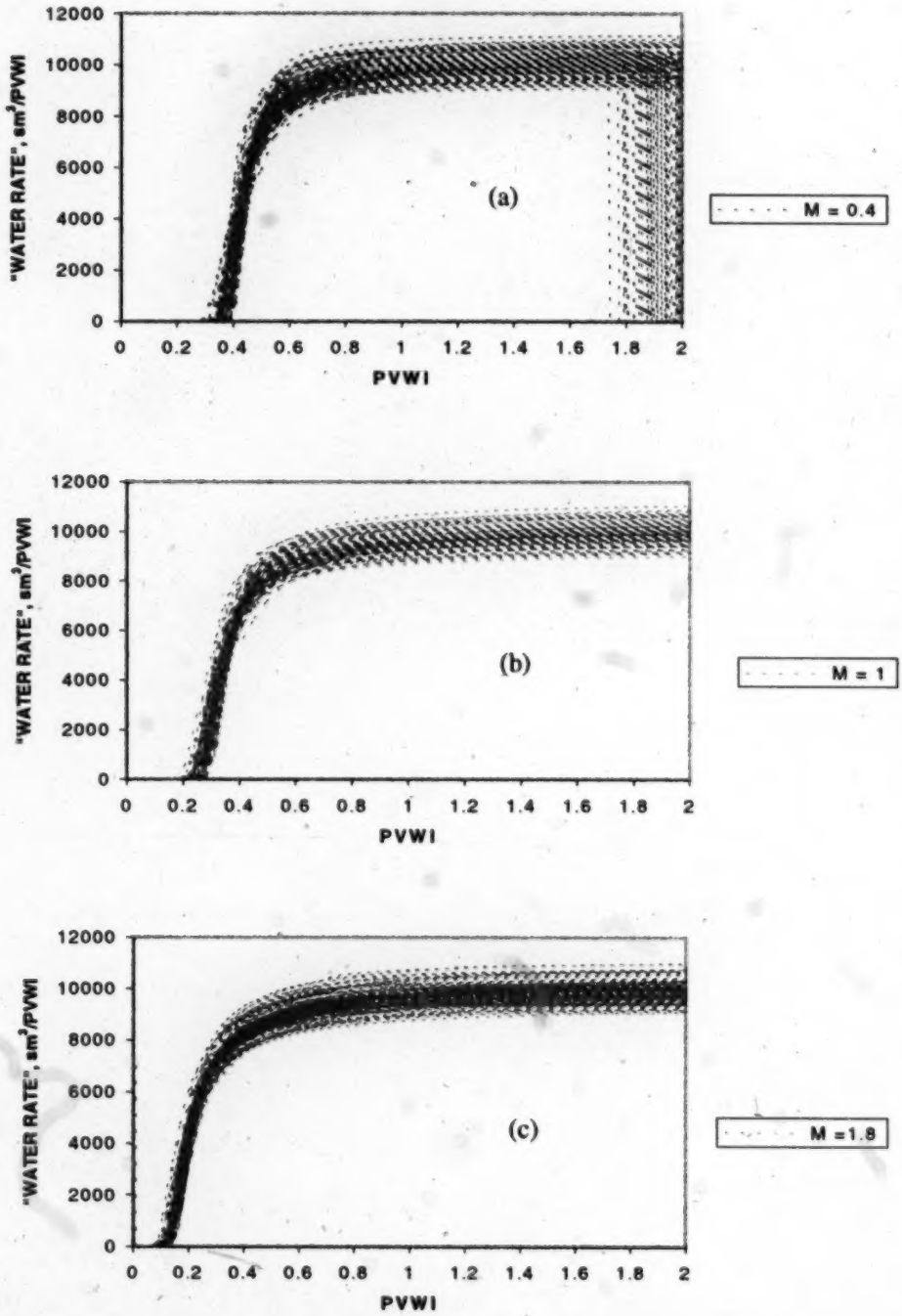

Figure A9-2: 16 x 12 grid – "water rate" plots for M = 0.4 (a), M = 1 (b), M = 1.8 (c)

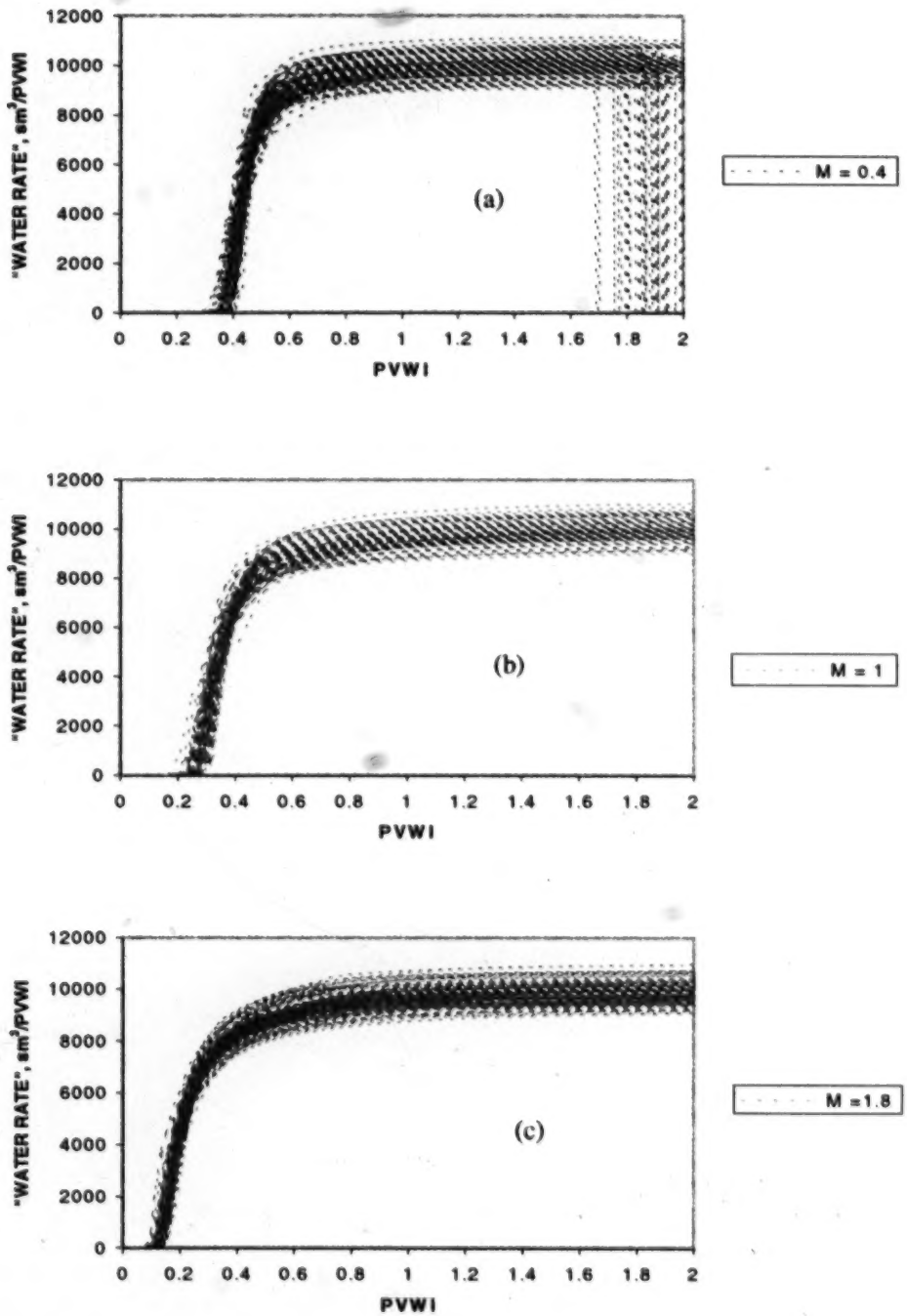

Figure A9-3: 32 x 24 grid – "water rate" plots for M = 0.4 (a), M = 1 (b), M = 1.8 (c)

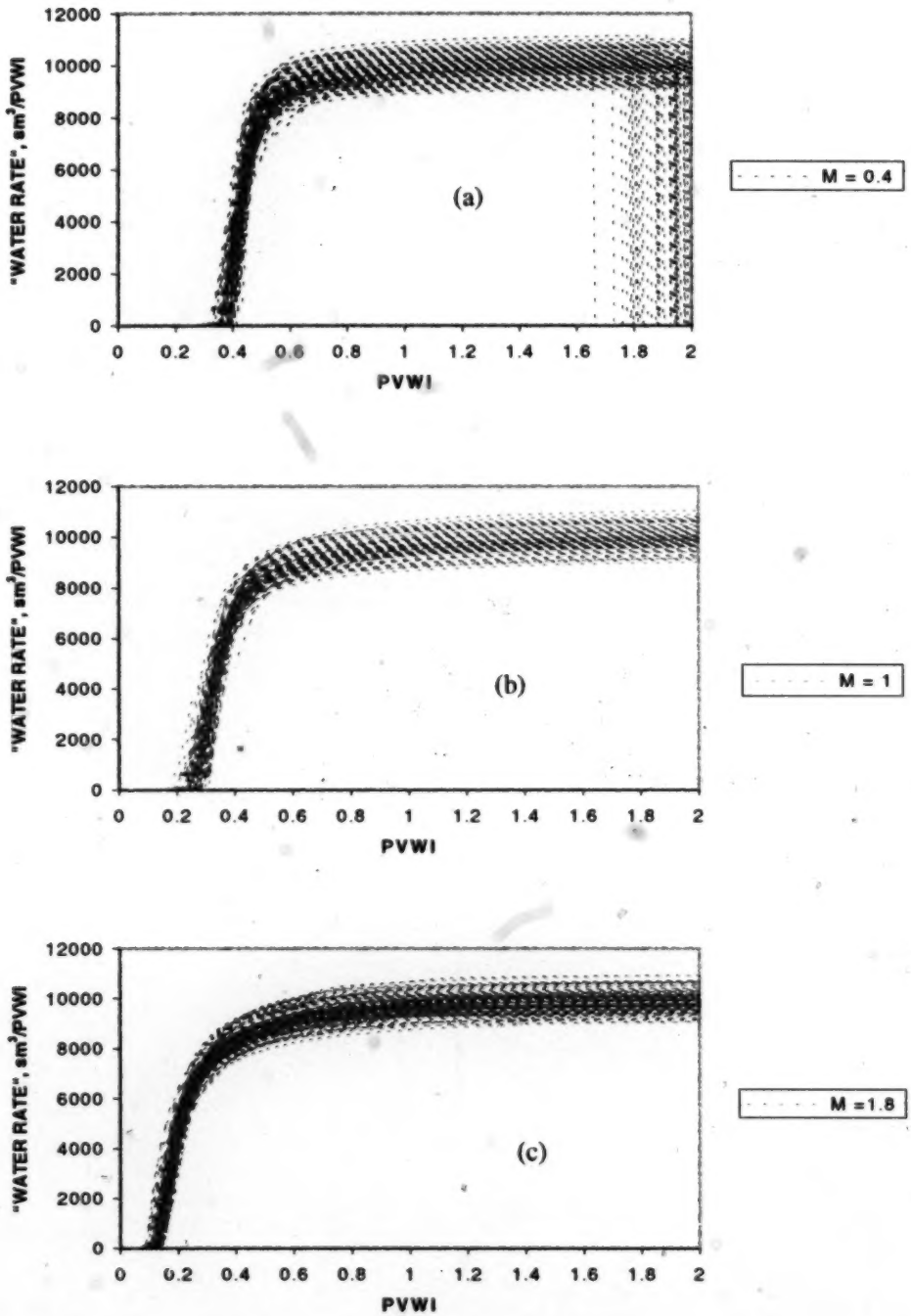

Figure A9-4: 64 x 48 grid – "water rate" plots for M = 0.4 (a), M = 1 (b), M = 1.8 (c)

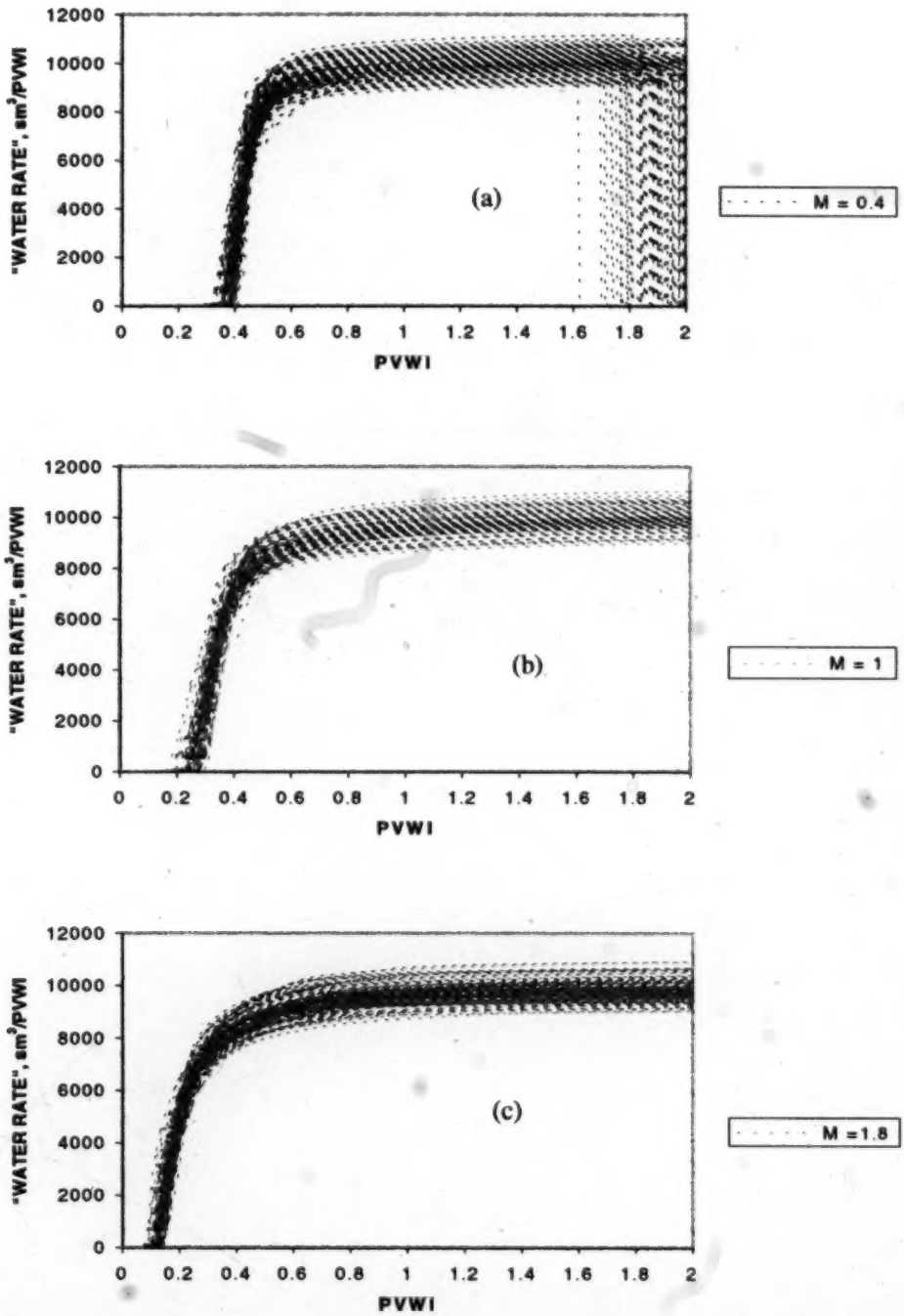

Figure A9-5: 128 x 96 grid – "water rate" plots for M = 0.4 (a), M = 1 (b), M = 1.8 (c)

APPENDIX 10: OIL RECOVERY FACTORS FOR 100 REALIZATIONS

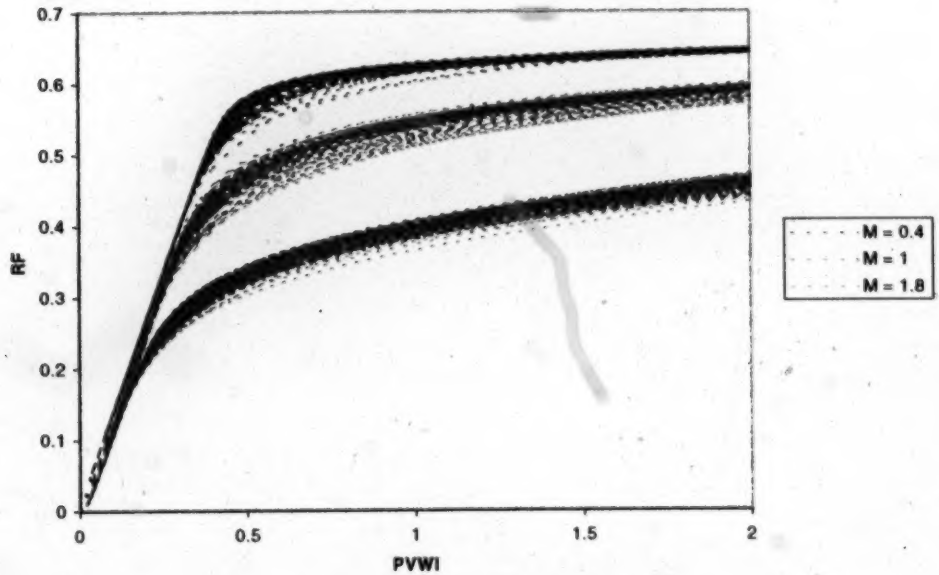

Figure A10-1: 8 x 6 grid – recovery factor plots for all three mobility ratios

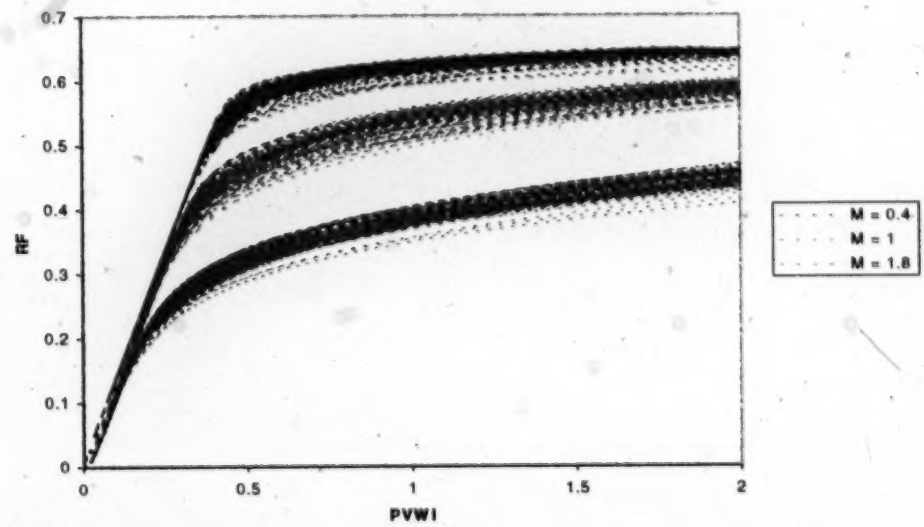

Figure A10-2: 16 x 12 grid – recovery factor plots for all three mobility ratios

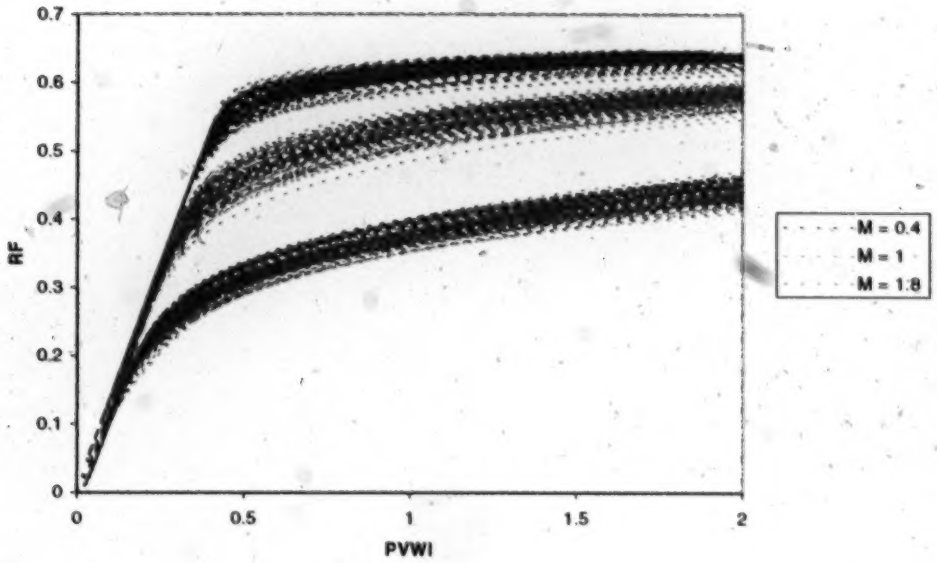

Figure A10-3: 32 x 24 grid – recovery factor plots for all three mobility ratios

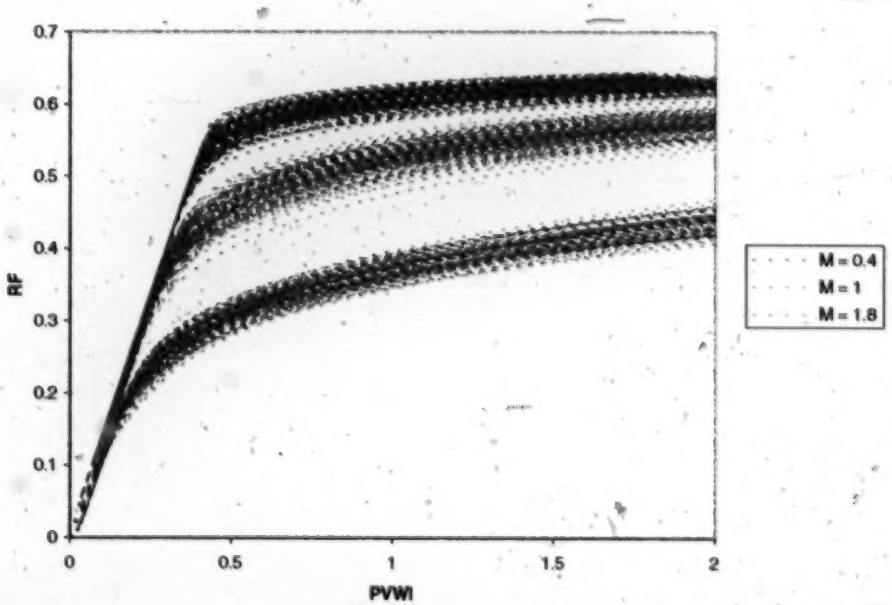

Figure A10-4: 64 x 48 grid – recovery factor plots for all three mobility ratios

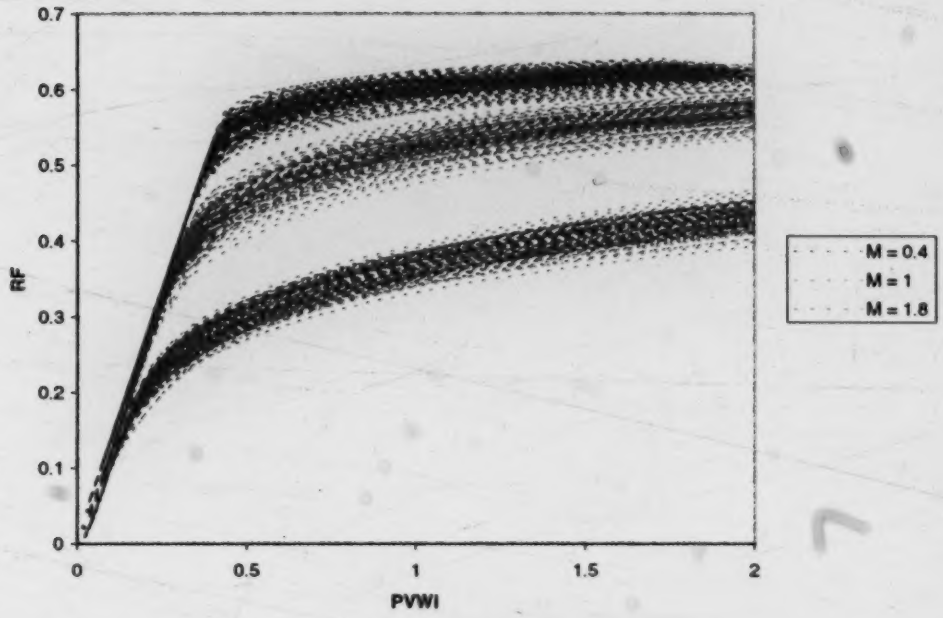

Figure A10-5: 128 x 96 grid – recovery factor plots for all three mobility ratios

APPENDIX 11: RECOVERY FACTORS TAKEN AT 1 PVWI

Table A11-1: Recovery factors taken at 1 PVWI for 100 realizations

Realization	8x6	8x61	8x6unf	16x12	16x121	16x12unf	32x24	32x241	32x24unf
1	0.6035	0.5195	0.3752	0.6049	0.5203	0.3726	0.6055	0.5159	0.3642
2	0.6258	0.5473	0.3903	0.6221	0.5421	0.3825	0.6090	0.5272	0.3655
3	0.6248	0.5474	0.3938	0.6208	0.5411	0.3776	0.6077	0.5260	0.3604
4	0.6172	0.5141	0.3930	0.6145	0.5130	0.3924	0.6046	0.5055	0.3798
5	0.6240	0.5418	0.3924	0.6238	0.5391	0.3853	0.6180	0.5356	0.3783
6	0.6242	0.5507	0.3989	0.6198	0.5401	0.3851	0.6162	0.5369	0.3801
7	0.6218	0.5341	0.3811	0.6242	0.5382	0.3844	0.6164	0.5242	0.3672
8	0.6256	0.5505	0.3991	0.6305	0.5523	0.3942	0.6287	0.5446	0.3810
9	0.6227	0.5404	0.3931	0.6088	0.5234	0.3764	0.6003	0.5234	0.3769
10	0.6267	0.5499	0.4049	0.6301	0.5501	0.3999	0.6284	0.5527	0.3998
11	0.6269	0.5517	0.4074	0.6294	0.5535	0.4060	0.6279	0.5524	0.4001
12	0.6246	0.5406	0.3972	0.6176	0.5308	0.3806	0.6125	0.5267	0.3730
13	0.6252	0.5436	0.3945	0.6267	0.5423	0.3926	0.6219	0.5398	0.3863
14	0.6227	0.5347	0.3990	0.6128	0.5215	0.3824	0.6116	0.5214	0.3758
15	0.6254	0.5489	0.3988	0.6209	0.5376	0.3837	0.6152	0.5329	0.3761
16	0.6200	0.5403	0.3970	0.5935	0.5126	0.3709	0.5832	0.5054	0.3633
17	0.6245	0.5422	0.4032	0.6198	0.5340	0.3915	0.6140	0.5302	0.3840
18	0.6253	0.5375	0.4075	0.6188	0.5278	0.4006	0.6176	0.5273	0.3965
19	0.6200	0.5451	0.3977	0.6142	0.5397	0.3904	0.6102	0.5370	0.3827
20	0.6259	0.5454	0.3974	0.6130	0.5196	0.3706	0.6066	0.5138	0.3627
21	0.6267	0.5515	0.4062	0.6309	0.5556	0.4055	0.6280	0.5543	0.3990
22	0.6247	0.5375	0.4031	0.6257	0.5443	0.4015	0.6213	0.5369	0.3935
23	0.6221	0.5362	0.3891	0.5953	0.5026	0.3527	0.5923	0.5041	0.3537
24	0.6239	0.5445	0.4030	0.6180	0.5339	0.3905	0.6142	0.5325	0.3816
25	0.6214	0.5377	0.3847	0.6160	0.5296	0.3743	0.6105	0.5241	0.3701
26	0.6246	0.5422	0.3981	0.6236	0.5374	0.3880	0.6085	0.5176	0.3631
27	0.6238	0.5243	0.3933	0.6238	0.5251	0.3852	0.6230	0.5249	0.3809
28	0.6002	0.5132	0.3670	0.5969	0.5061	0.3571	0.5913	0.5040	0.3525
29	0.6300	0.5578	0.4047	0.6334	0.5596	0.3999	0.6326	0.5624	0.4019
30	0.6267	0.5491	0.3910	0.6318	0.5545	0.3882	0.6270	0.5508	0.3812

31	0.6260	0.5441	0.4045	0.6276	0.5441	0.4001	0.6285	0.5495	0.4010
32	0.6146	0.5385	0.3847	0.6176	0.5400	0.3850	0.6247	0.5462	0.3837
33	0.6256	0.5476	0.4019	0.6255	0.5465	0.3919	0.6270	0.5505	0.3937
34	0.6232	0.5433	0.3971	0.6268	0.5452	0.3938	0.6210	0.5409	0.3882
35	0.6238	0.5443	0.3984	0.6232	0.5413	0.3869	0.6132	0.5336	0.3816
36	0.6227	0.5280	0.4082	0.6171	0.5187	0.3996	0.6180	0.5226	0.3955
37	0.6209	0.5383	0.3882	0.6157	0.5334	0.3774	0.6212	0.5376	0.3748
38	0.6160	0.5293	0.3828	0.6099	0.5254	0.3711	0.5949	0.5138	0.3606
39	0.6193	0.5150	0.3954	0.6179	0.5152	0.3913	0.6119	0.5105	0.3811
40	0.6266	0.5537	0.4023	0.6295	0.5557	0.3976	0.6332	0.5584	0.3953
41	0.6218	0.5390	0.3863	0.6235	0.5383	0.3820	0.6092	0.5229	0.3671
42	0.6277	0.5552	0.4071	0.6245	0.5501	0.3990	0.6265	0.5538	0.3945
43	0.6154	0.5188	0.3936	0.5978	0.5075	0.3775	0.5953	0.5053	0.3723
44	0.6209	0.5227	0.3902	0.6217	0.5189	0.3783	0.6053	0.5086	0.3708
45	0.6217	0.5213	0.3978	0.6228	0.5121	0.3911	0.6137	0.4994	0.3747
46	0.6268	0.5189	0.4060	0.6301	0.5520	0.4053	0.6249	0.5452	0.3953
47	0.6274	0.5466	0.3981	0.6204	0.5406	0.3898	0.6237	0.5451	0.3906
48	0.6164	0.5479	0.3975	0.6210	0.5471	0.3995	0.6210	0.5486	0.4011
49	0.6186	0.5385	0.3773	0.5998	0.4970	0.3486	0.6047	0.5078	0.3535
50	0.6270	0.5225	0.4022	0.6265	0.5482	0.3866	0.6234	0.5409	0.3794
51	0.6166	0.5537	0.3855	0.6141	0.5115	0.3797	0.6066	0.5150	0.3751
52	0.6251	0.5155	0.3988	0.6276	0.5473	0.3908	0.6255	0.5481	0.3912
53	0.6276	0.5480	0.3999	0.6245	0.5444	0.3883	0.6217	0.5414	0.3801
54	0.6269	0.5533	0.3966	0.6312	0.5579	0.3959	0.6259	0.5499	0.3897
55	0.6209	0.5538	0.3868	0.6190	0.5303	0.3734	0.6137	0.5205	0.3624
56	0.6231	0.5376	0.3968	0.6089	0.5202	0.3806	0.6058	0.5198	0.3773
57	0.6228	0.5320	0.3868	0.6231	0.5366	0.3727	0.6103	0.5280	0.3712
58	0.6181	0.5430	0.3818	0.6198	0.5261	0.3786	0.6109	0.5147	0.3608
59	0.6260	0.5268	0.4016	0.6208	0.5410	0.3959	0.6138	0.5378	0.3942
60	0.6225	0.5464	0.3976	0.5949	0.5093	0.3824	0.5918	0.5048	0.3718
61	0.6250	0.5253	0.3986	0.6226	0.5424	0.3904	0.6205	0.5408	0.3831
62	0.6242	0.5489	0.4013	0.6129	0.5359	0.3879	0.6057	0.5303	0.3777
63	0.6226	0.5495	0.3935	0.6226	0.5313	0.3920	0.6234	0.5313	0.3932
64	0.6228	0.5278	0.3939	0.6255	0.5461	0.3919	0.6216	0.5441	0.3870
65	0.6233	0.5422	0.3953	0.6227	0.5400	0.3946	0.6149	0.5304	0.3814
66	0.6208	0.5350	0.3904	0.6171	0.5279	0.3767	0.6077	0.5156	0.3616

67	0.6217	0.5378	0.3912	0.6236	0.5382	0.3847	0.6158	0.5321	0.3787
68	0.6277	0.5529	0.3990	0.6252	0.5467	0.3893	0.6153	0.5414	0.3819
69	0.6143	0.5277	0.3817	0.6081	0.5204	0.3737	0.6036	0.5195	0.3689
70	0.6252	0.5490	0.3940	0.6188	0.5367	0.3807	0.6156	0.5335	0.3728
71	0.6270	0.5496	0.4020	0.6273	0.5496	0.3979	0.6198	0.5449	0.3922
72	0.6233	0.5427	0.3950	0.6262	0.5407	0.3799	0.6214	0.5340	0.3677
73	0.6268	0.5488	0.4077	0.6256	0.5493	0.4010	0.6222	0.5458	0.3924
74	0.6185	0.5349	0.3863	0.6123	0.5304	0.3792	0.6165	0.5344	0.3762
75	0.6227	0.5352	0.3875	0.6163	0.5287	0.3787	0.6140	0.5255	0.3714
76	0.6208	0.5391	0.3886	0.6145	0.5322	0.3795	0.6065	0.5252	0.3754
77	0.6174	0.5112	0.3848	0.6201	0.5146	0.3794	0.5904	0.4866	0.3549
78	0.6210	0.5408	0.3878	0.6206	0.5388	0.3829	0.6167	0.5362	0.3761
79	0.6235	0.5466	0.3935	0.6227	0.5423	0.3816	0.6164	0.5312	0.3696
80	0.6231	0.5486	0.4019	0.6136	0.5402	0.3975	0.6054	0.5288	0.3849
81	0.6228	0.5470	0.4005	0.6190	0.5437	0.3978	0.6181	0.5467	0.3971
82	0.6257	0.5465	0.4019	0.6280	0.5466	0.3989	0.6291	0.5498	0.3977
83	0.6238	0.5387	0.3974	0.6160	0.5253	0.3782	0.6142	0.5290	0.3757
84	0.6259	0.5510	0.3986	0.6260	0.5506	0.3921	0.6267	0.5487	0.3879
85	0.6236	0.5367	0.3965	0.6250	0.5365	0.3871	0.6236	0.5404	0.3900
86	0.6285	0.5535	0.4096	0.6297	0.5539		0.6254	0.5505	0.3950
87	0.6245	0.5437	0.3901	0.6291	0.5511	0.3903	0.6318	0.5553	0.3889
88	0.6226	0.5363	0.3933	0.6214	0.5289	0.3804	0.6216	0.5318	0.3743
89	0.6252	0.5407	0.4031	0.6222	0.5391	0.3964	0.6103	0.5292	0.3856
90	0.6262	0.5462	0.4034	0.6268	0.5456	0.4011	0.6247	0.5462	0.3980
91	0.6234	0.5225	0.4023	0.6244	0.5257	0.4008	0.6237	0.5266	0.3958
92	0.6236	0.5370	0.3917	0.6197	0.5266	0.3729	0.6097	0.5102	0.3554
93	0.6188	0.5123	0.3835	0.6177	0.5041	0.3734	0.6034	0.5004	0.3631
94	0.6205	0.5339	0.3831	0.6177	0.5283	0.3740	0.6053	0.5191	0.3674
95	0.6249	0.5412	0.4077	0.6266	0.5425	0.4056	0.6217	0.5399	0.3972
96	0.6240	0.5421	0.3956	0.6213	0.5341	0.3800	0.6103	0.5237	0.3681
97	0.6235	0.5451	0.3943	0.6262	0.5474	0.3899	0.6222	0.5386	0.3793
98	0.6229	0.5421	0.3968	0.6250	0.5403	0.3919	0.6135	0.5284	0.3777
99	0.6248	0.5390	0.3940	0.6187	0.5302	0.3799	0.6067	0.5204	0.3704
100	0.6188	0.5250	0.3898	0.6041	0.5123	0.3770	0.5990	0.5075	0.3675

Realization	64x48	64x481	64x48unf	128x96	128x961	128x96unf
1	0.5988	0.5109	0.3613	0.5952	0.5108	0.3561
2	0.6038	0.5250	0.3592	0.5963	0.5204	0.3543
3	0.6031	0.5228	0.3552	0.5995	0.5205	0.3533
4	0.5810	0.4910	0.3658	0.5754	0.4845	0.3571
5	0.6098	0.5317	0.3697	0.6041	0.5269	0.3629
6	0.6104	0.5332	0.3761	0.6096	0.5330	0.3725
7	0.6055	0.5158	0.3610	0.5990	0.5139	0.3551
8	0.6181	0.5379	0.3734	0.6130	0.5321	0.3672
9	0.5900	0.5146	0.3657	0.5860	0.5129	0.3622
10	0.6259	0.5500	0.3887	0.6196	0.5478	0.3833
11	0.6190	0.5464	0.3935	0.6131	0.5403	0.3857
12	0.6028	0.5175	0.3626	0.5995	0.5180	0.3586
13	0.6154	0.5333	0.3764	0.6095	0.5288	0.3710
14	0.5995	0.5134	0.3685	0.5913	0.5081	0.3635
15	0.6092	0.5287	0.3690	0.5992	0.5236	0.3633
16	0.5791	0.5034	0.3629	0.5756	0.5014	0.3588
17	0.6049	0.5278	0.3780	0.5990	0.5255	0.3749
18	0.6109	0.5212	0.3898	0.6046	0.5146	0.3782
19	0.6001	0.5291	0.3785	0.5949	0.5239	0.3723
20	0.5927	0.5112	0.3577	0.5885	0.5086	0.3529
21	0.6200	0.5466	0.3902	0.6149	0.5439	0.3856
22	0.6184	0.5360	0.3887	0.6153	0.5322	0.3796
23	0.5872	0.5001	0.3474	0.5801	0.4986	0.3437
24	0.6072	0.5247	0.3761	0.6043	0.5243	0.3742
25	0.6007	0.5159	0.3590	0.5991	0.5176	0.3558
26	0.5946	0.5067	0.3498	0.5840	0.4979	0.3449
27	0.6166	0.5217	0.3725	0.6099	0.5183	0.3648
28	0.5840	0.5001	0.3486	0.5834	0.4916	0.3413
29	0.6288	0.5605	0.3998	0.6243	0.5587	0.3959
30	0.6196	0.5446	0.3742	0.6163	0.5446	0.3719
31	0.6198	0.5444	0.3965	0.6111	0.5374	0.3876
32	0.6168	0.5398	0.3760	0.6123	0.5384	0.3741
33	0.6235	0.5471	0.3892	0.6168	0.5428	0.3855
34	0.6111	0.5302	0.3761	0.6059	0.5280	0.3690
35	0.6001	0.5244	0.3747	0.5917	0.5167	0.3687

36	0.6066	0.5140	0.3830	0.5996	0.5123	0.3777
37	0.6134	0.5299	0.3653	0.6045	0.5255	0.3586
38	0.5881	0.5071	0.3481	0.5792	0.5035	0.3445
39	0.5961	0.4989	0.3677	0.5926	0.5020	0.3631
40	0.6270	0.5532	0.3861	0.6239	0.5524	0.3820
41	0.6055	0.5206	0.3571	0.6000	0.5190	0.3535
42	0.6231	0.5537	0.3933	0.6193	0.5528	0.3908
43	0.5815	0.4954	0.3625	0.5698	0.4904	0.3568
44	0.5946	0.5038	0.3623	0.5887	0.5030	0.3552
45	0.5993	0.4895	0.3660	0.5910	0.4848	0.3564
46	0.6166	0.5371	0.3842	0.6105	0.5332	0.3809
47	0.6151	0.5363	0.3777	0.6083	0.5339	0.3725
48	0.6100	0.5394	0.3893	0.6070	0.5376	0.3852
49	0.5938	0.5016	0.3477	0.5893	0.4981	0.3389
50	0.6122	0.5311	0.3626	0.6093	0.5307	0.3606
51	0.6107	0.5217	0.3723	0.6009	0.5144	0.3609
52	0.6203	0.5419	0.3835	0.6127	0.5347	0.3776
53	0.6168	0.5397	0.3784	0.6134	0.5391	0.3722
54	0.6229	0.5498	0.3862	0.6229	0.5485	0.3820
55	0.6010	0.5119	0.3544	0.6004	0.5086	0.3502
56	0.6001	0.5187	0.3755	0.5943	0.5153	0.3674
57	0.5996	0.5201	0.3635	0.5948	0.5173	0.3604
58	0.6030	0.5126	0.3550	0.5982	0.5077	0.3488
59	0.6007	0.5241	0.3795	0.5990	0.5210	0.3755
60	0.5869	0.5020	0.3647	0.5733	0.4945	0.3557
61	0.6090	0.5334	0.3797	0.6034	0.5273	0.3726
62	0.5976	0.5256	0.3727	0.5931	0.5225	0.3706
63	0.6065	0.5215	0.3812	0.6013	0.5196	0.3717
64	0.6167	0.5427	0.3838	0.6131	0.5365	0.3801
65	0.6070	0.5266	0.3763	0.6033	0.5246	0.3666
66	0.5953	0.5105	0.3554	0.5897	0.5078	0.3529
67	0.5990	0.5203	0.3655	0.5925	0.5171	0.3593
68	0.6168	0.5443	0.3809	0.6135	0.5423	0.3760
69	0.5999	0.5194	0.3658	0.5922	0.5167	0.3632
70	0.6088	0.5288	0.3688	0.6064	0.5298	0.3662
71	0.6135	0.5406	0.3827	0.6082	0.5381	0.3789

72	0.6078	0.5237	0.3561	0.5991	0.5194	0.3517
73	0.6168	0.5431	0.3880	0.6118	0.5396	0.3807
74	0.6128	0.5325	0.3666	0.6122	0.5321	0.3566
75	0.6053	0.5217	0.3645	0.6016	0.5201	0.3571
76	0.6043	0.5267	0.3745	0.5969	0.5242	0.3733
77	0.5795	0.4775	0.3393	0.5722	0.4775	0.3329
78	0.6111	0.5317	0.3716	0.6066	0.5286	0.3661
79	0.6007	0.5161	0.3608	0.5967	0.5136	0.3538
80	0.6000	0.5284	0.3834	0.5935	0.5269	0.3823
81	0.6124	0.5423	0.3913	0.6116	0.5412	0.3870
82	0.6190	0.5389	0.3853	0.6107	0.5345	0.3800
83	0.5991	0.5173	0.3647	0.5923	0.5134	0.3624
84	0.6224	0.5465	0.3819	0.6166	0.5437	0.3754
85	0.6144	0.5335	0.3833	0.6053	0.5254	0.3747
86	0.6126	0.5405	0.3912	0.6094	0.5362	0.3861
87	0.6267	0.5511	0.3868	0.6202	0.5486	0.3836
88	0.6097	0.5247	0.3623	0.6024	0.5196	0.3516
89	0.6054	0.5288	0.3787	0.6012	0.5279	0.3754
90	0.6205	0.5441	0.3932	0.6159	0.5395	0.3837
91	0.6090	0.5188	0.3819	0.6045	0.5172	0.3766
92	0.5995	0.5111	0.3546	0.5908	0.5041	0.3464
93	0.5922	0.4946	0.3531	0.5846	0.4867	0.3426
94	0.5951	0.5140	0.3577	0.5930	0.5099	0.3525
95	0.6129	0.5297	0.3850	0.6044	0.5228	0.3760
96	0.6033	0.5207	0.3645	0.6020	0.5194	0.3603
97	0.6110	0.5322	0.3725	0.6029	0.5299	0.3687
98	0.5998	0.5202	0.3704	0.5945	0.5162	0.3659
99	0.5845	0.5018	0.3507	0.5811	0.5004	0.3468
100	0.5926	0.5034	0.3604	0.5860	0.5001	0.3546

APPENDIX 12: BREAKTHROUGH TIMES - PVWI TAKEN AT ≈ 0.01 WATER CUT

Table A12-1: Breakthrough times for 100 realizations

Realization	8x6	8x61	8x6unf	16x12	16x121	16x12unf	32x24	32x241	32x24unf
1	0.3207	0.2386	0.1053	0.3207	0.2386	0.1245	0.3608	0.2387	0.1263
2	0.3623	0.2515	0.1116	0.3624	0.2516	0.1018	0.3624	0.2517	0.1083
3	0.3247	0.2416	0.0976	0.3653	0.2417	0.0868	0.3652	0.2416	0.1047
4	0.3555	0.2070	0.1075	0.3557	0.2221	0.1219	0.3950	0.2727	0.1275
5	0.3667	0.2422	0.1153	0.3669	0.2825	0.1309	0.4076	0.2828	0.1386
6	0.3429	0.2649	0.1015	0.3428	0.2647	0.1048	0.3809	0.2649	0.1269
7	0.3294	0.2040	0.1005	0.3706	0.2448	0.1185	0.3706	0.2448	0.1062
8	0.3507	0.2706	0.1092	0.3895	0.2706	0.1279	0.3896	0.2706	0.1307
9	0.3149	0.2337	0.1055	0.3150	0.2337	0.1071	0.3544	0.2340	0.1118
10	0.3903	0.2709	0.1261	0.3902	0.2709	0.1289	0.4292	0.3097	0.1325
11	0.3608	0.2783	0.1184	0.3610	0.2784	0.1216	0.4010	0.2786	0.1415
12	0.3509	0.2315	0.1173	0.3509	0.2701	0.1200	0.3511	0.2318	0.1109
13	0.3665	0.2420	0.1125	0.3665	0.2819	0.1120	0.4071	0.2822	0.1160
14	0.3296	0.2444	0.1003	0.3705	0.2444	0.1052	0.3707	0.2446	0.1085
15	0.3509	0.2706	0.1197	0.3507	0.2704	0.1202	0.3896	0.2706	0.1410
16	0.3659	0.2538	0.1125	0.3658	0.2537	0.1293	0.4023	0.2901	0.1219
17	0.3207	0.2380	0.1150	0.3605	0.2380	0.1177	0.3606	0.2778	0.1262
18	0.3512	0.2316	0.1135	0.3509	0.2695	0.1303	0.3898	0.2697	0.1344
19	0.3395	0.2622	0.1145	0.3397	0.2623	0.1339	0.3772	0.2998	0.1364
20	0.3525	0.2328	0.1081	0.3522	0.2323	0.1058	0.3523	0.2325	0.1099
21	0.3575	0.2757	0.1184	0.3972	0.3151	0.1381	0.3972	0.3152	0.1420
22	0.3560	0.2348	0.1092	0.3562	0.2738	0.1253	0.3956	0.2740	0.1276
23	0.3299	0.2700	0.0984	0.3301	0.2450	0.1025	0.3301	0.2452	0.1191
24	0.3190	0.2371	0.1067	0.3588	0.2371	0.1275	0.3589	0.2373	0.1176
25	0.3240	0.2407	0.1033	0.3644	0.2408	0.1080	0.3645	0.2408	0.1099
26	0.3586	0.2368	0.1202	0.3587	0.2370	0.1120	0.3587	0.2370	0.1026
27	0.3867	0.2651	0.1208	0.3870	0.2671	0.1242	0.3871	0.2673	0.1254
28	0.3406	0.2250	0.1082	0.3782	0.2623	0.1115	0.3783	0.2624	0.1287
29	0.3638	0.2809	0.1203	0.4040	0.3209	0.1407	0.4042	0.3210	0.1433

30	0.3729	0.2591	0.1126	0.4098	0.2590	0.1129	0.4100	0.2959	0.1290
31	0.3819	0.2649	0.1158	0.3439	0.2271	0.1281	0.3441	0.2651	0.1181
32	0.3386	0.2610	0.1190	0.3761	0.2611	0.1207	0.4201	0.2612	0.1231
33	0.3550	0.2114	0.1072	0.3902	0.2465	0.1116	0.3762	0.2817	0.1152
34	0.3599	0.2379	0.1121	0.3600	0.2380	0.1160	0.3904	0.2777	0.1380
35	0.3383	0.2514	0.1167	0.3384	0.2515	0.1058	0.3385	0.2515	0.1079
36	0.3469	0.2417	0.1144	0.3901	0.2493	0.1276	0.3902	0.2570	0.1313
37	0.3616	0.2389	0.1072	0.3617	0.2786	0.1255	0.4018	0.2788	0.1137
38	0.2910	0.2060	0.0864	0.3327	0.2062	0.0915	0.3326	0.2062	0.0955
39	0.3553	0.2137	0.1099	0.3555	0.2279	0.1149	0.3948	0.2339	0.1075
40	0.3937	0.2735	0.1123	0.3935	0.2734	0.1315	0.4327	0.3123	0.1319
41	0.3316	0.2465	0.1076	0.3728	0.2466	0.0975	0.3728	0.2056	0.1020
42	0.3798	0.2640	0.1118	0.3797	0.2639	0.1152	0.4176	0.3016	0.1348
43	0.3308	0.2150	0.1114	0.3309	0.2543	0.1189	0.3675	0.2546	0.1246
44	0.3317	0.2168	0.1041	0.3683	0.2182	0.1062	0.3685	0.2549	0.1016
45	0.3818	0.2640	0.1188	0.3817	0.2695	0.1302	0.3817	0.2417	0.1244
46	0.3701	0.2567	0.1279	0.4069	0.2934	0.1315	0.4071	0.2935	0.1354
47	0.3919	0.2716	0.1215	0.3918	0.3101	0.1359	0.3920	0.3102	0.1530
48	0.3377	0.2233	0.1087	0.3751	0.2605	0.1282	0.4124	0.2607	0.1328
49	0.3224	0.2124	0.0984	0.3580	0.2124	0.0927	0.3583	0.2126	0.0855
50	0.3650	0.2817	0.1170	0.3648	0.2816	0.1242	0.4053	0.2817	0.1273
51	0.3378	0.2069	0.1062	0.3799	0.2498	0.1171	0.3802	0.2504	0.1259
52	0.3522	0.2715	0.1154	0.3912	0.2715	0.1207	0.3913	0.2717	0.1400
53	0.3635	0.2805	0.1165	0.3766	0.2806	0.1374	0.4040	0.2807	0.1413
54	0.3390	0.2618	0.1016	0.3564	0.2618	0.1192	0.3393	0.2619	0.1381
55	0.3565	0.2356	0.1017	0.3410	0.2747	0.1198	0.3565	0.2748	0.1249
56	0.3410	0.2528	0.1010	0.3516	0.2529	0.1187	0.3411	0.2531	0.1112
57	0.3126	0.2327	0.1080	0.3594	0.2326	0.0932	0.3516	0.2327	0.1126
58	0.3196	0.2370	0.1028	0.3834	0.2370	0.1161	0.3596	0.2374	0.1122
59	0.3834	0.2663	0.1109	0.3613	0.2663	0.1162	0.3834	0.2665	0.1332
60	0.3612	0.2363	0.1237	0.3558	0.2776	0.1322	0.3613	0.2778	0.1207
61	0.3559	0.2356	0.1105	0.3687	0.2355	0.1148	0.3560	0.2748	0.1191
62	0.3319	0.2563	0.1103	0.3870	0.2563	0.1307	0.3687	0.2929	0.1352
63	0.3443	0.2547	0.1142	0.3851	0.2547	0.1238	0.3872	0.2550	0.1379
64	0.3425	0.2544	0.1072	0.3561	0.2966	0.1382	0.3854	0.2970	0.1425
65	0.3166	0.2352	0.1127	0.3216	0.2743	0.1274	0.3562	0.2744	0.1306

66	0.3216	0.2387	0.1065	0.3616	0.2386	0.1074	0.3617	0.2388	0.1121
67	0.3213	0.2385	0.0950	0.3215	0.2388	0.1125	0.3616	0.2389	0.1175
68	0.3513	0.2710	0.1152	0.3900	0.3094	0.1335	0.3902	0.3096	0.1338
69	0.3302	0.2450	0.0999	0.3713	0.2449	0.1262	0.3714	0.2858	0.1280
70	0.3494	0.2312	0.1103	0.3879	0.2695	0.1145	0.3880	0.2697	0.1171
71	0.3528	0.2718	0.1145	0.3919	0.2719	0.1297	0.3920	0.3107	0.1332
72	0.3783	0.2622	0.1184	0.3408	0.2251	0.0961	0.3785	0.2251	0.0977
73	0.3646	0.2811	0.1290	0.4051	0.2813	0.1362	0.4052	0.3216	0.1398
74	0.3365	0.2501	0.1115	0.3785	0.2503	0.1138	0.3787	0.2505	0.1196
75	0.3730	0.2460	0.1102	0.3730	0.2868	0.1258	0.4142	0.2872	0.1165
76	0.3226	0.2401	0.1054	0.3626	0.2400	0.1246	0.3627	0.2401	0.1106
77	0.3527	0.2224	0.1047	0.3527	0.2320	0.1187	0.3526	0.2321	0.1129
78	0.3557	0.2351	0.1047	0.3557	0.2351	0.1085	0.3952	0.2743	0.1114
79	0.3662	0.2542	0.1142	0.4026	0.2903	0.1182	0.4027	0.2905	0.1358
80	0.3446	0.2662	0.1096	0.3448	0.2663	0.1324	0.3829	0.2664	0.1363
81	0.3545	0.2344	0.1122	0.3545	0.2733	0.1280	0.3939	0.2735	0.1176
82	0.3928	0.2723	0.1193	0.3926	0.2722	0.1335	0.3746	0.3112	0.1378
83	0.3745	0.2471	0.1212	0.3745	0.2470	0.1244	0.4160	0.2883	0.1282
84	0.3610	0.2391	0.1026	0.4009	0.2787	0.1244	0.4011	0.2789	0.1270
85	0.3234	0.2398	0.1015	0.3636	0.2398	0.1173	0.3637	0.2800	0.1208
86	0.3731	0.2591	0.1269	0.4102	0.2961	0.0000	0.4102	0.2961	0.1369
87	0.3695	0.2443	0.1110	0.4106	0.2848	0.1250	0.4106	0.2849	0.1284
88	0.3498	0.2306	0.1110	0.3498	0.2306	0.1004	0.3887	0.2309	0.1048
89	0.3462	0.2285	0.1106	0.3464	0.2286	0.1254	0.3848	0.2667	0.1268
90	0.3851	0.2672	0.1204	0.3852	0.2672	0.1367	0.4235	0.3054	0.1403
91	0.3627	0.2258	0.1181	0.4030	0.2751	0.1420	0.4032	0.2389	0.1225
92	0.3502	0.2309	0.1128	0.3502	0.2309	0.1155	0.3503	0.2311	0.1050
93	0.3243	0.2322	0.1100	0.3646	0.2338	0.1192	0.3648	0.2794	0.1258
94	0.3284	0.2166	0.0976	0.3647	0.2526	0.1123	0.3647	0.2527	0.1156
95	0.3674	0.2546	0.1147	0.4040	0.2910	0.1291	0.4041	0.2549	0.1219
96	0.3447	0.2279	0.1104	0.3827	0.2657	0.1154	0.3828	0.2657	0.1202
97	0.3186	0.2371	0.1076	0.3583	0.2371	0.0951	0.3583	0.2371	0.1150
98	0.3094	0.2299	0.0932	0.3477	0.2677	0.1186	0.3862	0.2679	0.1092
99	0.3732	0.2869	0.1220	0.3732	0.2462	0.1256	0.3732	0.2462	0.1277
100	0.3537	0.2328	0.1027	0.3537	0.2716	0.1312	0.3928	0.2718	0.1340

Realization	64x48	64x481	64x48unf	128x96	128x961	128x96unf
1	0.3608	0.2388	0.1135	0.3609	0.2389	0.1178
2	0.3986	0.2159	0.0961	0.3986	0.2160	0.0993
3	0.3654	0.2418	0.0909	0.3654	0.2016	0.0924
4	0.3559	0.2731	0.1343	0.3560	0.2345	0.1146
5	0.4077	0.2830	0.1270	0.4078	0.2832	0.1297
6	0.3810	0.2650	0.1110	0.3811	0.2651	0.1133
7	0.3707	0.2450	0.1091	0.3707	0.2452	0.1114
8	0.3896	0.2707	0.1347	0.3897	0.2708	0.1197
9	0.3544	0.2731	0.1156	0.3545	0.2733	0.1181
10	0.4293	0.2713	0.1375	0.4294	0.3101	0.1250
11	0.4011	0.2788	0.1452	0.4011	0.2789	0.1488
12	0.3899	0.2319	0.1139	0.3900	0.2320	0.1155
13	0.4073	0.2422	0.1050	0.4074	0.2424	0.1076
14	0.3708	0.2448	0.1112	0.3709	0.2450	0.1135
15	0.3897	0.2707	0.1282	0.3898	0.2709	0.1317
16	0.3661	0.2542	0.1144	0.3662	0.2544	0.1027
17	0.3607	0.2781	0.1285	0.3608	0.2783	0.1321
18	0.3898	0.2698	0.1378	0.3510	0.2700	0.1297
19	0.3773	0.2999	0.1405	0.3773	0.3001	0.1430
20	0.3525	0.2327	0.1145	0.3525	0.2329	0.1173
21	0.3973	0.3153	0.1446	0.3974	0.3155	0.1483
22	0.3958	0.2741	0.1172	0.3565	0.2742	0.1173
23	0.3302	0.2453	0.1219	0.3303	0.2375	0.1234
24	0.3590	0.2374	0.1204	0.3590	0.2411	0.1411
25	0.3645	0.2409	0.1134	0.3646	0.2372	0.1009
26	0.3587	0.2371	0.1067	0.3587	0.2677	0.1092
27	0.3873	0.2675	0.1178	0.3873	0.2624	0.1204
28	0.3784	0.2625	0.1313	0.3784	0.2814	0.1167
29	0.4044	0.3213	0.1458	0.4044	0.2592	0.1489
30	0.4100	0.2959	0.1159	0.4101	0.2654	0.1191
31	0.3822	0.2653	0.1216	0.3442	0.2616	0.1243
32	0.3764	0.2614	0.1270	0.3764	0.2820	0.1131
33	0.3905	0.2818	0.1182	0.3905	0.2820	0.1211
34	0.3999	0.2777	0.1262	0.4000	0.2778	0.1305
35	0.3386	0.2518	0.1131	0.3386	0.2519	0.1152

36	0.3904	0.2571	0.1224	0.3904	0.2574	0.1256
37	0.4018	0.2790	0.1168	0.4019	0.2792	0.1204
38	0.3327	0.2063	0.0993	0.3328	0.2064	0.1011
39	0.3556	0.1951	0.0887	0.3949	0.1953	0.0913
40	0.4328	0.3126	0.1367	0.4328	0.3128	0.1391
41	0.3730	0.2058	0.0884	0.3731	0.2059	0.0917
42	0.4177	0.3018	0.1212	0.4178	0.3019	0.1235
43	0.3676	0.2547	0.1159	0.3677	0.2549	0.1203
44	0.3686	0.2551	0.1035	0.4052	0.2189	0.1060
45	0.3817	0.2501	0.1293	0.3818	0.2512	0.1191
46	0.4072	0.2937	0.1396	0.4073	0.2939	0.1289
47	0.3920	0.2718	0.1420	0.3921	0.2721	0.1467
48	0.4125	0.2979	0.1362	0.4126	0.2981	0.1402
49	0.3938	0.2127	0.0873	0.3939	0.2128	0.0907
50	0.4055	0.2819	0.1117	0.4056	0.2419	0.0948
51	0.3803	0.2506	0.1289	0.3803	0.2506	0.1171
52	0.3914	0.2719	0.1437	0.3914	0.2720	0.1282
53	0.4041	0.2809	0.1253	0.4041	0.2810	0.1285
54	0.3768	0.2620	0.1422	0.3769	0.2622	0.1262
55	0.3566	0.2357	0.1282	0.3566	0.2359	0.1140
56	0.3413	0.2534	0.1157	0.3413	0.2114	0.1029
57	0.3517	0.2328	0.1156	0.3907	0.2328	0.1176
58	0.3598	0.2377	0.1029	0.3995	0.2377	0.1030
59	0.3835	0.2665	0.1220	0.3836	0.2667	0.1096
60	0.3615	0.2384	0.1247	0.3616	0.2386	0.1148
61	0.3561	0.2358	0.1045	0.3562	0.2359	0.1073
62	0.4055	0.2931	0.1380	0.4055	0.2933	0.1411
63	0.3873	0.2552	0.1164	0.3874	0.2554	0.1318
64	0.3855	0.2973	0.1452	0.3856	0.2974	0.1463
65	0.3956	0.2745	0.1485	0.3957	0.2747	0.1360
66	0.3618	0.2391	0.1170	0.3618	0.2392	0.1204
67	0.3617	0.2391	0.1222	0.3617	0.2392	0.1256
68	0.4291	0.3098	0.1540	0.4292	0.3100	0.1394
69	0.3715	0.2452	0.1177	0.3716	0.2454	0.1207
70	0.3881	0.2700	0.1381	0.3882	0.2701	0.1228
71	0.3921	0.2722	0.1232	0.3922	0.2724	0.1268

72	0.3787	0.2254	0.0896	0.3787	0.2255	0.0920
73	0.4053	0.2816	0.1461	0.4053	0.2817	0.1324
74	0.3788	0.2507	0.1240	0.3789	0.2508	0.1087
75	0.4143	0.2874	0.1203	0.4144	0.2876	0.1247
76	0.3629	0.2402	0.1131	0.3630	0.2404	0.0979
77	0.3527	0.1937	0.1057	0.3528	0.2326	0.1109
78	0.3952	0.2744	0.0980	0.3953	0.2355	0.0998
79	0.4028	0.2906	0.1393	0.4029	0.2545	0.1267
80	0.3831	0.3046	0.1596	0.3831	0.3047	0.1637
81	0.3939	0.2737	0.1211	0.3940	0.2738	0.1247
82	0.4320	0.2727	0.1414	0.3748	0.2729	0.1303
83	0.3747	0.2886	0.1331	0.4162	0.2887	0.1340
84	0.4012	0.2392	0.1111	0.4013	0.2393	0.0942
85	0.3639	0.2402	0.1240	0.3639	0.2403	0.1248
86	0.4103	0.2962	0.1390	0.4105	0.2964	0.1418
87	0.4108	0.2853	0.1326	0.4109	0.2854	0.1174
88	0.3888	0.2310	0.1089	0.3889	0.2312	0.0986
89	0.3850	0.2670	0.1191	0.3851	0.2672	0.1224
90	0.4236	0.3057	0.1441	0.4238	0.2678	0.1330
91	0.3631	0.2391	0.1154	0.3632	0.2393	0.1067
92	0.3504	0.2312	0.1100	0.3504	0.2313	0.1124
93	0.4052	0.2528	0.1301	0.3650	0.2529	0.1317
94	0.3648	0.2550	0.1183	0.3648	0.2188	0.1213
95	0.4042	0.2659	0.1141	0.4042	0.2661	0.1175
96	0.4210	0.2372	0.1236	0.4211	0.2373	0.1269
97	0.3584	0.2299	0.1003	0.3585	0.2300	0.1025
98	0.3864	0.2465	0.1144	0.3865	0.2467	0.1026
99	0.3733	0.2334	0.1325	0.3735	0.2335	0.1167
100	0.3539	0.2721	0.1140	0.3931	0.2723	0.1300

APPENDIX 13: TURBO PASCAL PROGRAM TO CONVERT SATURATION VALUES FROM ECLIPSE

```
Program saturation (satfile,fout);
uses wincrt  ;
type
    row = 1..50;
    column =1..70;
    satarray = Array [row, column] of real;

Var
   dir: real;
   x, z, count, line: integer;
   sat : satarray ;
   satfile,fout: text;

Begin
     assign(fout,'33-1.out');
     rewrite(fout);
     Assign (satfile, '33-1');
     Reset (satfile);
  for z:=12 downto 1 do
  for x:=1 to 16 do
    Read (satfile, sat[x,z]);
    Close (satfile);

    writeln(fout, 'Saturation');
    writeln (fout,'1');
    writeln(fout, 'saturation');
  for z:=1 to 12 do
  for x:=1 to 16 do
    writeln(fout,'  ',sat[x,z]:2:5);
close(fout);
end.
```

APPENDIX 14: RANKING NUMBERS FOR RECOVERY FACTORS

Table A14-1: Ranking numbers of different realizations for recovery factors

Realization	8x6	16x12	32x24	64x48	128x96	8x61	16x121	32x241
1	99	93	84	80	68	92	83	81
2	22	48	74	59	67	27	34	61
3	35	54	76	61	56	26	36	64
4	92	80	89	98	97	97	90	92
5	44	36	42	42	43	50	47	41
6	41	60	48	40	27	12	42	38
7	71	34	47	53	63	77	50	68
8	25	5	5	17	17	13	8	24
9	66	91	92	91	88	55	80	71
10	13	7	7	4	5	14	13	6
11	9	10	9	14	15	9	7	7
12	37	73	63	63	57	54	64	62
13	28	18	28	25	28	41	33	33
14	64	87	65	75	81	76	81	74
15	26	53	52	44	58	19	52	46
16	83	100	100	100	96	56	91	93
17	40	61	57	57	62	47	59	54
18	27	65	43	38	38	67	73	60
19	84	82	71	69	69	36	45	37
20	21	85	79	88	87	34	85	86
21	15	4	8	11	12	10	4	4
22	36	24	34	16	11	68	27	39
23	70	98	96	93	94	72	99	96
24	45	68	55	49	42	37	60	47
25	75	77	67	65	60	65	68	69
26	38	37	75	86	91	45	53	80
27	46	35	25	24	26	87	79	67
28	100	97	98	96	92	98	97	97
29	1	1	2	1	1	1	1	1
30	14	2	11	13	9	17	5	8

31	18	14	6	12	23	39	28	13
32	97	72	19	20	19	62	43	19
33	24	26	10	5	7	25	22	9
34	56	16	36	35	36	42	25	29
35	47	40	62	68	80	38	35	44
36	63	75	41	51	55	81	87	73
37	78	79	35	29	40	63	61	36
38	95	89	95	92	95	80	77	85
39	85	69	64	82	76	96	88	87
40	16	9	1	2	2	4	3	2
41	72	39	73	54	54	59	49	72
42	4	32	13	6	6	2	12	5
43	96	96	94	97	100	94	96	94
44	79	49	87	85	86	88	86	89
45	74	42	59	77	82	91	93	99
46	12	6	17	23	25	93	9	21
47	6	57	20	26	31	30	39	22
48	94	52	37	41	33	24	19	15
49	88	95	88	87	85	61	100	90
50	7	20	24	34	30	89	16	28
51	93	83	80	39	52	5	94	83
52	31	13	15	10	18	95	18	16
53	5	31	30	21	14	23	26	26
54	10	3	14	7	3	7	2	11
55	77	64	60	64	53	3	66	75
56	57	90	82	70	72	66	84	77
57	60	41	69	74	70	79	55	59
58	90	59	66	62	64	43	75	84
59	19	55	58	66	61	84	37	35
60	69	99	97	94	98	32	95	95
61	32	46	38	46	44	85	31	30
62	42	86	83	81	74	20	57	53
63	68	45	23	52	50	16	63	50
64	62	27	32	22	16	82	23	25
65	55	44	53	50	45	46	44	52
66	80	74	77	83	84	74	72	82

67	73	38	49	79	77	64	51	48
68	3	28	51	19	13	8	20	27
69	98	92	90	72	79	83	82	78
70	30	66	50	47	35	18	54	45
71	8	15	39	28	32	15	14	23
72	54	22	33	48	59	44	38	43
73	11	25	27	18	21	21	15	20
74	89	88	45	31	20	75	65	42
75	65	76	56	56	49	73	70	65
76	81	81	81	58	65	57	62	66
77	91	58	99	99	99	100	89	100
78	76	56	44	36	34	52	48	40
79	51	43	46	67	66	29	32	51
80	58	84	85	71	73	22	41	57
81	61	63	40	33	22	28	29	17
82	23	12	4	15	24	31	21	12
83	48	78	54	78	78	60	78	56
84	20	23	12	8	8	11	11	14
85	50	29	22	27	37	70	56	31
86	2	8	16	32	29	6	6	10
87	39	11	3	3	4	40	10	3
88	67	50	31	43	47	71	69	49
89	29	47	68	55	51	53	46	55
90	17	17	18	9	10	33	24	18
91	53	33	21	45	39	90	76	63
92	49	62	72	76	83	69	74	88
93	87	71	91	90	90	99	98	98
94	82	70	86	84	75	78	71	79
95	33	19	29	30	41	51	30	32
96	43	51	70	60	48	49	58	70
97	52	21	26	37	46	35	17	34
98	59	30	61	73	71	48	40	58
99	34	67	78	95	93	58	67	76
100	86	94	93	89	89	86	92	91

Realization	64x48	128x96	8x6unf	16x12unf	32x24unf	64x48unf	128x96unf
1	83	77	99	93	86	78	75
2	50	53	75	60	85	82	81
3	56	52	62	80	95	89	84
4	98	99	69	28	49	62	70
5	35	39	70	52	53	55	59
6	32	27	32	54	48	42	37
7	74	72	97	57	83	79	79
8	25	30	29	25	45	48	49
9	75	75	68	85	57	64	61
10	5	6	10	11	5	13	12
11	10	13	6	1	4	3	6
12	70	61	46	67	68	74	68
13	31	34	57	27	32	38	43
14	78	81	30	62	61	58	55
15	44	48	34	58	59	56	56
16	89	88	48	95	87	72	67
17	46	42	14	34	35	36	31
18	61	70	5	9	11	9	22
19	41	47	41	39	38	34	39
20	81	80	44	96	90	84	85
21	8	8	8	3	6	8	7
22	28	28	15	5	20	12	20
23	94	91	79	98	98	99	96
24	52	45	17	38	41	41	33
25	73	62	91	86	76	83	76
26	86	93	38	47	88	95	94
27	59	60	67	53	46	50	54
28	93	95	100	97	100	96	98
29	1	1	11	12	1	1	1
30	11	7	73	46	43	47	41
31	12	20	12	10	3	2	3
32	21	17	90	55	36	43	34
33	7	10	24	31	19	11	8
34	38	36	47	26	29	40	45
35	53	67	37	50	40	45	46

36	77	76	2	13	13	25	23
37	39	41	81	82	65	66	69
38	85	85	94	94	94	97	95
39	95	87	54	35	44	59	58
40	3	3	18	19	15	17	15
41	63	59	86	63	84	86	83
42	2	2	7	15	17	4	2
43	96	96	63	81	70	75	72
44	87	86	76	78	74	77	78
45	99	98	40	36	66	61	74
46	26	26	9	4	14	20	16
47	27	25	39	43	25	37	38
48	23	19	43	14	2	10	9
49	92	92	98	99	99	98	99
50	37	31	20	51	50	73	63
51	57	71	88	72	64	52	62
52	18	23	33	37	24	22	24
53	22	16	28	45	47	35	40
54	6	5	51	23	27	16	14
55	80	79	85	89	91	92	90
56	69	69	49	66	56	44	48
57	66	63	84	92	73	71	64
58	79	83	95	77	93	90	91
59	54	51	25	22	18	32	28
60	90	94	42	61	71	68	77
61	30	38	36	40	37	31	36
62	49	50	26	48	54	49	44
63	60	56	65	30	21	29	42
64	16	21	61	32	31	21	18
65	48	44	55	24	42	39	50
66	84	82	74	84	92	88	86
67	64	65	72	56	52	65	66
68	13	11	31	44	39	30	27
69	67	66	96	88	78	63	57
70	42	33	59	65	69	57	51
71	19	18	21	17	23	26	21

72	55	57	56	71	80	87	88
73	15	14	4	7	22	14	17
74	33	29	87	75	58	60	73
75	58	54	83	76	72	70	71
76	47	46	80	73	63	46	35
77	100	100	89	74	97	100	100
78	36	35	82	59	60	53	52
79	72	73	64	64	77	80	82
80	45	40	22	20	34	23	13
81	17	12	27	18	10	6	4
82	24	24	23	16	8	18	19
83	71	74	45	79	62	67	60
84	9	9	35	29	30	28	29
85	29	43	52	49	26	24	32
86	20	22	1	100	16	7	5
87	4	4	77	41	28	15	11
88	51	55	66	68	67	76	89
89	43	37	16	21	33	33	30
90	14	15	13	6	7	5	10
91	68	64	19	8	12	27	25
92	82	84	71	91	96	91	93
93	97	97	92	90	89	93	97
94	76	78	93	87	82	85	87
95	40	49	3	2	9	19	26
96	62	58	53	69	79	69	65
97	34	32	58	42	51	51	47
98	65	68	50	33	55	54	53
99	91	89	60	70	75	94	92
100	88	90	78	83	81	81	80

APPENDIX 15: RANKING NUMBERS FOR BREAKTHROUGH TIMES

Table A15-1: Ranking numbers of different realizations for breakthrough times

Realization	8x6	16x12	32x24	64x48	128x96	8x61	16x121	32x241
1	91	99	79	81	82	59	77	84
2	29	56	75	28	29	40	58	69
3	83	49	69	72	72	52	71	78
4	41	73	29	89	90	97	97	43
5	20	46	12	13	13	49	12	24
6	63	89	53	55	56	22	44	57
7	81	42	65	68	69	100	69	75
8	54	21	40	43	45	15	32	46
9	97	100	89	91	91	74	87	89
10	4	18	2	3	2	14	31	8
11	33	60	25	26	26	6	19	33
12	52	81	93	40	43	80	34	94
13	21	47	13	14	14	50	13	25
14	80	43	64	67	68	47	70	76
15	53	82	41	42	44	16	33	47
16	23	48	22	71	71	38	55	19
17	92	61	80	82	83	61	79	34
18	51	80	39	41	94	79	36	49
19	67	92	58	60	61	27	46	12
20	48	78	91	94	93	75	89	92
21	36	11	26	29	30	7	2	3
22	38	69	27	30	88	72	24	41
23	79	96	100	100	100	17	67	74
24	94	64	82	84	84	64	80	86
25	85	53	72	74	75	53	72	79
26	35	65	83	85	85	66	83	88
27	5	24	45	47	49	21	40	51
28	66	33	57	59	60	88	47	58
29	26	6	17	20	20	4	1	2
30	16	3	11	12	12	31	51	15

31	8	88	95	53	96	23	95	56
32	69	35	4	62	63	29	49	60
33	43	17	59	38	41	96	65	27
34	34	62	36	27	27	62	78	36
35	70	93	98	98	98	41	59	70
36	58	19	37	39	42	51	62	62
37	30	57	23	24	24	57	18	32
38	100	94	99	99	99	99	100	99
39	42	74	30	90	33	94	94	90
40	1	12	1	1	1	8	25	4
41	76	40	62	65	66	44	64	100
42	10	31	5	7	6	24	45	11
43	77	95	68	70	70	93	54	66
44	75	45	67	69	19	91	98	64
45	9	29	52	54	55	25	35	77
46	17	4	14	15	15	32	7	16
47	3	15	33	36	38	11	3	7
48	72	36	8	9	9	89	50	61
49	88	67	85	34	35	95	99	98
50	24	50	15	16	16	2	14	26
51	71	30	54	56	57	98	61	72
52	49	16	35	37	39	12	30	45
53	27	34	19	22	22	5	16	28
54	68	68	97	61	62	28	48	59
55	37	90	86	87	87	68	22	38
56	65	79	96	97	97	39	56	67
57	98	63	92	95	40	77	88	91
58	93	27	81	83	28	65	82	85
59	7	59	49	51	53	19	41	53
60	31	71	78	80	81	67	20	35
61	39	44	88	88	89	69	84	37
62	74	23	66	17	17	33	52	17
63	62	26	44	46	48	34	53	63
64	64	70	47	49	51	36	5	13
65	96	97	87	31	31	70	23	39
66	89	58	76	78	79	58	76	83

67	90	98	77	79	80	60	75	81
68	50	20	38	4	3	13	4	9
69	78	41	63	66	67	46	68	22
70	57	22	43	45	47	81	37	48
71	46	14	34	35	37	10	28	6
72	11	91	56	58	59	26	96	97
73	25	5	16	18	18	3	15	1
74	73	32	55	57	58	42	60	71
75	15	39	7	8	8	45	10	21
76	87	55	74	77	78	54	73	80
77	47	77	90	93	92	90	90	93
78	40	72	28	32	32	71	85	40
79	22	9	21	23	23	37	9	18
80	61	87	50	52	54	20	42	54
81	44	75	31	33	34	73	26	42
82	2	13	60	2	64	9	27	5
83	12	37	6	63	7	43	63	20
84	32	10	24	25	25	56	17	31
85	86	54	73	75	76	55	74	29
86	14	2	10	11	11	30	6	14
87	18	1	9	10	10	48	11	23
88	56	84	42	44	46	83	92	96
89	59	86	48	50	52	85	93	52
90	6	25	3	5	4	18	39	10
91	28	8	20	76	77	87	21	82
92	55	83	94	96	95	82	91	95
93	84	52	70	19	73	78	86	30
94	82	51	71	73	74	92	57	68
95	19	7	18	21	21	35	8	65
96	60	28	51	6	5	86	43	55
97	95	66	84	86	86	63	81	87
98	99	85	46	48	50	84	38	50
99	13	38	61	64	65	1	66	73
100	45	76	32	92	36	76	29	44

Realization	64x48	128x96	8x6unf	16x12unf	32x24unf	64x48unf	128x96unf
1	79	73	78	40	46	75	56
2	95	94	46	92	88	95	91
3	71	99	96	100	94	96	96
4	32	82	69	46	41	25	68
5	19	16	27	17	11	36	25
6	49	45	89	90	44	82	71
7	68	62	91	59	91	84	74
8	41	36	62	28	32	24	52
9	33	29	76	85	79	67	55
10	39	3	4	24	29	21	36
11	25	23	17	47	5	6	3
12	90	87	21	51	82	74	65
13	70	64	40	78	70	88	79
14	69	63	92	89	87	80	70
15	40	35	13	50	7	34	20
16	58	54	41	22	57	70	85
17	26	24	29	61	47	33	18
18	43	38	36	19	23	20	26
19	8	7	32	9	17	14	7
20	89	84	65	87	85	69	60
21	2	1	19	4	4	8	4
22	30	27	61	37	40	59	61
23	66	76	95	91	63	48	42
24	82	66	73	30	65	52	9
25	72	78	82	83	84	76	89
26	84	40	12	79	95	86	77
27	44	46	9	43	50	57	50
28	50	20	64	81	35	29	64
29	1	49	11	2	2	5	2
30	12	44	39	75	34	64	53
31	48	48	25	26	64	49	40
32	52	17	15	48	54	37	72
33	21	18	70	80	72	56	46
34	27	25	44	67	13	38	22
35	61	56	23	88	89	78	66

36	53	50	33	29	31	45	35
37	24	22	71	35	74	61	49
38	97	97	100	99	99	93	88
39	99	100	59	71	90	98	99
40	3	2	42	15	30	22	13
41	98	98	68	94	96	99	98
42	7	6	45	70	22	50	41
43	57	52	48	55	52	63	51
44	55	92	81	86	97	90	82
45	64	57	16	20	53	31	54
46	13	11	2	14	20	15	27
47	38	33	7	8	1	12	5
48	9	8	63	25	28	23	11
49	96	95	94	98	100	100	100
50	20	65	22	44	42	79	94
51	63	59	75	64	48	32	62
52	37	34	26	49	9	10	29
53	23	21	24	5	6	39	28
54	51	47	87	54	12	11	33
55	86	80	86	52	51	35	69
56	59	96	90	57	81	65	84
57	88	85	66	97	76	66	57
58	81	75	83	66	77	91	83
59	46	42	51	65	26	47	76
60	80	74	5	13	59	40	67
61	85	79	53	72	62	89	80
62	14	12	55	18	21	19	10
63	54	51	35	45	14	62	19
64	10	9	72	3	3	7	6
65	28	26	38	31	33	3	14
66	78	71	74	84	78	60	48
67	77	72	98	76	67	46	34
68	4	4	28	11	25	2	12
69	67	61	93	32	38	58	47
70	42	37	56	73	68	18	43
71	35	31	31	21	27	44	31

72	94	91	18	95	98	97	97
73	22	19	1	7	10	4	17
74	62	58	47	74	61	41	78
75	17	14	57	33	69	53	39
76	74	67	77	39	83	77	93
77	100	86	79	56	75	87	75
78	29	81	80	82	80	94	90
79	15	53	34	60	19	16	32
80	6	5	60	12	18	1	1
81	31	28	43	27	66	51	38
82	34	30	14	10	15	13	23
83	16	13	8	41	37	26	15
84	75	69	85	42	43	81	95
85	73	68	88	62	58	42	37
86	11	10	3	63	16	17	8
87	18	15	49	38	36	27	59
88	92	89	50	93	93	85	92
89	45	41	52	36	45	54	44
90	5	39	10	6	8	9	16
91	76	70	20	1	55	68	81
92	91	88	37	68	92	83	73
93	60	55	58	53	49	30	21
94	56	93	97	77	71	55	45
95	47	43	30	23	56	72	58
96	83	77	54	69	60	43	30
97	93	90	67	96	73	92	87
98	65	60	99	58	86	71	86
99	87	83	6	34	39	28	63
100	36	32	84	16	24	73	24

APPENDIX 16: CROSSPLOT OF RANKING NUMBERS OF RECOVERY FACTORS AND BREAKTHROUGH TIMES FOR DIFFERENT GRIDS

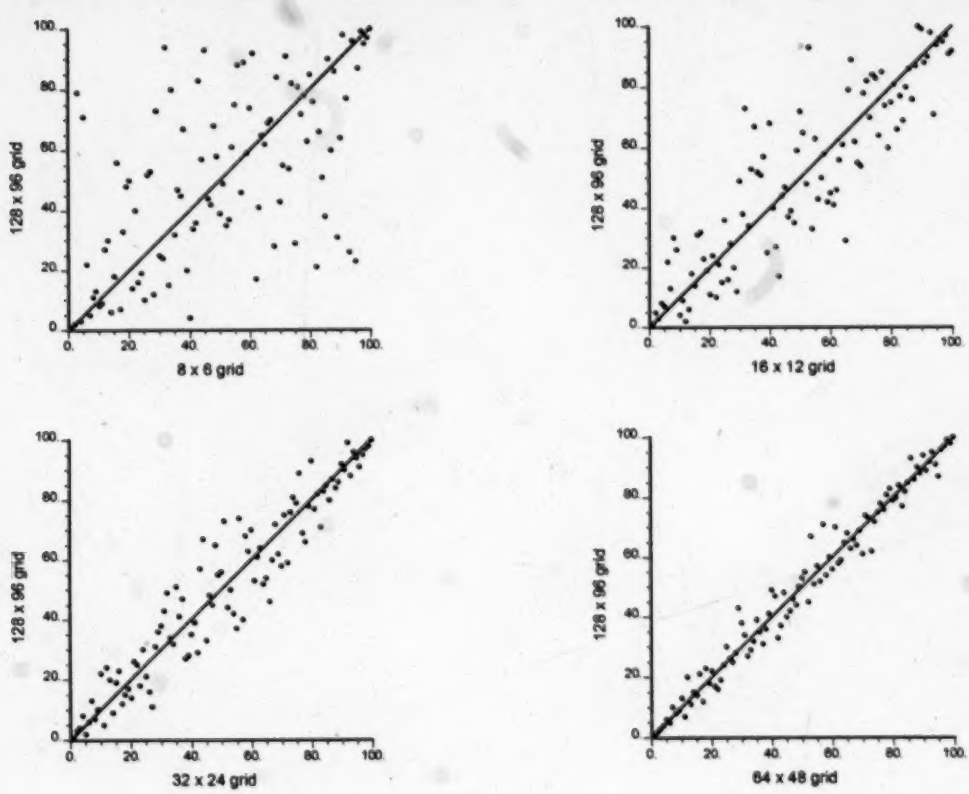

Figure A16-1: Ranking plots for RFs, M = 1

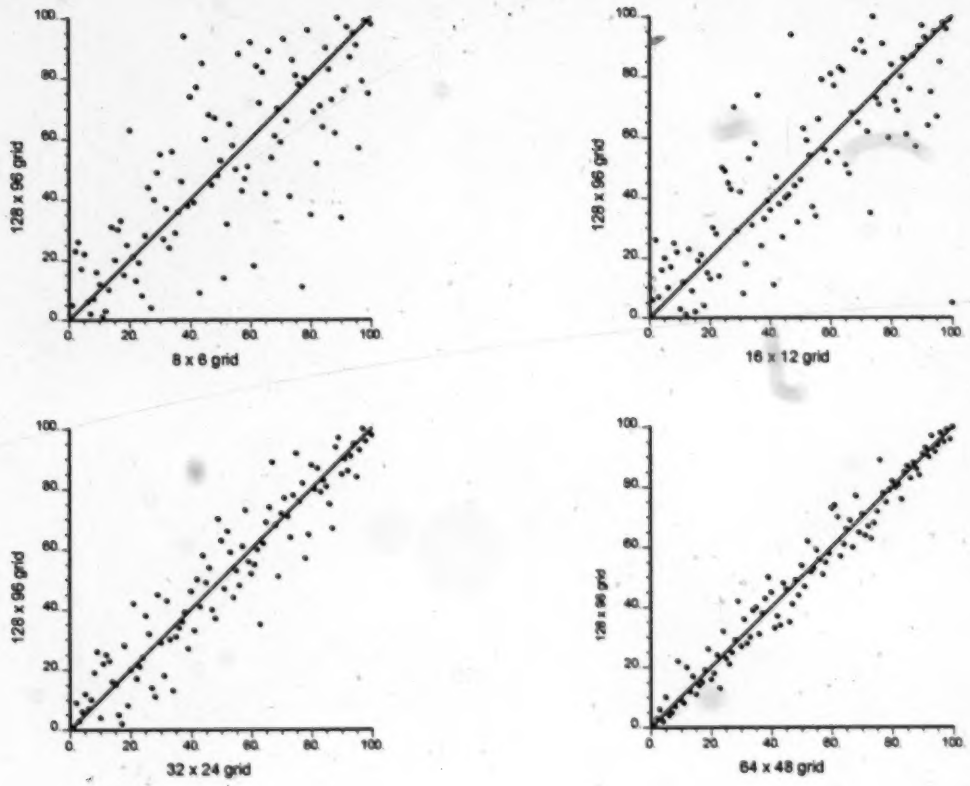

Figure A16-2: Ranking plots for RFs, M = 1.8

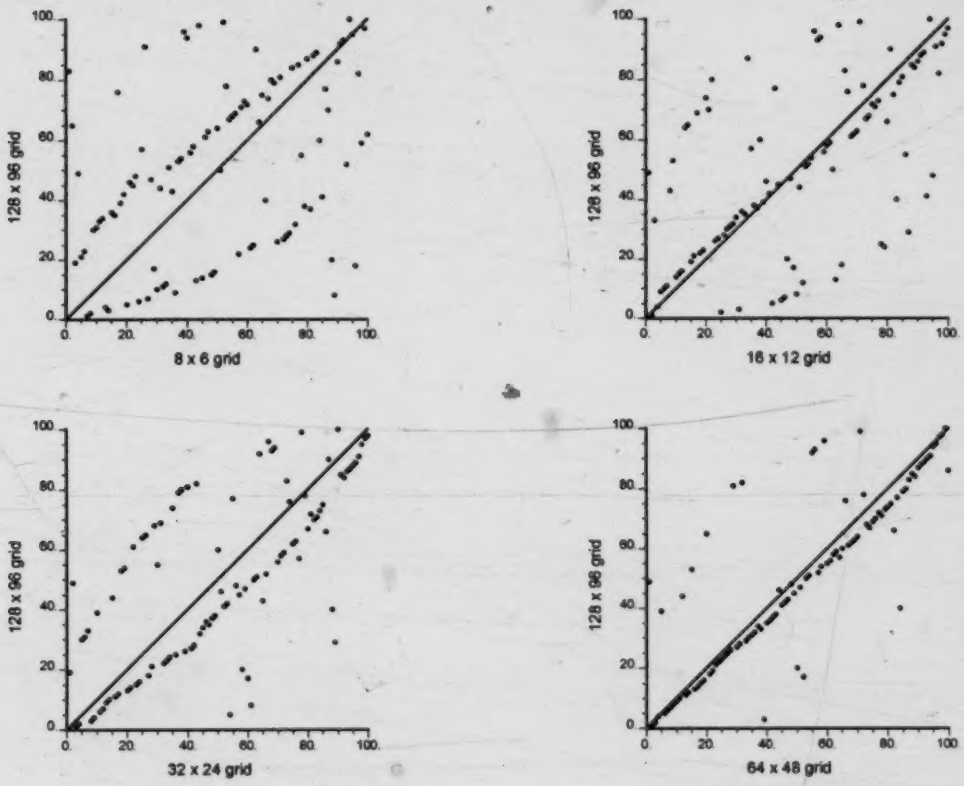

Figure A16-3: Ranking plots for BTs, M = 1

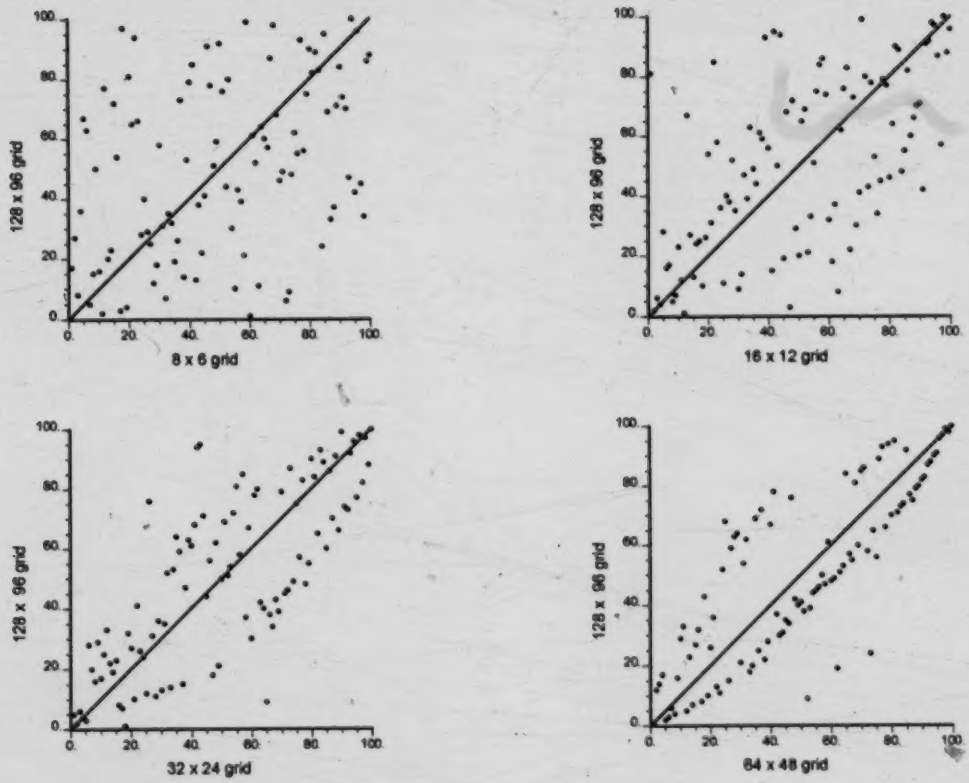

Figure A16-4: Ranking plots for BTs, M = 1.8

APPENDIX 17: TURBO PASCAL PROGRAM TO CALCULATE K_{min} FOR 8 x 6 GRID

```
Program permeability (permfile,fout);
uses wincrt  ;
type
    row = 1..50;
    column =1..70;
    permarray = Array [row, column] of real;
    karray = array [column] of real ;

Var
   k,k1, revk, revk1: real;
   x, z, r: integer;
   perm, revperm : permarray ;
   khar : karray;
   permfile,fout: text;

BEGIN

{Read the data in}

     assign(fout,'8x6kmin.out');
     rewrite(fout);
     Assign (permfile, '8x6fperm.out');
     Reset (permfile);

{Read in the data for 100 realizations}

for r:=1 to 100 do
Begin {start loop for 100 realizations}

  {Assign the data into 8 x 6 matrix}

  for z:=1 to 6 do
  for x:=1 to 8 do

    Read (permfile, perm[x,z]);

  {Calculate the reverve of permeability}

  for z:=1 to 6 do
  for x:=1 to 8 do

  begin

    revperm[x,z]:=1/perm[x,z];

  end;

{Calculate harmonic averages in x direction}

for z:=1 to 6 do
```

```
    repeat

      x:=1 ;
      revk:= revperm[x,z];

      for x:=2 to 8 do
          repeat
            revk1:=revk+revperm[x,z]  ;
            revk:=revk1;
          until x<=8;

      khar[z]:=8/revk;

    until z<=6;

{Calculate arithmetic averages in z direction}

z:=1;
k:=khar[z];
for z:=2 to 6 do
  repeat
    k1:=k+khar[z];
    k:=k1;
  until z<=6;

k:=k/6;
writeln(fout, k:4:3);

End; {End of looping for 100 realizations }
close(permfile) ;  {close the data file}
close(fout);     {close the output file}
END.
```

APPENDIX 18: TURBO PASCAL PROGRAM TO CALCULATE k_{max} FOR 8 x 6 GRID

```
Program permeability (permfile,fout);
uses wincrt  ;
type
    row = 1..50;
    column =1..70;
    permarray = Array [row, column] of real;
    karray = array [row] of real ;

Var
   k,kz, kz1, revk, revk1: real;
   x, z, r: integer;
   perm: permarray ;
   karith, revperm : karray;
   permfile,fout: text;

BEGIN

{Read the data in}

     assign(fout,'8x6kmax.out');
     rewrite(fout);
     Assign (permfile, '8x6fperm.out');
     Reset (permfile);

{Read in the data for 100 realizations}

for r:=1 to 100 do
Begin {start loop for 100 realizations}

  {Assign the data into 8 x 6 matrix}

  for z:=1 to 6 do
  for x:=1 to 8 do

    Read (permfile, perm[x,z]);

 {Calculate arithmetic averages in z direction}

  for x:=1 to 8 do
  begin
      z:=1;
      kz:= perm[x,z];
     for z:=2 to 6 do
     repeat
           kz1:= kz + perm[x,z];
           kz:= kz1;
     until z<=6;
     karith[x]:= kz/6;
  end;
```

```
  {Calculate the reverve of permeability}

  for x:=1 to 8 do

    revperm[x]:=1/karith[x];

  {Calculate harmonic averages in x direction}

    x:=1;
    revk:= revperm[x];

    for x:=2 to 8 do
          repeat
            revk1:=revk+revperm[x]  ;
            revk:=revk1;
          until x<=8;

    k:=8/revk;

writeln(fout, k:4:3);

End; {End of looping for 100 realizations  }
close(permfile) ;  {close the data file}
close(fout);     {close the output file}

END.
```

APPENDIX 19: SUMMARY OF k_{min} AND k_{max} CALCULATIONS BASED ON CARDWELL AND PARSONS' METHOD

Table A19-1: Permeability values calculated based on Cardwell and Parsons' method

				8 x 6 grid			
Realization	**Earlier BTs**	**Same BTs**	**Later BTs**	**k_{min}**	**k_{max}**	**k_{min}/k_{max}**	**RD**
1		x		956.593	1126.265	0.849	0.163
2		x		1004.46	1116.92	0.899	0.106
3		x		1042.651	1155.947	0.902	0.103
4			x	656.739	775.402	0.847	0.166
5		x		877.908	1033.133	0.850	0.162
6		x		1174.219	1275.339	0.921	0.083
7		x		924.671	1087.019	0.851	0.161
8		x		1074.807	1176.912	0.913	0.091
9		x		906.492	1015.11	0.893	0.113
10		x		953.381	1061.262	0.898	0.107
11		x		1014.592	1085.663	0.935	0.068
12		x		920.287	991.005	0.929	0.074
13		x		949.007	1007.268	0.942	0.060
14		x		857.181	938.421	0.913	0.090
15		x		999.087	1105.499	0.904	0.101
16			x	902.742	1038.649	0.869	0.140
17		x		874.65	1001.968	0.873	0.136
18			x	832.631	918.959	0.906	0.099
19		x		1110.037	1256.103	0.884	0.123
20			x	935.054	1031.851	0.906	0.098
21		x		958.784	1122.632	0.854	0.157
22			x	841.408	929.224	0.905	0.099
23			x	904.399	1024.587	0.883	0.125
24		x		900.823	1030.877	0.874	0.135
25		x		887.597	1083.334	0.819	0.199
26			x	905.491	992.209	0.913	0.091
27			x	781.249	873.908	0.894	0.112
28		x		889.863	1027.571	0.866	0.144

29		x		1111.077	1216.365	0.913	0.090
30		x		1063.425	1206.769	0.881	0.126
31			x	929.07	996.652	0.932	0.070
32		x		1003.304	1135.436	0.884	0.124
33		x		1009.53	1089.606	0.927	0.076
34		x		952.724	1039.266	0.917	0.087
35			x	902.742	1047.967	0.861	0.149
36		x		735.179	823.904	0.892	0.114
37		x		987.041	1111.177	0.888	0.118
38		x		856.956	1014.826	0.844	0.169
39		x		690.187	815.081	0.847	0.166
40		x		1065.541	1162.881	0.916	0.087
41		x		975.903	1082.071	0.902	0.103
42		x		1122.252	1198.111	0.937	0.065
43		x		752.642	868.273	0.867	0.143
44	x			771.18	862.25	0.894	0.112
45			x	700.042	840.442	0.833	0.182
46		x		901.383	999.618	0.902	0.103
47			x	906.376	1029.572	0.880	0.127
48	x			949.495	1088.743	0.872	0.137
49	x			791.354	937.37	0.844	0.169
50		x		1110.892	1189.729	0.934	0.069
51		x		739.176	867.321	0.852	0.160
52		x		1000.77	1075.763	0.930	0.072
53		x		1071.62	1177.85	0.910	0.094
54		x		1136.553	1258.742	0.903	0.102
55			x	911.877	1074.323	0.849	0.164
56			x	801.637	950.245	0.844	0.170
57	x			914.068	1149.954	0.795	0.229
58	x			854.333	1010.204	0.846	0.167
59			x	905.901	1022.858	0.886	0.121
60			x	782.192	884.975	0.884	0.123
61			x	1082.787	1168.495	0.927	0.076
62	x			1092.47	1223.564	0.893	0.113
63		x		814.853	884.803	0.921	0.082

64		x		883.05	1062.879	0.831	0.185
65	x			925.586	1045.539	0.885	0.122
66		x		893.608	1009.266	0.885	0.122
67		x		916.092	1048.156	0.874	0.134
68	x			1083.722	1211.692	0.894	0.112
69		x		907.598	1013.535	0.895	0.110
70		x		1080.76	1182.386	0.914	0.090
71		x		985.758	1091.272	0.903	0.102
72			x	939.006	1039.82	0.903	0.102
73		x		918.124	1060.427	0.866	0.144
74		x		924.88	1097.029	0.843	0.170
75		x		932.834	1012.241	0.922	0.082
76		x		979.269	1086.118	0.902	0.103
77			x	729.596	868.327	0.840	0.174
78		x		986.443	1107.519	0.891	0.116
79		x		979.407	1119.449	0.875	0.133
80		x		1037.829	1195.456	0.868	0.141
81		x		917.906	1048.636	0.875	0.133
82			x	919.532	1012.238	0.908	0.096
83		x		878.197	971.272	0.904	0.101
84		x		1047.239	1206.958	0.868	0.142
85		x		865.818	943.505	0.918	0.086
86		x		1016.046	1098.25	0.925	0.078
87		x		986.966	1100.532	0.897	0.109
88		x		854.379	956.269	0.893	0.113
89		x		876.915	960.397	0.913	0.091
90		x		944.513	992.084	0.952	0.049
91			x	753.046	838.364	0.898	0.107
92			x	890.433	952.834	0.935	0.068
93		x		753.884	822.602	0.916	0.087
94		x		841.765	957.607	0.879	0.129
95		x		841.564	941.646	0.894	0.112
96	x			947.607	1059.303	0.895	0.111
97		x		1026.721	1113.842	0.922	0.081
98	x			955.065	1030.903	0.926	0.076
99			x	889.106	991.388	0.897	0.109
100		x		805.916	891.626	0.904	0.101

	128 x 96 grid				Ratios 8 x 6/128 x 96	
Realization	kmin	kmax	kmin/kmax	RD	kmin/kmax	RD
1	367.985	1168.612	0.315	1.042	2.697	0.156
2	447.172	1148.667	0.389	0.879	2.310	0.121
3	370.775	1186.102	0.313	1.047	2.885	0.098
4	212.915	808.9693	0.263	1.167	3.218	0.142
5	264.95	1063.268	0.249	1.202	3.410	0.135
6	598.529	1304.723	0.459	0.742	2.007	0.111
7	441.564	1121.682	0.394	0.870	2.161	0.185
8	450.913	1205.787	0.374	0.911	2.442	0.100
9	360.63	1043.757	0.346	0.973	2.585	0.116
10	384.743	1094.779	0.351	0.960	2.556	0.112
11	406.409	1113.928	0.365	0.931	2.561	0.073
12	313.551	1018.894	0.308	1.059	3.018	0.070
13	327.378	1038.855	0.315	1.042	2.990	0.057
14	308.508	971.8499	0.317	1.036	2.877	0.087
15	475.197	1135.467	0.419	0.820	2.159	0.123
16	287.397	1073.098	0.268	1.155	3.245	0.121
17	337.317	1034.997	0.326	1.017	2.678	0.133
18	278.138	951.6257	0.292	1.095	3.100	0.090
19	499.441	1289.537	0.387	0.883	2.282	0.140
20	284.729	1067.742	0.267	1.158	3.398	0.085
21	364.207	1153.617	0.316	1.040	2.705	0.151
22	239.588	961.5481	0.249	1.202	3.634	0.083
23	404.79	1053.893	0.384	0.890	2.298	0.140
24	348.992	1066.647	0.327	1.014	2.671	0.133
25	267.285	1119.879	0.239	1.229	3.433	0.162
26	320.459	1024.392	0.313	1.047	2.917	0.087
27	279.342	906.5529	0.308	1.058	2.901	0.106
28	445.559	1062.092	0.420	0.818	2.064	0.176
29	480.763	1245.854	0.386	0.886	2.367	0.102
30	366.355	1239.287	0.296	1.087	2.981	0.116
31	352.467	1025.755	0.344	0.977	2.713	0.072

32	412.184	1166.299	0.353	0.955	2.500	0.129
33	380.354	1117.962	0.340	0.985	2.723	0.077
34	371.224	1068.594	0.347	0.969	2.639	0.090
35	301.951	1079.46	0.280	1.126	3.080	0.132
36	182.884	853.5586	0.214	1.294	4.165	0.088
37	427.811	1144.158	0.374	0.911	2.376	0.130
38	246.134	1044.318	0.236	1.237	3.583	0.136
39	231.348	848.4784	0.273	1.143	3.106	0.145
40	364.232	1193.329	0.305	1.065	3.002	0.082
41	290.634	1115.358	0.261	1.173	3.461	0.088
42	481.187	1227.087	0.392	0.873	2.389	0.075
43	286.646	895.7248	0.320	1.030	2.709	0.138
44	311.183	890.533	0.349	0.964	2.560	0.116
45	192.381	874.0614	0.220	1.278	3.784	0.143
46	342.971	1027.772	0.334	0.999	2.702	0.103
47	323.28	1060.736	0.305	1.066	2.889	0.119
48	398.237	1119.807	0.356	0.951	2.452	0.144
49	334.718	972.4504	0.344	0.976	2.453	0.173
50	473.75	1218.263	0.389	0.880	2.401	0.078
51	247.648	899.5543	0.275	1.137	3.096	0.140
52	361.105	1110.732	0.325	1.019	2.861	0.071
53	470.963	1209.768	0.389	0.879	2.337	0.107
54	496.655	1292.996	0.384	0.890	2.351	0.115
55	341.3	1105.908	0.309	1.057	2.750	0.155
56	221.455	982.7103	0.225	1.264	3.744	0.134
57	470.207	1183.096	0.397	0.862	2.000	0.265
58	278.205	1045.798	0.266	1.160	3.179	0.144
59	346.981	1055.385	0.329	1.010	2.694	0.120
60	250.526	920.5179	0.272	1.144	3.248	0.108
61	453.102	1194.982	0.379	0.900	2.444	0.085
62	460.609	1255.065	0.367	0.926	2.433	0.122
63	271.377	917.1939	0.296	1.087	3.113	0.076
64	368.418	1097.377	0.336	0.995	2.475	0.186
65	390.116	1080.37	0.361	0.939	2.452	0.130
66	254.841	1046.291	0.244	1.217	3.635	0.100

67	422.004	1084.438	0.389	0.879	2.246	0.153
68	527.15	1248.218	0.422	0.812	2.118	0.137
69	349.32	1048.503	0.333	1.000	2.688	0.110
70	403.615	1216.56	0.332	1.004	2.755	0.089
71	367.953	1124.295	0.327	1.014	2.760	0.100
72	402.567	1071.159	0.376	0.907	2.403	0.112
73	396.748	1089.891	0.364	0.932	2.378	0.154
74	359.039	1127.291	0.318	1.034	2.647	0.165
75	351.389	1045.791	0.336	0.994	2.743	0.082
76	436.54	1120.983	0.389	0.879	2.315	0.118
77	192.818	906.7641	0.213	1.299	3.951	0.134
78	322.154	1136.877	0.283	1.117	3.143	0.104
79	358.039	1157.258	0.309	1.055	2.828	0.127
80	427.992	1225.007	0.349	0.964	2.485	0.146
81	378.343	1076.863	0.351	0.960	2.491	0.138
82	358.473	1040.213	0.345	0.975	2.636	0.098
83	358.791	1002.753	0.358	0.946	2.527	0.106
84	448.36	1237.971	0.362	0.936	2.396	0.151
85	339.642	974.9291	0.348	0.967	2.634	0.089
86	354.171	1128.396	0.314	1.044	2.948	0.074
87	351.079	1129.638	0.311	1.052	2.886	0.103
88	216.188	989.9303	0.218	1.283	4.091	0.088
89	312.981	989.5922	0.316	1.039	2.887	0.087
90	389.105	1019.88	0.382	0.895	2.495	0.055
91	191.331	870.7646	0.220	1.279	4.088	0.084
92	394.245	984.4914	0.400	0.856	2.334	0.079
93	239.108	854.3425	0.280	1.125	3.275	0.077
94	339.478	988.6649	0.343	0.978	2.560	0.132
95	183.895	974.4301	0.189	1.365	4.736	0.082
96	439.979	1088.928	0.404	0.849	2.214	0.131
97	319.105	1145.916	0.278	1.129	3.310	0.072
98	385.461	1063.149	0.363	0.936	2.555	0.082
99	292.549	1019.989	0.287	1.108	3.127	0.098
100	331.334	923.2898	0.359	0.944	2.519	0.107

APPENDIX 20: RANKING BASED ON THE NUMBER OF CONNECTED CELLS AND PERMEABILITY SCALING

Table A20-1: Ranking for 8 x 6 and 128 x 96 grids based on the connected cells

				600 md threshold				500 md threshold			
				8 x 6 grid		128 x 96 grid		8 x 6 grid		128 x 96 grid	
Realization	Earlier BTs	Same BTs	Later BTs	Cells	Rank	Cells	Rank	Cells	Rank	Cells	Rank
1		x		31	97	0	59	33	100	0	98
2		x		40	46	0	76	44	29	0	97
3		x		44	5	3789	25	44	32	4005	45
4			x	36	68	617	48	37	92	2938	58
5		x		40	44	0	69	43	39	6640	15
6		x		41	35	0	63	43	44	0	90
7		x		33	90	3292	32	40	77	3623	52
8		x		40	45	2145	42	43	41	3857	47
9		x		32	94	5759	13	41	66	6075	26
10		x		42	18	0	60	45	9	4667	37
11		x		43	12	0	99	46	8	0	70
12		x		40	42	498	49	45	14	561	66
13		x		43	9	2847	40	45	16	6612	16
14		x		41	40	3105	35	43	45	3317	55
15		x		42	17	0	57	45	13	0	80
16			x	36	74	0	86	40	75	6005	29
17		x		38	61	3579	29	42	54	4976	34
18			x	40	41	2924	39	43	49	3195	57
19		x		41	36	0	66	42	51	6138	25
20			x	41	29	0	84	44	22	1368	62
21		x		41	30	3386	31	44	23	6842	10
22			x	39	54	0	52	41	69	4065	44
23			x	35	83	830	47	41	67	876	65
24		x		34	85	0	64	39	85	6273	20
25		x		40	43	5456	16	43	48	6813	11
26			x	38	60	0	80	43	38	0	68
27			x	34	87	0	55	37	88	0	95
28		x		36	77	4844	21	39	84	4842	36

29		x		44	2	3122	34	47	1	7355	1
30		x		42	27	0	51	44	31	4483	40
31			x	44	3	6101	7	46	5	6531	17
32		x		42	20	6685	2	44	30	7016	6
33		x		42	22	0	96	45	15	0	93
34		x		36	75	3891	24	41	70	4531	39
35			x	41	32	0	95	44	25	4478	41
36		x		37	67	0	93	42	50	0	87
37		x		36	70	0	89	39	80	0	75
38		x		31	98	0	81	40	78	0	85
39		x		34	88	948	46	37	94	2222	60
40		x		42	28	6801	1	46	3	7089	4
41		x		41	39	3000	36	42	52	6156	24
42		x		45	1	0	79	46	7	0	69
43		x		32	92	0	77	35	98	0	83
44	x			33	89	0	73	39	83	0	73
45			x	35	79	0	61	39	79	0	99
46		x		43	8	382	50	46	2	2890	59
47			x	42	25	6333	4	45	21	6670	14
48	x			43	10	0	56	44	37	4575	38
49	x			35	80	0	53	37	91	3509	54
50		x		43	6	5956	10	45	10	6229	23
51		x		35	84	1746	44	39	82	1920	61
52		x		42	24	0	54	45	20	0	96
53		x		44	4	3598	28	45	17	3765	51
54		x		43	13	0	98	45	12	0	88
55			x	36	71	0	100	44	24	0	84
56			x	35	81	5994	9	37	95	6464	18
57	x			37	65	0	65	40	74	0	78
58	x			31	96	0	67	36	96	0	76
59			x	41	37	6082	8	44	28	6458	19
60			x	36	72	0	71	42	61	0	72
61			x	39	53	6249	5	42	59	6708	12
62	x			41	38	0	75	42	53	0	100
63		x		36	69	2936	38	44	35	3226	56

64		x		37	64	3626	27	39	81	3829	48
65	x			38	62	4037	23	42	63	6675	13
66		x		35	82	0	83	38	86	0	81
67		x		39	51	0	85	42	58	3612	53
68	x			42	26	0	87	45	19	7049	5
69		x		35	78	5939	12	37	93	6234	22
70		x		38	58	0	91	44	33	0	74
71		x		41	34	6177	6	43	43	6941	7
72			x	38	57	2077	43	42	64	4079	43
73		x		40	47	5080	20	43	40	6912	8
74		x		36	73	0	72	40	72	0	82
75		x		42	23	3178	33	44	36	4140	42
76		x		34	86	0	74	38	87	0	86
77			x	28	99	1028	45	36	97	1100	63
78		x		41	33	6445	3	42	65	6882	9
79		x		39	49	0	62	43	42	0	92
80		x		42	19	0	78	43	46	0	94
81		x		43	7	5705	15	43	47	6027	28
82			x	43	15	5757	14	46	6	6058	27
83		x		39	50	2745	41	42	56	3790	49
84		x		43	11	0	82	44	34	7208	3
85		x		32	93	3499	30	42	62	3785	50
86		x		42	21	5166	19	45	11	5410	32
87		x		40	48	2959	37	45	18	7238	2
88		x		39	55	4607	22	40	71	4916	35
89		x		42	16	3667	26	46	4	3897	46
90		x		43	14	0	88	44	26	0	67
91			x	27	100	0	68	42	57	0	89
92			x	36	76	0	90	37	90	0	77
93		x		31	95	0	58	34	99	0	91
94		x		37	63	0	92	40	73	0	71
95		x		39	52	0	70	40	76	1048	64
96	x			38	59	0	94	42	55	0	79
97		x		41	31	5193	18	42	60	5447	31
98	x			38	56	0	97	41	68	4990	33
99			x	37	66	5955	11	44	27	6253	21
100		x		33	91	5233	17	37	89	5591	30

	400 md threshold				Flow-based scaling			
	8 x 6 grid		128 x 96 grid		8 x 6 grid		128 x 96 grid	
Realization	Cells	Rank	Cells	Rank	k	Rank	k	Rank
1	41	91	0	80	1090.4	27	1167.41	30
2	44	68	0	76	1099.7	20	1184.91	24
3	45	46	7242	11	1137.1	17	1238.67	14
4	39	98	5727	43	761.85	100	806.89	100
5	43	72	6889	22	1016	52	1100.73	60
6	46	14	0	93	1260.8	1	1400.48	1
7	41	89	6445	36	1052.2	40	1142.36	40
8	47	9	4109	56	1166.2	12	1235.3	16
9	45	44	6313	40	999.36	61	1111.4	54
10	46	13	4873	52	1042.6	42	1132.51	44
11	47	12	0	81	1072.8	33	1182.2	26
12	46	15	672	75	981.08	71	1109.45	55
13	46	16	6976	18	997.01	63	1095.24	62
14	44	63	4912	51	920.75	83	1044.73	75
15	45	43	7003	16	1093.6	24	1165.03	34
16	43	78	6364	37	1020.1	51	1118.54	48
17	45	38	5216	48	977.09	73	1037.27	77
18	45	54	3550	65	901	86	942.941	89
19	44	61	6505	31	1238.9	3	1330.07	3
20	46	18	1587	73	1012.3	54	1071.56	69
21	46	19	7206	13	1095.9	23	1176.46	27
22	45	35	6655	27	912.61	85	962.67	86
23	46	24	3864	62	1004.8	57	1112.64	53
24	44	60	6711	26	1004.6	58	1086.78	65
25	43	73	7180	14	1056.9	38	1161.17	36
26	47	6	0	96	979.18	72	1067.13	70
27	44	56	3207	68	854.45	91	1004.08	83
28	40	94	5049	50	1004.2	59	1087.39	64
29	48	2	7645	2	1202.5	5	1327.33	4
30	47	10	7560	3	1192.7	7	1270.51	10
31	47	11	6900	21	986.77	67	1063.8	72

32	44	55	7333	7	1120.7	19	1222.57	18
33	46	27	0	98	1073.3	32	1162.51	35
34	44	62	6498	32	1026.8	47	1125.98	45
35	44	59	6717	25	1028.6	46	1115.12	51
36	45	34	5360	46	809.73	98	869.642	98
37	43	75	6489	33	1093.2	25	1227.14	17
38	42	86	5166	49	993.43	65	1080.67	67
39	39	96	3317	67	790.28	99	834.007	99
40	47	7	7373	6	1148	16	1218.55	19
41	45	39	6488	34	1062	36	1166.95	32
42	47	5	7965	1	1184	9	1281.31	8
43	42	88	0	84	856.55	90	927.44	93
44	45	42	0	78	848.45	92	933.913	91
45	44	57	5956	42	818.98	96	884.281	97
46	47	3	3105	70	984.16	69	1029.73	79
47	46	33	6977	17	1011.1	55	1100.65	61
48	45	49	4783	53	1066.3	35	1142.65	39
49	41	90	3790	63	916.09	84	982.331	84
50	46	17	6507	30	1180.2	10	1273.48	9
51	42	85	2068	72	845.15	93	928.769	92
52	46	30	0	100	1060.5	37	1184.69	25
53	47	8	3934	61	1165.5	13	1258.77	12
54	48	1	0	99	1240.9	2	1338.96	2
55	45	50	0	97	1055.4	39	1139.46	43
56	42	81	6759	24	930.43	80	1027.95	81
57	42	84	0	95	1129.2	18	1205.18	22
58	41	92	0	91	984.5	68	1106.5	58
59	44	64	6802	23	1010.8	56	1106.64	57
60	45	53	0	89	859.68	89	951.804	88
61	44	58	6969	19	1157.2	15	1236	15
62	42	83	7163	15	1205.5	4	1270.47	11
63	46	20	3375	66	871.56	88	934.148	90
64	42	80	4031	59	1039.9	43	1125.23	46
65	43	79	6953	20	1023.7	49	1089.35	63
66	44	65	0	87	988.42	66	1063.49	73

67	43	74	3717	64	1023.9	48	1116.44	50
68	46	32	7317	8	1186.1	8	1303.9	5
69	39	97	6540	28	1000.2	60	1141.83	41
70	46	22	0	79	1160.8	14	1242.67	13
71	44	69	7265	10	1073.7	31	1167.3	31
72	46	26	4320	55	1021.7	50	1116.57	49
73	44	71	7282	9	1036.1	44	1149.79	38
74	41	93	0	86	1080.1	30	1196.71	23
75	46	25	4387	54	993.94	64	1141.14	42
76	42	82	3147	69	1068.2	34	1150.97	37
77	39	99	2522	71	836.57	94	887.695	96
78	45	51	7220	12	1092.2	26	1210.01	20
79	45	52	0	83	1097.7	22	1167.6	29
80	44	67	0	85	1177.9	11	1282.86	7
81	43	76	6335	39	1036	45	1104.77	59
82	46	28	6487	35	998.01	62	1071.88	68
83	43	77	4084	58	955.22	75	1041.72	76
84	45	48	7480	5	1193.7	6	1286.55	6
85	45	47	3976	60	929.73	81	1066.92	71
86	45	45	5628	45	1084.9	29	1171.77	28
87	47	4	7528	4	1085.6	28	1209.94	21
88	40	95	6355	38	940.28	78	1081.79	66
89	46	29	4103	57	945.89	76	1015.05	82
90	46	21	0	88	983.25	70	1056.89	74
91	45	37	0	77	820.23	95	921.806	95
92	46	31	0	90	945.06	77	1035	78
93	37	100	0	82	810.48	97	924.353	94
94	45	36	0	92	937.76	79	1028.36	80
95	45	41	1088	74	924.32	82	979.812	85
96	44	66	0	94	1044.7	41	1113.5	52
97	45	40	5638	44	1098.2	21	1165.41	33
98	44	70	5329	47	1015.8	53	1107.67	56
99	46	23	6522	29	977.03	74	1121.84	47
100	42	87	6135	41	875.16	87	955.559	87

APPENDIX 21: VARIANCES OF FLOW RATES

Table A21-1: Flow rate variances for 8 x 6 and 128 x 96 grids

		Flow rate variances		Standardized flow rate variances	
Realization	d (8 x 6)	8 x 6	128 x 96	8 x 6	128 x 96
1	9	53.7	0.675	3.107	1.755
2	0	31.859	0.568	1.057	0.759
3	11	24.91	0.636	0.405	1.392
4	-49	10.346	0.289	-0.961	-1.836
5	7	9.375	0.426	-1.053	-0.562
6	7	38.139	0.769	1.647	2.629
7	12	43.641	0.579	2.163	0.862
8	9	21.08	0.587	0.046	0.936
9	6	27.03	0.495	0.604	0.080
10	2	11.482	0.411	-0.855	-0.701
11	7	12.596	0.475	-0.750	-0.106
12	9	13.473	0.41	-0.668	-0.710
13	7	16.093	0.407	-0.422	-0.738
14	12	8.617	0.394	-1.124	-0.859
15	9	13.795	0.569	-0.638	0.769
16	-48	20.384	0.524	-0.019	0.350
17	9	20.5	0.401	-0.009	-0.794
18	-43	7.434	0.344	-1.235	-1.324
19	6	52.01	0.718	2.948	2.154
20	-45	10.035	0.545	-0.991	0.545
21	6	15.771	0.46	-0.452	-0.245
22	-50	11.306	0.375	-0.871	-1.036
23	-21	22.871	0.478	0.214	-0.078
24	10	19.286	0.503	-0.123	0.155
25	10	25.903	0.491	0.498	0.043
26	-50	10.74	0.499	-0.924	0.117
27	-44	5.627	0.313	-1.404	-1.613
28	6	40.673	0.536	1.884	0.462

29	6	15.692	0.529	-0.460	0.397
30	4	21.273	0.585	0.064	0.917
31	-88	5.908	0.393	-1.378	-0.868
32	6	36.349	0.561	1.479	0.694
33	2	17.37	0.494	-0.302	0.071
34	7	21.572	0.509	0.092	0.210
35	-28	26.642	0.552	0.568	0.610
36	16	4.675	0.284	-1.494	-1.882
37	6	28.052	0.557	0.700	0.657
38	1	32.078	0.623	1.078	1.271
39	9	11.111	0.331	-0.890	-1.445
40	0	14.406	0.513	-0.580	0.248
41	10	18.754	0.562	-0.172	0.703
42	4	14.622	0.514	-0.560	0.257
43	7	16.334	0.36	-0.400	-1.175
44	56	17.144	0.351	-0.324	-1.259
45	-46	7.293	0.271	-1.248	-2.003
46	2	9.553	0.395	-1.036	-0.850
47	-35	5.813	0.42	-1.387	-0.617
48	63	25.311	0.505	0.443	0.173
49	53	24.592	0.506	0.375	0.183
50	8	23.365	0.688	0.260	1.875
51	14	16.724	0.317	-0.363	-1.575
52	10	14.61	0.421	-0.561	-0.608
53	5	19.683	0.568	-0.085	0.759
54	6	30.23	0.665	0.904	1.662
55	-50	32.475	0.569	1.115	0.769
56	-32	9.244	0.391	-1.065	-0.887
57	58	44.225	0.569	2.218	0.769
58	65	31.482	0.466	1.022	-0.189
59	-46	16.033	0.519	-0.428	0.304
60	-50	6.613	0.362	-1.312	-1.157
61	-50	33.755	0.635	1.235	1.382
62	57	42.067	0.675	2.015	1.755
63	14	12.392	0.307	-0.769	-1.668
64	13	22.328	0.46	0.163	-0.245

65	65	32.135	0.492	1.083	0.052
66	10	22.616	0.494	0.190	0.071
67	10	30.869	0.545	0.964	0.545
68	47	23.582	0.636	0.281	1.392
69	11	27.27	0.514	0.627	0.257
70	10	24.652	0.654	0.381	1.559
71	9	15.061	0.522	-0.519	0.331
72	-48	14.087	0.567	-0.610	0.750
73	7	13.464	0.447	-0.669	-0.366
74	15	28.92	0.583	0.782	0.899
75	7	12.131	0.435	-0.794	-0.478
76	9	39.443	0.587	1.769	0.936
77	-45	13.999	0.364	-0.619	-1.138
78	8	26.486	0.551	0.553	0.601
79	-1	23.783	0.627	0.299	1.308
80	7	40.238	0.624	1.844	1.280
81	10	20.275	0.424	-0.030	-0.580
82	-62	10.222	0.38	-0.973	-0.989
83	5	17.226	0.384	-0.316	-0.952
84	7	28.261	0.579	0.720	0.862
85	10	22.749	0.407	0.202	-0.738
86	3	18.747	0.511	-0.173	0.229
87	8	11.175	0.422	-0.884	-0.599
88	10	17.545	0.413	-0.286	-0.682
89	7	7.82	0.416	-1.198	-0.655
90	2	13.519	0.426	-0.664	-0.562
91	-49	5.354	0.287	-1.430	-1.854
92	-40	11.003	0.451	-0.900	-0.329
93	11	21.585	0.324	0.093	-1.510
94	8	24.612	0.425	0.377	-0.571
95	-2	10.164	0.373	-0.978	-1.055
96	55	27.079	0.493	0.609	0.062
97	9	27.664	0.59	0.664	0.964
98	49	22.28	0.523	0.158	0.341
99	-52	10.606	0.477	-0.937	-0.087
100	9	14.079	0.386	-0.611	-0.934